Assessment of the Performance of Corn Cob Ash as a Partial Replacement for Portland Cement in Concrete

Oluwadamilola Adepeju Fadele

A thesis submitted to the Faculty of Engineering and the Built Environment, University of the Witwatersrand, Johannesburg in fulfilment of the requirements for the degree of Doctor of philosophy in Civil Engineering

Johannesburg, 2023

DECLARATION

I, Oluwadamilola Adepeju Fadele, hereby declare that this thesis is my own unaided work. It is being submitted for the degree of Doctor of Philosophy in Engineering to the University of the Witwatersrand, Johannesburg. It has not been submitted before for any degree or examination to any University.

(Signature of Candidate)

20th day of March year 2024

ABSTRACT

The production of Portland cement is associated with the release of greenhouse gases especially carbon dioxide which is estimated to be about a ton per every ton of clinker produced contributing to climate change. Several mitigation strategies have been proposed but the most viable remains the use of supplementary cementitious materials as partial replacement for Portland cement. There have been considerable success with the use of some industrial by-products (fly ash and slag) and natural materials (calcined kaolin clay) as supplementary cementitious materials. However, the non-availability of these by-products in countries like Nigeria calls for the investigation of locally available substitutes. Supplementary cementitious materials are either pozzolanic or possess latent hydraulic properties making them choice materials as partial Portland cement replacement. The classification and choice of a material as supplementary cementitious material lies in the understanding of their characteristic properties (chemical composition and mineralogy) and subsequent performance in cementitious systems.

The performance of corn cob ash calcined at 700°C and 800°C as partial replacement for Portland cement (PC) compared to Portland cement and fly ash (FA) was studied with the following objectives: to determine the influence of calcination temperature on the reactivity of corn cob ash; investigate the effects of corn cob ash content at varying w/b ratio on the i) hydration reaction of Portland cement; ii) the compressive strength of concrete iii) drying shrinkage strain of mortar iv) penetrability of concrete v) microstructure of concrete

The laboratory investigation involves using corn cob ash to partially replace Portland cement at two levels of 15% and 30% by mass using two w/b ratios of 0.4 and 0.6 at a water content of 205 kg/m^3. The corn cob ashes in binary combination with either Portland cement or fly ash were used to prepare concrete samples which were used for the determination of compressive strength, durability index tests (namely oxygen permeability, water sorptivity and chloride conductivity) to assess the durability of concrete, and microstructural development. The concrete was designed using the South African Cement and Concrete Institute method of mix design. Also, mortar samples made from one part of cement to three parts of sand were prepared for the investigation of drying shrinkage and estimation of strength activity index while paste samples were prepared for determining reactivity of the ashes and effect on Portland cement hydration.

Reactivity of the ashes was measured using both strength activity index and R3 reactivity test. Strength activity index was estimated from the compressive strength of 50 mm cube mortars at the ages of 28, 56 and 90 days of curing in order to better understand the mechanism of reaction of the ash, while R3 test was performed on model paste using the bound water approach at the age of 7 days.

The amorphous content of ash calcined at 700°C and 800°C is 1.9% and 2.4% respectively while the gain in strength of mortar cubes prepared with only Portland cement, Portland cement/fly ash, Portland cement/corn cob ash calcined at 700°C and 800°C between 28 and 90 days are 14%, 24%, 10% and 9% respectively. The surface area of the Portland cement, fly ash, corn cob ash calcined at 700°C and at 800°C is 2.38, 2.224, 3.122 and 2.751 m^2/g respectively. The results indicate that the corn cob ashes (CCA) calcined at 700°C (C700) and 800°C (C800) are low reactive materials with limited pozzolanic reactivity while the mechanism of reaction is largely influenced by filler effect due to finer particle size than plain PC. The compressive strength of concrete containing 15% CCA calcined at 700°C and 85% Portland cement ranges between 40 to 58 MPa between 3 and 90 days of curing at w/b ratio of 0.4 compared to 56 to 83 MPa for Portland cement concrete and 48 to 82 MPa for fly ash/Portland cement concrete at the same replacement level. The porosity of concrete containing 15% C700 and C800 at w/b ratio of 0.4 is 9.66 and 6.9% respectively at 28 days of curing compared to 8.37% for PC and 6.52% for fly ash at the same age and replacement level.

The presence of CCA affects the heat of hydration of plain PC by prolonging the induction phase by about 12 hours which delayed the evolution of main heat peak. The use of CCA lead to a reduction in strength compared to PC/FA system with compressive strength decreasing with increasing w/b ratio and increasing PC replacement level. CCA has a high potassium oxide content which is highly soluble with a high concentration in the pore solution of concrete. CCA influences volume change leading to a high drying shrinkage strain compared to plain PC and FA. CCA also affects the durability of concrete by increasing the penetrability of concrete which increases with increasing ash content. In terms of the studied properties of cementitious systems, there is no marked difference in the effect of C700 compared to C800 while the effects recorded becomes significant with increasing PC replacement level. In comparison to FA, the effect of CCA on the properties studied was inferior due to the largely crystalline nature resulting in limited pozzolanic activity.

ACKNOWLEDGEMENTS

I would like to sincerely appreciate my supervisor Prof. Mike Otieno for the guidance, support and encouragement during the course of this study.

I would also like to appreciate the support and encouragement received from Prof. Yunus Ballim, Prof. Sunny Nwaubani, Prof. John Ndiritu and Ms Janina Kanjee.

I would like to extend my appreciation to the technical staff of: the concrete lab (Mr Ronny Lambani and Mr Ronald Manameni), the Environmental Engineering laboratory (Ms Namhla Maquebela), the geotechnical laboratory (Ms Tumelo Sithole and Mr Sam Mabote) and the administrative staff (Ms Lubica Korac, Ms Pinkie Steyn and Mrs Rishandani Govender). I also appreciate Miss Areej Gamieldien of the University of Cape Town for her assistance.

To my family; my husband Dr Ayangbenro, my children Praise and Joy, my siblings, my parents and In-laws, I am indeed indebted to you all. Thank you for the support and encouragement.

I acknowledge the financial support received from National Research Fund of South Africa Grant number 110818 and Postgraduate Merit award, University of the Witwatersrand, Johannesburg.

TABLE OF CONTENTS

LIST OF FIGURES

LIST OF TABLES

NOMENCLATURE

15-4	15% plain Portland cement replacement at w/b ratio of 0.4
15-6	15% plain Portland cement replacement at w/b ratio of 0.6
30-4	30% plain Portland cement replacement at w/b ratio of 0.4
30-6	30% plain Portland cement replacement at w/b ratio of 0.6
C700	Corn cob ash calcined at 700°C
C800	Corn cob ash calcined at 700°C
CCA	Corn cob ash
CCI	Chloride conductivity index
FA	Fly ash
OPI	Oxygen permeability index
PC	Plain Portland cement
SCM	Supplementary cementitious materials
WSI	Water sorptivity index
w/b	Water to binder ratio
w/c	Water to cement ratio

1.1 Background

The production of Portland cement is associated with the release of CO_2 (a greenhouse gas) which must be overcome to lessen its impact and improve environmental sustainability (Miller, Roijen, Cunningham, & Kim, 2021). CO_2 mitigation strategy suggested include increasing energy efficiency, fuel substitution, clinker substitution and carbon capture and storage or use (Scrivener, John, & Gartner, 2018). The most successful strategy so far to reduce the emission of CO_2 in the production of cement globally is the reduction of the clinker content through the use of supplementary cementitious materials (SCMs) (Scrivener, Martirena, Bishnoi, & Maity, 2018). The first generation of SCMs (ground granulated blast furnace slag, GGBS, fly ash, FA and silica fume) are majorly by-products and/or waste materials from industrial activities, and are found to have good compatibility with Portland cement (PC) and improves the performance of cementitious systems (Lothenbach, Scrivener, & Hooton, 2011). However, the availability of these streams of SCMs is dwindling globally (Scrivener et al., 2018) and this has resulted in an increase in the streams of materials being investigated and used as SCMs in cement, mortar and concrete production in order to reduce the environmental impact of PC production and usage. SCMs are used as effective partial substitutes to PC to reduce cost, reduce need for landfilling these industrial wastes and improve environmental sustainability with respect to cement production. Current investigation into the use of SCMs is embracing new sources of materials such as calcined clays, some naturally occurring materials and SCMs from agricultural wastes. Industrial SCMs (fly ash, GGBS, silica fume and metakaolin) are well researched and widely available materials in commercial quantities in developed countries (Luxán *et al.*, 1989; Gutteridge and Dalziel, 1990b; Suprenant and Papadopoulos, 1991; Lumley *et al.*, 1996; Singh, Singh and Rai, 2000; Escalante *et al.*, 2001; Haha, *et al.*, 2010; Otieno, *et al.*, 2010; Deschner *et al.*, 2013; Monteagudo *et al.*, 2014; Bullard *et al.*, 2015).

SCMs processed from agricultural wastes (agro-based SCMs) are being investigated as potential binder sources in agrarian developing nations, partly because of the availability of agro wastes which are renewable in nature and essentially due to their material properties which makes them potential source of SCMs. In terms of availability, it was reported that the theoretical residue from maize and sugarcane in South Africa based on area of land cultivated and which can be harnessed

for energy production is about 28Mt and 6Mt respectively (Barahira, Okudoh, & Eloka-Eboka, 2021). Also, the available volume of biomass ash was estimated at about 100-140Mt/yr with zero utilisation as SCM compared to fly ash volume of about 700-1100Mt/yr with 330-400Mt/yr utilised as SCM (Juenger, Snellings, & Bernal, 2019). With the increasing research into the use of agricultural wastes for energy production, it is believed that the quantity of biomass ash will also increase and the major challenge remains enhancing the use as alternative source of SCMs by understanding the mechanism of influence on the properties of cementitious systems.

Agricultural wastes here refer to waste materials resulting from the harvest and/or post-harvest processing of plant and tree crops often generated in large quantities and disposed of. Examples of such wastes include rice husk, corn cobs, sugarcane straw and bagasse, wheat straw, groundnut shell, palm kernel fibre and shell, coconut husk and shell. While a fraction of some of these wastes is utilised as fuel for cooking or as animal feed, a substantial part is mostly openly burnt in air or heaped up in open field and left to decay. Although, open air burning results in emission of pollutants (particulate matters and gases like carbon dioxide and methane) (Cogut, 2016), it is often unavoidable in some climes given the need to dispose-off wastes, it is therefore necessary to seek for alternative ways to utilise these wastes.

One sustainable and efficient way to handle agricultural wastes is by recycling them to produce value added materials in construction activities, which can be economical given the dire need for durable materials to address the deficit in housing and infrastructure requirement of developing countries (World Bank Group, 2015). This often requires the thermal processing of the raw waste into usable form suitable for use in construction application. Although, processing agricultural wastes into SCMs may require substantial energy input which often times is not readily available in most developing countries, the required energy is not as high as that required for Portland cement (PC) production (Choate, 2003). Studies have investigated the calcination of these wastes at temperatures less than 1000°C while the production of Portland cement takes place at temperature above 1000°C (Bahurudeen & Santhanam, 2015; Muthadhi & Kothandaraman, 2010). However, these materials in themselves can be used to generate the needed energy for their conversion into SCMs either solely or in combination with conventional fuels such as coal (Wang *et al*., 2012; Asonja *et al*., 2017). Furthermore, combusting these wastes in the production of energy is noted by Commission for environmental cooperation report (2014) as a cheaper option than conversion to biofuel. More importantly, these waste can be used as fuel for agro-processing

and agro-allied industry at source and this requires more concerted efforts in research and development to obtain suitable production approaches.

The utilization of these materials as SCMs depends on their impact on the properties of cementitious systems especially with respect to how the hardened paste structure and pore structure is affected. Both the hardened paste and pore structure influence the mechanical and durability behaviour of cementitious system and can impact the service life of structural concrete to a considerable extent. Aside strength, the performance of these materials with respect to durability in reinforced concrete structures is important and more importantly with respect to the penetrability of the matrix. A proper understanding of the influence on and contribution of these materials to the penetrability by aggressive agents is essential to their development and use as viable clinker substitution strategy. As these materials often require thermal processing for conversion into useable form as SCM, this often has a significant effect on the characteristics of the ash and behaviour in cementitious systems. Also important is the mechanism of reaction and impact on the properties of cementitious systems, as a good understanding of this is essential to the development and utilisation of these types of SCM.

Corn cob ash (CCA) can be obtained from uncontrolled (open air burning) and controlled burning (combustion and/or calcination) of corn cobs, which is a post-harvest waste of maize (*Zea mays*). Maize is widely cultivated in the humid tropics and sub-Saharan Africa, with South Africa, Nigeria and Egypt being the three largest producers of the crop in sub-Saharan Africa (Suberu *et al*., 2012). The cobs constitute about 20% of the total residue of maize harvesting (Danje, 2011) resulting in about 11 million tons of corn cobs produced yearly in South Africa (South African Department of Agriculture, 2016). There are limited studies (Adesanya & Raheem, 2009a, 2010; Ikponmwosa *et al.,* 2015; Memon & Khan, 2018; Mujedu *et al*., 2014; Nimityongskul & Daladar, 1995; Serbanoiu *et al*., 2022) that have investigated the usage of CCA as SCM in cement-based systems with divergent views on its pozzolanicity. However, most of these studies have worked mostly with CCA obtained from open air burning and shown that it contained significant amount of silica, traces of alumina, iron oxide and alkalis while the nature of the silica in terms of reactivity could not be established. Aside the chemical composition, is a need for the understanding of the mechanism by which it react with PC and contributory effect to performance in cementitious systems in order to establish its suitability as a Portland cement replacement given the gains which can ensue from sustainable utilisation of corn cob wastes.

1.2 Problem Statement

Nimityongskul and Daladar (1995) reported that CCA may not be a pozzolan given the oxide composition and the strength activity index (SAI) for samples recorded in the study while Ikpowonsa *et al.* (2015) reported that CCA up to 30% PC replacement level met the 28 day strength activity index requirement. The CCA used in both studies have similar chemical composition and high carbon content, it is not clear the contributory factors to the differences reported. For pozzolans, the reactivity and particle fineness can be said to be of importance as British standard (BS EN 197:1) recommends a reactive silica content of at least 25% while ASTM C618 requires that a maximum of 34% of the particles can be retained on a 45 μm sieve when wet sieved. Memon & Khan (2018) reported that increasing the fineness of CCA increases the strength activity index and hence its performance as a pozzolan. It could not be established from any of the studies the reactive content of the ash to be able to understand the difference in results. This is further complicated by the method of ash preparation from raw corn cobs. For one it is clear is that the calcination method of obtaining ash from raw cobs contributes to the properties of the ash but how this affects the performance of cementitious systems need to be understood.

Variability in pozzolanic behaviour of agricultural based pozzolans may be traced to the variation in the contents and composition of the ash-forming elements, type of thermal treatment adopted and operating conditions (temperature of burning, burning duration and rate of cooling) of the heating system (Gilbe et al., 2008). Resolving the differences therefore requires a comparison of different calcination methods and understanding their effect on the characteristics and reactivity of the resulting ash.

Beyond the chemical composition requirements for pozzolanic materials given by ASTM C618-12 and BS EN 197-1, the wide variability in performance of materials that met the requirements indicates the need for additional requirement(s) with direct effect on reactivity and/or interaction with PC. This information could not be established by any of the previous studies on CCA, while other studies (Kroehong, Sinsiri, Jaturapitakkul, & Chindaprasirt, 2011; Megat Johari, Zeyad, Muhamad Bunnori, & Ariffin, 2012; Memon & Khan, 2018) further showed the information gap with respect to reactivity. Reactivity reflect to a certain extent the material behaviour, reaction and interaction with plain PC and extent of improvement of the internal structure of the system and its

impact on the performance and response of cementitious system to external effects (load, aggressive fluids etc.).

From previous studies, it is clear that there is a need for proper classification of CCA by understanding its properties, mechanism of reaction and contribution to the performance of cementitious systems in order to enhance its development and adoption or otherwise in countries where the raw material abounds.

1.3 Aim and Objectives of the study

The aim of this study is to investigate the performance of CCA as a partial replacement of Portland cement in cementitious system with a view to determining its suitability as a supplementary cementitious material.

The specific objectives of the study are to:

1. determine the influence of calcination temperature on reactivity CCA;
2. investigate the effects of CCA content at varying w/b ratio on the
    (i) hydration reaction of PC;
    (ii) compressive strength of concrete
    (iii) drying shrinkage of mortar;
    (iv) Penetrability of concrete; and
    (v) microstructure of concrete.

1.4 Research Significance

The design of concrete structures to satisfy strength and durability requirements is crucial to the functionality of structures during the design life to which the material properties and interaction play a role. Field utilization of non-conventional binders requires thorough understanding of their properties and behaviour prior to use in the construction of concrete structures. Laboratory investigation of the material properties, interaction with other constituents and performance in cementitious systems is therefore a crucial step in both its development and utilisation.

The use of SCMs from agricultural waste in concrete such as corn cob ash no doubt is an evolving field worth exploring. It offers the benefit of reducing emission of greenhouse gases associated with the production of conventional Portland cement with an added advantage of reduced energy

required in its production. Subsequently, the use of these SCMs has the potential of improving the strength and durability properties of concrete (Juenger & Siddique, 2015) thereby giving rise to concrete with better performance characteristics.

Furthermore, since in most developing African countries these agricultural wastes are generated annually in several tonnes and improperly disposed of, their utilisation in concrete will result in a cleaner environment. Subsequently, post-harvest collection of the cobs may generate additional income in the downstream (either to farmers and/or through the utilisation of the waste for energy generation). Also, in developing countries where industrial activities are limited due to poor power supply, advantage can be taken of the abundance of agricultural wastes as alternative source of energy and construction materials to enhance local content and capacity development in materials research and development.

1.5 Research Questions

This study will attempt to proffer answers to the following questions in order to understand the pozzolanic behaviour of CCA in cementitious systems:

1. What is the influence of processing method on the properties of CCA?
2. How does CCA content influence the hydration of cement paste?
3. How does CCA content affect the microstructure of concrete?
4. How does CCA content affects drying shrinkage of mortar?
5. What is the effect of CCA content on compressive strength development of blended cement systems?
6. How does CCA content impact the transport properties of blended cement systems?

1.6 Scope

This study investigates the use of CCA as a partial replacement for PC compared with PC and fly ash which is believed to have similar pozzolanic reaction behaviour with CCA. CCA was used as a partial replacement for PC at two replacement levels of 15% and 30%. Also, two w/b ratios of 0.4 and 0.6 were investigated while the maximum curing age for this study was 270 days of water curing at about 23°C.

1.7 Challenges

There is a limited availability of facility for the calcination process of obtaining the ash for the study. This had an impact on the type of thermal treatment adopted as well as the quantity and quality of the ash obtained.

1.8 Thesis layout

This thesis is presented in five chapters with the remaining chapters explained as follows, chapter two is the literature review, which presents the definition of terms, description of supplementary cementitious materials and their behaviour in cementitious systems. Also, hydration reaction and filler effects of SCMs were discussed.

Chapter three presents the research methodology and discussion of the experimental procedure for each test carried out on the study material in details. The chapter discusses the materials and methods employed to achieve the stated objectives by giving a vivid description of each test carried out as well as the test instrument required.

Chapter four presents the analyses and discussion of the results obtained from the laboratory investigations. The tests carried out includes the compressive strength, hydration using isothermal calorimetry method, transport properties (durability indices), and drying shrinkage.

Chapter five presents discussion on the relationship between strength and porosity of concrete as it relates to the experimental data.

Chapter six presents the conclusions and summary of findings of the study while other results not presented in chapter four are presented in the appendix.

2.1 Introduction

This chapter presents a critical review of the different subject matters considered important to this study using information available from different published journal articles, reports, conference articles, and textbooks. Inferences were drawn from the information available to identify differences in information, and create a niche for this study. The discussion divided into sections, provides information on definition and classification of SCMs, development around CCA as a pozzolan from agricultural wastes (availability, challenges and research findings), behaviour of SCMs in cementitious systems, and propositions on the influence and behaviour of Portland cement blended with fillers and cementitious materials, and in cementitious compounds at early reaction age.

2.2 Discussion on definitions and classification of SCMs from literature

Pozzolans according to BS EN 197-1:2000 and ASTM C125-03 are materials rich in silica or silica and alumina which may not have hydraulic properties but in the presence of moisture and in finely divided form will react at room temperature with calcium hydroxide produced from PC hydration process to form strength enhancing calcium silicates and/or calcium aluminate compounds. Pozzolanic materials described by the standards include fly ash, silica fume, metakaolin, calcined clay, natural pozzolans, natural calcined pozzolans which are thermally activated.

On the other hand, materials which behave hydraulically in the presence of water are referred to as cementitious, they are chemically active in the presence of water and can harden to form strength enhancing compounds, e.g. burnt oil shale and slag (ASTM C125-03). However, ‘cementitious’ is used to describe a material that may have some similarities with cement either with respect to chemical reactivity, nature of setting/hardening or formation of compounds. Hence, either pozzolanic materials or those possessing some form of hydraulicity can be considered cementitious but since they are often used in combination with PC, the term supplementary cementitious materials (SCMs) may be more appropriate.

Further, several reports (Lawrence, Cyr, & Ringot, 2003; Monteagudo et al., 2014; Nehdi, Duquette, & El Damatty, 2003) have used the term ‘mineral admixture’ to collectively describe pozzolanic, cementitious and filler materials but was noted in ASTM C 125-03 as not suitable

since each material differ from the other. The differences being traced to their reactivity and influence on the properties of cementitious systems. The standard suggests specific material name such as pozzolan, slag or finely divided aggregate, thus distinguishing SCMs from finely divided aggregates (e.g. limestone, quartz powder, silica sand). As further noted from (Schlorholtz, 2006) the term SCMs may best describe both pozzolanic (like fly ash, natural/calcined natural pozzolan and ashes from agricultural wastes) and cementitious materials (like slag) while the term mineral admixture include finely divided aggregates if at all appropriate.

Supplementary cementitious materials describe the use in improving the properties of cementitious systems and as extenders (to reduce cost) (Schlorholtz, 2006). The term inert fillers here refers to finely divided aggregates like limestone, quartz etc., which are relatively inert and only affect systems properties by being present. Ultimately, understanding the interaction of each material with Portland cement will help to understand their contribution to the performance of cementitious systems and enhance their efficient use.

2.3 Supplementary Cementitious materials (SCMs)

The initial use of SCMs in concrete was to reduce bleeding but were found to improve some other properties alongside (Schlorholtz, 2006), and in recent times are now an important part of concrete technology most especially as partial replacement of Portland cement (PC). Pozzolanic SCMs react with the excess CH given off during the hydration of cement to produce more C-S-H or C-A-S-H hydrates, thereby enhancing properties of concrete (Lothenbach et al., 2011). SCMs that behaves hydraulically do not entirely depend on PC hydration for their reaction but hydrate in the presence of moisture to produce strength enhancing products similar to PC. SCMs investigated for cement and/or concrete production have been from three major sources namely, natural materials (pozzolana, natural calcined pozzolana, volcanic ash), industrial wastes or product (fly ash, GGBS and metakaolin) and agricultural wastes (rice husk ash, palm oil fuel ash, bagasse ash, palm kernel shell ash, corn cob ash). There have been considerable advances in the use of industrial SCMs on field as these materials are often readily available requiring little or no processing prior to use. In recent times, new streams of materials are being investigated for their potential as SCM and subsequent utilisation in cementitious systems

Also, some agricultural residues have potential use as pozzolanic SCMs especially in developing countries where agricultural wastes abound. In countries like Malaysia, Brazil and Thailand,

residues from palm oil husk, fibre and shell, sugarcane bagasse and rice husk are being used as fuel source in agro-allied sector or power plants (Chao-Lung, Anh-Tuan, & Chun-Tsun, 2011; Kroehong et al., 2011; Singh et al., 2000). As a result, the waste ashes can be readily obtained but may require further thermal treatment to obtain an amorphous material for use as partial cement replacement (Megat Johari et al., 2012). However, some other developing countries like Nigeria, is yet to fully harness such potentials despite the abundance and challenges of improper disposal of these wastes every farming season. The development and subsequent field utilization of agricultural based SCMs therefore require an assessment of the current state of research and field activities on these materials with respect to the extent, limitations and prospect of the current methods and specifications for standardization where necessary.

Even though, there are several studies on industrial SCMs properties and interaction with PC in concrete, it suffice to say the interdependence and interference on system hydration and performance is yet to be fully understood. Proper classification of SCMs, widening their scope of application and sources, and understanding their behaviour is crucial to their utilisation.

2.3.1 Material properties requirement for pozzolanic SCMs

ASTM C618 specify the classification requirements for fly ash (class F and C) and natural pozzolans (class N) based on chemical and physical characteristics. A combined oxide composition (SiO_2, Al_2O_3, Fe_2O_3) of 70% for class N and F; and 50% for class C is required. The maximum amount of particles allowed to be retained on a 45μm after wet sieving is 34% for all classes. The minimum compressive strength development allowed for the three classes of pozzolans is 75% of the control at 7 and 28-days. However, some SCMs may achieve this strength requirement at a later age than the specified age and as such may require additional requirement for qualification for use and/or for classification.

On the other hand, BS EN 197:1 specifies that the reactive silica content should be at least 25%, while it silica, alumina or iron oxide were identified as likely oxide constituents of pozzolans. The standard identifies and describe limits for individual pozzolans based on chemical composition, loss on ignition, soundness, compressive strength and/or surface area. Pozzolanic materials which can be used as main constituent of cement discussed in the standard are natural pozzolana (P), natural calcined pozzolana (Q), fly ashes (siliceous V, calcareous W) and silica fume (D).

A careful examination of both standards showed that the requirements may be extended to SCMs of agricultural origin for the purpose of identification and/or classification towards the understanding of their mechanism of reaction. It can also be inferred that the behaviour and/or influence of pozzolanic SCMs depend largely on their reactivity, there is a need to develop guidelines along this line for the use of pozzolans from agricultural wastes.

2.3.2 Characteristics of ashes from thermally treated crop residues

Type and properties of crop residues, type of thermal treatment method coupled with temperature range and duration of burning impact on ash transformation process, properties (physical, chemical and mineralogical) and hence reactivity (Boström et al., 2012; Cordeiro, Toledo Filho, & Fairbairn, 2009; Grimm, Skoglund, Boström, & Öhman, 2011; Vassilev, Vassileva, Song, Li, & Feng, 2017; Wang et al., 2012). The presence of alkalis and fusion of some chemical constituents (potassium, chloride, phosphorus, calcium and magnesium) with silicates at low temperature is typical, leading to slagging and/or melting of the ash (Boström et al., 2012; Wang et al., 2012). Also, the concentration of the oxide of potassium (Wang et al., 2012) and phosphorus (Boström et al., 2012) in relation to the silica was reported to affect ash properties variation with temperature. Importantly, for cementitious systems, is the need to consider the influence of the oxide composition, reactivity of ash and/or interaction with admixtures as these affect their performance as SCM. The reactivity and subsequent performance in cementitious systems is key to the adoption of this category of SCMs and should be known.

2.4 Influence of SCMs in cementitious systems

The influence of SCMs in cementitious matrices has been attributed to both microfiller effects and pozzolanic reactions each occurring at different stages of the hydration process due to intrinsic material properties. Gutteridge and Dalziel (1990a) often referenced in filler effect studies reported that SCMs (pulverised fly ash, slag and silica fume) have retarding effect on PC hydration within the first few hours after contact with water, and this is often consistent with prolonged setting times reported for some SCMs (Florian Deschner et al., 2012; Givi, Rashid, Aziz, & Salleh, 2010; Singh et al., 2000; Zhang & Islam, 2012). This retarding effect noticeable during the induction period is also associated with a lower main heat peak and lower rate of heat release (Figure 2.1). A comparison with PC-inert fillers (PC-IFs) pastes showed that PC-IF system often have shorter induction period and higher rate of heat release which further increases with increasing fineness

and quantity of the filler (Berodier & Scrivener, 2014; Dittrich, Neubauer, & Goetz-Neunhoeffer, 2014; Kumar et al., 2017). The noticeable differences in hydration behaviour (induction and main heat peak phases) may be associated with the reactivity characteristics of SCMs and IFs (i.e. degree of crystallinity or amorphousness). Crystalline inert fillers seems to have little or no interference with PC hydration and mechanisms controlling each phase evolution. For instance, quartz was reported to enhance the rate of reaction of clinker, a higher main peak and steeper acceleration slope (Berodier & Scrivener, 2014).

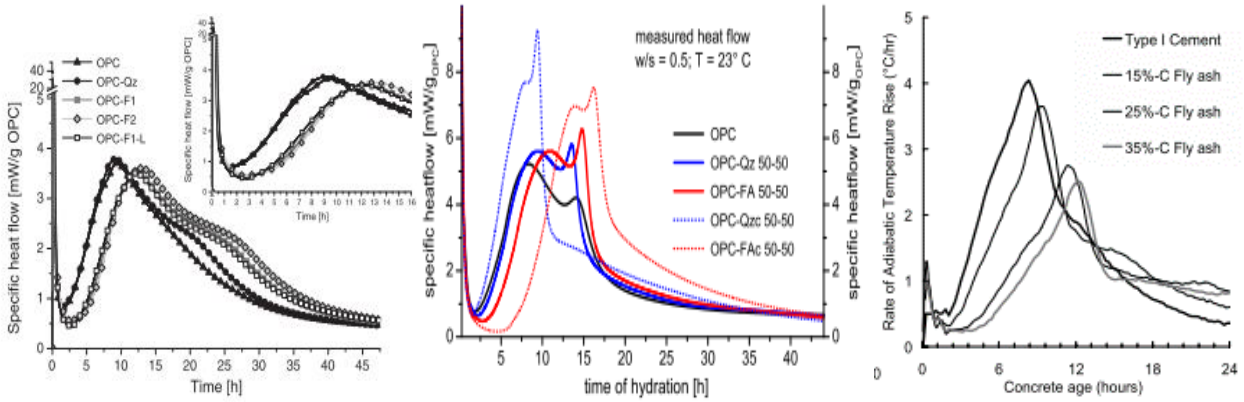

(a) (b) (c)

Figure 2.1: Heat of hydration (isothermal and semi-adiabatic calorimetry) of PC containing SCMs

(source: (Florian Deschner et al., 2012; Dittrich et al., 2014; Schindler & Folliard, 2005) for (a) (b) and (c) respectively

In another instance, the influence of silica fume was attributed to both water reduction and its reactivity (inherent effect), the inherent effect having both physical and chemical components (Goldman & Bentur, 1989). The physical effect described as a microfiller effect was linked to the shape and size of the particles. Further, prior to significant contribution to strength development, SCMs (silica fume, fly ash) were reported to have effect on hydration and strength of cementitious systems similar to micro-fillers (carbon black, rutile), and linked to the creation of more nucleation sites for C-S-H (Gutteridge & Dalziel, 1990a; Lothenbach et al., 2011).

Micro-filler effect is a physical influence due to densification of the microstructure and enhanced packing of hydration products (at later ages), grain refinement due to particle fineness and reduced bleeding at transition zone which enhances interfacial bonding in concrete, and as such has a direct

bearing on the compressive strength (Detwiler & Mehta, 1989; Goldman & Bentur, 1989). Furthermore, Berodier and Scrivener (2014) attributed the contribution to hydration reaction to the inter particle distance evident in increased shearing with reduced inter particle distance. However, there is a need to carefully examine the concept of the micro-filler effect with respect to age and material type given the various reported mechanisms and limitations of the various studies.

Also, pozzolanic SCMs are believed to undergo pozzolanic reaction which involves the reaction between the amorphous phase and the portlandite produced during the hydration of PC. With the availability of portlandite and significant glassy content, the extent and rate of formation of hydration products is further enhanced by the fineness and surface area of particles and likely disposition to CH (Lothenbach *et al*., 2011). This distinguishes SCMs from IFs especially the formation of additional C-S-H which may differ in properties to that of plain PC. The C-S-H produced by SCMs was reported to have a different calcium to silica (Ca/Si) ratio compared to plain PC which results from the active participation of the silica constituent of SCM in the reaction (Duchesne and Berube, 1995; Lothenbach *et al*., 2011). Detwiler and Mehta (1989) also noted that the pozzolanic effect of SCMs particularly silica fume is significant to the fracture toughness of the transition zone. Consequently, the interdependence and contribution of these processes to the performance of concrete structures remain the ultimate goal and of concern from engineering perspective. This further gives credence to the need to determine the glassy phase which actively participate in pozzolanic reaction and may aid the further understanding of the actual filler and pozzolanic effect of materials.

2.4.1 Filler effect of SCMs

The filler effect of SCMs is much reported in literature with some level of investigation to support it (Detwiler & Mehta, 1989; Goldman & Bentur, 1993; Isaia, Gastaldini, & Moraes, 2003). This effect is sometimes considered to be as important as the pozzolanic effects, even though, the initial use of SCMs in concrete was to reduce bleeding but found to improve some other properties aside reducing bleeding (Schlorholtz, 2006). Detwiler & Mehta (1989) noted that this effect is a fresh state effect in cementitious systems. Consequently, the reduction of bleeding leads to a reduction in pores filled by free water in the system and hence a close packing of particles than in plain PC system at the same w/b ratio. This impact on the strength and durability of the system but the effect of inert fillers can further be separated from that of SCMs over time. Some authors reported this

effect as continuous up to 28 days and sometimes beyond (Isaia et al., 2003), since the pozzolanic reaction of some SCMs occurs beyond the first 28 days. In concrete, lower w/b ratio is synonymous to increase in strength but not necessarily improved durability. It follows then that the actual filler effect of each SCM may vary with particle size and reactivity and this will determine the eventual behaviour and usability of new SCMs.

2.4.2 Perspectives on the filler effects of SCMS

The filler effect often attributed to SCMs has two contributory mechanism as noted by Goldman & Bentur (1993), the microfilling effect and modification of the microstructure of the transition zone. Detwiler & Mehta, (1989) attributed the 28 days compressive strength enhancement in cementitious systems to physical mechanisms resulting from better packing of hydration products, reduced bleeding and refinement of grain by the presence of fine particles (SCMs or inert fillers). Pozzolanic reaction was reported to influence the fracture toughness of the transition zone than compressive strength, while the microfilling effect is more pronounced in concrete than its corresponding paste. There is a synergy between the microfiller effect and the pozzolanic effect of pozzolanic SCMs as the formation and growth of hydration products further enhances the microstructure initially modified by the microfilling effect due to physical mechanism. A reason why quantitative analysis of this phase remains semi quantitative is that the formation of hydration products is at microscopic scale with a consequent macroscopic effect. Also, as hydration progresses, the volume of the system shrinks due to consumption of water during hydration process while the anhydrous binder material(s) and water may not be recoverable. It is not certain that the strength at 28 days can be attributed to physical mechanisms alone as there is a substantial chemical reaction which contribute to the properties attained at this age.

Furthermore, concrete containing SCMs or inert fillers exhibit composite property evident in higher compressive strength than the corresponding paste sample (Goldman & Bentur, 1989, 1993). The higher strength in concrete containing silica fume (SF) and carbon black at the same w/b was linked to improved bonding at the transition zone compared to plain PC concrete. The enhanced strength in concrete was attributed to the improved bonding between the aggregates and paste, reduced bleeding and hence porosity at their interface. The compressive strength was deconvoluted into several effects considered to influence it (Fig. 2.2). The same method of estimation was used by Isaia et al. (2003) which considered the filler effect up to and beyond 28

days. Pozzolanic effect was estimated as the difference between the total effect and filler (limestone) effect. The total effect was taken as the difference between the strength of the pozzolanic and plain PC concrete.

The microfiller effect as presented in this way contributes more to compressive strength than the pozzolanic effect and is overestimated as shown in Figure 2.2, given that at the same w/b ratio, plain PC concrete has lesser fine particles and more water-filled spaces compared to the other two systems. This further underestimate the pozzolanic effect of SCMs given the reduction in volume of hydration products compared to the anhydrous materials but with improvement in microstructure and especially, the transition zone and pore characteristics. Also, it is clear that the overall influence of using an inert filler or SCM with cement will vary, hence the application of the separation principle will depend on the reactivity of the microfiller and the value of compressive strength obtained for each mix considered. However, another question that comes to mind is whether the filler effect is actually at early ages below 28 days or is inclusive of ages beyond 28 days.

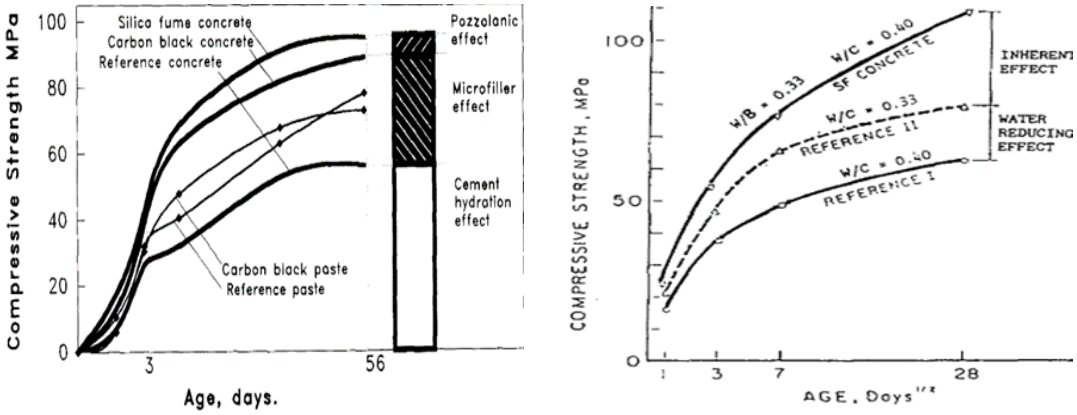

Figure 2.2: Comparison of the physical and chemical effects of different concrete matrices
(source: (Goldman & Bentur, 1993))

The filler effect of SCMs is further attributed to creation of more surfaces for heterogeneous nucleation of the hydration products with associated increase in the degree of hydration of PC (Lawrence et al., 2003; Lothenbach et al., 2011). This effect was also reported for IFs. The increase in the degree of hydration of PC and heterogeneous nucleation considered both SCMs and IFs as inert materials hence, a higher w/c ratio in both system due to more water available for PC reaction. Enhanced PC hydration based on cement chemistry is linked with the higher w/c ratio and

increased space for hydration products. The enhanced PC hydration is an early age effect which has a consequent impact on the later age properties of the system. It is associated with both SCM and IF, and could be regarded as a surface effect due to the creation of extra nucleation points for the hydration products of PC and the reduced interparticle space compared to plain PC system.

The interdependence and contribution of these processes to the performance of concrete structures remain the ultimate goal and of importance from engineering perspective. The reduced bleeding with the use of SCMs or IFs compared to plain PC system at the same w/b ratio reflects differences in the way the available water is accessible for hydration subject to the chemical activity level of water demanding materials. Also, interparticle spacing for systems containing either SCM or IF will be different from that in plain PC system at the same w/c ratio. Therefore, the mechanism responsible for each materials behaviour and performance will be different relative to the spacing between cement particles and surface activity of other fine materials included in the system.

2.5 Portland cement (PC) hydration: Process and products

The major oxides of PC studied as calcium silicates (tri and di calcium silicates) and calcium aluminates (tricalcium aluminate and tetra calcium aluminate ferrite) form the basis for understanding its hydration and interaction with SCMs and or inert fillers. The emphasis on the importance of the calcium silicates is their significant influence on strength development, shrinkage and microstructure of cementitious systems (Scrivener et al., 2016). At early stages of hydration, C-S-H formed is described as dimer of both 1.4-nm tobermorite and jennite with C/S ratio of 1.25 and 2.25 while the jennite formed at later stages has C/S ratio of about 1.8 and significant anions present. The porosity of portlandite produced forms the basis for the beneficial use of SCMs in cementitious systems to improve microstructure and engineering (strength and durability) properties. The morphology of the hydrating species viewed from a scanning electron microscope is shown in Figure 2.3.

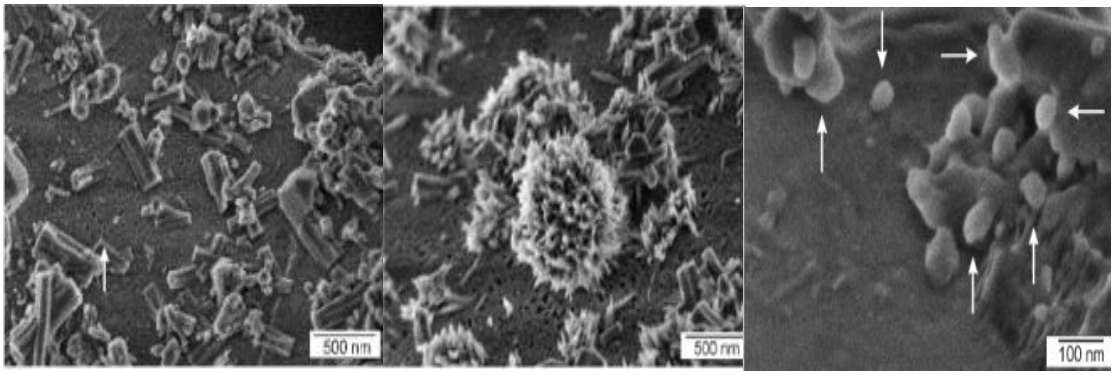

Figure 2.3: Morphology of hydrated aluminates (during induction period), silicates (end of induction period) and CH of plain PC paste observed in SEM.

Source: (Makar and Chan, 2008)

The hydration of the anhydrous calcium aluminates phase is believed to be more rapid and occurs at the initial stage of cement hydration resulting in the formation of ettringite (AFt) and monosulphate (AFm) phases (Odler & Abdul-Maula, 1984). Hydrating aluminate appears as prismatic formation when viewed under a scanning electron microscope (SEM), Figure 2.3. The stability and/or transformation of ettringite to hemi and monocarboaluminate in the presence of limestone fillers has been reported for plain PC and some SCMs (De Weerdt, Kjellsen, Sellevold, & Justnes, 2011; Kakali, Tsivilis, Aggeli, & Bati, 2000; D. Wang et al., 2018). This may imply their potential to enhance carbonation given favourable conditions in the system, this may be beneficial to some extent.

2.5.1 Evolution of water during the hydration of PC

The initial mix water in cementitious systems is transformed over time into physically and chemically bound water during the hydration of PC. Physically bound (evaporable) water consist of the capillary (free) water and the absorbed water in gel pores, and chemically combined (non-evaporable water) in form of hydroxyl is found in the interlayer of hydration products (Brouwers, 2011; Jennings, Thomas, Chen, & Rothstein, 2002). Estimation of the CH, physically bound and chemically bound water is often used to evaluate the degree of hydration of cementitious materials with time and to develop hydration models (Bhatty & Reid, 1985; Brouwers, 2011; Isaia et al., 2003; Lam et al., 2000; Pane & Hansen, 2005; Park et al., 2016; Poole et al., 2007; Zeng et al., 2012). Also, the measurement of the bound water has been used as a basis for the estimation of the chemical reactivity of SCMs (Avet, Snellings, Alujas, Ben, & Scrivener, 2016).

2.5.2 Estimation of the degree of hydration for cement pastes

Thermal analysis of hydrated cement paste has shown that dehydration, dehydroxylation of portlandite and decarbonation occur at temperature range 40–300°C, 400-500°C and 600-800°C respectively (Snellings et al., 2018). This has enabled the estimation of the degree of hydration, quantification of bound water and the assessment of the reactivity of SCMs. The estimation of the degree of hydration for cement pastes stems from different laboratory tests, the estimation from thermogravimetry is further discussed in the following paragraphs:

Bhatty and Reid (1985) used thermogravimetric analysis (TGA) and differential thermal analysis to follow the decomposition of cement pastes made from tailing cement and type I PC and identified three main temperature phases. The first phase was linked to dehydration reaction due to water loss by C-S-H and it occurs between 105 and 440°C. It was also noted that the phase could include dehydroxylation and some desorption as it is not well defined on the endotherm. The second phase identified was between 440 and 580°C due to mainly dehydroxylation of calcium hydroxide produced during the hydration of the calcium silicates in PC. The third phase was between 580 and 1000°C and was linked to the decarbonation of calcium carbonate which is as a result of exposing the paste to air.

The study gave the estimation of the chemically bound water (Wn) at a reference temperature of 105°C and at a given time as

$$W_n = (L_{dh} + L_{dx}) + 0.41L_{dc} \quad \text{.....2.1}$$

And the estimation of the free calcium hydroxide (W_{CH}) is given as

$$W_{CH} = 4.11L_{dx} + 1.68L_{dc} \quad \text{.....2.2}$$

And the degree of hydration as $\propto = \frac{W_n}{W_{n\infty}}$ 2.3

L_{dh} is the mass loss due to dehydration, L_{dx} is the mass loss due to dehydroxylation and L_{dc} mass loss due to decarbonation. $W_{n\infty}$ is taken as 0.21, while the correction factor 0.41 accounts for water loss equivalent to decarbonation of portlandite as a result of carbon dioxide and CH during hydration, and the factors 4.11 and 1.68 are correction factors which accounts for the formation of CH during hydroxylation and decarbonation respectively.

Pane & Hansen (2005) put into consideration the carbonation of the anhydrous material in the estimation of the chemically combined water at a reference temperature of 140°C, and used a $W_{n\infty}$ of 0.23 as a typical value for type 1 PC while the values for blended cements were obtained by extrapolation at the lowest possible temperature taken to be 0.5°C. The mass loss between 600-780°C for the anhydrous material was subtracted from that of the hydrated paste to give the mass loss due to decomposition of $CaCO_3$, the equation for the estimation of Wn is given as

$$W_n = L_{dh} + L_{dx} + (L_{dc} - L_{dca}) \quad \ldots\ldots\ldots\ldots\ldots\ldots 2.4$$

The L_{dca} in a way accounted for the decomposition of the unhydrated cement in the paste while the experiment was performed between 21-1100°C. A three parameter equation was used to estimate the ultimate chemically combine water thus

$$W_B = W_{B\infty}\, e^{(-\left(\frac{\tau}{t}\right)a)} \quad \ldots\ldots\ldots\ldots\ldots\ldots\ldots\ldots\ldots 2.5$$

Where τ and a are the intercept and curvature of the plot on logarithmic scale, and t the curing age

Monteagudo et al.(2014) factored in the carbonation of the anhydrous materials and the factor for carbonation of portlandite in the estimation of the chemically combined water. The estimated values of L_{dh}, L_{dx} and L_{dc} were obtained by taking the second derivative of the DTA curve for each sample investigated while the estimation of the ultimate chemically bound water was done with a modified Michaelis-Menten equation thus;

$$W_n = {W_{n\infty} + t}/{t + k} \quad \ldots\ldots\ldots\ldots\ldots\ldots\ldots\ldots\ldots 2.6$$

$W_{n\infty}$ and W_n are expressed in parts per unit, t is the curing time in hours and K is a constant. The chemically combined water was calculated from the equation;

$$W_n(\%) = L_{dh} + L_{dx} + 0.41(L_{dc} - L_{dca}) \quad \ldots\ldots\ldots\ldots 2.7$$

And the degree of hydration from the equation below with $W_{n\infty}$ taken as 0.24

$$\propto (\%) = \frac{W_n}{W_{n\infty}} \quad \ldots\ldots\ldots\ldots\ldots\ldots\ldots\ldots 2.8$$

Also, Deboucha et al. (2017) took 25-400°C as the dehydration phase, 400-600°C as the dehydroxylation phase and 600-800°C as decarbonation phase, 25-105°C as free water and 105-400°C as dehydration phase.

Generally, it was noted that the temperature range considered by the various authors is dependent on the Tga plot obtained in the individual studies which may have been affected by different factors. Lothenbach et al. (2016) identified the heating rate, kind of vessel, sample weight, sample pretreatment method as factors influencing the temperature of the main weight loss and hence position of the peaks. Also, the correction factors being considered and applied to the estimation of the bound water or degree of hydration will depend on the prevailing logical reasoning at the time of estimation.

Table 2.1: Temperature range for different phases of Tga experiment

Phase	**Temperature range of phase evolution (°C)**		
	Bhatty	**Pane et al**	**Monteagudo et al**
Dehydration	105-440	140-440	105-430
Dehydroxylation	440-580	440-520	430-530
Decarbonation	580-1000	520-1100	530-1100
Reference temperature	105	140	105

2.5.3 Heat of hydration evolution in cementitious system

The heat of hydration development in cementitious systems is an early-age property which commences as water is added to cement. The reaction of cement with water is exothermic and this enables the heat evolution to be measured using calorimetry. Calorimetry (isothermal, adiabatic or semi-adiabatic) study have enabled the breaking down of the complex hydration process into different distinct stages by monitoring the rate of heat released. Each of the stages are widely reported to be caused by different mechanisms, however, the most debated stage till date is the induction phase as mechanism responsible for it is yet to be fully unravelled. Pratt and Jennings (1981) noted that any mechanism explaining the induction phase must be sufficient to explain the subsequent heat rise while the effect of other contributory factors (like particle size, temperature and the use of admixture) should also be accounted for.

Furthermore, beyond the induction phase is the evolution of the acceleration or peak heat of hydration associated with the precipitation of the formed C-S-H. Also, a second peak on the curve associated with aluminate phase have also been reported (Rahhal & Talero, 2004, 2005) beyond which the rate of reaction reduces steadily till PC hydration is completed. However, the duration

of each stages of hydration can be influenced by the water/binder ratio, reaction condition, inherent reactivity and particle distribution of the C_3S studied (Gatner et al., 2002; Kumar et al., 2017). Aside the rate of reaction, of importance is the nature and type of products formed which have significant effect on the strength and durability performance of concrete and as such will impact the service life of concrete structures. Also, the reaction chemistry and kinetics is equally important to understand behaviour towards maximizing performance.

2.5.4 Understanding the hydration of Portland cement .

To understand the complex hydration reaction of PC, several authors (Bellmann, Sowoidnich, Ludwig, & Damidot, 2015; Bullard et al., 2015; Damidot & Nonat, 1994; Gartner & Jennings, 1987; Jennings & Pratt, 1979; Taylor, 1986) have tried to relate it to the hydration of alite (C_3S) which is the most abundant phase in anhydrous PC and believed to greatly influence the early age properties of cementitious systems. Gartner et al. (2002) noted that relating alite to PC is made possible by the similar mechanisms of reaction of C_3S with water in pure (C_3S) or impure form (alite in PC) despite differences in their hydration kinetics. A perceived benefit of understanding the mechanisms of cement hydration is that it may help understand the likely effect of some SCMs on hydration reaction (which may be complicated by the use of admixtures) in order to improve their performance and hence applicability. This is necessary as some of the SCMs from agricultural origin have shown wide variability in behaviour while they feature promising material characteristics in cementitious systems.

To date, the actual mechanism of C_3S (hence PC) hydration is yet to be fully understood most especially the slow reaction preceded and succeeded by increase in rate of reaction observed for few hours after cement comes in contact with water. Several studies have focused on investigating the pre-induction and induction stages using pure C_3S (or laboratory prepared C_3S) in dilute forms or investigating the structure of the C_3S formed at different stages of the hydration as a step forward in understanding the hydration kinetics and hence the mechanism(s) responsible (Bellmann, Sowoidnich, Ludwig, & Damidot, 2012; Damidot & Nonat, 1994; Damidot et al., 1995; Gartner & Jennings 1987; Jansen, Neubauer, Goetz-Neunhoeffer, Haerzschel, & Hergeth, 2012; Juilland, Gallucci, Flatt, & Scrivener, 2010; Juilland P, 2015; Rodger, Groves, Clayden, & Dobson, 1988; Taylor, 1986). This have resulted in some propositions/theories put forward to explain the existence of induction period, however, the extent to which these theories have been able to justify

the existence of the phase and their acceptability as viable theory is yet another question for consideration.

2.5.5 Hypotheses explaining the induction phase of Portland cement hydration

A consideration of thermodynamics and kinetics of reaction supposed that the addition of water to either C_3S or PC should result in increase in reaction rate due to the dissolution of C_3S and subsequent formation of C-S-H, however, the noticeable induction period negates this stance (Frank Bellmann, Damidot, Möser, & Skibsted, 2010). To explain this contrast, some notable propositions were put forward to explain the likely mechanism responsible for the slow reaction rate of the induction period and subsequent increase in the reaction rate after this period. These propositions were based on experimental data, thermodynamic relationships and/or kinetics of hydration behaviour, with experimental results used to further substantiate other evidences. The most prominent views are discussed further.

2.5.6 Theory of protective layer

Proponents of the theory of protective layer believed that the formation of a layer of hydration product inferior to the actual hydration product (C-S-H) is responsible for the induction period. In the opinion of Jennings and Pratt (1979), the evidences presented by the images obtained through transmission electron microscopy (TEM) showed convincingly the existence of a membrane (protective layer) being responsible for the slow rate of reaction during the induction period; the presence of aluminium (Al) likely enhancing the stability of the layer. The study further attributed the termination of the induction period to the removal of the Al by its likely reaction with OH and hence the disintegration of the layer overtime. Consequently, the study suggested further characterisation of the membrane in a bit to determine the conditions that may be responsible for its formation.

In a bit to identify the structure of the early product of alite hydration, Taylor (1986) hypothesized that the product is probably a mix of both dimeric tobermorite-type and jennite-type C-S-H, while the later product of hydration is likened to jennite-type comprising larger pentameric anions. In a similar vein, Gartner and Jennings (1987) also attributed the existence of the induction period to the formation of a protective kind of metastable C-S-H which undergoes a solid state transformation resulting in the termination of this hydration phase. Subsequently, the protective layer is said to have monomeric structure which distinguishes it in structure from the C-S-H formed

beyond the induction phase. This premise was further substantiated with NMR results from the study of Rodger et al. (1988) which also linked the early product to monomeric silicates contained in C-S-H. However, the study was not specific as to the actual location of the formed product, but further noted that by the end of the induction period only about 2% of the C_3S has hydrated. Similarly, Damidot and Nonat (1994) reported that the C-S-H formed during and after the induction period differs with respect to nucleation rate and the protective layer formed around the C_3S grain but that a structural distinction is still required to prove Taylor's (1986) hypotheses. Gartner et al. (2002) concluded that the protective layer formed is a kind of C-S-H different from the main C-S-H resulting from the hydration process.

However, a reason this theory is not totally accepted by some is the fact that the amount of soluble silicate observed during this period is very small and as such not easy to quantify (Pratt and Jennings, 1981; Rodger *et al.*, 1988; Damidot and Nonat, 1994). Also, evidences supporting it have inferred from the kinetics of diluted rather than concentrated solutions (Damidot & Nonat, 1994; Damidot & Nonat, 1994; Jennings & Pratt, 1979) and thermodynamic relationship (Gartner and Jennings, 1987). Gartner and Jennings (1987) further noted that direct experimental measurement to explain the actual composition of the so-formed C-S-H backed by thermodynamic relations is yet to be done, while Juilland et al. (2010) opined that experimental observation of this layer is somewhat impossible.

However, to disprove this, direct experimental investigation was done by Garrault et al. (2005) using SEM and AFM with evidence of C-S-H nuclei growth covering the C_3S grains surface while the study further linked the growth of C-S-H to lime concentration. Also, Bellmann et al. (2010) used ^{29}Si magic angle spinning nuclear magnetic resonance with ^{1}H cross polarisation to substantiate the existence of an intermediate phase containing uncondensed silicate monomers different from both alite and C-S-H hydrates. This phase was reported to be distinct from the hydroxylation of C_3S surface. Bellmann et al. (2012) further upheld the formation of the intermediate phase as a layer of about 2nm covering the entire C_3S surface using X-ray photoelectron spectroscopy while it further noted that the nucleation and growth of C-S-H is responsible for the kinetics of the reaction of the induction period.

2.5.7 Dissolution theory

Some critics of the protective layer theory have in recent times attributed the existence of the induction period to dissolution theory which is rooted in geochemistry theory of crystal dissolution (Juilland et al., 2010). The theory explains dissolution of minerals as involving three phases defined by two activation energies and related to the undersaturation of the solution. The phases relate to the formation of 2D vacancy islands, the formation of etch pits at dislocations and step retreat at pre-existing surface roughness (Lasaga & Luttge, 2001). The first activation energy correspond to the free energy barrier required for 2D pits nucleation on grain surface, $\Delta G^{n}_{crit.}$ The second is the free energy barrier at point where the first energy no longer controls etch pit formation indicating that pit formation at this point is due to intersection between dislocations and the surface. The application of the theory to induction period upheld that the slow reaction is due to the low dissolution rate resulting from undersaturation of the solution with respect to alite while the onset of the induction period was probably linked to critical dissolution level of alite in the solution. However, the study was probably able to explain the beginning of induction period while end of the period and onset of accelerated hydration is yet to be accounted for.

Contrary to this, Gartner (2011) pointed out the high critical undersaturation from Juilland et al. (2010) as differing to the undersaturation recorded in geochemical experiments used to validate the theory of dissolution. In response to Gartner (2011), Juilland et al. (2011) further affirmed the application of the dissolution theory to alite hydration especially the induction period. Furthermore, Makar et al. (2011) noted that the formation of pits on alite surface reported in (Makar, *et al.,* 2007; Makar and Chan, 2008) occurs at the end of the induction period and not at the onset as reported by (Juilland et al., 2010). Makar et al. (2011) further argued against pit formation at dislocation noting that the sides and not bottom of the pits are more susceptible to dissolution. The study also noted that existing evidence implies the existence of some form of protective barrier which probably hinders dissolution and formation of C-S-H, but suggested further investigation to substantiate both theories.

Bullard and Flatt (2010), however noted that existing data on hydration of alite can be so explained by both the theories of site deactivation (dissolution and protonation of surface) and the protective layer (passivating layer) using simulation model, while the inhibition of CH precipitation have different effect on both theories. Scrivener et al. (2015) on the other hand, upheld the dissolution

theory rather than protective layer formation as responsible for the induction period and that the main heat peak is not due to diffusion control.

It is worth noting from several interpretation of calorimetry data especially the rate of heat release on addition of water to PC and at the end of induction period, that there is a rise in the rate of heat released. This is often associated with silicate species reaction with either same or different products reported, but aluminate reaction will have commenced with consumption of gypsum up to the end of the induction period. The deceleration slope leading to induction period and after the main heat peak have also been associated with aluminate species reaction. Then, the mechanism controlling the induction and main hydration phase should be able to relate with both species, their interaction and interference and likely impact of hydrating system pH. Given the debates on the induction phase of PC hydration, the understanding of the kinetics and/or mechanisms of reaction of supplementary cementitious materials with PC especially during the induction phase may pose a challenge since these materials often vary in materials characteristics and depend on the alkalinity of the system

2.6 Drying shrinkage

Drying shrinkage is the volume change due to moisture loss from hardened concrete to the environment which is not load or temperature induced (Beushausen et al., 2021). Drying shrinkage is time-dependent and it is the linear component (one-dimensional) that is often considered important and it is not independent of the initial water content and the relative humidity of the environment. During the early age of hydration, free water in the capillary pores that have not reacted moves to the surface and moisture is lost to the environment, and as drying continues it results in micro-cracks when the induced stress exceeds the tensile strength of the concrete (Mokarem, Weyers, & Lane, 2005).

2.6.1 Mechanisms of drying shrinkage

According to Li (2011), three mechanisms are responsible for the drying shrinkage of Portland cement concrete; the first is the disjoining pressure which is a differential pressure associated with the water adsorbed on the surface of C-S-H and it is dependent on relative humidity. This pressure is of importance when the relative humidity exceeds 75% and it is of no effect when the relative humidity is below 45%. When relative humidity is above 50%, there is an increase in the thickness

of the interlayer water between overlapping C-S-H layer (Tran et al., 2021). Disjoining pressure tends to separate the C-S-H layer by overcoming the van der Waals forces of attraction resulting from increasing adsorption of water on the C-S-H surface at hindered adsorption region at a given relative humidity (Di Bella, Wyrzykowski, & Lura, 2017). At high relative humidity, disjoining pressure causes a swelling as the C-S-H layers tends to pull apart while at low humidity, the converse is the case. At low humidity, below 50%, there is desorption of water from the hindered adsorption region, there is a reduction in the van der Waals forces which tends to draw the C-S-H layers together leading to shrinkage. The mechanism of disjoining pressure as proposed by Powers was to explain the continuous shrinkage at relative humidity below 40% (Idiart, 2009). However, Beltzung and Wittmann (2005) opined that hygral expansion above 50% relative humidity is significantly influenced by disjoining pressure as capillary meniscus cannot be formed by pore solution at a nano-scale. This brings to the fore the influence of pore size and their distribution on drying shrinkage mechanism which is further influenced by the internal relative humidity of the system.

The second mechanism is the capillary surface tension which develops in capillary pores and is hydration dependent. The volume of air increases with hydration progress leading to an increase in the meniscus between the air and water in a capillary pore thereby inducing capillary stress. Bentz (2005) suggest that a significant part of shrinkage occurring during drying is influenced by capillary pressure formed in partially filled water pores. As drying progresses, internal relative humidity decreases while capillary tension developed in the pore water inducing capillary tensile stresses which tends to compress the solid skeleton thereby resulting in deformation of mortar or concrete. This effect can be explained by the Kelvin equation given in equation 2.9 and the Laplace equation given in equation 2.10

$$\ln(RH) = -\frac{2\sigma}{r}\frac{M}{vRT}\cos\theta \quad \ldots\ldots\ldots\ldots\ldots\ldots 2.9$$

$$P_c - P_v = \frac{2\sigma}{r}\cos\theta \quad \ldots\ldots\ldots\ldots\ldots\ldots\ldots\ldots 2.10$$

RH is the relative humidity, σ the surface tension of water in contact with air, M the mass of a mole of water, θ the contact angle of water and solid, r the radius of pore, v the density of water, R the ideal gas constant, T the temperature in Kelvin, pc is the capillary pressure of water in a pore and pv is the vapour pressure.

However, a major limitation of this mechanism in explaining the drying shrinkage behaviour of cementitious systems is that it cannot adequately account for the shrinkage occurring below 50% going by the Kelvin equation as the maximum hydrostatic stress is attained at relative humidity of 40%-50% (Idiart, 2009).

Surface free energy is another mechanism put forward to explain the shrinkage and swelling of cementitious systems below relative humidity of 40% through the adsorption and desorption of water film on C-S-H outer layer (Di Bella et al., 2017). As drying progresses, the adsorbed water layer on C-S-H surface is desorbed leading to an increase in the contact between the gel layers which increases the surface tension between the interlayer water inducing a compressive stress on the gel layers and thus a deformation (Tran et al., 2021). This mechanism is significantly influenced by the moisture content and particularly the adsorbed water layers on the C-S-H gel (Idiart, 2009).

It is worth noting that these mechanisms hardly exist in isolation as they influence the drying shrinkage of cementitious systems while their influence is significantly affected by the internal relative humidity as well as the relative humidity of the exposure environment.

2.6.2 Factors influencing drying shrinkage

Most factors that influence drying shrinkage of cementitious systems pertains to their effect on the paste which is said to be the source of shrinkage (Beushausen et al., 2021). The relative humidity of the exposure environment as well as the initial water content of cementitious systems greatly affect the rate and magnitude of drying shrinkage (Zongjin Li, 2011). It is believed that the initial difference in the relative humidity of the environment and the internal relative humidity of the sample influence to a greater extent the rate of drying shrinkage at early ages of drying. At early ages, the net loss to the environment is higher as the capillary moisture is reducing as drying proceeds. At this stage, the microstructure is just developing and as such the shrinkage is controlled by loss of capillary moisture.

Water to cement ratio affects the shrinkage of concrete, with higher w/c ratio tending to exhibit higher shrinkage strain most especially at later ages although in terms of the magnitude of scale, the shrinkage strain of higher or lower w/c ratio is not so different (Beushausen et al 2021). It is also believed that the effect of drying shrinkage can be significant when the water to cement ratio is above 0.4 (Tran et al., 2021), this is further shown in Figure 2.4. The effect of w/c ratio on drying

shrinkage is considered alongside the degree of hydration both of which influence the microstructure of cementitious systems especially the porosity (Juenger & Jennings, 2002). It is reported that alkali oxides contribute to hygral shrinkage by influencing the composition of the pore solution (Beltzung & Wittmann, 2005). The mechanism of influence of alkali oxides on drying shrinkage is related to the concentration of alkali in pore solution and the influence on the solubility of portlandite (Beltzung & Wittmann, 2005). The addition of SCMs and the exposure condition of samples have also been reported to influence drying shrinkage. Alexander (1994) found that the addition of blastfurnace slag results in a small increase in shrinkage at early ages while the effect was reversed at later ages for samples that were exposed but for sealed samples, shrinkage strains were significantly reduced. The reduced shrinkage strain at later ages can be linked to cement paste stability effected by the hydration reaction of slag which over time contributes to the formation of C-S-H and hence reduced deformation. The use of fly ash has a minor effect on the shrinkage of concrete with shrinkage similar to plain PC concrete for a range of fly ash content u to 30% (Beushausen et al., 2021). Similar to slag, the effect of fly ash on shrinkage is attributed to the pozzolanic reaction contributing to the formation of additional C-S-H, which enhanced the stability of the system to deformation. The reactivity of SCMs is considered essential to the exhibited influence on the property of cementitious systems given that the inclusion of SCMs is a dilution strategy resulting in the reduction of the quantity of plain PC which is essentially the main binder phase.

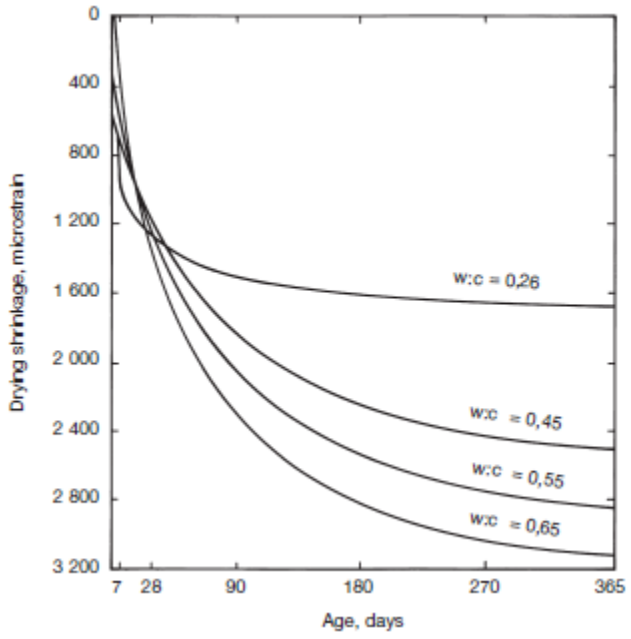

Figure 2.4: Effect of water to cement ratio on the shrinkage of cement pastes

(Source: Beushausen et al. 2021)

2.6.3 Requirements of ASTM versus SANS on drying shrinkage experiment

ASTM C 157/ C157M-04 specifies the standard test method for determining the length change in hardened hydraulic-cement mortar and concrete. If mortar sample is to be tested, the standard specified a prism of 25 mm cross section by 285 mm long while for concrete sample, the prism is to be 100 mm cross section for aggregates size passing the 50 mm sieve and 75mm cross section for aggregates passing the 25 mm sieve. The standard requires the samples to be cured in lime saturated water for 28 days prior to the commencement of the test in either water or air. This extent of curing will allow the hydration of the system to certain extent but is different to what is obtainable on field. To be representative of field practice the curing period may need to be shortened to allow the early age shrinkage determination. Another argument with respect to systems containing pozzolanic materials is the fact that pozzolanic reaction takes place beyond the first 28 days of curing. The 28 days of curing will have allowed significant degree of hydration reaction of plain PC which is required to facilitate pozzolanic reaction and the study of the shrinkage behaviour under standard laboratory condition. However, it is necessary that laboratory experiments be representative of actual service conditions as much as possible as this enhances the application of laboratory findings to actual practice.

The South African standard SANS 6254:2006 specifies the procedure for carrying out initial drying shrinkage and wetting expansion of mortar. The standard specifies the use of sample of nominal size 280 mm x 50 mm x 50 mm which is larger in cross section than the specification of the ASTM. It is likely that the differences in size may have some effect on the measured drying shrinkage however, this may not be quite significant as there are other factors which influences drying shrinkage related to composition of the matrix and exposure condition. The standard further recommends water curing the samples after demoulding for a period of 6 days at a temperature of between 22°C and 25°C. This would allow some degree of hydration in the samples prior to testing. The test samples are placed in a vented cabinet or drying oven operating at a temperature of between 50°C and 55°C for 7 days after which the measurement is taken. The samples are returned to the oven or drying facility and every subsequent 48 hours measurement is taken until the difference between two successive readings do not exceed 5 μm. It is noted that this method allows

an accelerated drying of the specimens which may interfere with the continuous hydration reaction of plain PC and may not be reflective of actual drying conditions in service. Nonetheless, the method can be seen as an accelerated approach to measuring the drying shrinkage of samples and may have the advantage of shortening the measurement time required provided that the required difference between successive readings can be attained in a short period of time.

2.6.4 Shrinkage prediction models

A good number of the existing shrinkage prediction models are equations that have been developed for use in the design of structures. It is noted that most of the models incorporates the time dependency of shrinkage. The American concrete Institute model (ACI 209) for prediction of drying shrinkage in concrete for moist cured samples is presented in equation 2.11 and for steam cured samples is presented in equation 2.12.

$$\varepsilon_{sh}\left(t, t_{sh,0}\right) = \frac{(t-t_{sh,0})}{35+(t-t_{sh,0})}\varepsilon_{sh\infty} \quad \text{.....2.11}$$

$$\varepsilon_{sh}\left(t, t_{sh,0}\right) = \frac{(t-t_{sh,0})}{55+(t-t_{sh,0})}\varepsilon_{sh\infty} \quad \text{.....2.12}$$

$\varepsilon_{sh}\left(t, t_{sh,0}\right)$ is the shrinkage strain in in/in; t is time in days; $t_{sh,0}$ is the time at the start of the drying in days; $\varepsilon_{sh\infty}$ is the ultimate shrinkage strain in in/in.

The model presents the prediction of shrinkage strain as a time-dependent function requiring the ultimate shrinkage to be known. The model was shown by Mokarem et al. (2005) to be unsuitable to predict the drying shrinkage of mixtures containing slag and fly ash while it is suitable for mixture containing microsilica. Also, Mushtaq, Siddique, Goyal, & Kaur (2021) reported that the method is suitable for control mix up to 56 days of drying beyond which it gives higher shrinkage values while it was unsuitable for the prediction of the drying shrinkage of concrete containing waste foundry sand. Gardner (2004) suggested that the absence of size effect in the time term is the reason why the model is inaccurate as the model overestimates at early ages and underestimates at later ages. It can be inferred that the model is suitable to conventional concrete and may not correctly predict the drying shrinkage of concrete containing SCMs or other unconventional materials.

Mushtaq et al. (2021) proposed a modification of the ACI model based on empirical data to include the effect of drying times and percentage waste foundry sand. The model presented is said to be able to predict the drying shrinkage of concrete at any time and is presented in equation 2.13 thus

$$\varepsilon_{sht} = \frac{671.5t}{17+t} + 1.92p - 76.11 \ldots\ldots\ldots\ldots\ldots\ldots 2.13$$

Where ε_{sht} is the shrinkage at any time t, t is the time in days at which the shrinkage is calculated, p is the percentage content of waste foundry sand used in the experiment.

The model was based on multiple regression relationship and was found to correlate well with the experimental results. However, the adaptability of the model to other experimental data outside the study has not been established.

Another model is the RILEM B3 model based on the work of Bazant and co-researchers. The model is rather complex and noted by Beushausen et al. (2021) the model is recommended for structures that are sensitive to deflection. The model put into consideration the effects of water to cement ratio, cement type, cement content and aggregate to cement ratio and it is presented in equation 2.14. The model also accounts for the effect of relative humidity on drying shrinkage

$$\varepsilon_{sh}(t, t_0) = -\varepsilon_{sh\infty} k_h S(t) \ldots\ldots\ldots\ldots\ldots\ldots\ldots\ldots\ldots\ldots\ldots\ldots 2.14$$

Where $\varepsilon_{sh\infty}$ is given as

$$\varepsilon_{sh\infty} = -\propto_1 \propto_2 (26(w^{2.1})(fc^{-0.28} + 270)10^{-6} \ldots\ldots\ldots\ldots\ldots 2.15$$

$$k_h = 1 - h^3 \ldots\ldots\ldots\ldots\ldots\ldots\ldots\ldots\ldots\ldots\ldots\ldots\ldots\ldots\ldots\ldots\ldots 2.16$$

$$S(t) = \tan h \sqrt{\frac{t-t_0}{T_{sh}}} \ldots\ldots\ldots\ldots\ldots\ldots\ldots\ldots\ldots\ldots\ldots\ldots\ldots\ldots\ldots 2.17$$

The terms in the equations are as defined, $\varepsilon_{sh}(t, t_0)$ is the shrinkage strain in in/in, $\varepsilon_{sh\infty}$ is the ultimate shrinkage strain in in/in, $\propto_1 and \propto_2 = 1.0$, w is the water content in the concrete mix in lb/ft^3, k_h is the shape factor of the cross section, h is the relative humidity in %, t is the age of concrete in days, t_0 is the age of concrete at beginning of shrinkage and s(t) is the time function for shrinkage.

The Euro- International concrete committee- CEB 90 code model put into consideration the effect of concrete compressive strength and relative humidity in the prediction of drying shrinkage. The drying shrinkage is obtained from a relative humidity chart. The challenge with the model is the

practicality of using the chart for data obtained outside the environment for which the chart was derived as this will have introduced some level of variability and uncertainties in the estimation process. The equations are presented below

$$\varepsilon_{cso} = \varepsilon_s(f_{cm})\beta_{RH} \quad \text{.....2.18}$$

$$\varepsilon_s(f_{cm}) = (160 + 10\beta_{sc}\left(9 - \frac{f_{cm}}{1450}\right))10^{-6} \text{.....2.19}$$

$$\beta_{RH} = -1.55\beta_{ARH} \text{.....2.20}$$

$$\beta_{ARH} = 1 - (\frac{RH}{100})^3 \text{.....2.21}$$

ε_{cso} is the drying shrinkage of Portland cement concrete in in/in, ε_s is the drying shrinkage obtained from relative humidity chart, β_{sc} is a coefficient which depends on the type of cement, β_{RH} is the coefficient for relative humidity and f_{cm} is the average 28-day compressive strength in psi .

Gardner and Zhao (1993) developed a model that attempts to overcome the drawback of the ACI 209-82 and the CEB model code by using an empirical ultimate shrinkage rather than a hypothetical shrinkage used in the two previous models. The model was developed for normal strength concrete structures for the estimation of the total deformation in the design of structures. The model attempted to calculate the shrinkage at any time from the shrinkage of concrete at 40% relative humidity, and correcting for the effect of age of loading, duration of loading, strength of concrete, member size and relative humidity. The model also make provision for the application of the model to concrete containing SCMs by adjusting the value of K using the strength data available from such concrete. The equation for the estimation of drying shrinkage is presented in equation 2.22 while the correction for the effect of relative humidity is given in equation 2.23. Equation 2.23 holds for h value less than 0.99 and it is given as -0.20 for h value of 1.0 while swelling occurs when the concrete is not stressed. The correction for time effect and member size effect is given by equation 2.25. The correction for relative humidity indicates zero volume change and zero shrinkage at relative humidity of 99%.

$$\varepsilon_{sh} = \varepsilon_{shu}\beta(h)\beta(t) \text{.....2.22}$$

$$\beta(h) = 1 - h^4 \text{.....2.23}$$

$$\varepsilon_{shu} = 900K\left(\frac{f_{cm28}}{f_{cmtc}}\right)^{0.5} \times \left(\frac{25}{f_{cm28}}\right)\text{^}0.5 \times 10^{-6} \quad \text{.....2.24}$$

$$\beta(t) = \left[\frac{7.27+\ln(t-t_c)}{17.18}\right] \times \left(\frac{t-t_c}{t-t_c+0.0125(V/S)^2}\right)\text{^}2 \times 10^{-6} \text{.....2.25}$$

The Gardner and Lockman (2001) model estimated the shrinkage at any time t, from the ultimate shrinkage rather than using an empirical value as done by Gardner & Zhao (1993). The model builds on the model of (Gardner & Zhao, 1993) and also accounts for the effects of relative humidity and time on shrinkage. Equation 2.22 is used to estimate the shrinkage at any time while the correction factor for the effect of time and relative humidity were modified as follows

$$\varepsilon_{shu} = 1000K\left(\frac{30}{f_{cm28}}\right)^{0.5} \times 10^{-6} \text{.....2.26}$$

$$\beta(h) = (1 - 1.18h^4) \text{.....2.27}$$

$$\beta(t) = \left(\frac{t-t_c}{t-t_c+0.15(V/S)^2}\right)^{0.5} \quad \text{... ... ...}\text{.....2.28}$$

ε_{sh} is the shrinkage strain, ε_{shu} is the ultimate shrinkage strain, $\beta(h)$ is a correction factor for the effect of relative humidity on shrinkage, $\beta(t)$ is a correction factor for the effect of time on shrinkage, h is the relative humidity expressed as a decimal, t_c is the age at which drying started in days, t is age of concrete in days, f_{cm28} is the average compressive strength of concrete at 28 days in MPa and V/S is the volume to surface area ratio in mm. The K value is taken as 1 for type I cement, 0.70 for type 2 cement and 1.15 for type 3 cement.

The EN 1992-1-1:2004 shrinkage prediction model accounts for the effect of relative humidity, compressive strength and cement type on drying shrinkage. The model predicts shrinkage development as a function of time, concrete cross section and nominal unrestrained drying shrinkage. The unrestrained drying shrinkage is obtained from

$$\varepsilon_{cd,0} = 0.85\left[(220 + 110.\propto_{ds1}).exp\left(-\propto_{ds2}.\ \frac{f_{cm}}{f_{cmo}}\right)\right].10^{-6}.\beta_{RH} \text{.....2.29}$$

$$\beta_{RH} = 1.55\left[1 - \left(\frac{RH}{RH_0}\right)^3\right] \text{.....2.30}$$

The development of the drying shrinkage strain in time is obtained from

$$\varepsilon_{cd}(t) = \beta_{ds}(t, t_s).k_h.\varepsilon_{cd,0} \quad \text{.....2.31}$$

$$\beta_{ds}(t,t_s) = \frac{(t-t_s)}{(t-t_s)+0.04\sqrt{h_0^3}} \quad \text{.....2.32}$$

The final value of drying shrinkage can be obtained from

$$\varepsilon_{cd,\infty} = k_h . \varepsilon_{cd,0} \quad \text{.....2.33}$$

Where:

f_{cm} is the mean compressive strength (MPa); f_{cmo} = 10 MPa

$\propto_{ds1}$ is a coefficient depending on the type of cement; 3 for class S, 4 for class N and 6 for class R; $\propto_{ds2}$ is a coefficient depending on the type of cement; 0.13 for class S, 0.12 for class N and 0.11 for class R; RH is the ambient relative humidity (%) and RH_O is 100%; k_h is a coefficient that depends on the notional size h_o of the cross section given by $\frac{2A_c}{U}$; Ac is concrete cross-sectional area and U is the perimeter of the part of cross section exposed to drying; t is the age of concrete at the time of consideration, in days; t_s is the age of concrete (in days) at the start of drying shrinkage which is normally at the end of curing

The WITS model (Gaylard, Ballim, & Fatti, 2013): the model was developed from statistical analysis of 30 years shrinkage data in South Africa. The variables considered in the development of the model include cement type and content, water content, sand and stone type, stone content, aggregate to binder mass ratio, specimen volume to surface area ratio and temperature. The mean shrinkage strain in a cross section is estimated from

$$\varepsilon_{sh}(t-t_o) = \alpha\left(1-e^{-\beta(t-t_o)}\right)\gamma \quad \text{.....2.34}$$

$\varepsilon_{sh}(t-t_o)$ is the mean shrinkage strain in the cross section in microstrain at drying time t-t_o in days, t is the age of the concrete, t_o is the age at first drying in days, α is the ultimate shrinkage, β is the rate of shrinkage development with time and γ is the growth curve shape parameter.

2.7 Compressive strength of hardened concrete

Compressive strength of concrete is a time-dependent function which measures the load carrying capacity of the material. Till date compressive strength remains an important performance criteria for concrete structures. The compressive strength of concrete is quite often determined in the laboratory with cubes or cylinder specimen using three replicates of each mix to be tested. The acceptance criterion of the test is that the range of strength for the three test samples should not be

more than 15% of the mean strength (SANS 5863:2006). Compressive strength is calculated from the expression given in equation 2.35, where f_{cc} is the compressive strength in MPa, F is the maximum load at failure, and A_c is the cross sectional area of the specimen in contact with the load

$$f_{cc} = \frac{F}{A_c} \quad \text{.....2.35}$$

Materials related factors that influence the strength of concrete are the microstructure of concrete, age of concrete, type and nature of aggregate, the strength of the aggregate-paste interface, type and amount of binder, water to cement ratio (Boshoff et al. 2021). Other factors related to the testing procedure are specimen curing temperature, loading rate, height to width ratio of the specimen, shape and size of specimen. The standard loading rate specified by the ASTM for cylinder samples is 0.15-0.34 MPa/sec and for cube samples the BSI specifies 0.2-0.4 MPa/sec (Zongjin Li, 2011). SANS 5863:2006 specifies a loading rate of 0.3 ± 0.1 MPa/s for cube samples.

2.8 Transport properties of concrete

The durability of concrete is hinged on two factors which are the concrete system and the aggressiveness of the exposure environment (Beushausen et al., 2021). The transportation properties of concrete system relates to the penetrability of the pores and the interconnectivity of the pores present in cementitious systems by aggressive fluids. The properties of the hardened cement paste and the interfacial transition zone contributes significantly to the transport properties of concrete. The transport properties of concrete is controlled by different mechanisms of capillary action, flow under pressure and flow under a concentration gradient (Beushausen et al., 2021). The flow of fluid through a porous material under the influence of capillary action is controlled by absorption while sorptivity relates to the rate of such flow controlled by the larger capillaries and the interconnectivity of the capillaries. Permeation is the flow of fluids through the pore structure of concrete under externally applied pressure. Permeability of concrete is affected by the microstructure of concrete, characteristics of the permeating fluid and the moisture condition of the material (Beushausen et al., 2021). Diffusion is the movement of fluid or ion through a porous material under the influence of concentration gradient. It is an important transport mechanism in structures exposed to salts ingress.

The transport of fluids or ions through concrete is often influenced by the age of the concrete. Hydration of cement in concrete is a continuous process and it affects the microstructure, and as concrete ages, deterioration sets in and with the ingress of aggressive fluids, the microstructure of concrete changes thus influencing the service life of structures (Beushausen et al., 2021; Zongjin Li, 2011). The quality of the cover concrete plays a significant role in the transportation of aggressive fluids through concrete and it is the basis of most laboratory based durability tests.

2.8.1 Oxygen Permeability Index test (OPI)

The oxygen permeability test assesses the flow of oxygen through the concrete cover under the influence of applied pressure. The test measures the drop in pressure as oxygen passes through a 30 mm thick concrete disc. The sample preparation and test procedure is given by SANS 3001-CO1-1 and 2 of 2015 respectively. The schematic for the experimental set-up for the test is presented in Figure 2.5. The significance of the test lies in being used to assess the resistance of concrete to the ingress of aggressive gas, in this case carbondioxide. As noted in Fultons (2021), the test is sensitive to macro voids and cracks which can aid the permeation of the permeating gas and can be used as an indication of the state of compaction, presence of bleed voids and path and the interconnectivity of the pore structure.

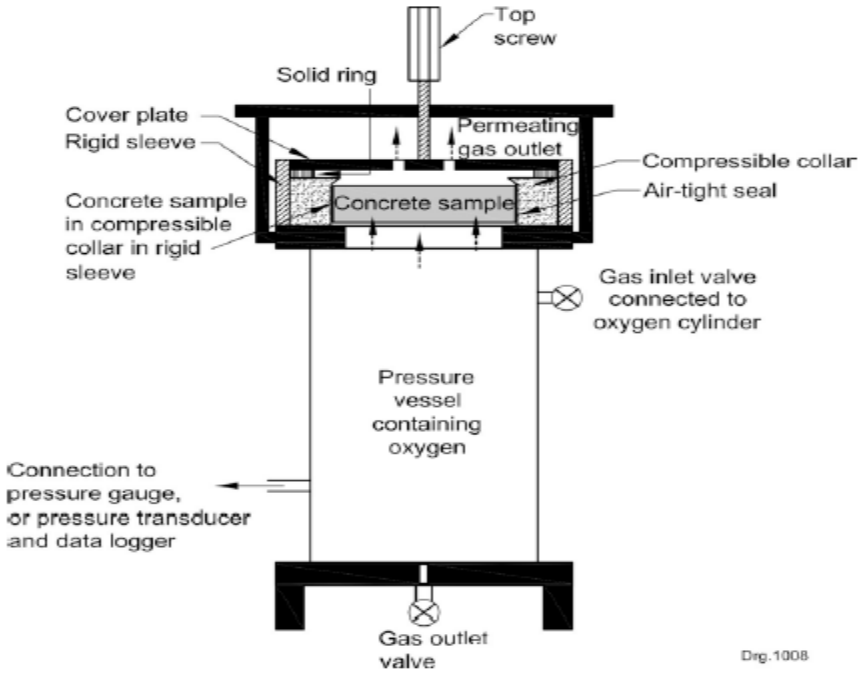

Figure 2.5: Experimental set-up for oxygen permeability test (UCT-WITS DI Manual, 2018)

Stanish et al. (2006) found the reproducibility and repeatability of the OPI test to be 1.8% and 1.4% respectively, with a very similar coefficient of variation between and within the participatory laboratories. Also, Gouws (2001) found that poor site practices like inadequate compaction and insufficient curing affects the OPI of site prepared samples compared to laboratory prepared samples. Likewise, Alexander & Griesel (2004) reported that relative humidity and temperature influences OPI, as inadequate curing leads to rapid moisture loss at elevated temperature (35°C) and for high strength concrete, the OPI values were impaired, an effect likely influenced by micro-cracking resulting from internal stresses during thermal expansion and rapid changes in volume.

2.8.2 Chloride conductivity Index test (CCI)

The CCI test is a measure of the diffusion of chloride ions through a concrete or mortar in order to determine its resistance to chloride ingress. Two transport mechanisms are involved in the test; diffusion of chlorides and migration of chlorides ions resulting from the induced potential difference and are related by the Nernst-Planck equation (Otieno, 2018) given in Equation 2.36

$$J = \left(D \times \frac{zF}{RT}\right)\left(\frac{du}{dx}\right) \quad \text{.....2.36}$$

J is the unidirectional flux of the ionic species (mol/cm^{2}s), D is the diffusion coefficient of the ionic species (cm^2/s), z is the electrical charge of the ionic species, F is the Faradays' constant (96500C/mol), T is the absolute temperature (k), U is the potential difference across the sample (v), x is a distance variable (cm) and R is the universal gas constant (8.314J/mol-K).

The specimen to be tested are oven dried at 50°C between 7 and 8 days, and then vacuum saturated with 5M NaCl solution. Afterwards, the specimens are placed in the test rig which comprise of two cells which are filled with the same concentration of NaCl solution, then a 10V potential difference is applied across the specimen and the current through the specimen is measured within 10s. The chloride conductivity is then determined using the Equation 2.37 and the CCI is taken as the average of at least three individual test measurements. Also, higher values of CCI implies a lower resistance to chloride penetration.

$$\sigma = \frac{id}{VA} \quad \text{.....2.37}$$

σ is the chloride conductivity of the specimen, in millisiemens per centimetre (mS/cm), *i* is the electric current, in milliamperes (mA), *d* is the average specimen thickness, in centimetres (cm), *V* is the voltage difference, in volts (V) and *A* is the cross-sectional area of the specimen, in square centimetres (cm^2).

The test has been found to be sensitive to differences in binder type, water to binder ratio and curing condition with a high statistically significant level. At international level, the test also has a good correlation with other accepted chloride resistance test methods. On like Portland cement, the addition of SCMs (i.e fly ash, ground granulated blast furnace slag, and condensed silica fume) leads to a decrease in chloride conductivity, and likewise increasing moist curing duration and increasing grade of concrete leads to a decrease in chloride conductivity (Beushausen et al. 2021). The test has been standardised and the specification regarding the test is provided in SANS 3001-CO3-3:2015. Also, the test rig has gone through some design modification and this is presented by Otieno & Alexander (2015) but the major difference between the old and the new test rig is the higher values of CCI obtained using the new compared to low values obtained with the old rig. This differences has been linked to the differences in the cross sectional area exposed to the 5M sodium chloride solution. To correct this effect, a hole can be drilled in the anode and cathode compartment for filling in the salt solution as obtainable in the new rig. Otieno (2018) further noted that to obtain valid results from the test, the correct concentration of salt and capillary voltage as stated in the SANS standard should be used, and in addition, the applied capillary voltage should be taken within a very short period of time about 10 secs after closing the test rig.

2.8.3 Water sorptivity index test (WSI)

This is the only durability index test that is yet to be standardised but nonetheless is in use to assess the transport property due to absorption in concrete. Sorptivity is a material property that measures the flow of water by capillary action through a porous material (Hall, 1989). The South African water sorptivity test entails the measurement of the mass of a preconditioned concrete disc subjected to uni-directional water absorption over a predetermined time interval (Gouws et al., 2001). The sorptivity of a given concrete is calculated from equation 2.38

$$S = \frac{Fd}{M_{sv} - M_{so}} \quad \text{……..2.38}$$

Where S is sorptivity (mm/√h), d is the samples' thickness (mm), Msv and Mso are respectively the saturated mass and dry mass of the sample (g), F is the slope of best fit obtained by plotting the mass of water absorbed by the sample per time against the square root of time.

The lower the value of sorptivity obtained the better is the durability potential. As the test measures a surface property of concrete, it is affected by the method and extent of early curing of concrete and as such can be used as quality control measure on construction site. The test further requires the determination of the porosity of the sample which is estimated from equation 2.39

$$n = \frac{M_{sv} - M_{so}}{Ad\rho_w} \times 100 \quad \text{.....2.39}$$

Where n is the porosity (%), A is the cross section area of the sample, ρ_w is the density of water and other terms are as previously defined.

The importance of porosity as a durability indicator for consideration alongside the sorptivity has been emphasized (Moore, Bakera, & Alexander, 2021). Porosity was considered as an input in the estimation of sorptivity by considering the rate of mass gain as a function of porosity of the sample. This in a way give credence to the interdependence between sorptivity and porosity as a measure of the durability potential of a material with respect to water ingress through capillary pores. However, the relation between the two parameters may not be a simple one, as porosity and the rate of absorption of water are influenced by interconnectivity of pores, tortuosity of pore, pore volume and pore size distribution all influenced by the degree of hydration (and pozzolanic) reaction and initial w/b ratio.

2.9 SCM reactivity assessment

The laboratory assessment of SCMs reactivity especially for the qualification of new materials involves two phases; one is the characterisation of the anhydrous material which entails checking for requisite material properties (chemical and/or glassy phase content), and two testing for characteristic performance in hydrated system. The reactivity of SCMs is essential to their use in cementitious systems and a number of methods have been used in its assessment as further discussed.

2.9.1 Methods based on calcium hydroxide consumption

These methods are based on the reaction mechanism of pozzolanic SCMs based on the consumption of portlandite produced from the hydration reaction of plain Portland cement. Fratinni test given in BS EN 196-5:1995, determines the amount of CH in aqueous solution of the hydrated cement compared to the CH required to saturate a solution of the same alkalinity. The concentration of Ca^{2+} and OH^- ions are determined by titrating suspension containing the SCM and Portland cement against 0.025mol/l EDTA and 0.1mol/l HCl solution. Pozzolanicity is determined by noting the position of the data points relative to the saturation curve, with points below the curve indicating pozzolanicity or reactivity of the SCM. Some studies have used the method to assess the pozzolanicity of SCM (Antiohos, Papadakis, & Tsimas, 2014; Bahurudeen & Santhanam, 2015; Donatello, Tyrer, & Cheeseman, 2010; Snellings & Scrivener, 2016). The major disadvantage of the method is the relatively long time and high temperature required to achieve equilibrium (at least 8 days at a temperature of 40˚C) higher than the temperature at which hydration occurs. On the other hand, it is suitable for cement matrix to be cured at high temperature.

Chapelle test determines the amount of $Ca(OH)_2$ consumed by SCM in solution containing 1 g of SCM and 1 or 2 g of $Ca(OH)_2$. The SCM and CH are added to about 200ml of water at 60˚C for about 16 hours; the free CH is estimated using sucrose extraction and titrating against HCl solution (Arif, 2016). The procedure is specified in NFP 18- 513:2009 for metakaolin (with metakaolin to lime ratio of 1:2) and NBR 15895:2010 for natural and artificial pozzolans (Quarcioni, Chotoli, Coelho & Cincotto, 2015). The test is carried out at a much higher temperature than the Fratinni test thus reducing the time required to complete the experiment to less than 24 hours. The application of the method to selected pozzolans from agricultural wastes has been reported by Cordeiro et al. (2008), Perraki et al. (2005), Rego et al. (2015) and Quarcioni et al. (2015).

A major drawback of the chemical method is that the conditions (i.e. temperature and duration of test) under which the test is carried out is different from the actual condition at which pozzolanic reaction occurs in cementitious systems, hence this can affect the accuracy of the reaction of the pozzolan being determined. Also, the dissolution of the alkali content of the SCM can affect the alkalinity of the test mix (Snellings & Scrivener, 2016), thereby influencing the accuracy of the titration. This implies that the concentration of CH determined may not be truly indicative of CH

content liberated by the SCM during the reaction. Hence, a correction factor based on the concentration of unreacted and liberated lime may be necessary if feasible within the test set-up.

2.9.2 Methods based on heat of hydration or bound water determination

The rapid, relevant and reliable method dubbed R^3 method is based on the use of either the bound water approach or the heat of hydration approach to determine reactivity of SCMs. The method was initially developed to determine the reactivity of calcined kaolinite clays (Avet et al., 2016) but has been extended to include other SCMs. The methods require that model paste be prepared containing the SCM and calcium hydroxide in mix proportion 1:3 and mixed with a potassium-based solution containing 4g of KOH and 20g of K_2SO_4 dissolved in one litre deionized water. The paste thus prepared is cured at a temperature of 40°C for 7 days for the determination of the bound water by calculating the mass loss of the paste at a temperature of 350°C. For the determination of the heat of hydration, the paste thus prepared is placed in an isothermal calorimeter at a temperature of 40°C for 7 days while the cumulative heat released is recorded. As both test approaches assesses the activity of the SCM with calcium hydroxide, it assumes silica as the dominant reactive phase present in the SCM. Also, the use of a model paste eliminates the interference of Portland cement with the reaction while the potassium-based solution is used to mimic an alkaline condition similar to that with Portland cement.

2.9.3 Method based on strength determination

Assessing reactivity of SCMs on compressive strength basis offers a more direct means of evaluating reactivity based on performance in a cementitious system. The method is based on estimating the strength activity index as a function of strength development at specified age. The determination of the strength activity index requires that compressive strength of mortar cubes be determined at either 7 or 28 days at 20% SCM content and mix proportion 1:3 for cement and sand respectively. The strength activity index of mix containing SCM is required to be at least 75% of the control (plain PC) at each of the test age for a material to be used as a pozzolan (ASTM C618). Strength activity index as a reactivity indicator has it challenges as the w/b ratio of mix containing the SCM often has to be adjusted to achieve equivalent workability with the control mix and this has an effect on strength development. The difference in w/b ratio between the test mix and the control mix can become significant with increase in fineness of SCM as well as the presence of porous component which can increase the water demand of SCMs (Snellings, 2016). Although,

some authors (Al-Shmaisani, Kalina, Ferron, & Juenger, 2022) suggest the use of workability aid to achieve similar workability between the control mix and test mix, the likely interference of such workability aid with the reaction and performance of the mix can limit their use. Also, the use of variable w/b ratio gives a better understanding of the SCM performance although this can affect the classification based on strength performance which is affected by the varying w/b ratio.

Another challenge with the use of strength activity index is that some inert materials have been reported to pass the 75% strength activity requirement (Kalina, Al-shmaisani, Ferron, & Juenger, 2019). This is not seen entirely as a limitation of the requirement but rather that the scope if the standard may be broadened to include such materials given satisfactory performance in use. This is because going by the scope of ASTM C618, the requirement can be used where "other properties normally attributed to fly ash or pozzolans may be desired". The filler effect identified as the reason why inert materials pass the activity requirement is a desired property of fly ash known to enhance its performance in cementitious systems. This filler effect can be used to advantage in inert materials satisfying the activity requirement to widen the scope of use of such materials even though their reaction mechanism may differ to that of pozzolans in terms of chemical reactivity.

2.10 Corn cob waste

Maize (Zea mays) is an annual crop cultivated at least once in a year in most of the African countries where it is cultivated while a wide variety of species is available depending on market needs and climatic conditions (Department of agriculture and fisheries, 2018). The Food and agriculture organisation (2016) statistics showed that Nigeria followed closely by Egypt, Ethiopia and South Africa are the leading countries in maize production in sub-Sahara Africa, accounting for about 78% of the total production (Figure 2.6). Corn cob constitute between 18% and 20% of the total wastes stream of harvesting or post-harvest processing of mature corn, the others are the leaves, stalk and husks (referred to as the stover) (Danje, 2011; Kianirad, Muazardalan, Savaghebi, Farahbakhsh, & Mirdamadi, 2010). This implied that at least about 1874522.15, 1440253.98, 1412491.5 and 1400130 tonnes of corn cobs resulted from maize harvesting in Nigeria, Egypt, Ethiopia and South Africa respectively according to FAO (2016) statistics.

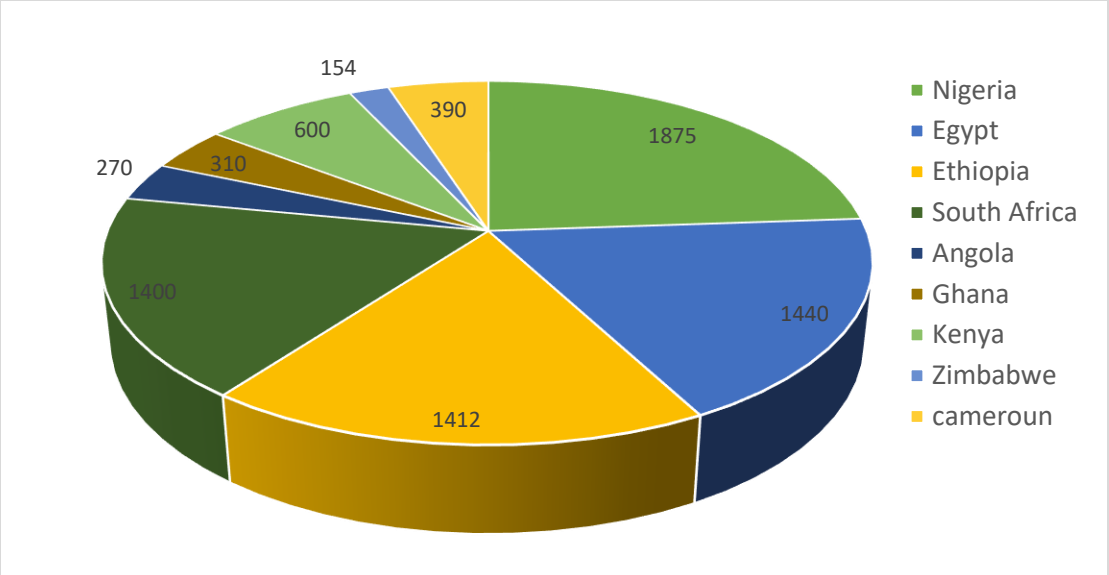

Figure 2.6: Estimate of corn cob wastes (in thousand tons) generated in Africa based on FAO statistics in 2016 (Source: Faostat, 2016)

2.10.1 Potential economic use of corn cob

Corn cobs like other fuel materials has significant carbon and oxygen content which is an essential requirement for energy production (Jenkins, Baxter, & Miles, 1998; L. Wang et al., 2012). The calorific value of corn cob according to Suberu et al. (2012) is about 16MJ/kg and Mohlala et al. (2016) reported a heating value of 19.14MJ/kg which is said to be comparable to low grade South African coal. As a potential fuel, Suberu et al. (2012) noted that Nigeria can generate up to 2900MW of electricity from corn cobs alone. Energy generation from it and other suitable crop residues can cater for agricultural and agro-allied energy requirement since the fuel source is renewable given that most of these wastes are generated annually in substantial quantities (Asonja et al., 2017).

Another alternative is co-firing the cobs with conventional fuels like coal and other crop residues especially in countries with existing coal plants, but may require retrofitting the plants to accommodate the new fuel (Batidzirai et al., 2016). The utilisation of corn cobs (and other crop residues) as alternative fuel source will further reduce the exploitation of non-renewable fuel sources, resulting in lower net CO_2 and net life-cycle CO_2 emissions of more than 50% (Batidzirai et al., 2016; Choate, 2003). Also, co-firing with coal can result in significant cost savings compared to other power generation sources as indicated in Table 2.2 below. Availability of electricity in agro-economic areas will improve socio-economic status as it will encourage the citing of agro-

processing industries in such location thereby reducing post-harvest loss of crops while providing a wide range of employment opportunities (unskilled, artisans and technocrats alike). It will also enhance infrastructural development and reduce rural-urban migration of agile workforce from rural economy. This will further foster a good cooperation between the industry, research institutes and academic institutions.

Table 2.2: Comparison of power production cost from different energy sources

Energy source	**Estimated/Average power production cost ($MWh^{-1})**	
Coal[a]	10.27	
Co-firing (coal-biomass)[a]	23.24-31.42	
Wind	86.6[b]	99[c]
Wind-offshore	221.5	264.5
Solar PV	144.3	282.5
Solar thermal	261.5	-
Hydro	90.3	69

Source:(Batidzirai et al., 2016)
a,b,c average generation cost in South Africa, U.S and Germany respectively

Furthermore, the combustion of corn cobs (and other crop residues) for energy production like other fuel materials will generate ashes which can be converted for other economic use. The waste ashes can be utilized as supplementary cementitious materials in cementitious systems. This has been demonstrated by some studies (Adesanya & Raheem, 2009b; Ikponmwosa et al., 2015; Memon & Khan, 2018; Mujedu et al., 2014) using ashes obtained mostly from open air burning of corn cobs. The ash obtained (Adesanya & Raheem, 2009b) met the chemical content requirement (ASTM C618, BS EN 197-1) for utilisation as partial replacement for cement. This has the advantage of reducing the use and cost of Portland cement which is the major binder currently in use in most developing countries while reducing the attendant negative impact of cement production on the environment. Subsequently, this will reduce the challenges associated with the disposal of crop residues which is a major environmental issue in most developing countries while enhancing cleaner environment with reduced pollution.

Firing of crop residues at and below 900ºC prevent melting of ash and will enhance the efficiency of combustion plants (Asonja et al., 2017). As type and extent of thermal treatment impact on the characteristics and performance of the ash in cementitious systems, consideration of this is imperative in designing energy production plants to significantly minimize or eradicate (where

possible) waste ashes and the need for landfilling as it is currently practiced for fly ash. This will benefits developing economies in deploying appropriate technologies or upgrading of existing facilities to fit this requirement. Therefore, a good understanding of the factors and conditions that may enhance the material's optimal performance given its potentials is necessary for sustainable utilisation.

2.10.2 Previous findings on the use of corn cob ash in cementitious systems

Nimityongskul & Daladar (1995) found that corn cob ash prepared by burning cobs in a ferrocement incinerator has a low strength activity index (SAI), lesser than 50% when compared to PC at 28 days while the ash has a loss on ignition (LOI) of 16.18. The ash thus reported did not meet the ASTM C618 strength activity index (SAI) requirement of 75% of the control (PC) and as such the study concluded that CCA was not a pozzolan. The ash has a combined oxide (silica, alumina and iron oxide) of 41% and a high potassium oxide content and a low Blaine fineness. The low SAI though maybe traced to the low oxide composition but this may not be totally responsible as the reactivity of the ash could not be established. Also, there is a need for further investigation on the suitability of corn cob ash as a pozzolan or otherwise.

The effect of CCA on setting times reported by Adesanya & Raheem (2009b) showed that increasing CCA content in CCA blended cement prolonged both the initial and final setting times of cement. This effect is attributed to the coarseness of the blended cement as a result of the reducing fineness of the blended cement with increasing CCA content in the cement. As fineness reduces with increasing CCA content, the percentage residue on a 45μm sieve increases thereby reducing the surface area of the blended cement. This was further linked to slowing down of the hydration process. However, the link between surface area and hydration reaction is not clear as surface area is envisaged to have an influence on water demand during mixing of the paste rather than on hydration kinetics. Hydration reaction is more of a chemical interaction than physical a physical effect, although it is possible that physical properties of the material can influence the available water for reaction.

Adesanya & Raheem, (2009a) reported on factory prepared CCA blended cement with PC replacement by CCA ranging between 2 and 25%. The CCA used was prepared in a blacksmith furnace prior to blending with plain PC. The blended cement showed chemical composition comparable to PC with a low LOI but higher initial and final setting times. The setting times

increases with increasing CCA content in the blended cement. Adesanya & Raheem, (2009a) reported an optimum ash content of 8% for factory blended cement, based on 180-day compressive strength of 57.10MPa, 40.30MPa and 28.07MPa for mix ratios 1: 1.5: 3, 1:2:4 and 1:3:6. The ash blended cement concrete gained strength at a much later age compared to plain PC, with the reported strength improvement comes the challenge of improving the early age strength which will be of advantage in structural cocrete. Also, Adesanya & Raheem, (2010) reported an optimum content of 10% for 1:1.5:3, 15% for 1:2:4 and 1:3:6 for reduction in water absorption of CCA blended cement concrete. The study further reported an improved resistance to acid attack up to 15% CCA content in mortar bars. The study showed the potential of CCA in improving the durability of concrete between 10% and 15% replacement levels, while there is the need for further study to corroborate the findings and establish the behaviour of CCA with respect to durability performance. It should be noted that only the studies of Adesanya and Raheem used factory blended CCA cement while the CCA has a combined oxide composition of 78.3% however this do not translate to high strength gain in the blended cement concrete. The improvement in strength gain with age was attributed to pozzolanic reaction of CCA in the blended cement concrete. As the amount of amorphous content of the CCA used could not be established, there is a need for further investigation to ascertain the pozzolanicity of CCA given the reported performance.

Also, Olafusi & Olutoge, (2012) and Augustine & Michael, (2016) reported a decrease in strength gain with increasing CCA content but an increase in strength with curing age. The studies reported an increase in setting times with increasing CCA content with an optimum content of 10% CCA for structural application. Augustine & Michael (2016) reported a 28-day compressive strength range of 28.78-17.33 MPa for a grade 30 concrete at replacement levels of between 5% and 25%. Olafusi & Olutoge (2012) reported a 28-day compressive strength of 29 MPa at 10% CCA content and water to cement ratio of 0.45 for a grade 35 concrete. The findings of this study showed considerable improvement in the early age strength of concrete containing CCA, although at a lower CCA replacement level of 10%. It was also noted that the method of ash processing was not reported by the study and as such it could not be inferred whether this could have been responsible for the improved strength reported compared to other studies reported above.

Suwanmaneechot et al. (2015) studied CCA collected from a thermal power plant in Thailand. The ash was further subjected to calcination in a laboratory furnace at temperature range of 200°C - 600°C for 4 hrs. The ash has a high potassium oxide content of 12% and a high specific surface

area greater than that of plain PC which was used as the reference material. The combined oxide composition on further thermal treatment of the ash was 71.87% which satisfied the requirement of ASTM C 618 for class F fly ash. Both the initial and final setting time increases with increasing ash content which showed that CCA has an effect on plain PC setting related to the quantity of PC in the paste. The result of the 28-day compressive strength done of concrete showed that strength improved with further thermal treatment, with strength at 10% ash content slightly higher than that of the reference PC and strength at 15% and 20% similar to that of the reference PC. The improvement in strength recorded in CCA blended concrete compared to plain PC concrete may be attributed to the quality of the ash which when compared to other studies could mean that ash obtained from power plant and further calcined may be beneficial subject to durability perfromance. The reactivity of the ash could not be ascertained to be able to establish its contribution to the reported performance.

Memon & Khan, (2018) determined the reactivity of CCA based on variation in calcination temperature. Corn cobs were first burnt in open air before being calcined in a controlled environment at temperature range 400-800°C with step difference of 100°C. The study reported an optimum incineration temperature, incineration time and grinding time for CCA to be 500°C, 30 and 60 minutes respectively based on strength activity index test, Chapelle test and Fratinni test results. The variability of these parameters with quantity of raw corn cob incinerated and repeatability or reproducibility of the results could not be ascertained, as the optimum incineration time and temperature will be influenced by several other factors like the quantity of raw material feed into the furnace per time, the size of the furnace etc. The study further showed that crystallinity of ash increases with increasing temperature beyond the optimum temperature. The result presented also showed that strength activity varies with calcination temperature while the 75% strength activity index requirement of ASTM C618 at 28 days was satisfied by ashes produced at 400°C, 500°C and 600°C. It is noted that the ash produced at the optimum temperature reported by the study contains some unburnt carbon content evident in the colour of the ash. However, the study could not establish the loss on ignition for the ash obtained at each of the calcination temperature as this could help ascertain the unburnt carbon content in each of the ash. Also, the amorphous content of each batch of ash could not be established as the information contained on XRD pattern is not sufficient to determine the quantity of the reactive phase present

in the ash. This is of importance as it can help ascertain the contribution of the reactive phase to the reported perfromance of the material in cementitious systems.

Shakouri et al. (2020) reported on CCA obtained from burning ground corn cobs in a cyclonic ashing furnace at temperature range of between 600°C and 700°C. The ash was further calcined in a muffle furnace at 550°C for 30 minutes in order to reduce the carbon content. The ash has a high loss on ignition of 23.6% and a high potassium oxide content of 38%. The high loss on ignition can be attributed to unburnt carbon present in the ash. The CCA has a specific surface area of 604.2 m^2/kg and mean and median particle sizes of 33.5 μm and 43.5 μm respectively. The reactivity of the material was inferred from the plot of heat released against calcium hydroxide consumed, on which CCA fell near the inert zone showing it to have limited pozzolanic activity. This can be said to be responsible for the low compressive strength recorded in the study compared to plain PC. Also, the bulk resistivity reported for CCA containing concrete was lower than that of plain PC concrete. Analysis of the pore solution showed that the concentration of potassium and sodium were higher in CCA samples than in plain PC samples. Although, CCA has an effect on the heat flow at dissolution, induction and main heat peak phases, the total heat released is similar to that of fly ash. It could be drawn from the study that the method of ash processing had an effect on the performance of the ash most especially the high loss on ignition. The possibility of reducing the surface area and improving on fineness could be explored in order to further understand the behaviour of the material and if necessary to improve its performance.

Serbanoiu et al. (2022) reported on CCA obtained by burning the cobs in a brick kiln at around 570°C. The study used two quality of ash with the second quality having more carbon than the first and subjected to a further calcination at about 500°C but subjected to the same grinding regime of 120min. The CCA has a high carbon and potassium oxide content of between 14% and 22%, and 21% and 23% respectively while the replacement levels studied were 2.5% and 5% batched by volume. The compressive strength result showed that the ashes do not differ in strength as the 28-day strength for quality A was 26.83 MPa and 21.93 MPa at 2.5% and 5% respectively while quality B was 26.62 MPa and 22.62 Mpa respectively compared to the 31.33 MPa reported for the control (PC). It could be inferred that the ash physical properties do not significantly impact the strength characteristics even though further treatment was required. Also, the study reported a low mass loss due to HCl acid attack compared to the control, this further substantiated the findings of Nimityongskul & Daladar (1995) and Adesanya & Raheem (2010) that CCA can withstand HCl

acid attack better than H_2SO_4 acid attack. It was noted from the study that the percentage replacement levels investigated were lower than 10% while the reactivity of the ash could not be established.

2.11 Summary of literature review

There have been a number of studies on the investigation of CCA as a pozzolan with most of the studies reporting on its potential use in concrete. From the studies that have been reviewed, different calcination methods have been explored in the preparation of ash from raw corn cobs and this has an influence on the properties of the ash reported. It is also noted that most of the ash reported have a high potassium oxide content which indicates a peculiarity to CCA while the effect of such high content of potassium content on the properties and behaviour of CCA in cementitious systems was hardly considered. Also, it is pertinent to give attention to understanding the early age behaviour of CCA and interaction with plain PC towards the proper classification and development of the material. This is important as it will determine the suitability of CCA in actual construction works for use in structural application especially as it affects the striking of formwork.

The use of CCA showed some potentials as noted from the compressive strength reported in most of the studies, however, CCA showed a low strength development compared to plain PC, it is considered important to understand the mechanism contributing to the low strength development as this can help determine the suitability of the material and limit of use in construction application. Given the dearth of information on the holistic characterisation of the ash most especially with respect to the reactive phase of the ash used in most of the studies, there is a need for proper characterisation of the material towards understanding its contribution to the performance of the material in cementitious systems.

There is also a dearth of information on the effect of the material on durability performance of cementitious systems most especially with respect to microstructural development of cementitious systems. This is considered essential as this can give a better understanding of the contributory factors to the penetrability by aggressive fluids most especially as it relates to the properties of the concrete cover which is important to durability studies. Also, as cementitious systems (especially mortar and concrete) undergo some degree of volume change in service, it is good to know the contribution of the material to such changes which could have an impact on the service life of structures.

3.1 Introduction

This chapter presents the detailed experimental materials and methods used in this investigation to collect data for analysis on the reactivity and performance of corn cob ash in cementitious systems. The laboratory experiments consist of characterisation of the materials, determination of the compressive strength of concrete samples prepared with different replacement levels of PC with the ash, determination of the effect of the replacement material on the hydration of PC, determination of the transport properties using durability index tests, microstructural characterisation of the ashes and concrete samples and determination of drying shrinkage. The specimen for the strength tests were cubes while circular discs cored from concrete cube samples were used for the durability index tests. Cement paste was used to study the effect of the ash on the hydration of PC while mortar bars were used for the drying shrinkage test. The binders used in the study were Portland cement, corn cob ash and fly ash.

3.2 Materials

The materials that were used in the laboratory investigation include a CEM I 52.5R Portland cement which is the main binder. Fly ash and corn cob ash were used as supplementary binders to partially replace plain PC while ground crusher sand from andesite rock was used as a filler material to compare effect of the test materials. Crusher sand from andesite was used as fine aggregate for the investigation except for strength activity index determination where silica sand was used as the fine aggregate, and 22 mm crushed andesite stone was used as coarse aggregate.

3.3 Preparation of corn cob ash

Dried corn cobs were collected in sacks from farms in Ilora, Oyo state, Nigeria and two methods of ash preparation were explored. For the first method, the corn cob ash was prepared by subjecting corn cobs to heat treatment in a drum furnace (Fig 3.1). The temperature of the drum furnace was monitored using a temperature probe connected to a measuring meter. The temperature was measured when the initial raw cobs have turned to carbon black at which time the burning temperature was adjudged to be fairly stable. The drum furnace operated at an average stable temperature of between 705 - 708°C and the corn cobs were subjected to continuous burning in the furnace until ash was formed. The temperature of the ash was allowed to cool to the temperature

of the environment before collection. This method of ash preparation is the most common reported in literature obtainable in developing countries and this is largely because of lack of industrial activities utilising the waste in energy generation. Corn cobs being a light weight lignocellulosic material, its controlled calcination in large quantity for laboratory experiment remains a challenge as there is often no suitable facility that can process the material from raw cobs to ash. Another challenge with the calcination of untreated lignocellulosic material is their large volatile gases which is released during calcination. To overcome this challenge, the second method of calcination was adopted.

For the second method, attempt was made to calcine carbon black obtained from pyrolysed corn cobs as a means of improving on the first method of calcining in a drum furnace. This offers the advantage of completing the calcination process in a controlled environment and comparing the effect of modification of the process on the performance of the ashes obtained. The pyrolysed corn cob were milled to powder before subjecting the powder to calcination in a furnace at about 800°C until ash is obtained. The ash was allowed to cool in the furnace to the temperature of the environment before collection. This calcination temperature is higher than the optimum reported by Memon & Khan,(2018) while the carbon content at this temperature was considerably reduced (see Table 4.1 in chapter four) evident in the pinkish colour of the ash compared to the dark grey at 500°C reported by Memon and Khan (2018). The elimination and/or reduction of the carbon content is necessary for quality control purposes as the carbon content can have an impact on water demand and behaviour of the ash. Aside water demand, the specification of ASTM C618-12a on loss on ignition requires a maximum of between 6 and 10% for flyash and natural pozzolans. The requirements of the ASTM is often inferred for other materials with similar composition and/or characteristics. For this second method, the ash yield was about 6kg of ash from 50kg of mill med pyrolysed corn cobs powder. Both ashes were subjected to mechanical grinding using a disk mill in the laboratory to obtain finer particles.

The ash collected was subjected to chemical analysis using the X-ray fluorescence method, determination of the amorphous content using X-ray diffraction method and determination of some physical properties such as the particle size and surface area were also carried on the ashes. Particle size analysis was done using wet dispersion method with Anton Paar particle size analyser. The characterisation was done to assist in the classification of the materials, understanding of the

influence of material properties on the performance in cementitious systems and comparisons to standard specification.

Figure 3.1: Drum furnace for the calcination of the corn cob

3.4 Experimental Variables

The variables selected for the experimental work include water to binder ratio (w/b), curing age, binder type and percentage replacement level by mass. These variables were chosen base on engineering judgement from literature review and known to contribute significantly to and enable comparison of the engineering properties of cementitious systems being investigated (Adesanya & Raheem, 2009a).

3.4.1 Water to binder (w/b) ratio

Two w/b ratios of 0.4 and 0.6 were investigated and these represent low and high w/b ratio commonly used in concrete production. Water/binder ratio influence significantly the properties of cementitious systems both in the wet and hardened state, and w/b of 0.4 is believed to be ideal for complete cement hydration and it is considered to be a critical value for practical purposes (Jacobs and Kiliswa, 2021) while 0.6 represents common site practices where concrete admixture especially superplasticizer is not in use based on workability requirement. Aside this, the two w/b ratios were chosen to enable comparison and understanding of the test material performance with respect to the other selected variables to enable within and between groups comparison.

3.4.2 Binder type

Also, three binder types namely, Portland cement, fly ash and corn cob ash were used in the investigation. Fly ash and corn cob ash were used as SCMs to partially replace Portland cement. The Portland cement and fly ash were used as reference materials for comparison of the properties and performance of corn cob ash. Fly ash was selected as it is a SCM with known properties and behaviour in cementitious systems and having a similar chemical composition as corn cob ash (see Table 4.1), it is envisaged it would have a similar reaction mechanism against which corn cob ash can be assessed. The choice of PC for comparison is on the basis that it remains a major component of most cements and its reaction and products form the basis for the reaction of other supplementary materials used to partially replace it and serves as a basis for comparisons where fly ash is not available. Also, as most cement contains Portland cement, using it as a reference material enables the understanding of its interaction with SCMs and influence on the performance of cementitious systems.

3.4.3 Curing age

Another variable studied is curing age and for compressive strength, curing ages of 3, 7, 28, 90, 180 and 270 days were investigated. The curing age for the compressive strength were chosen such that the early and later age strength development can be established for the test material. For durability index tests, curing ages of 28 and 90 days were investigated. The curing age was chosen to allow sufficient reaction of the cements and to enable distinction in the pore structure characteristics of concrete with age as hydration progresses. For drying shrinkage, curing age of two weeks was adopted prior to testing the samples to allow a certain degree of reaction especially for the SCMs containing samples.

3.4.4 Replacement level

The fly ash and corn cob ash were used to partially replace PC at two levels of 15% and 30% by mass of Portland cement. The effect of replacement level is significant in understanding the effectiveness of the supplementary cementitious materials as a good replacement and in determining the optimum replacement level based on performance in cementitious systems. The commonly used replacement level for fly ash in South Africa is 30% for strength and durability requirements. The replacement levels were chosen to enable comparison of effects of the SCMs at

low and moderate substitution levels which allows distinction of the effects of the SCMs in cementitious systems.

3.5 Mix Design

The concrete mix for the experiment was designed using the Cement and Concrete institute of South Africa absolute volume method as described by Van Heerden (2021) and the materials were batched by weight. Reference mixes were adopted for the experiment which are; 100% PC and fly ash partially replacing PC at 15% and 30% in order to enable comparison of performance of the test material. The test mixes contain corn cob ash partially replacing PC at 15% and 30% levels. Each of the control mixes and the test mixes was prepared using two w/b ratio. The mix design is presented in Table 3.1. The mix proportioning for mortar bar and 50 mm cubes is according to BS EN196:1-1995 except that river sand was used in place of standard graded sand based on availability. River sand was used as it is believed to be an inert material thereby leaving PC and the SCMs as the only reactive materials in the system. This enhances the comparison of the performance of the test materials within and between groups to enable proper understanding of the behaviour of the materials.

Table 3.1: Mix proportioning for concrete samples

Mix/Material	**PC (kg/m^3)**	**FA (kg/m^3)**	**CCA (kg/m^3)**	**Water (kg/m^3)**	**Sand (kg/m^3)**	**Stone (kg/m^3)**	**w/b**
100PC	512.50	-	-	205	582	1126	0.4
100PC	342	-	-	205	725	1126	0.6
85/15/PC/FA	436	77	-	205	582	1126	0.4
85/15/PC/FA	291	51	-	205	725	1126	0.6
70/30/PC/FA	358.75	153.75	-	205	582	1126	0.4
70/30/PC/FA	239	103	-	205	725	1126	0.6
85/15/PC/C-700	436	-	77	205	582	1126	0.4
85/15/PC/C-700	291	-	51	205	725	1126	0.6
70/30/PC/C-700	358.75	-	153.75	205	582	1126	0.4
70/30/PC/C-700	239	-	103	205	725	1126	0.6

N/b: The mix 100PC denotes 100% PC without SCM, 85/15/PC/FA denotes 85% PC and 15% fly ash, 85/15/PC/C-700 denotes 85% PC and 15% corn cob ash calcined at 700°C, 70/30/PC/FA denotes 70% PC and 30% fly ash and 70/30/PC/C-700 denotes 70% PC and 30% corn cob ash calcined at 700°C.

3.6 Preparation of samples for chemical reactivity test

Chemical reactivity of the test material (CCA) was determined using the R3 (rapid, reliable and relevant) test procedure developed by (Avet et al., 2016) for assessing the reactivity of calcine clay with limestone. The test was done to assess the chemical reactivity of the ashes in a simulated pore solution environment and to substantiate the result of the strength activity index test carried out which is based on compressive strength. R3 test is based on the measurement of either the cumulative heat released or bound water content of hydrated cement paste with simulated pore solution conditioned to mimic the chemical environment of a hydrating system. The procedure of the test is given in ASTM C1897 (2020) and do not distinguish between the reactivity of pozzolanic or hydraulic materials. This however is seen as a limitation as the mechanism of reaction of pozzolanic material differs from that of hydraulic material. The bound water determination method was used by heating cured paste sample in a furnace at 350°C. The test involves preparation of paste containing the SCM, calcium hydroxide, potassium solution and calcium carbonate. The potassium solution contains both alkali and sulphate used to condition the mix to simulate the pore solution in a blended cement system and also to mimic Portland cement hydration which include sulphate adjustment. The test also include curing of the paste sample at elevated temperature (which in this case is taken to be 50°C) in order to accelerate the reactivity of the material. The paste sample was cured for 5 days since the curing temperature used is slightly higher than that given in the standard. A typical proportioning of the paste mixture is given below

Table 3.2: Mix proportioning for the paste

Material	SCM	$Ca(OH)_2$	$CaCO_3$	Potassium solution
Mass(g)	10	30	5	54

3.7 Preparation and testing of concrete samples for compressive strength test

Compressive strength was carried out to determine the strength development with time and load carrying performance of the test material compared to its references. Compressive strength remains a fundamental property required for the design of concrete structures and can assist in making informed decision on the suitability of a material as a partial replacement for plain PC. The sample

for the determination of compressive strength were 100 mm cubes prepared from freshly mixed concrete samples batched by weight and mixed in a pan mixer. The concrete samples were prepared using two w/b ratios as stated in section 3.4. Fresh concrete was placed in oiled moulds in two layers, each layer was vibrated for about a minute on a vibrating table operating at a frequency of 50Hz. The cubes were covered with polythene sheet to prevent moisture loss to the surrounding and the cubes were demoulded after 24 hours of casting. The concrete cubes were cured in water in the laboratory up until the testing date.

The compressive strength test was carried out in accordance with the provisions of SANS 5863:2006. The testing age are 3, 7, 28, 90, 180 and 270 days. At the testing age, 100 mm cubes were tested in saturated surface dry condition immediately after removal from water. The test cube is placed in the compression machine such that the loading face is perpendicular to the as-cast face. The loading rate of the machine is 0.25MPa/s. The cube was loaded to failure and the load at failure recorded.

3.7.1 Preparation and testing of mortar samples for compressive strength

The preparation of mortar cubes was done to establish the strength activity index to allow the comparison of and ascertain the reactivity of the ash obtained from the two methods as stated in section 3.3. Strength activity index is used as a measure of reactivity and suitability of a material as a pozzolan. Silica sand was used in lieu of standard sand and w/b ratio of 0.5 was used to prepare the mortar mix. The mortar cubes (50 mm) were demoulded after 24 hours of casting and cured under water till the testing age. However, the mortar cubes prepared using the calcined ash from the second method were demoulded after 48 hours of casting but it was not certain whether the inclement weather alongside the material characteristic was responsible for the slow setting or hardening as the case maybe. At 24 hours, the samples were not strong enough to be submerged in water for curing without disintegration hence the extension of the demoulding period. For the mortar cubes, the same procedure for the concrete cubes was followed and the test was carried out at the ages of 28, 56 and 90 days to allow sufficient reaction of the SCM and distinction in material behaviour with time.

3.7.2 Preparation of samples for testing dilution and filler effect of SCM

The use of SCMs in cementitious systems is associated with both filler and dilution effects each contributing to the overall performance of the system and most especially concrete. The test was

done in order to understand the mechanism by which the test material contributes to the performance of the system. The dilution effect of SCMs have two phases; increased water to plain PC content and reduced plain PC content due to its partial substitution with SCMs. For each of the w/b ratio of 0.4 and 0.6, the binder content correspond to the combination of plain PC and SCM. To study the dilution effect of the SCMs, 100mm cubes were cast with 100% plain PC but with w/b ratio corresponding to water to plain PC content only (w/pc) for each of the w/b ratio. The w/pc ratio also varies with the replacement level, for instance at 15% content and w/b ratio of 0.4, the w/pc ratio was 0.47 while at 30% it was 0.57. For w/b ratio of 0.6, the w/pc ratio was 0.72 and 0.86 for 15% and 30% replacement levels respectively. This was used to assess the dilution effect of the CCA containing samples and fly ash reference samples in order to quantify the effect of the increased w/pc ratio due to the inclusion of SCMs in concrete. The dilution effect measured in this way attributes the free water to PC as the only hydrating binder in the system since w/c ratio is a factor influencing the compressive strength of concrete.

To study the filler effect of the SCM in concrete, 100 mm cubes of concrete were cast with ground crusher sand at 15% and 30% replacement level of PC using a w/b ratio of 0.4 and 0.6. Crusher sand (andersite) is known to be an inert material and in this case it is used as an inert filler material to compare the filler effect of the CCA and fly ash. The crusher sand was sieved through 300, 150 and 75μm and the particles retained on and passing through 75μm sieve were further ground in the disk mill to increase its fineness. The filler effect measured in this enables the comparison of strength of concrete containing an inert material whose main influence on strength is largely physical, with that of concrete containing either fly ash or CCA as SCM in order to understand the mechanisms of reaction of the materials.

3.8 Preparation and testing of samples for drying shrinkage test

The drying shrinkage test measures moisture loss from concrete or mortar to the environment beyond setting of the cement. Drying shrinkage determination would help to understand the influence of the test material on the drying (shrinkage) behaviour which can often induce cracks and impair durability performance. For the test, mortar prisms of size 50 by 50 by 300 mm were cast from freshly prepared mortar mix containing one part of cement to three parts of crusher sand using two w/b ratios of 0.4 and 0.6. Mortar was placed in oiled moulds and compacted in two layers using a vibrating table while the samples were demoulded after 24 hours of casting. Two

sets of samples were tested, one set was cured in water for two weeks and another set was not cured prior to testing. The test was done according to the provisions of SANS6254:2006, the initial drying shrinkage of mortar, with some modifications.

To each of the mortar prisms, aluminium targets were affixed to one side of the longitudinal face perpendicular to the as-cast face at 50 mm interval (Fig.3.2). Using this approach, three independent readings of strain can be taken per sample using a 100 mm gauge length dial gauge. For the samples that were cured, the targets were fixed upon removal from water prior to placing in the test room while for the samples that were not cured, the targets were fixed after demoulding the samples. The samples were placed in the test room on a steel rack such that each sample is adequately exposed to the environment (Fig. 3.3) and the measurement of the microstrain was done every day for the first two weeks. For the samples that were not cured, the first reading was taken immediately after demoulding and the targets have been fixed while for the cured samples, the first reading was taken after removal from water and the targets have been fixed. Subsequent readings were taken every three days and then every week till the shrinkage stabilise. The readings were taken for seven months.

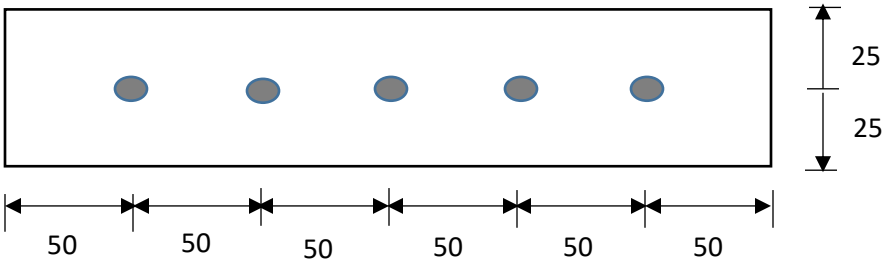

Figure 3.2: Plan of aluminium stud arrangement on drying shrinkage sample


Figure 3.3: Drying shrinkage samples with stud arrangement and placement on steel rack

3.9 Preparation and testing of samples for durability index tests

Durability index tests were carried out to characterise the pore structure and penetrability of concrete made from the test material compared to that made of plain PC and fly ash. More important than strength is the durability of concrete structures to satisfy the designed service life to which the ingress of aggressive fluids and ions contribute significantly. The tests assess different mechanisms of deterioration to infer concrete quality and hence durability of concrete based on certain performance criteria. Three durability index tests, oxygen permeability, water sorptivity and chloride conductivity were carried out at 28 and 90 days of water curing. The test sample consist of concrete discs cored from cured 100 mm concrete cubes at the testing age. The 28 and 90 days curing was to allow for some degree of pozzolanic reaction of the SCMs (which is slow compared to hydration reaction) as the reaction influences pore structure development and pore size distribution in concrete. Also, both reactions develop with time as they are time dependent and this allows for comparison of age effect on the microstructure of concrete which gives an indication on the durability of concrete. Sample preparation for durability index testing was done according to SANS 3001-CO3-1:2015. The schematic for sample cutting from cored 100mm cube is as shown in Fig. 3.4. The three durability index tests gives an assessment of the transport mechanism of fluids movement into concrete through the cover concrete.

Beushausen, Otieno and Alexander (2021) noted that oxygen permeability test is used to assess the resistance of concrete to the flow of gases through the capillary pores at near surface concrete, and as a result can give information on the tortuosity and interconnectivity of the pores. The test measures the pressure decay of oxygen gas passed through the sample in a permeability cell as the gas flows through the sample under pressure. The specimens were subjected to pressure of between 95 and 105 kPa at the start of the experiment and the experiment last for about 6 hours. The schematic of the permeability cell with sample is as shown in Fig. 3.5. The test was carried out according to SANS 3001-CO3-2:2015. The chloride conductivity index (CCI) test assesses concrete resistance to the diffusion and conduction of chloride ions by measuring the flow of current and voltage through a sample in a conduction cell. A 5M NaCl solution is poured into the anode and cathode cell of a conduction rig and the cell connected to the ammeter and voltmeter connected to a DC power supply such that the voltage across the specimen is about 10V. The current and voltage reading were taken simultaneously within 10 seconds. The conduction cell

arrangement is shown in Figure 3.6. The test was carried out according to SANS 3001-CO3-3:2015.

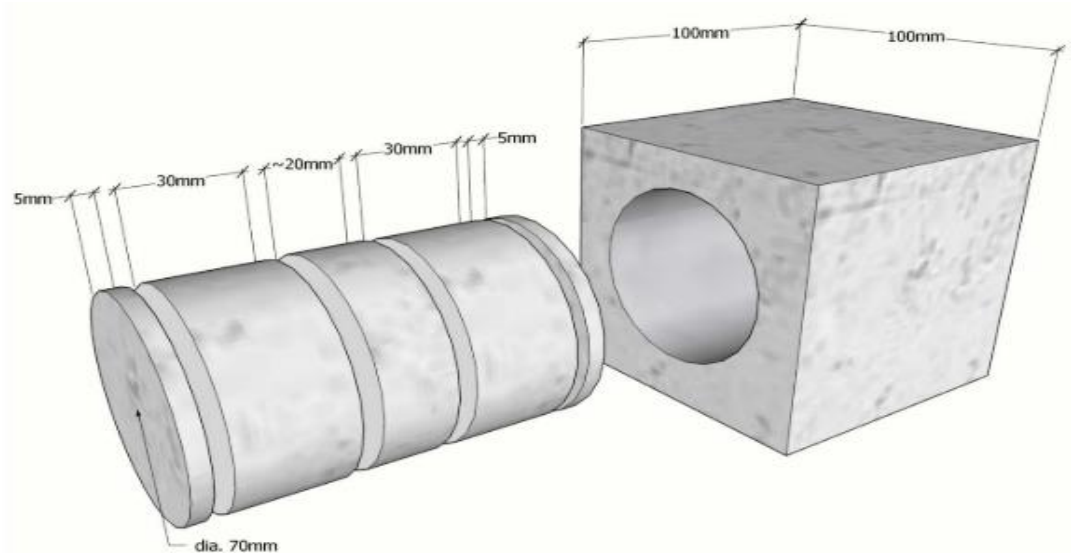

Figure 3.4: Details of discs cutting from cubes for durability indices determination (source: UCT-WITS DI Manual, 2018)

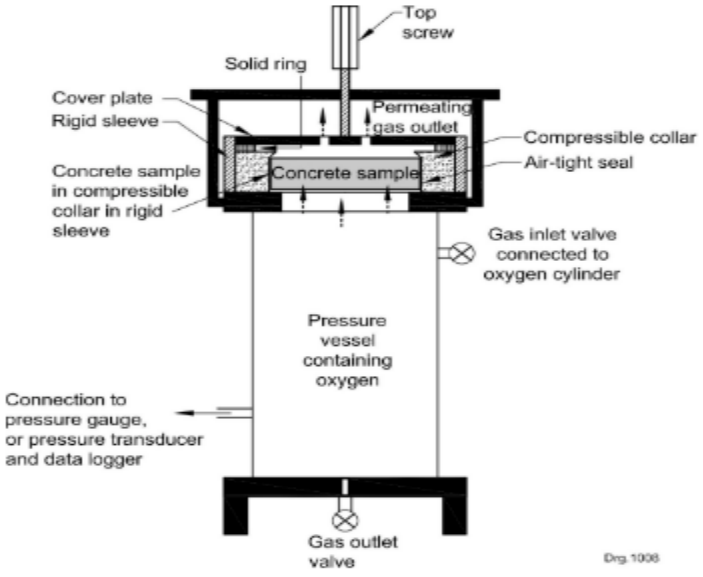

Figure 3.5: Diagram of the permeability cell arrangement (source: SANS 3001-CO3-2:2015)

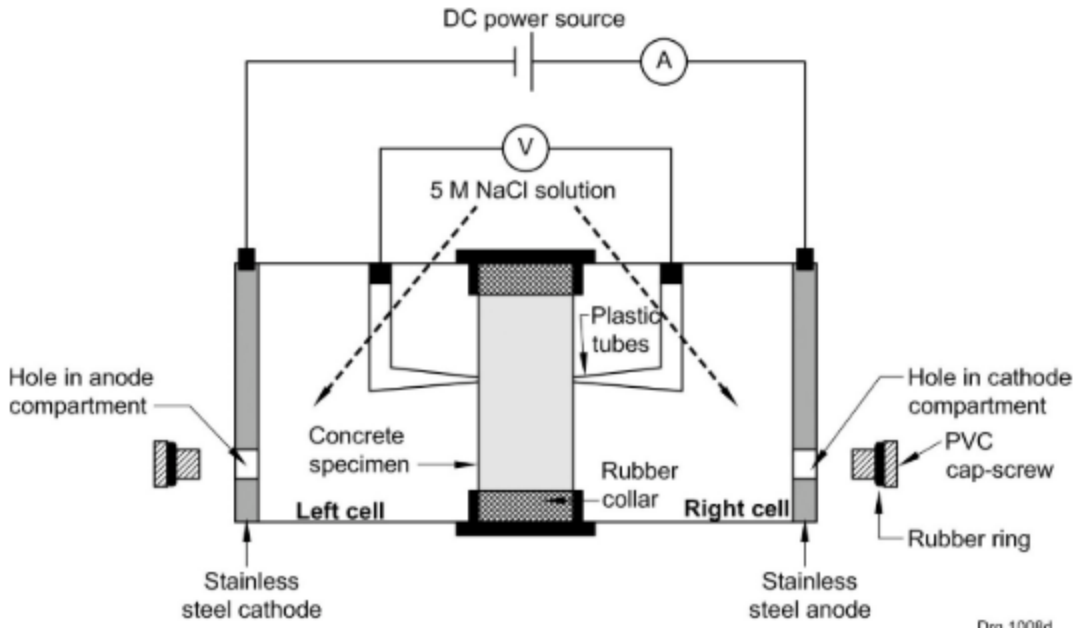

Figure 3.6: longitudinal section of the conduction cell (source: SANS 3001-CO3-3:2015)

The conduct of the water sorptivity and porosity test was guided by the (UCT-WITS DI Manual, 2018). The test is used to assess the absorption of moisture through the capillary pores of the concrete cover. As exposed concrete structures are subjected to intermittent moisture absorption in service, a measurement of this mechanism of transport enables the assessment of concrete quality and susceptibility of the concrete cover to moisture absorption in order to understand the potential durability of the concrete. The same samples used for the oxygen permeability test were used for this test. A solution of tap water saturated with calcium hydroxide (3g of $Ca(OH)_2$ to a litre of water) at 23°C was used for the testing.

The discs curved edges were sealed with cellotape and the dry mass (Mso) measured to an accuracy of 0.01g. The thickness and diameter of the discs were measured to the nearest 0.02 mm taking four different points on each disc. 10 layers of paper towel was placed in the tray and saturated with calcium hydroxide solution. The external surface of the disc was then placed on the towel with the solution being visible above the paper towel and at a maximum of 2mm above the sample face (Fig.3.7). The surface of the discs was patted dry on a dry paper towel and weighed at different intervals 3, 5, 7, 9, 12, 16, 20 and 25 minutes.

For the porosity test, after weighing was completed, the samples were vacuum saturated and the tank evacuated to between 75 and 80 kPa with samples maintained for 3 hours ± 15 minutes. After

this, calcium hydroxide solution was allowed into the tank to about 40 mm above the samples, the vacuum was re-established and maintained for 1 hour ± 15 min. The vacuum was released after 1 hour and the specimen allowed to soak for 18 ± 1 hr after which the samples were surfaced dried with a paper towel and weighed to an accuracy of 0.01 g. This mass was recorded as the vacuum saturated mass (Msv). The density of each sample was obtained from the equation 3.2

$$n = \frac{Msv - Mso}{Ad\rho_w} \times 100 \quad \ldots\ldots\ldots\ldots\ldots\ldots\ldots 3.2$$

Msv is the vacuum saturated mass of the sample to an accuracy of 0.01 g, Mso is the mass of the sample at start of the test, A is the samples' cross sectional area to the nearest 0.02 mm^2, d is the average thickness of the sample and ρ_w is the density of water.

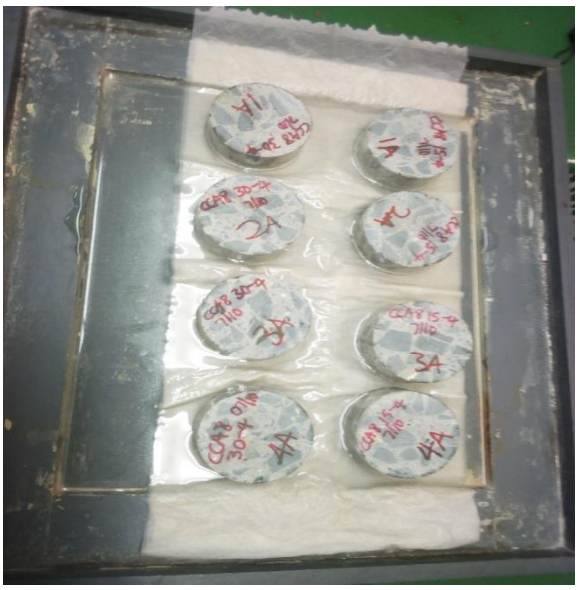

Figure 3.7: Testing of concrete cores for water sorptivity determination

3.10 Preparation and testing of samples for hydration test

Hydration test involves the measuring of the effects of cement reaction upon the addition of water. Isothermal calorimetry allows the monitoring of the rate of heat evolution as cement undergoes reaction with time. In principle, the sample is kept at a constant temperature while the heat liberated from within the sample is removed to a heat sink with known specific heat capacity and this enables the heat flow and thermal power to be determined for the sample (Ballim and Otieno, 2021). The method was used as it enables small quantity of material to be tested and allows for the

characterisation of the paste which is the main hydrating material in concrete without the interference of the aggregates. This further enables the understanding of the effect of the test material on the different phases of hydration reaction of PC and influence on heat evolution over time

Sample preparation involves weighing and dry mixing of the powder samples for each of the replacement levels investigated. The required quantity of powder was measured and mixed thoroughly manually in a container. The powder samples were then stored in airtight ziplock bags prior to commencement of the test. The hydration test was done using isothermal calorimetry method. Deionized water was weighed and conditioned to 20°C (which is the target isothermal temperature) prior to mixing. The required quantity of the sample was weighed and mixed with the preconditioned water inside the sample vial to prepare a paste of 30g. The ratio of the mix water to the powder is 0.4. The paste with the sample vial was placed in the calorimeter in less than two minutes from the time the mix water was added to the sample, in order to maintain the temperature of the paste as close as possible to that of the calorimeter. Once the vial containing the paste is placed in the calorimeter, the logging of the data commenced and the total duration of the test is 48 hours. The calorimeter used was I-Cal 2000 HPC.

3.11 Preparation of samples for microstructural analysis

Microstructural analysis involves the characterisation of the hydrated phases of cement hydration reaction in order to understand the effects of the replacement materials studied on the properties of concrete and their interaction with PC. The microstructural analysis is in two phases; hydrated paste analysis and pore solution analysis to enable the understanding of the contribution of the microstructural properties to the performance of concrete. The samples used for analysis were thin slices of concrete cut from concrete cores at the testing age. The slices were oven dried for at least 48 hours at 50°C after which the samples were stored in a ziplock bag prior to testing. Oven drying was used as a means of stopping the hydration of the samples beyond the testing age and the temperature considered sufficient to prevent modification of the hydrates and to preserve the microstructure. For pore solution analysis, oven dried thin slices of concrete were milled to powder using a laboratory disk mill. The powder was then stored in airtight ziplock bags prior to testing to prevent exposure to the environment and likely carbonation of the samples.

Pore solution analysis was done in order to determine the concentration of alkalis and metals that can easily go into solution in the presence of moisture as this has an influence on the durability of cementitious systems. The pore solution was extracted from hydrated concrete powder at 28 and 90 days, and for the analysis, pore solution was extracted using the cold water extraction method described by Plusquellec & Weerdt (2017). The pore solution thus extracted was stored in plastic vials prior to testing. For the determination of the OH concentration, 1ml of sample was added to 1.5ml of deionized water (and this gives a dilution factor of 4) in a cell, the test reagent was added as appropriate and the concentration determined. The concentration was measured by a spectrometer with a measuring range of 0.4-8 mmol/l for OH. For potassium content determination, no dilution was done except for samples with high concentration above the measuring range of the spectrometer which is 5-50 mg/l. A spectroquant Pharoo 300 M spectrometer was used for the determination of OH, potassium and sodium content while atomic absorption spectrometry was used for the determination of calcium, alumina and silica.

For the hydrated phase analysis, scanning electron microscopy (SEM) coupled with electron dispersive spectrometry (EDS) was used. This was done to obtain the morphology of the cement particles, the paste structure and the interfacial characteristics. Samples were obtained from the thin slices cut from cored concrete and carbon coated. Images of the cement paste and interface with aggregates were obtained as well as mappings in order to characterise the phases present in the sections. The images were acquired using the back scattered electron imaging mode and the acceleration voltage was 30kV. The equipment used is a Bruker TESCAN Vega SEM.

3.12 Preparation of samples for setting times determination

Setting time test to determine the initial and final setting times of cement paste containing CCA was conducted to assess the effect of CCA on the setting of cement. The test was carried out according to EN 196-3:2005+A1 with modification to the water content used to prepare the paste. Cement paste containing either 15% or 30% CCA was prepared with a w/b ratio of 0.4 and placed in vicat apparatus mould. The time at the beginning of mixing of the paste was noted as time zero from which time the duration required for the distance between the initial set needle and the base plate to be between 3 mm and 9 mm is recorded as the initial setting time. The final set time is determined at the time elapsed between time zero and the time the final set needle first penetrated 0.5 mm into the specimen without a ring inscription on the specimen.

3.13 Framework for the study

The framework for the study (Fig. 3.8) which aligns the study aim and objectives with the laboratory experiment is presented. The investigation of CCA as an SCM involved the setting out of variables which include material and test variables considered important to assist in the understanding of the test material performance compared to both plain PC and fly ash which are the reference material for the study. The study set out to investigate the suitability of CCA as a supplementary cementitious material (SCM) by comparing its reactivity and performance with those of plain PC and fly ash. The material variables include two water- to-binder ratios (0.4 and 0.6 w/b), two plain PC replacement levels (15% and 30%).

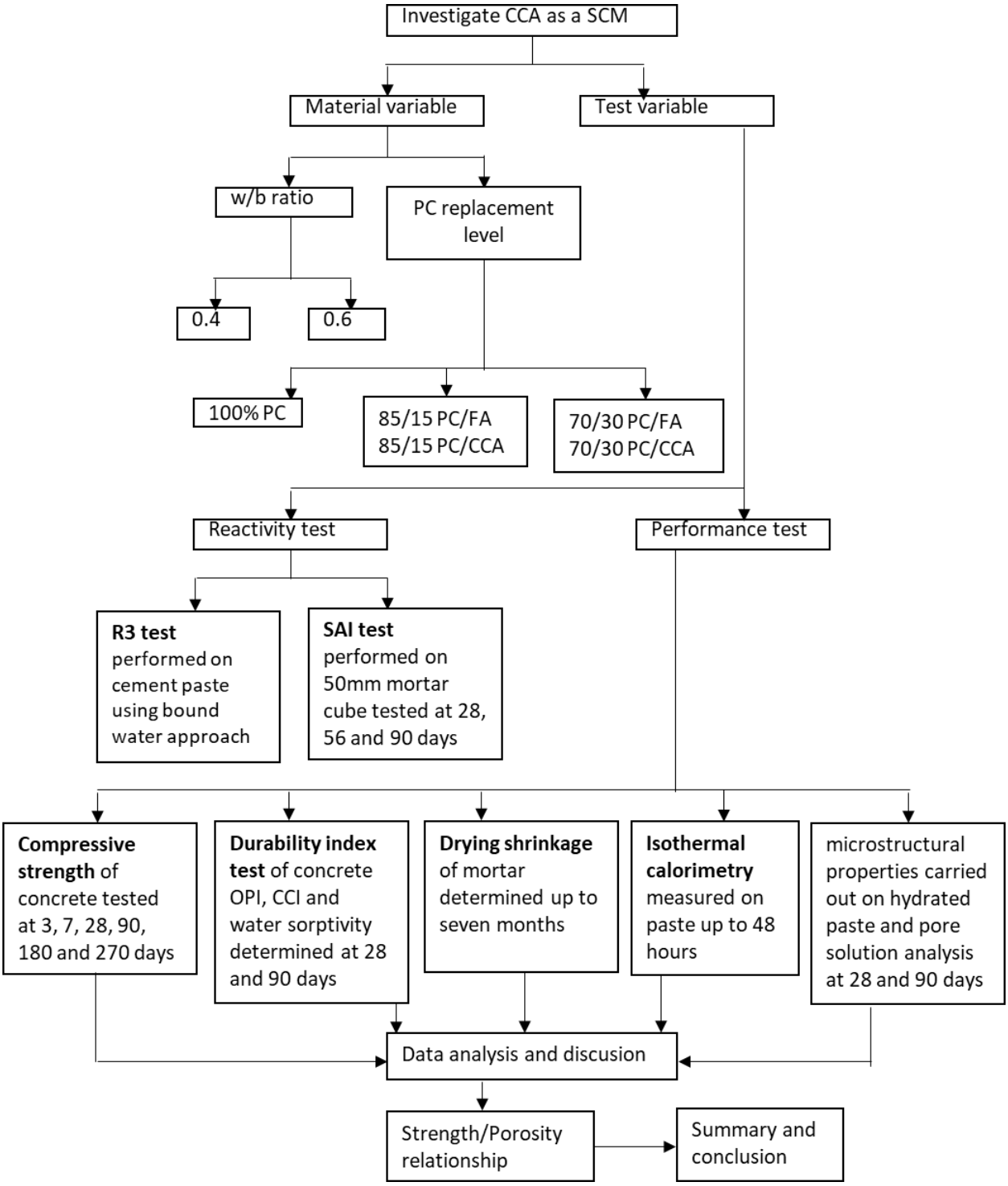

Figure 3.8: Framework of the study

4.1 Introduction

This chapter focusses on the presentation and analyses of the results obtained from the experimental investigations carried out in the laboratory and subsequently discusses the results. There is a section covering the presentation and discussion of the physical and chemical properties of the input materials followed by the presentation of the main results of the study. The main results cover the results and discussion of the reactivity tests and performance tests. The reactivity tests results include those from R3 test using bound water approach and compressive strength determination on mortar cubes to obtain the strength activity index. The performance tests results cover those from compressive strength determination on concrete cubes, isothermal calorimetry test, pore solution analyses`, drying shrinkage and durability indices as indicators of the durability performance of concrete samples with respect to ingress of fluids.

It should be noted with respect to the notation for each of the mix that; PC4 and PC6 implies a mix with 100% plain PC and w/b ratio of 0.4 and 0.6 respectively; FA15-4 and FA15-6 implies a mix containing 15% fly ash and 85% PC with w/b ratio of 0.4 and 0.6 respectively; FA30-4 and FA30-6 implies a mix containing 30% fly ash and 70% PC with w/b ratio of 0.4 and 0.6 respectively; C-700 15-4 and C-700 15-6 implies a mix containing 15% corn cob ash calcined at 700°C and 85% PC with w/b ratio of 0.4 and 0.6 respectively; C-700 30-4 and C-700 30-6 implies a mix containing 30% corn cob ash calcined at 700°C and 70% PC with w/b ratio of 0.4 and 0.6 respectively; C-800 15-4 and C-700 15-6 implies a mix containing 15% corn cob ash calcined at 800°C and 85% PC with w/b ratio of 0.4 and 0.6 respectively; C-800 30-4 and C-800 30-6 implies a mix containing 30% corn cob ash calcined at 800°C and 70% PC with w/b ratio of 0.4 and 0.6 respectively.

4.2 Characterisation of materials

A description of the material properties is considered given its import in understanding the contribution of the materials properties towards the understanding of the performance of the materials, mechanisms of reaction and behaviour exhibited in cementitious systems. The properties reported include surface area, chemical composition and amorphous content and particle size distribution.

The raw materials were characterised for physical and chemical properties and the result is presented in Table 4.1. The Brunauer-Emmett-Teller (BET) surface area analysis using nitrogen gas showed that the fly ash has a surface area of 2.224m^2/g while C-700 and C-800 have a surface area of 3.122 m^2/g and 2.751 m^2/g respectively. Corn cob ash has a higher surface area than fly ash, this is expected to have an effect on the surface property of the material with respect to absorption of water and thus an implied effect on the workability of cementitious systems (leading to increase in water demand) prepared from both materials given the same water content and cement content (Mehdipour & Khayat, 2017; Walker & Pavía, 2011). Apart from the effect on workability, surface area of the materials may also have an influence on reactivity of reactive materials and interaction with PC in cementitious systems (Walker & Pavía, 2011). The surface area can also be used as an indication of fineness and for this, fly ash is finer than the CCAs while C-800 is finer than C-700.

The oxide composition for the chemical constituent of each of the ashes is presented in Table 4.1. Fly ash is an alumino-silicate material with both silica and alumina making up more than 80% of the total oxide composition. On the other hand, corn cob ash is mainly siliceous with the alumina content less than 5% and a high content of potassium oxide, which is reflective of its agricultural origin. The combined silicon oxide, aluminium oxide and iron oxide for C-700 and C-800 is 65% and 72% respectively which is lower than that of fly ash which is 91%. ASTM C 618-05 required a combined oxide of 70% for class F fly ash and natural pozzolans and this requirement is often used by extension for siliceous and/or alumina-siliceous materials. CCA is compared to class F fly ash given its similar oxide composition except for its high potassium and low aluminium oxide. This difference can be expected given the differences in the origin of both materials as fly ash is obtained from the combustion of naturally occurring material which is why its silica and alumina content is high. Likewise, the loss on ignition (LOI) for corn cob ash is above the 10% required for class F fly ash. This shows that CCA contains some ignitable matter and this is evident in the dark grey and pinkish grey colour of C-700 and C-800 respectively. This ignitable matter is linked to unburnt carbon and this may have contributed to the high surface area of both CCAs compared to that of fly ash. This will have an influence on the water demand during concrete production and hence workability as well as the reactivity of the ash (Hill, Sarkar, Rathbone, & Hower, 1997). Subsequently, the oxide composition of each of the ashes is expected to have an impact on the formation of hydration product as well as interaction with PC in cementitious systems.

Table 4.1: Oxide analyses and particle size distribution of the ashes

Oxide / phase / particle size	Percentage (%)			
	CEM I 52.5R	C-700	C-800	FA
SiO_2	19.57	59.37	63.68	56.01
Al_2O_3	4.93	2.79	4.42	31.74
Fe_2O_3	2.64	2.62	4.05	3.31
MnO	0.37	0.07	0.11	0.01
MgO	2.06	1.38	2.07	1.22
CaO	62.57	1.26	2.37	5
Na_2O	0.00	0.16	0.24	<0.01
K_2O	0.45	15.83	11.22	0.77
TiO_2	0.35	0.41	0.5	1.59
P_2O_5	0.10	1.76	3.2	0.56
Cr_2O_7	0.03	0.07	0.09	0.04
LOI	3.60	13.19	6.76	0.81
Amorphous content	-	1.9	2.4	57.5
D10 (μm)	30.11	1.63	1.06	0.15
D50 (μm)	38.72	12.41	6.11	1.17
D90 (μm)	225.72	54.93	24.50	3.37
Mean size vol (μm)	95.09	22.00	9.96	1.38
BET surface area (m^2/g)	2.38	3.122	2.751	2.224

The amorphous content result showed that both C-700 and C-800 have very low amorphous content of 1.9% and 2.4% respectively compared to 58% amorphous content of fly ash. The CCAs understudy are mainly crystalline and this can be linked to the calcination process which is ineffective in producing a desirable amorphous ash typical of pozzolanic material. The duration of calcination may need to be shortened when using a drum furnace but a major challenge remains that the obtained ash contains unburnt matters reflected in its dark grey colour. Although, calcining

in an electric furnace eliminated the unburnt particles, the slight difference in the amorphous content also suggest there is a need for further improvement in the method to be able to obtain a more amorphous material.

The particle size distribution for each of the ashes as presented in Table 4.1 (see Appendix for the graphs) showed that fly ash particles are much finer than those of the CCAs while C-800 is finer than C-700. The finer particles of fly ash reflects a programed and controlled calcination process and quality control typical of industrial process. However, being able to optimize the laboratory calcination process to obtain amorphous material maybe a step forward in the upscale of CCA production in industrial scale. The particle size distribution for the crusher sand used as fine aggregate is presented in appendix A. The sand consist of about 2% stone fraction (i.e. fraction retained on the 4.75 mm sieve) and 1% dust particle. About 77% of the mass of sand is retained between the 2.36 and 0.3 mm sieves and 21% passed through 0.3 mm sieve. The sand has coarser fraction than the fine fraction and can be classified as a coarse sand in line with its fineness modulus which is 3.2. in line with literature classification as specified in Bonser and Alexander (2021) fineness modulus greater than 2.9 implies a coarse sand.

The results of the setting time test is presented in Table A13 in appendix. The result showed that CCA calcined at 700°C shortens both the initial and final setting time compared to both PC and fly ash cement paste. CCA calcined at 800°C shortens the initial setting time but prolonged the final setting time compared to PC and fly ash. The rather short initial setting time observed for both CCAs is contrary to the reports in literature as Adesanya and Raheem (2009b) reported a longer setting time compared to PC. The result obtained in this study is inexplicable although a likely reason for this is the high surface area of the CCAs compared to either PC or FA (see Table 4.1) and possibly a porous structure. This is likely to increase the water demand of CCA in the paste resulting in the CCAs absorbing free water in the system. This is so as setting times in principle measures the stiffness of cement paste as hydration reaction progresses and the stiffness of paste in influenced by the free water within the paste with time.

4.3 Strength activity index

Figure 4.1 presents the 28-, 56-, 90-day compressive strength results of mortar samples made using the different binders. It is worth noting that the 56-d and 90-d strengths determination exceeded the 7-day or 28-day strength determination required by ASTM C618. The later-age strength

determination was to assess the effect of delayed pozzolanic reaction on strength, if any. This is to aid the proper classification of the materials and better understanding of the material behaviour. To achieve this, the percentage increase in strength with time was estimated. The increase in compressive strength from 28-day to 90-day was 14%, 24%, 10% and 9% respectively for PC, PC/FA, PC/C-700 and PC/C-800. The strength increase were minimal except for fly ash. This trend of result is expected for fly ash, as it is a known pozzolanic material and the amorphous content from Table 4.1 further corroborates this. More importantly, these results depict the corn cob ashes to be non-pozzolanic, and this is also evident in the amorphous content of the ashes (Table 4.1).

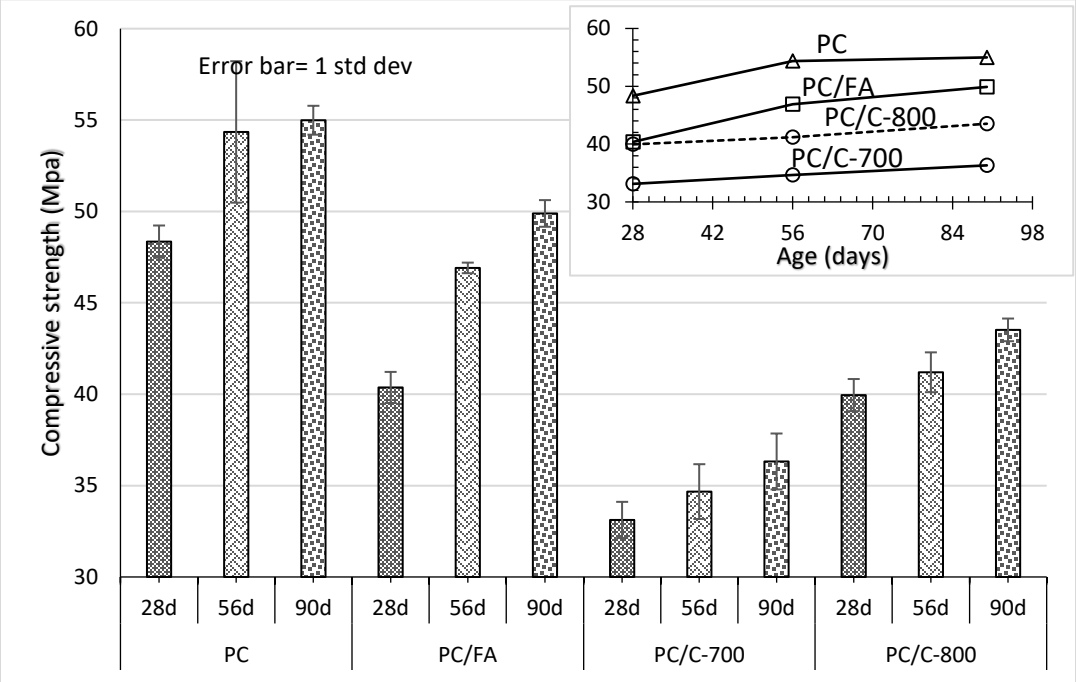

Figure 4.1: Compressive strength development of mortar cubes

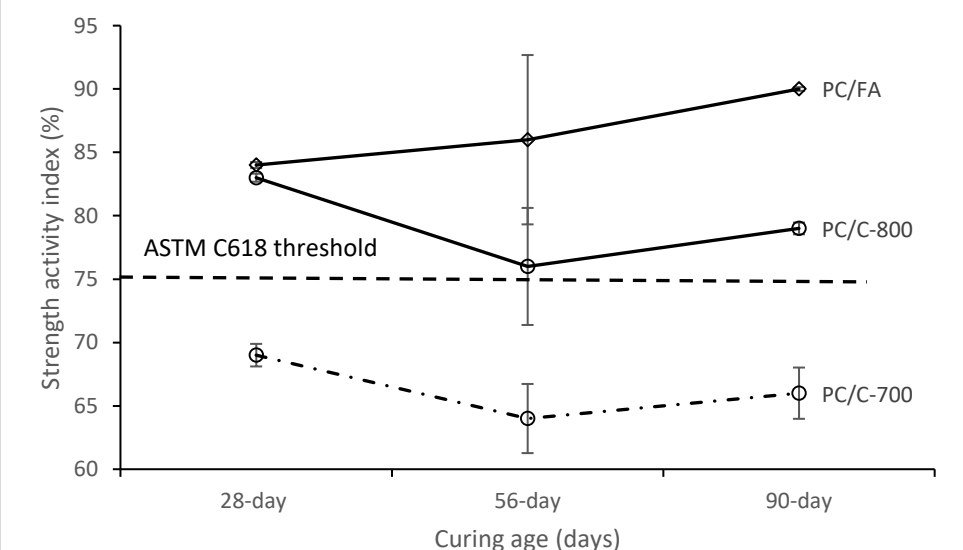

The plot of strength activity index (SAI) for the mortar mixes is presented in Figure 4.2. ASTM C618 stipulates a minimum SAI of 75% for a material to be classified as pozzolanic. The results show that both PC/FA and PC/C-800 exceeded the minimum requirement at all ages. This is expected for PC/FA, fly ash being pozzolanic as already discussed. However, the interpretation of this requirement as applied to C-800 does not depict it as being pozzolanic going by the low amorphous content of the ash and the low percentage increase in strength. This implies that the strength development is influenced by a different mechanism aside pozzolanic reaction and it is an indicator of the filler effect of CCA. This is one of the limitations of strength activity index as an indicator of pozzolanicity of SCMs as it is possible that largely crystalline materials can satisfy the 75% strength activity requirement. This limitation of SAI was also noted by Kalina et al. (2019).

The differences between the SAI of C-700 and C-800 beyond 28 days points to the differences in the surface activity of the two CCA samples, with C-800 being more surface active. It is believed that prior to the commencement of significant pozzolanic reaction in cementitious systems, the surfaces of SCMs acts as extra nucleation points to enhance the degree of reaction of plain PC. The creation of nucleation sites is further enhanced by the so called filler effect of SCMs, which is pronounced at early stage of cement hydration (Juenger & Siddique, 2015). The differences in the surface activity of the two CCAs is largely impacted by the calcination method with C-700 having more unburnt carbon evident in its dark grey colour. This further showed that calcination in a controlled environment can be beneficial to the performance of the material in cementitious system. Although the study of Memon & Khan, (2018) could not establish the amorphous content variation with calcination temperature, increasing temperature affects the reactivity of the material while a compromise need to be reached between obtaining a reactive material and eliminating the unburnt carbon.

The consistence in the SAI with increasing age for FA compared to C-700 and C-800 implies pozzolanic reaction in addition to hydration reaction of plain PC. The contribution of pozzolanic reaction to strength development increases with age. This shows the active participation of the amorphous phase in hydration process with pozzolanic reaction taking place through the consumption of portlandite released from the hydration of PC resulting in the formation of more C-S-H. The formation of more C-S-H enhances the performance i.e. the compressive strength and thus, the strength activity index of the mortars.

4.4 R3 Reactivity test results

The bound water contents of pastes prepared with FA, sand, C-700 and C-800 are presented in Table 4.2. The test R3 (rapid, relevant and reliable test) developed initially to assess the reactivity of calcined clay (Avet et al., 2016) was used by measuring the bound water given off by paste heated at 350°C for 2 hours. The conditioning of the paste with $Ca(OH)_2$ and sulphate to simulate hydration environment similar to plain PC brings about the formation of hydrates with bound water. R3 paste containing crushed andesite sand was used to benchmark the reactivity of each material.

Table 4.2: Bound water content of R3 paste

Material	**Bound water (g/100g)**
FA	6.16
C-800	3.44
C-700	2.89
Sand	1.73

The results depict the chemically bound water in the hydrates formed in the R3 paste that is released when the sample is heated at a temperature of 350°C. A correction for the bound water in the SCM in line with ASTM C1897-20 requirement was made by heating each SCM at a temperature of 350°C. While this correction may be necessary, applying it to ash accounts for the loss on ignition of the material at 350°C and its deduction from the bound water due to hydrates formation.

The values of the bound water for both C-700 and C-800 fall within the range of bound water defined by that for the sand (an inert material) and that for FA (a pozzolanic material). The bound water for FA is that formed in the hydrates emerging from the silicate and aluminate compounds (Al-Shmaisani et al., 2022). This is expected, FA being a known pozzolanic material. The higher bound water content in the corn cob ashes than in the sand is a clear indication that some degree of pozzolanic reaction took place, leading to the formation of hydrates. This was however limited by the low amorphous content of the materials. A comparison of this trend of results showed some similarity with the trend of result obtained for the SAI discussed in the previous section with FA having a higher activity index than the corn cob ashes.

4.5 Calorimetry test results

Figures 4.3 to 4.5 shows the heat flow curve during the first 48 hours of hydration for PC/FA paste and PC/CCA paste compared to PC/sand paste and 100% plain PC paste. The main characteristic features of the hydration reaction had occurred for all the mix within the 48 hours studied. Isothermal calorimetry has been useful in the study of the interaction of SCMs with plain PC and to understand the underlying hydration kinetics. The main outputs; the heat flow rate and the total heat have been useful to distinguish between reactive and non-reactive SCMs. In addition, it has enabled the distinction of the hydration reaction into different phases based on the rate of heat flow and the heat evolved with time since cement reaction with water is exothermic. The heat flow rate curve of common cements can be distinguished into four phases: dissolution period, dormant period (induction period), acceleration period (main heat peak period) and deceleration period (Bullard et al., 2011). Each of the phases has been linked to different mechanisms controlling the heat flow pattern most especially associated with the reactions of the main phases in PC namely the calcium silicates and the calcium aluminates.

FA and andesite crusher sand showed similar trend of heat evolution at the two replacement levels 15% and 30%. The slight difference in the heat flow rate of PC/FA and PC/sand (Fig. 4.3) compared to plain PC can be attributed to the decrease in PC content as the difference is proportional to decrease in PC content. This shows that the contribution to heat evolution is mainly from PC; PC reaction with water being exothermic. The heat flow curves in Figure 4.4 and Figure 4.5 show that the trend for the PC/C-700 and PC/C-800 differ appreciably from those of plain PC, PC/FA or PC/sand blends. Contrary to the effect of the andesite crusher sand, the replacement of

PC with corn cob ash affected the heat evolution process. This effect is pronounced at the induction phase and the acceleration phase than at the dissolution and deceleration phases of the hydration process.

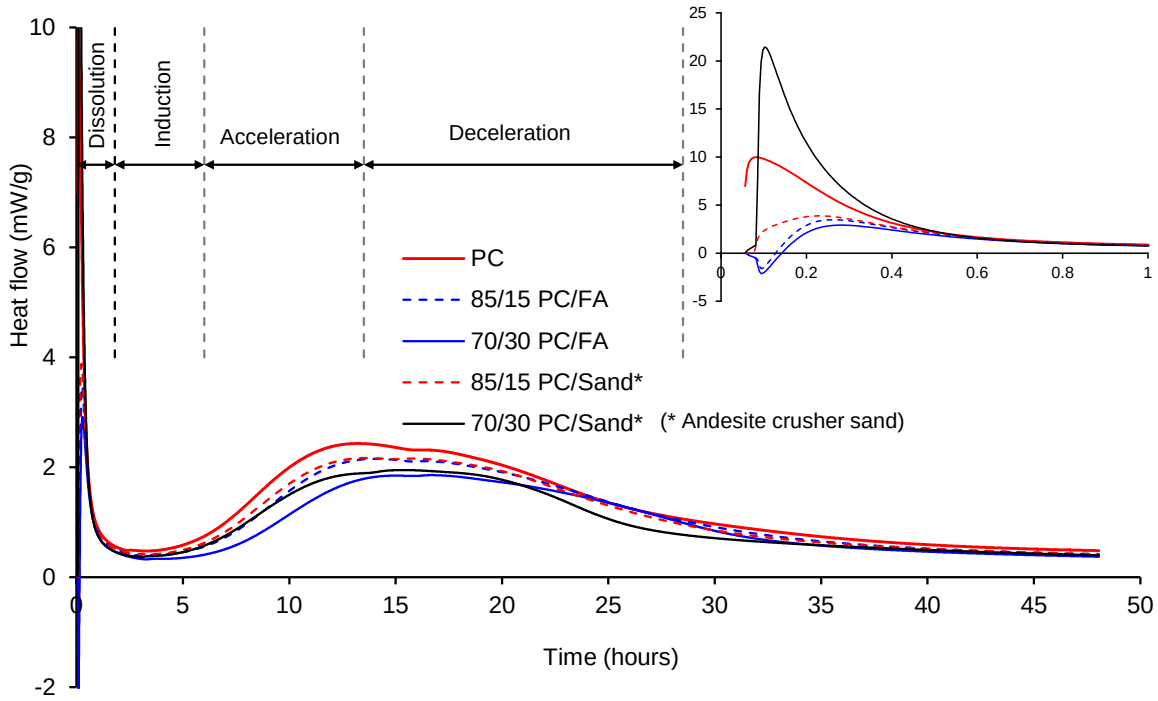

Figure 4.3: Heat flow curve of FA compared to PC and filler sand

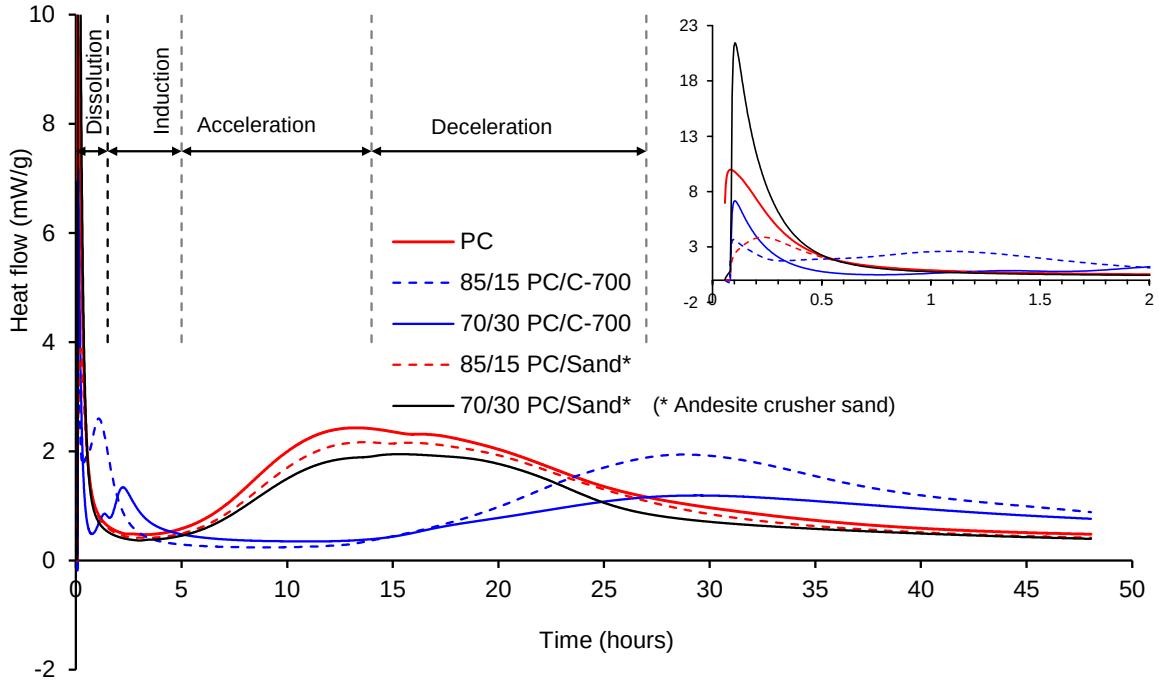

Figure 4.4: Heat flow curve of C700 compared to PC and filler sand

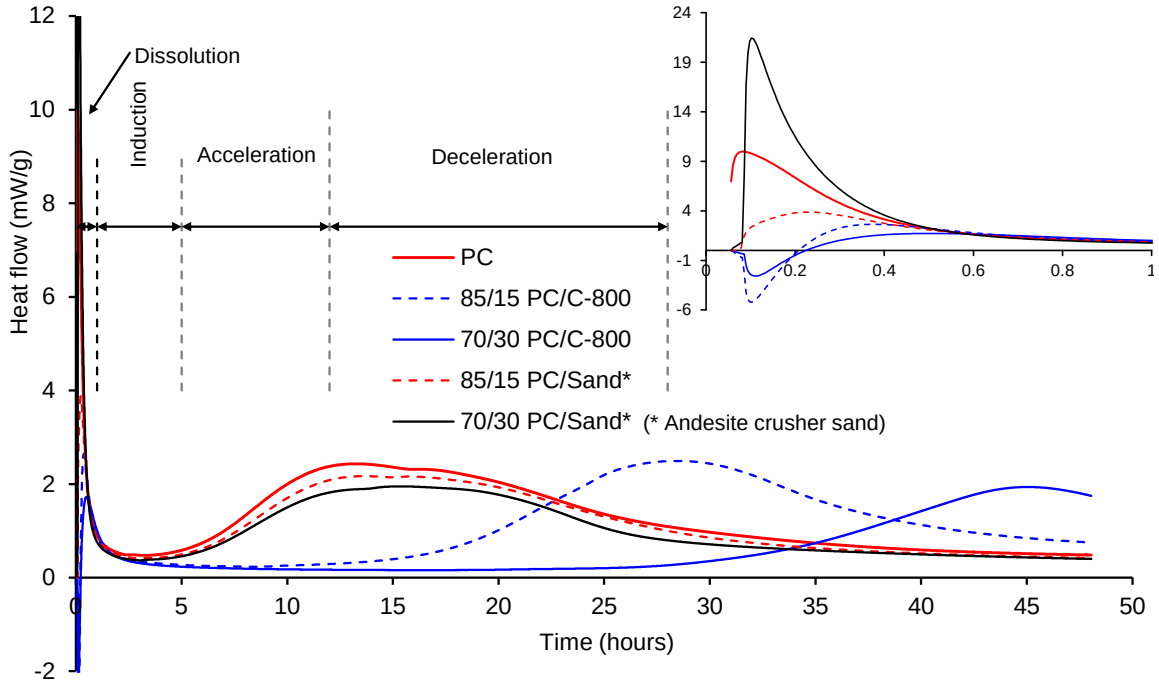

Figure 4.5: Heat flow curve of C800 compared to PC and filler sand

4.5.1 Dissolution period

Dissolution phase is often attributed to the dissolution of tricalcium silicate (C_3S) and the initial reaction of cement particles with water upon wetting (Bullard et al., 2011). Both reactions add up to the heat released and the heat flow measured for this phase in an isothermal calorimetry. The dissolution of C_3S is said to occur rapidly in the first few seconds in contact with water. From the heat flow curves, for both FA and CCA, there is an initial gain of heat from the environment resulting in a negative heat flow recorded within the first few minute of contact with water. This was subsequently followed by heat loss to the environment still within few seconds of contact with water. It could be said that the subsequent positive heat flow is due to the dissolution of C_3S, which far outweighs the heat flow of the initial reaction of cement upon the addition of water, although when compared to plain PC, this heat flow is lower. The lower heat flow depicts a lower dissolution rate of C_3S in the blends coupled with the reduced PC content as a result of replacement with either FA or CCA.

The first deceleration leading to the induction phase following the initial rapid reaction can be observed in all the blends and this phase has been attributed to formation of a thin protective layer of initial C-S-H, which is metastable and different from the C-S-H formed at later ages (E.M. Gartner et al., 2002). The transition due to the formation of this layer terminates the initial rapid reaction of C_3S. The nucleation and precipitation of this layer of hydrate is as a result of the concentration of calcium and silica reaching a critical solubility product. Gartner and Gaidis (1989) further opined that the protective layer is a metastable C-S-H formed on the surface of the dissolving C_3S, while the layer is not uniform in thickness but with greater thickness around the reactive sites (Juilland et al., 2010). It is said that the progressive consumption of the metastable hydrate by the precipitation of a more stable C-S-H results in a more rapid dissolution of the anhydrous C_3S and terminates the slow reaction process. It is obvious from the results that if this mechanism is considered, it was further compounded by the inclusion of CCA and to certain extent by FA resulting in a lower heat flow rate than plain PC and andesite crusher sand, while the heat flow rate further varies with quantity of ash. This first deceleration phase extends into the induction period characterised by slowdown of reaction evident in a trough on the heat flow curve.

4.5.2 Induction period

The induction period is associated with low heat flow immediately after the dissolution phase as shown on each of the curves above. The phase is associated with the retardation of the initial reaction of the silicates compound in plain PC most especially C_3S (alite) (Juilland et al., 2010). Several mechanisms have been said to be responsible for this phase; the formation of a protective layer of hydrate on the surface of C_3S which limits the further dissolution of the anhydrous phase and in recent times, it has been attributed to the slow dissolution rate due to undersaturation of the solution with respect to alite. Each of the mechanisms put forward showed that the dissolution of C_3S contributes significantly to the existence of this phase. This also implied that the prolongation of this phase is as a result of a likely interference with the dissolution of C_3S and nucleation of C-S-H.

A slight difference can be noticed between the heat evolution of andesite crusher sand and plain PC attributed to the dilution effect of the sand. Report has shown that inert fillers like limestone and quartz powder have little or no effect on this phase compared to plain PC (Berodier & Scrivener, 2014; Dittrich et al., 2014). A consideration of the effect of FA and CCA on the induction period showed that FA had a little interference with the reaction of C_3S taking place, while CCA had a significant effect evident in the prolonged duration of the phase. This effect most especially for CCA can be linked to the low rate of heat evolution during the dissolution phase leading to the slow dissolution of C_3S and slow growth of initial C-S-H formed (Bullard et al., 2011). This results in a low concentration of Ca^{2+} ions in solution, while the absorption of these ions on the surface of the CCA further delays the nucleation and growth of C-S-H (Han, He, Zhang, & Liu, 2017). The interference with the rate controlling mechanism is significant in the presence of CCA than in the presence of FA. Going by the protective layer theory, the formation and disruption of this layer is prolonged in the presence of CCA than in FA. This can be linked to the dissolution of K^+ ion from CCA competing with the dissociated Ca^{2+} ions from C_3S in solution and at the surface of the C_3S and CCA thereby retarding the rate of nucleation of C-S-H on the surfaces. The prolonged induction phase is expected to have an effect on compressive strength development of CCA due to the delayed nucleation and growth of C-S-H.

A further consideration of the induction phase showed that C-800 prolonged the length of this phase longer than C-700. This is however not expected with C-800 given its lower potassium oxide

content and LOI compared to C-700. Compared to the andesite crusher sand, CCA (being largely crystalline) has an inherent material behaviour that elongates the induction phase by delaying the mechanism responsible for the acceleration phase. Although prolongation of the induction phase is sometimes reported for FA when compared to plain PC and inert fillers (De la Varga et al., 2018; Dittrich et al., 2014), the CCAs are largely crystalline, which affects their reactivity. The influence of the CCAs on the induction and acceleration periods is dependent on the replacement level with the effect more pronounced at higher replacement level. This is as a result of the dilution effect due to reduced PC content and this implies that increasing CCA content has an effect on plain PC hydration and as such increasing content has no advantage on the system.

4.5.3 The main heat peak

This phase comprises of an acceleration phase which succeed the induction phase and a deceleration phase, which follows the acceleration phase. This phase is attributed to the nucleation and growth of C-S-H, formation of ettringite, consumption of gypsum (E.M. Gartner et al., 2002). The evolution of the main heat peak was observed in all the systems studied, while each material presents different influence on the phase. Both FA and andesite crusher sand have a similar heat flow trend with plain PC but a slightly lower heat flow peak indicative of the reduced plain PC content in both systems. For fly ash, the heat flow is further influenced by the content of the ash with the acceleration slope occurring slightly later at 30% than at 15%. This can be linked to its dilution effect indicating that FA did not contribute to the chemical reaction taking place. In the PC-CCA systems, the evolution of this phase was delayed due to the prolonged induction phase yielding a different trend line compared to plain PC, PC-FA and PC-sand systems. For the CCA, effect on this phase is dependent on the replacement level with effect more pronounced at higher replacement level. This is largely due to the crystalline structure of the CCAs with a likely effect on the nucleation and growth of C-S-H due to the dilution effect of using CCA. Similar to the induction phase, effect on main heat peak is influenced by increasing ash content. PC/C-800 has a higher main peak than PC/C-700, an effect that can be linked to the differences in their LOI and this can have an effect on their effectiveness in bridging the hydrating PC particles with C-800 more effective than C-700. This is evident in the similar heat peak of C-800 (at 15%) to that of plain PC and those of PC/sand and PC/FA at 15% content.

The mechanisms controlling the evolution of the acceleration phase (the nucleation and growth of stable C-S-H, reaction of the aluminates phases and formation of the AFt and AFm phases) terminates the induction period, although, the second peak on the deceleration slope attributed to the reaction of aluminate is not clearly distinguishable on the heat flow curves, especially for PC/C-700 and PC/C-800. This can be linked to the alumina content of the plain PC, which is the main hydrating particle. A consideration of the mechanisms controlling this phase showed that CCA has more significant effect on the mechanism than FA. The differences can be traced to the differences in their effect on the induction phase as previously explained. The lower heat flow peak in PC/C-700 could mean a lower nucleation and growth rate of C-S-H and reaction of aluminates compared with plain PC, PC/sand and PC/FA. The different behaviour of the two CCAs point to the enhanced surface activity of PC/C-800 due to the lower LOI resulting in a higher heat peak compared to C-700. The particle surface providing more surface area for the nucleation and growth of hydration products.

4.5.4 Intermediate heat peak effect of C700

The intermediate heat peak notable on the heat flow curve of PC/C-700 between the dissolution phase and induction phase is absent in PC/C-800. The intensity of the peak decreases with increasing ash content. The peak has an acceleration and deceleration slope, which is sharp and occurred over a shorter period compared to the main heat peak. The peak is associated to chemical reaction (s) taking place linked to the high K_2O content of C-700. The dissolution of K_2O on contact with water increases the pH of the solution which can induce further dissolution of the C_3S and a likely reaction of the C_3A beyond the first deceleration and prior to induction period. The addition of alkali was found to be beneficial to the formation of AFt at very early ages especially for PC with high C_3A content (Huang & Yan, 2019). A likely interference between the dissociated Ca^{2+} and K^+ ions may have contributed to the retardation of the hydration reaction, hence, delaying progress to the induction phase.

A similar peak was observed in the heat flow curve presented by Shakouri et al. (2020). The ash used in the study has a higher potassium oxide content (38%) and loss on ignition (23%) than C-700. This further showed that this exhibited behaviour is impacted by the material characteristics. It is also likely that the appearance of this peak may have been impacted by the carbon content linked to the calcination method, as the absence of this peak in C-800 further confirmed this. The

appearance of the peak between the dissolution phase and the induction phase needs further investigation, especially with respect to the formation of hydration product that may have resulted in its development as well as understanding the likely interference with plain PC hydration. This will further aid the understanding of the mechanism of reaction of CCA and its interaction with PC towards enhancing its use as SCM.

4.5.5 Total heat output

The total heat output per mass of binder as a function of time is presented in Figures 4.6 to 4.8. The total heat released by each of the system studied varied. For PC/FA blend, the trend line of heat released is similar to that of plain PC and PC/sand showing a slow rate of heat released between time zero and around the first 10 hours. This slow rate of heat output is influenced by the induction period on the heat flow curve and at the termination of this period there is a progressive release of heat. Between 10 hours and about 25 hours of hydration, the increase in the slope showed this increasing rate of reaction, which can be attributed to the increase in the reaction of the hydrating phases. Beyond this, the slope of the curve tends to flattens showing a further decrease in reaction rate. Compared to plain PC, both fly ash and filler sand system have a lower total heat which varied with replacement level beyond the first 10 hours. A closer look showed that the effect of replacement level on heat release is more noticeable in fly ash than in the filler sand. In terms of the total heat output, the heat released is found to be in the order PC > filler sand > fly ash. The lower heat output in both the filler sand and fly ash can be seen as a result of the reduction in the PC content in both systems due to partial replacement by the materials. The variation of the heat released with replacement level further alludes to this. However, that the heat released in both fly ash and filler sand is not equal showed that there is an inherent material characteristic effect responsible for the difference in the heat output in both systems.

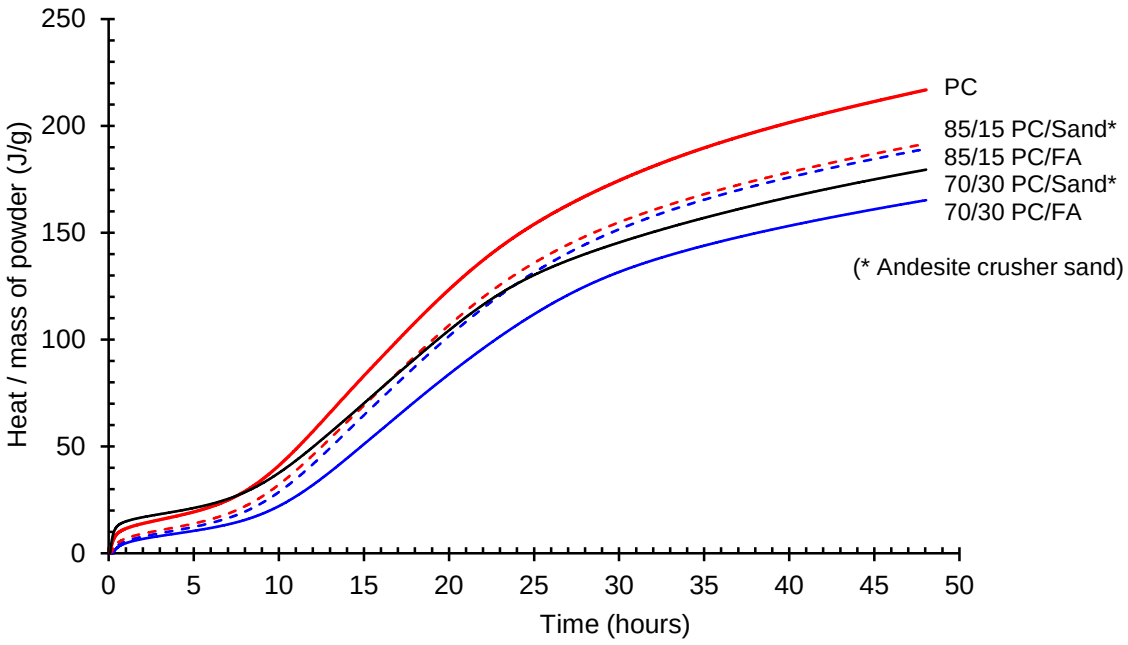

Figure 4.6: Comparison of total heat output PC, PC/FA and PC/sand

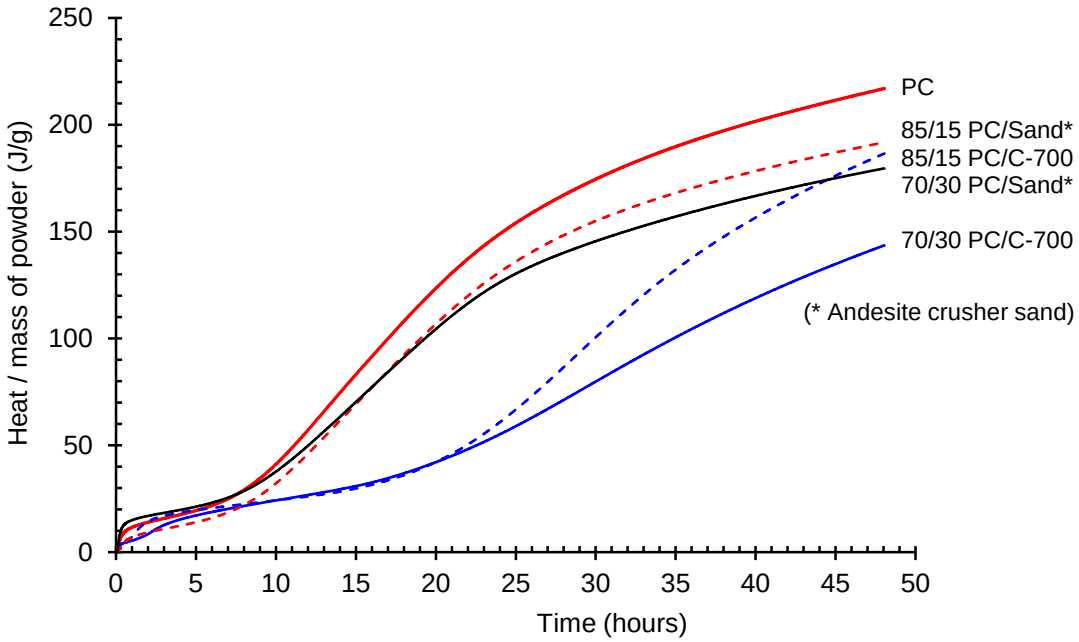

Figure 4.7: Comparison of total heat output for PC, PC/C700 and PC/sand

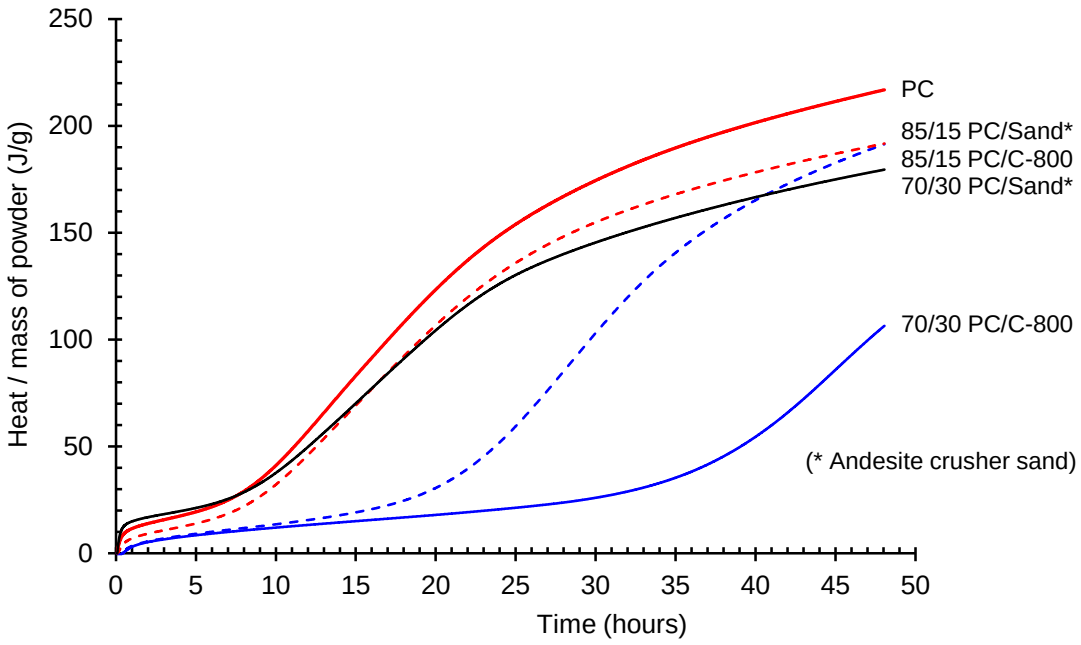

Figure 4.8: Comparison of total heat output for PC, PC/C800 and PC/sand

The total heat output for the CCAs showed a different trend line compared to that of plain PC and filler sand. The period of slow heat release rate is extended beyond the first 10 hours unlike in fly ash system, for C-700, the period is extended to up to about 22 hours, while for C-800 the period is extended up to about 15 hours and 30 hours for replacement levels 15% and 30% respectively. The total heat output for the two CCAs is lower than that of plain PC and is similar to that of fly ash except for C-800 at 30% replacement level, which is very low and this is affected by the extended induction period. The difference in the trend line of CCAs and the filler sand showed a difference in the behaviour of both materials despite both being largely crystalline, while the filler sand showed no significant interference with PC hydration, the CCAs has a noticeable effect on PC hydration evident in the shape and slope of the curve compared to that of the filler sand and plain PC. The evolution of the main slope for C-700 began at around 22 hours and for C-800 at around 20 hours, although this is further influenced by the ash content. The evolution of the main slope almost coincides with the evolution of the main heat peak on the heat flow curve attributed to the reaction of reacting phases (C_3S and C_3A). A comparison with the calorimetry data presented

in the study of Shakouri et al. (2020) for CCA showed that there is no delay in the evolution of the main slope recorded in their study as obtained in this study. This could probably be linked to the chloride content in the study of Shakouri et al. (2020), although the chloride content was not determined in this study. $CaCl_2$ is known to be an accelerator, the combined effect of dissociating Ca^{2+} and the Cl^- could have had an accelerating effect eliminating the delay noticed in this study. This further showed the variability in properties of SCMs from agricultural origin mostly impacted by the geographical location and agricultural practices as most of this wastes are lignocellulosic in nature. The minerals are often picked up from the soil and soil nutrients during the lifecycle of the crop (Gilbe et al., 2008).

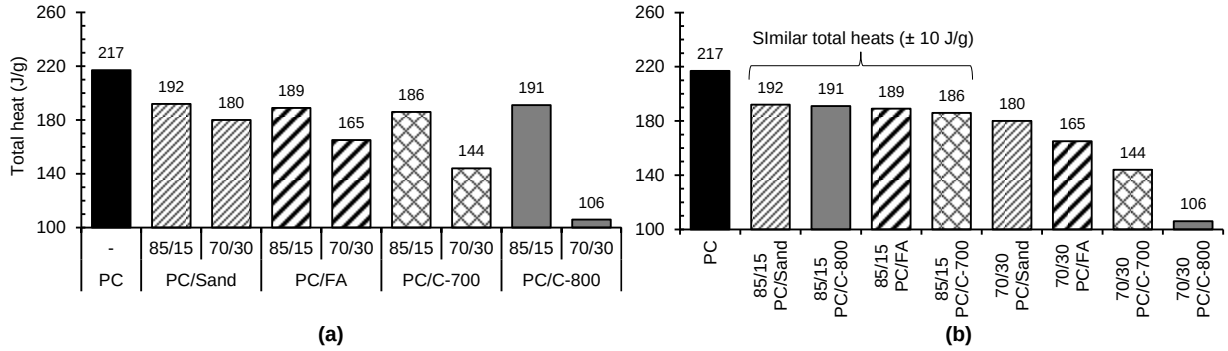

Figure 4.9: Values of total heat measured up to 48 hours

The values of total heat at the end of 48 hours of isothermal calorimetry test is presented in Figure 4.9. The values decreases with increasing replacement level for all blends depicting the effect of reducing plain PC content. The total heat value for C-700 and C-800 is similar to those of FA and sand at 15% content. This shows that replacement of PC with CCA at 15% do not affect the total heat output, although it does influences the rate of heat rise.

4.6 Compressive strength of concrete results

The performance of C-700 with respect to compressive strength development in concrete was investigated in furtherance to understanding the material behaviour and aid proper classification of the material. C-700 being the least reactive from SAI results gives the worst case scenario with respect to strength development given its largely crystalline nature and the high potassium oxide content. The mechanism of its contribution to strength development is also considered vis-à-vis

the dilution effect and filler effect. The result of the compressive strength is presented in Figures 4.10 and 4.11 while the rate of gain of strength for each of the mixes is presented in Table 4.3.

The results show that compressive strength varies with both curing age and w/b ratio and this is consistent with strength development pattern in cementitious systems (Simnani, 2017; Singh, Munjal, & Thammishetti, 2015). There is a gain in strength depicting that hydration is taking place in all the mixes studied and this is consistent with strength development characteristics of conventional concrete. For plain PC system, at w/b ratio of 0.4, the rate of gain of strength increases up to 28 days and subsequently decreases with increasing curing age which shows an increase in rate of hydration of PC particles up to 28 days. For w/b ratio of 0.6, the rate of gain of strength decreases with increasing curing age and this is observed to be a decrease in the rate of hydration of PC with age and increasing w/b ratio depicting an early higher degree of hydration. For PC-FA system, the rate of gain of strength increases with increasing FA content for all the ages investigated depicting the active participation of FA in strength development process despite the reduction in plain PC content. This is expected and further confirms the pozzolanic reaction of FA and its contribution alongside hydration reaction of PC to strength development in concrete (Deschner et al., 2012). The rate of gain of strength at w/b ratio of 0.6 is higher than at w/b ratio of 0.4. This is attributed to a higher degree of hydration relative to the w/b ratio and the lower strength values which is more sensitive to small variation in measured values. There is a significant strength gain between 7-day and 28-day (23%, $p= 0.0076$) than between 28-day and 90-day (15%, $p=0.101$), which shows that there is an early compensation for the dilution effect of PC reduction through the contribution of pozzolanic reaction at early ages in addition to the filler effect of FA (Florian Deschner et al., 2012).

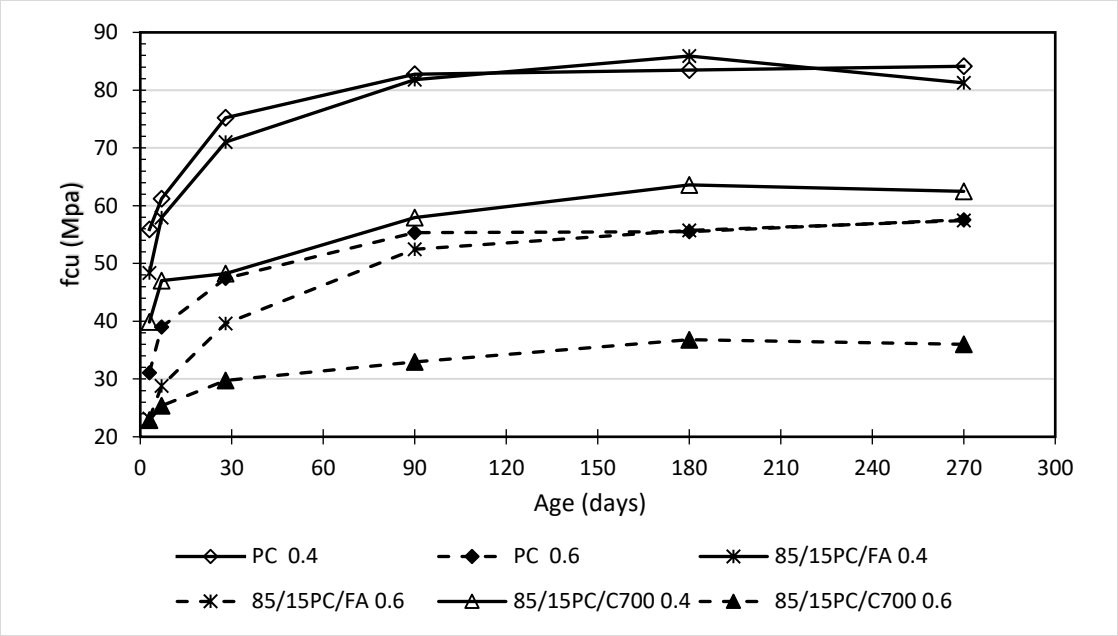

Figure 4.10: Comparison of compressive strength of concrete at 15% replacement level

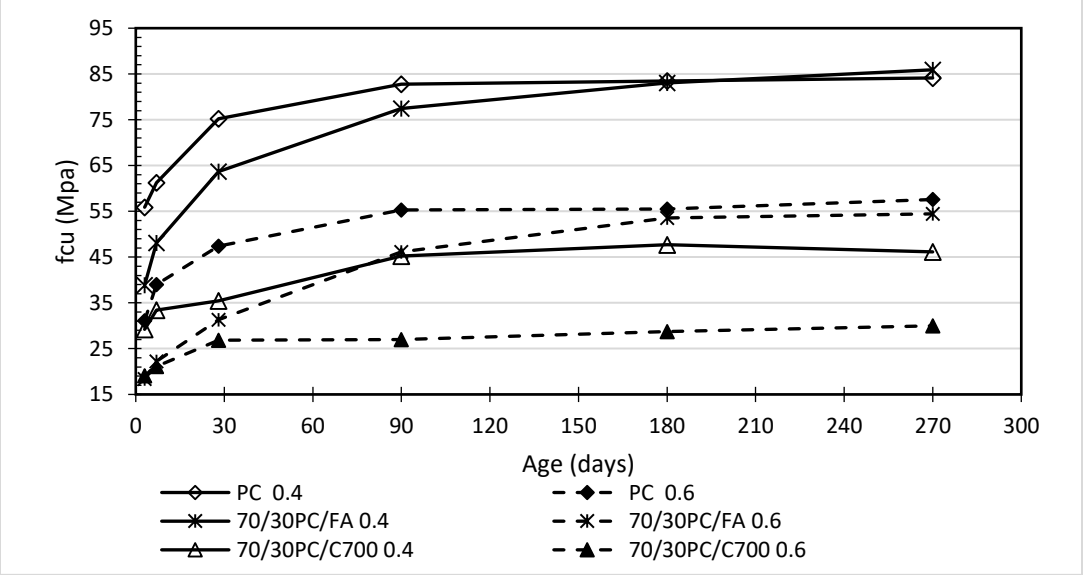

Figure 4.11: Comparison of compressive strength of concrete at 30% replacement level

Table 4.3: Rate of gain of compressive strength in percentage

Mix/Age	**Percentage strength gain (%)**				
	7d	**28d**	**90d**	**180d**	**270d**

PC4	9.52	22.89	10.04	0.83	0.08
85/15FA-4	19.83	22.59	15.19	5	-0.05
70/30FA-4	23.67	32.52	21.59	7.27	3.41
85/15C-700-4	18.04	2.55	20.06	9.76	-1.76
70/30C-700-4	14.27	6.11	27.59	5.48	-3.23
PC6	25.37	21.60	16.68	0.36	3.71
85/15FA-6	24.21	37.63	32.47	6.25	3.01
70/30FA-6	20.77	41.06	47.37	16.03	1.64
85/15C-700-6	10.98	17.19	10.86	11.68	-2.17
70/30C-700-6	10.36	27.41	0.48	6.48	4.31

For PC-C-700 blend, similar to PC and PC/FA, compressive strength increases with increasing curing age up to 180 days and decreases with increasing w/b ratio and increasing ash content. The reduction in strength with increasing ash content and increasing w/b ratio is evidenced of the dilution effect of partially replacing plain PC with CCA and increasing water content beyond that required for hydration. Also, compared to PC/FA blend, there is no clear trend in the rate of gain of strength with age and replacement level compared to PC/FA at the same w/b ratio and replacement level. This shows that the inclusion of CCA affects the rate of gain of strength and this is attributed to its filler effect given the largely crystalline nature of the CCA particles. The strength values of PC/FA blend is significantly higher at all ages and replacement levels except 180-day than those of PC/C-700 with a corresponding p-values of 0.0032, 0.00061, 0.00078, 0.031 and 0.026 for 3-, 7-, 28-, 90, and 270-day respectively for 15% content, while for 30% content the p-values are 0.00032, 0.00073, 0.0012, 0.00019 and 0.00065 for 3-, 7-, 28-, 90-, and 270-day respectively. The higher strength of PC/FA is expected given the moderate amorphous content of FA compared to the largely crystalline particles of CCA. This implies that strength development in PC/C-700 is mainly controlled by the hydration of plain PC particles which is the dominant chemical reaction contributing to the formation of C-S-H and hence strength development.

Generally, for the PC/C-700 mixes, there is a significant strength gain up to 90-days beyond which the strength gain is marginal. This shows a decrease in the rate of PC hydration with age, hence, the 90 day strength can be said to be sufficient to explain the long term strength gain of the mixes. Also, there is a reduction in strength at 270 days typical of all replacement levels and w/b ratio showing that there is no strength gained beyond 180 days. Although, a similar effect was noticed in fly ash sample at 15% replacement level and w/b ratio of 0.4, the reason for this could not be ascertained. To better understand the mechanism of strength development in C-700 given its high crystalline structure, the filler and dilution effect were further investigated.

4.6.1 Dilution effect of PC/C700 compared to PC/FA

The partial replacement of plain PC with C-700 results in a dilution effect which has two phases; one is the reduction in the quantity of plain PC and second is the increase in the water to plain PC ratio (w/c) (Cyr, Lawrence, & Ringot, 2006). The dilution effect is considered for only w/b ratio of 0.4 corresponding to w/b ratio of high strength concrete and theoretical w/b ratio for complete hydration. The increased w/c ratio considers the water to plain PC only (i.e. minus the SCM) and this varies with replacement level. The dilution effect of each SCM was studied by considering the increased w/c ratio corresponding to each replacement level, by comparing the compressive strength at each replacement level for each material with the compressive strength of plain PC at the increased w/c ratio. Thus for w/b ratio of 0.4, at 15% and 30% replacement level, the corresponding w/c ratios are 0.47 and 0.57 respectively. The dilution effect is considered up to 28 days at which significant degree of PC hydration would have taken place in each of the system and the influence of the difference in w/pc ratio can be distinguished in the systems.

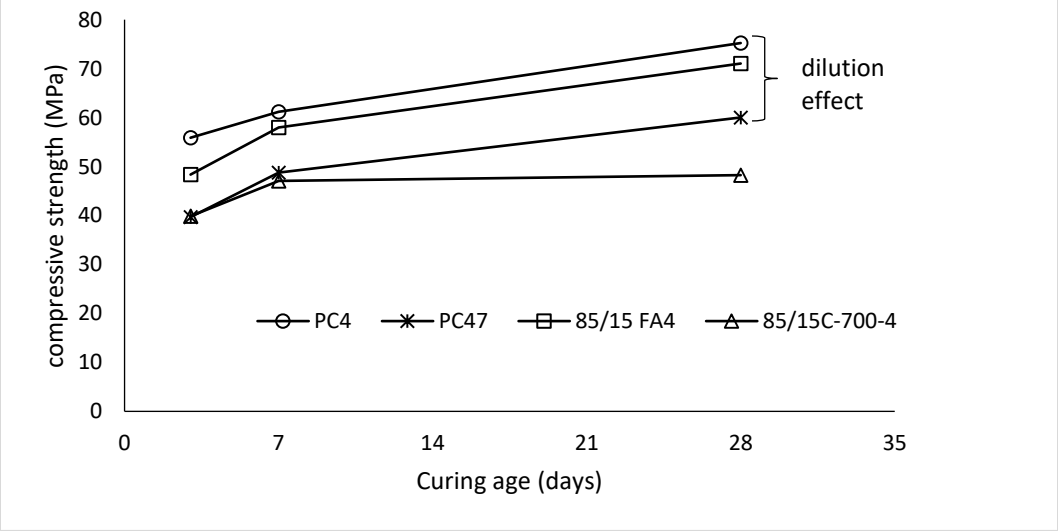

Figure 4.12: Comparison of dilution effect at 15% replacement level

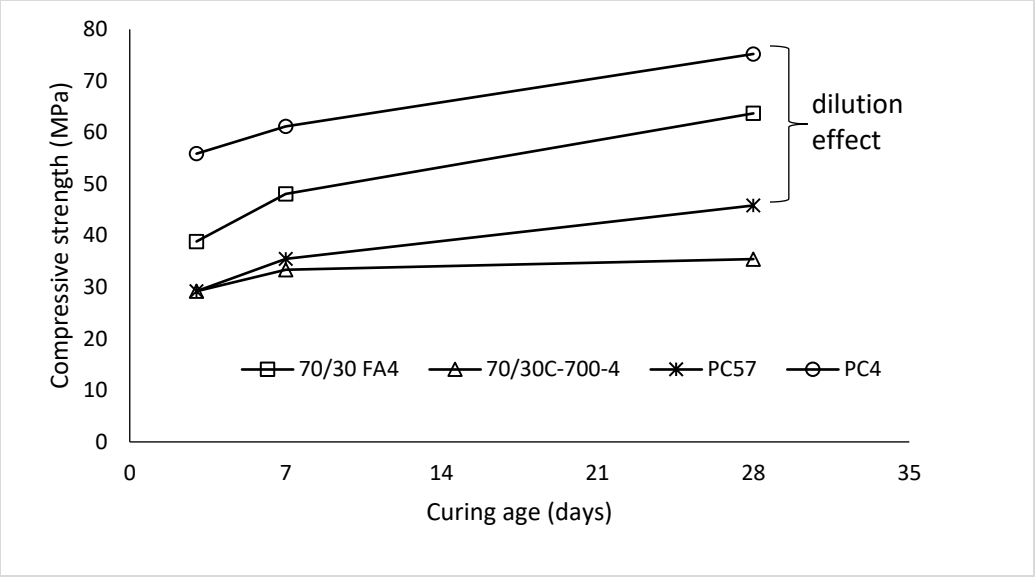

Figure 4.13: Comparison of dilution effect at 30% replacement level

Dilution effect of SCMs in cementitious system has an effect on the porosity and packing of particles within the systems and thus, a consequential effect on the compressive strength development (Cyr, Lawrence, & Ringot, 2005; Lothenbach et al., 2011). In spite of the increased w/pc ratio, the w/b ratio is lower, hence, the particles in PC/SCM system are better packed with a reduction in the size of the pores but it is also likely that there will be increase in the total porosity necessitated by the increase in the fine particles present in the system. Increased fine particles implied increase interparticle space within the paste. The extent of hydration and pozzolanic product formation reduces the interparticle space.

Figures 4.12 and 4.13 showed that the strength of PC/FA is higher than the strength at the increased w/pc ratio (i.e. PC47 and PC 57) for all replacement levels, while the strength of PC/CCA is either similar to or lower than the strength of the increased w/pc ratio depending on the age. This means the inclusion of both CCA and FA has a dilution effect given a lower strength than plain PC at w/b ratio of 0.4, which is consequential of the reduction in PC content. The reduction in PC content means a reduction in the hydration product formation with an impact on the compressive strength.

On the other hand, the higher strength in FA than the increased w/pc ratio means that part of the dilution effect had been compensated for either through enhanced hydration of PC and/or better packing of the hydration products with an implied effect on the porosity of the system. The particles of the fly ash are packed between PC particles thereby reducing the interparticle spaces

and spaces between the paste and the aggregates. As the interparticle spaces is reduced, the surfaces of the SCM creates extra surface for the nucleation and growth of hydration products thereby densifying the microstructure of the system. This was noted in the work of Detwiler & Mehta (1989) on silica fume that compressive strength can be enhanced by the use of fine particles of SCM through the mechanism of better packing of particles and hydration products and grain refinement.

However, for PC/CCA, the strength of the increased w/pc ratio is higher at both 7 and 28 days. With the inclusion of the CCA, it is expected that there is a better packing of the particles (given its finer particle size than plain PC, Table 4.1) but the dilution effect resulting from PC content reduction outweighs the improved packing of particles and hydration products within the interparticle spaces. This coupled with a likely retardation effect on PC hydration resulted in a lower strength than the increased w/pc ratio, hence the dilution effect was not adequately compensated for. The likely slowdown of PC hydration may be associated with the unburnt carbon present in the ash and possibly the high potassium oxide content although the mechanism of influence is not clearly understood. A likely explanation may be that the precipitation of calcium silicate is hindered by the increased potassium oxide concentration in the pore solution while enhancing calcium aluminate precipitation. This may have contributed to the similar strength in CCA samples and the increased w/pc ratio samples at early age notably at age 3 days beyond which there is a reduction in strength in CCA samples compared to the increased w/pc ratio showing an interference with strength development.

In addition, another property that may have contributed to the dilution effect mechanism is the particle size effect, as the fly ash is finer than CCA. The finer particle size (see Table 4.1) of FA implies that concrete made from it is denser than concrete made from CCA due to the better packing of particles which contributed to the enhanced strength in PC-FA concrete. This was noted in the study of Goldman & Bentur (1993) that compressive strength of microfillers increases with increasing fineness of particles. The effect of the dilution effect on strength is more dominant in CCA than in FA and as such can limit the extent of CCA use in cementitious systems.

4.6.2 Filler effect of PC/C700 compared to PC/FA

Another effect attributed to the use of SCMs in cementitious systems is the filler effect leading to better packing of particles and enhanced heterogeneous nucleation contributing to improved

properties and performance of the system (Berodier & Scrivener, 2014). Filler effect is a physical

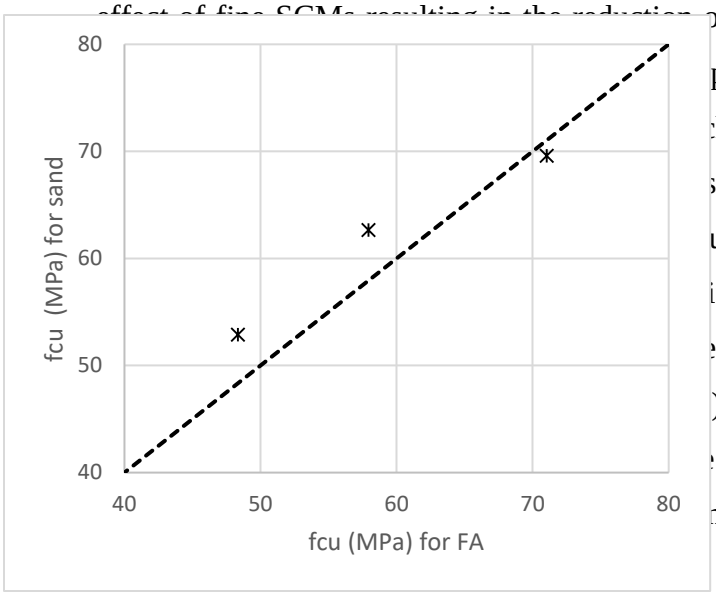

(a)

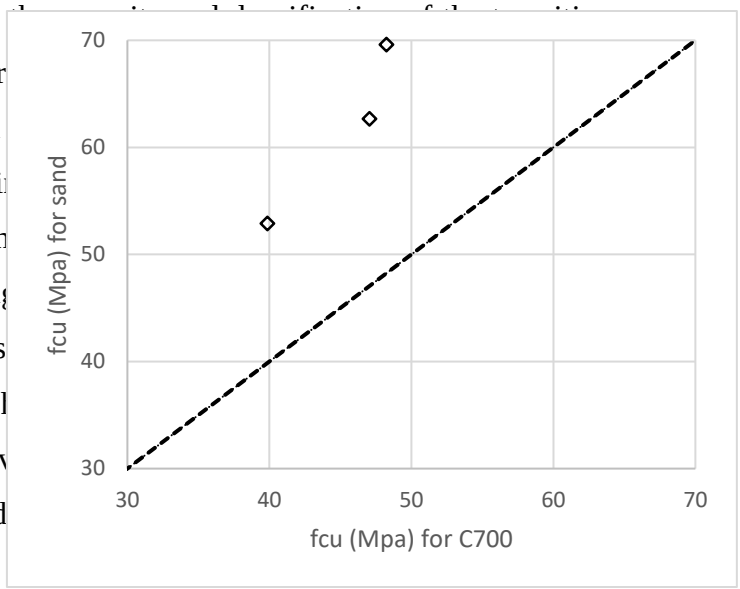

(b)

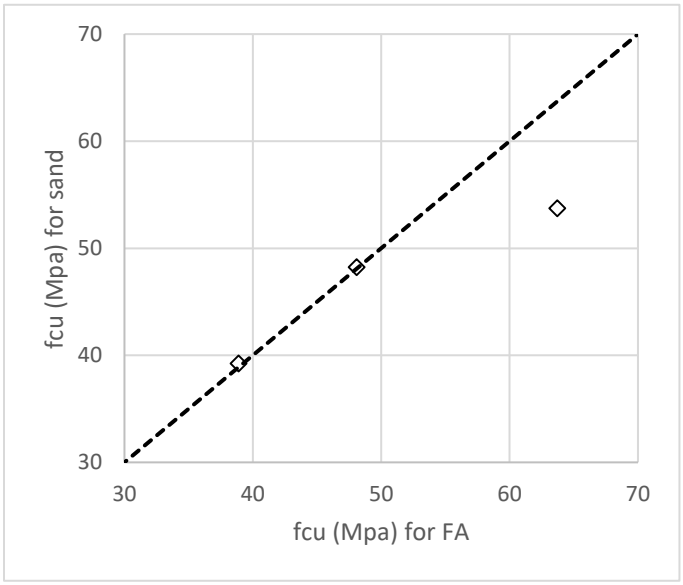

(a)

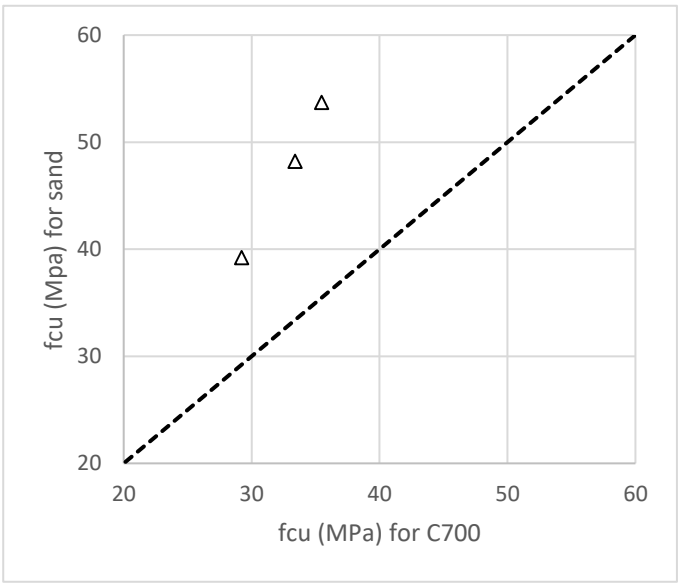

(b)

Figure 4.15: Comparison of filler effect at 30% replacement level and w/b ratio of 0.4

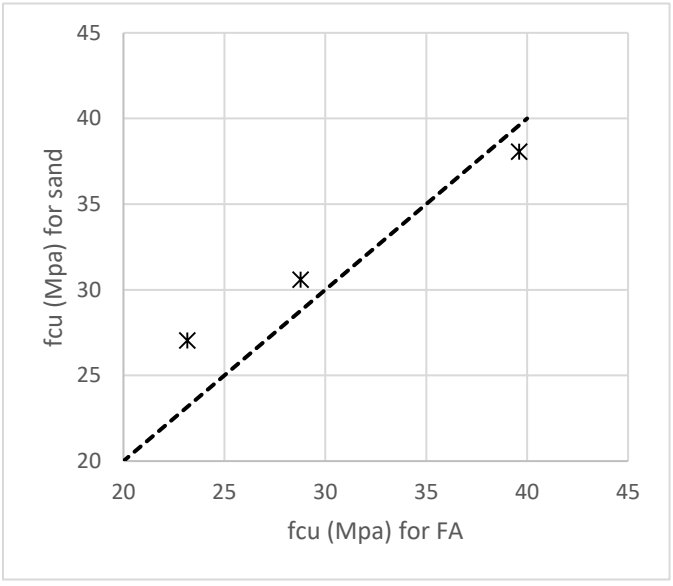

(a)

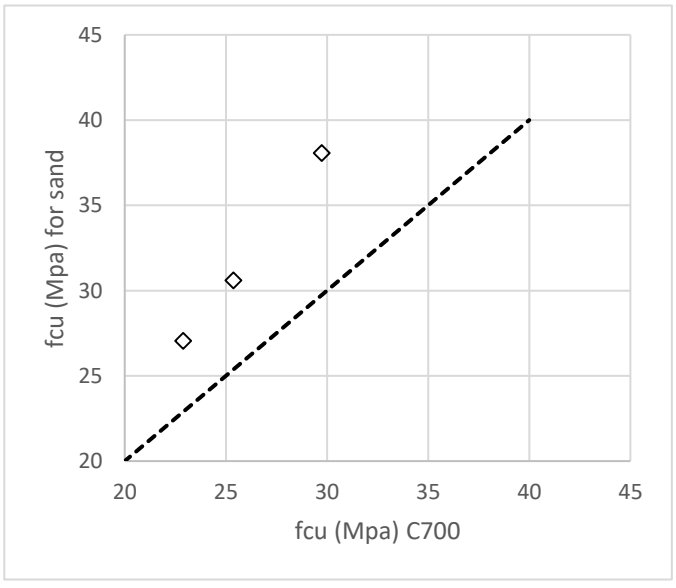

(b)

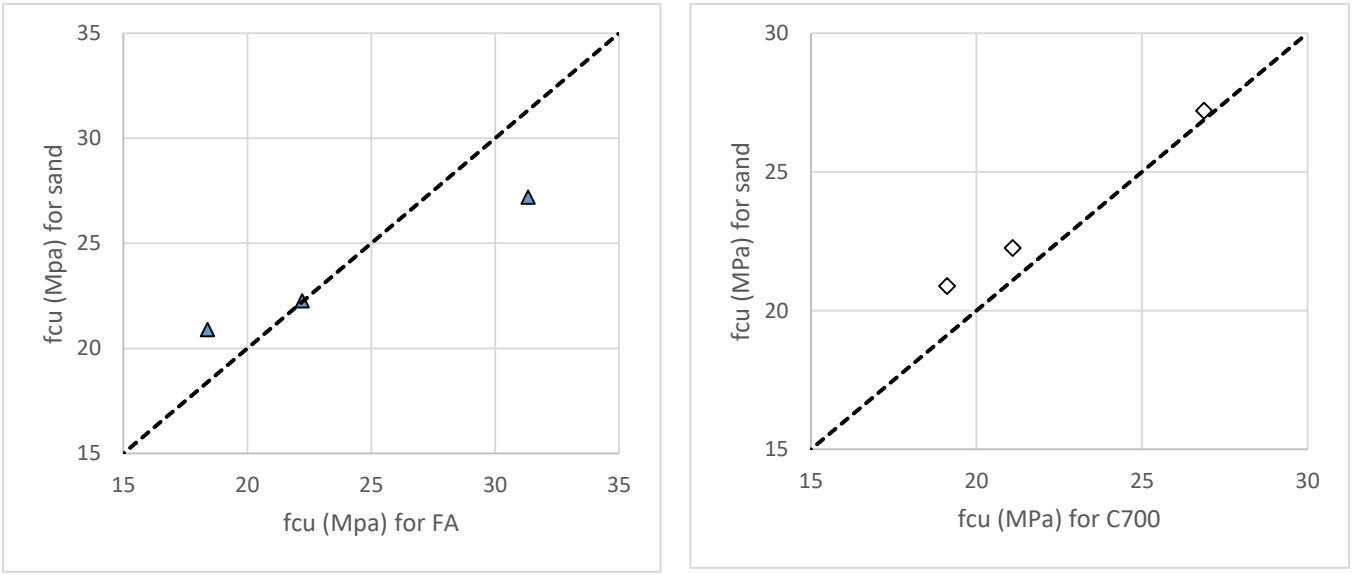

(a) (b)

Figure 4.17: Comparison of filler effect at 30% replacement level and w/b ratio of 0.6

The plot of the filler effect of CCA and FA is presented in Figures 4.14 to 4.17 with more details presented in Appendix B. The filler effect of each material varies with replacement level. From Figures 4.14(a) and 4.16(a), the strength of PC/FA was lower than that of the PC/sand (inert material) at early ages (3 and 7 days). This shows that the contribution of the filler effect to strength was more significant in the andesite crusher sand than in FA at early ages. The filler effect of FA at higher replacement level (30%) results in a strength similar to those of the sand at early age (Figure 4.15(a) and 4.17(a)). The filler effect of FA is significant at 30% than at 15% showing that the influence of the filler effect on strength is a function of PC replacement level. This confirmed the effectiveness of FA as a PC replacement material up to 30% content. The higher strength in PC/FA at 28-days, implies that the filler effect of FA is an early age effect, while the higher strength is an evidence of additional mechanism contributing to strength development. The

contribution of pozzolanic effect to strength development is evident at both replacement levels with the strength being higher than that of the sand.

Figure 4.14 (b) to 4.17(b) shows that compared to FA, the strength of C-700 is lower than that of the andesite crusher sand at all ages despite the similarity in particle size distribution of both materials. The contribution to strength by the filler effect is minimal for C-700 and the effect extended to 28-days compared to the 7-days of FA. The lower strength compared to the sand showed the superior quality of the sand as a filler material than C-700 despite the highly crystalline structure of the two materials. This further indicates that a good quantity of amorphous content is essential for C-700 to compensating for its dilution effect and hence maximise the filler effect of its fineness. It is therefore necessary to optimise the calcination process of C-700 to obtain amorphous CCA. It is important to note that corn cob ash obtained through open air burning and milled to improve its fineness can still be useful in non-structural applications while its use in structural application will be subject to durability requirement(s). Also, for the filler effect to be significant in CCA samples, the particle size may need to be finer than that of the sand (inert filler) and likewise the unburnt carbon should be reduced to minimise its effect on the properties of concrete. It is possible that the unburnt carbon contributes to the high surface area with water adsorbing at these surfaces and limiting availability of water for PC hydration while creating pockets of weak points within the paste.

From the results, the influence of the microfiller effect on strength development affected by the particle size effect is significant in FA with finer particle size than in C-700 (Goldman & Bentur, 1993; Jaturapitakkul, Tangpagasit, Songmue, & Kiattikomol, 2011). Microfiller effect in concrete is linked to the densification of the transition zone as a result of reduced bleeding and efficient packing at the interface (Goldman & Bentur, 1993). This mechanism was seen in effect in PC/FA concrete leading to higher strength than in PC/CCA concrete and the difference in behaviour is not totally due to differences in particle size. The crystallinity of the CCA also contributes to its behaviour but may not be the only limitation to its performance given that the inert filler used is also largely crystalline. There is an inherent material behaviour in CCA, which can limit its use as a filler and/or SCM.

4.7 Influence of alkali content on compressive strength development

To explain the low strength development in CCA concrete, the effect of the high alkali content is considered. There has been evidence of binding of silica to potassium or sodium rather than to calcium (L'Hôpital, Lothenbach, Scrivener, & Kulik, 2016) resulting in the modification of the C-S-H and C-A-S-H structure. The modification of C-S-H structure was noted by Li, et al. (2016) to be responsible for the inferior mechanical performance of the C-S-H gel leading to a lower compressive strength as the C-S-H formed has a lower Ca/Si ratio. The binding of alkalis in the C-S-H structure showed a competition between the calcium cations and alkali cations to make up for the negative surface charge due to high pH (Lothenbach & Nonat, 2015). The net negative charge at C-S-H surface was linked to the de-protonation of the silanol (≡SiOH and ≡SiO^-) sites with Ca^{2+} being able to balance the negative charge than the monovalent cations (K^+ and Na^+). However, the binding of either divalent or monovalent ions depends on the pH and Ca/Si ratio with lower Ca/Si ratio favouring uptake of monovalent cations in the presence of hydroxides. For PC/CCA system, the binding of alkali cations (K^+ and Na^+) to the C-S-H formed creates a weak link between the Calcium and silicate site with the C-S-H formed (C-K(Na)-S-H) being less strong than that formed with calcium (Ca^{2+}), which has a stronger electrostatic interaction (Lothenbach & Nonat, 2015). This also explains the difference in the strength between the ground crusher sand (SS) and CCA despite having a similar particle size, which are mostly crystalline. The high solubility of the monovalent ions in the pore solution further attest to the less strong bond formed compared to the divalent calcium ions

4.8 Pore solution analysis

The composition of the pore solution was analysed in order to understand the mechanisms and interaction between the solid and liquid phases in hydrating compounds (Vollpracht, Lothenbach, Snellings, & Haufe, 2016). The concentration of alkalis (K^+ and Na^+ ions), hydroxyl ion (OH^-), Ca, Al and Si in the extracted pore solution were measured in order to further understand the stability of phases and the likely contribution to the performance of the system. The concentration of the alkalis and hydroxide is considered important given that their concentration impact on the durability of cementitious system most especially mortar and concrete. The later age pore solution analysis was considered in this study to help in the understanding of the likely influence of the test materials on the durability of cementitious systems most especially with respect to the dissolution

of phases in the presence of moisture if such favourable condition occur. Both the hydration of plain PC and pozzolanic reaction of SCMs are continuous processes, which influence pore solution chemistry and as such the concentration of the alkali oxides and hydroxides can be useful in predicting the durability of concrete structures due to solubility of phases in hardened concrete and as diagnostic tool in ascertaining the state of deterioration with respect to deterioration process associated with dissolution of phases.

4.8.1 Concentration of alkalis and hydroxyl ion

The hydroxyl ion (OH^-) concentration at 28 and 90 days curing is presented in Figure 4.18. Portlandite (CH) is precipitated during the hydration of the calcium silicate phases but significantly during C_3S hydration. The solubility of this phase has been linked to deterioration of concrete induced by carbonation due to reaction of carbon dioxide with CH (D. C. Park, 2008). The measured concentration varies with mix type and SCM content in the mix and also with w/b ratio of the mix. Generally, for all the mixes investigated, OH^- concentration decreases with increasing w/b ratio and increasing replacement level. This can be seen as a dilution effect due to the reduced cement content with increasing w/b ratio at the same water content and the diminishing growth rate of C-S-H with increasing w/b ratio (Ley-hernandez, Lapeyre, Cook, Kumar, & Feys, 2018), hence a reduction in OH^- concentration. This trend is expected given that plain PC is the only source of CH in the system. The OH^- concentration reduces with increasing curing age which implies its precipitation reduces with age and hence increase in stability with increasing age. On careful observation of each material, the mechanism differs. For FA, the high OH at 28 days implies that significant pozzolanic reaction is yet to take place, as the reactive phase of FA is expected to react with the CH produced from PC hydration. The variation of concentration with replacement level is a consequence of the reduction in plain PC content due to the inclusion of FA in the mix. The result do not show a clear pattern regarding the consumption of CH by the reactive phase of FA as the trend do not show a clear reduction in OH concentration as this is expected to contribute to strength development in concrete. The contribution of SCMs to strength development in concrete is often influenced by a combination of mechanisms one of which is the reaction between SCM and CH resulting in the formation of extra C-S-H leading to reduction in the CH content of the system (Lothenbach et al., 2011). In another instance, the high concentration comparable to PC in FA is inexplicable as pozzolanic reaction is expected to have commenced at later ages, it is rather envisaged to be due to enhanced PC hydration at the early ages of cement

hydration. A cross comparison with pH (Fig. 4.19) showed a similar trend in the pH value of FA compared to plain PC. At 90 days, the concentration varies with w/b ratio, while it is higher than that of plain PC at w/b ratio of 0.4, it is lower at w/b ratio of 0.6. The higher concentration showed evidence of continued PC hydration as discussed earlier while the lower concentration is a pointer to the dilution effect of increased w/b ratio.

For both C-700 and C-800, concentration varies with replacement level with lower concentration at higher replacement level reflective of the reduction in PC content and thus a dilution effect. Also, the concentration at w/b ratio of 0.6 is lower than at w/b ratio of 0.4 also indicative of a dilution effect. This dilution effect compared to FA is influenced by the largely crystalline structure of the CCAs and inherent effect of CCA on PC hydration with respect to dissolution of calcium silicate phases. The lower OH concentration in CCA compared to plain PC showed that the effect of replacing PC with CCA dominates over enhanced PC hydration compared to FA which enhances PC hydration. This is an indication that the dissolution and precipitation of alite and belite phases which produces CH is reduced leading to lower OH concentration. A cross comparison of pH value (Figure 4.19) shows that CCA unlike FA lowers the pH of the system slightly compared to plain PC system. This may have been influenced by the unburnt carbon content (LOI), which is likely to reduce the alkalinity of the system as carbon is non-reactive.

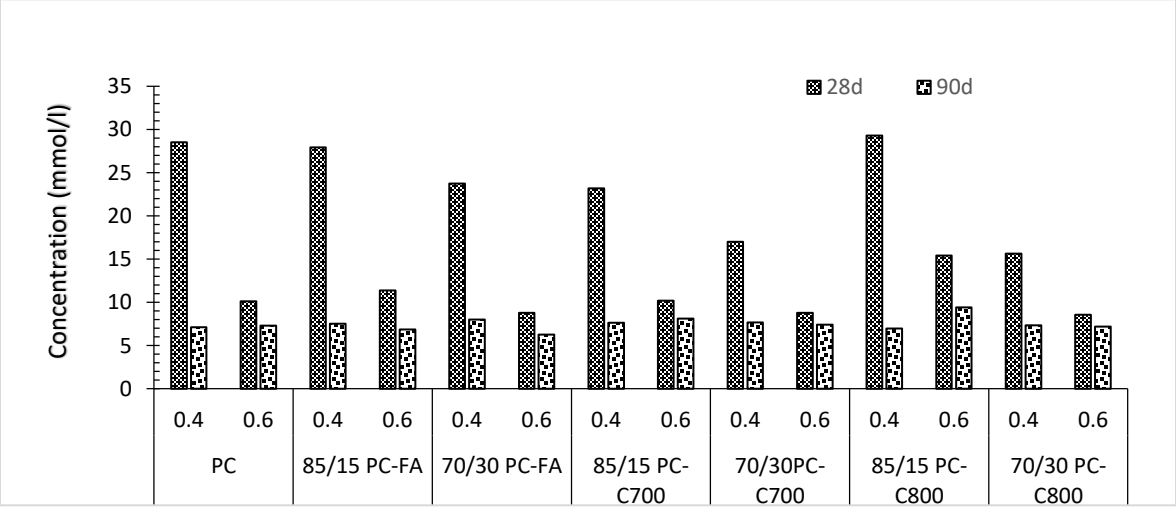

Figure 4.18: Variation of OH ion concentration with age and w/b ratio

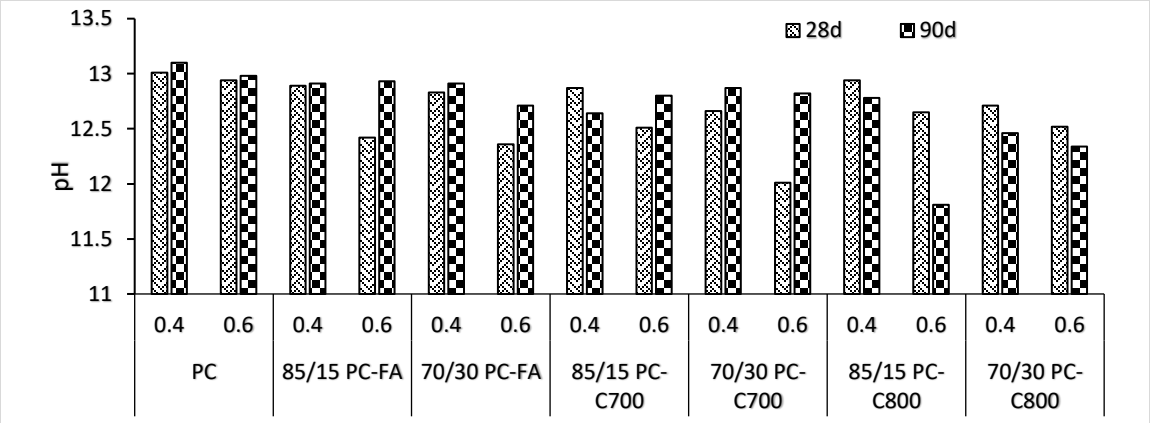

Figure 4.19: Variation of pH of pore solution with age and w/b ratio

For alkalis, the alkalis of interest are those of potassium and sodium, which have been noted to have an impact on pore solution due to their high solubility. Figure 4.20 shows that the concentration of potassium in the CCA samples is quite higher than those of plain PC and FA. This reflects the high potassium content in the raw material and indicates that a significant part of potassium is highly soluble in the presence of water. It can be said that the concentration increases with age to for some mix showing weak binding of potassium ion to C-S-H with an increase in the precipitation of potassium with age or the high solubility of potassium ion in solution. Likewise, concentration mostly reduces with w/b ratio showing a dilution effect with increasing w/b ratio. For FA, potassium concentration is similar to that of plain PC irrespective of replacement level or w/b ratio.

Also, Figure 4.21 shows the concentration of sodium and its variation with age. For CCA, like potassium, the concentration of sodium is higher than those of plain PC and FA. For CCA, sodium concentration increases with age and replacement level showing that there is an increase in precipitation with age and replacement level. This also implies that sodium like potassium is highly soluble in the presence of water and given favourable condition may easily be leached out of cementitious systems. The solubility of both potassium and sodium (alkali) in the presence of moisture had been linked to deterioration mechanism of alkali-silica/aggregate reaction (ASR/AAR) given favourable condition most especially the presence of reactive aggregates (L'Hôpital et al., 2016).

Alkali content in cement is expressed as a sodium oxide equivalent (Na_2O_e) by converting the potassium content to a sodium equivalent with a limit of 0.6% by weight of cement (Fulton, 2021). The Na_2O_e for both CCA studied exceeds the 0.6 limit and when compared to other studies on CCA use in cementitious system (Adesanya & Raheem, 2009b; Shakouri et al., 2020), it further showed that Na_2O_e of CCA is higher than 0.6 and this is a likely indication that its use may increase the risk of ASR if favourable conditions exist. Other consequences of high alkali content of cement are prolonged final setting, reduced compressive strength, increased drying shrinkage and increase in the volume of permeable voids in high performance mortar (Zhengqi Li et al., 2016). Also, low amount of portlandite at high concentration of alkali with a preferential binding of silica to potassium or sodium rather than to calcium has been reported (L'Hôpital et al., 2016). As part of the calcium is being replaced by the alkali ion at the surface and in the interlayer, there is a modification of the structure of the C-S-H and C-A-S-H with a likely effect on the strength and pore structure of the hydration product formed. Therefore, the high alkali content of CCA may be a limitation to its use in cementitious system, especially where alkali silica reaction or alkali aggregate reaction is envisaged to be a challenge. This is also an indication of the need for pre-treatment of the raw cobs (e.g. leaching with water (Jenkins, Bakker, & Wei, 1996)) prior to calcination in order to reduce significantly and/or eliminate the alkali content.

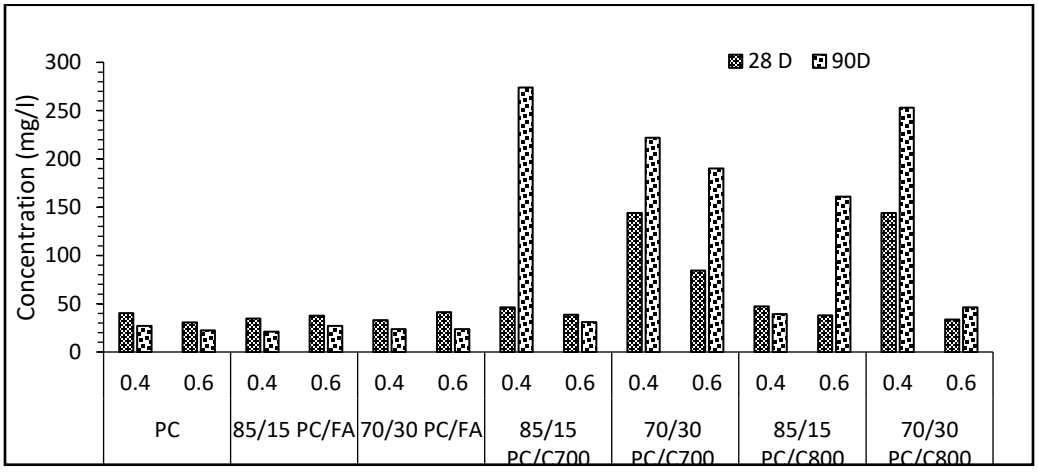

Figure 4.20: Variation of potassium ion concentration with age and w/b ratio

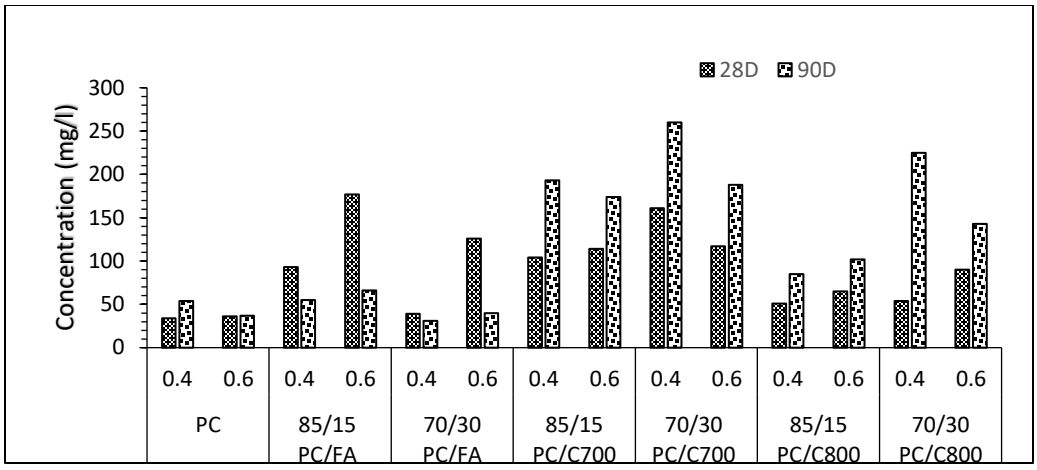

Figure 4.21: Variation of sodium ion concentration with age and w/b ratio

4.8.2 Concentration of calcium, silica and aluminium ions in solution

The variation in the concentration of calcium, silica and aluminium in the pore solution is presented in Figures 4.22 to 4.24. The concentration of calcium in the pore solution is high compared to the others and this is due to the solubility of CH, which is considered a major contributor to the calcium concentration. The higher concentration in PC system is majorly due to the continued PC hydration, which led to an increase in concentration with age while the decrease in concentration with increasing w/b ratio showed a dilution effect, which is expected. For FA, the lower concentration compared to plain PC is an indication of the dilution effect due to its inclusion in the system as well as the likely pozzolanic reaction, which consumes part of the CH produced in the system. The result also showed that Calcium concentration is a better indicator of pozzolanic reaction with age than OH^- concentration. This is so as the variation with age and w/b ratio can be seen. The low concentration of both silica and aluminium in the pore solution is an indication of the stability of phases containing them and binding in hydration product with a higher concentration in the paste than in the pores. The contents in pore solution are likely from the unreacted cement particles.

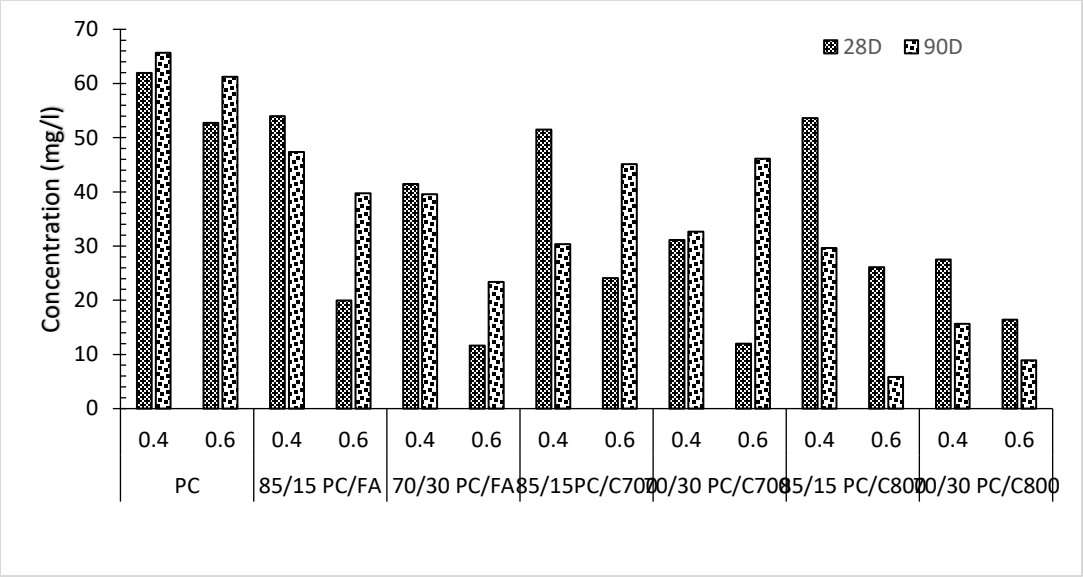

Figure 4.22: Variation of calcium ion concentration with age and w/b ratio

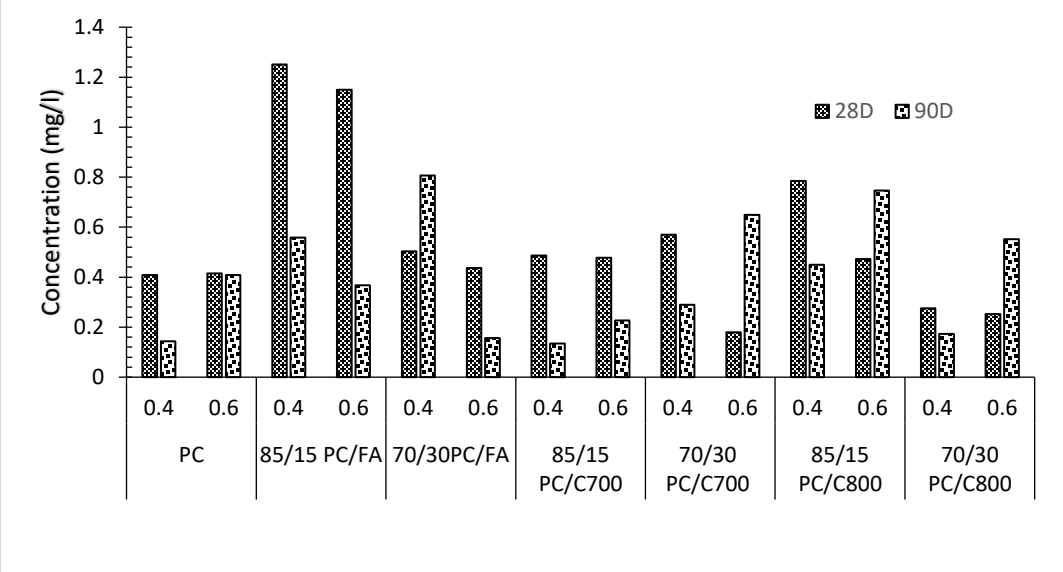

Figure 4.23: Variation of silica ion concentration with age and w/b ratio

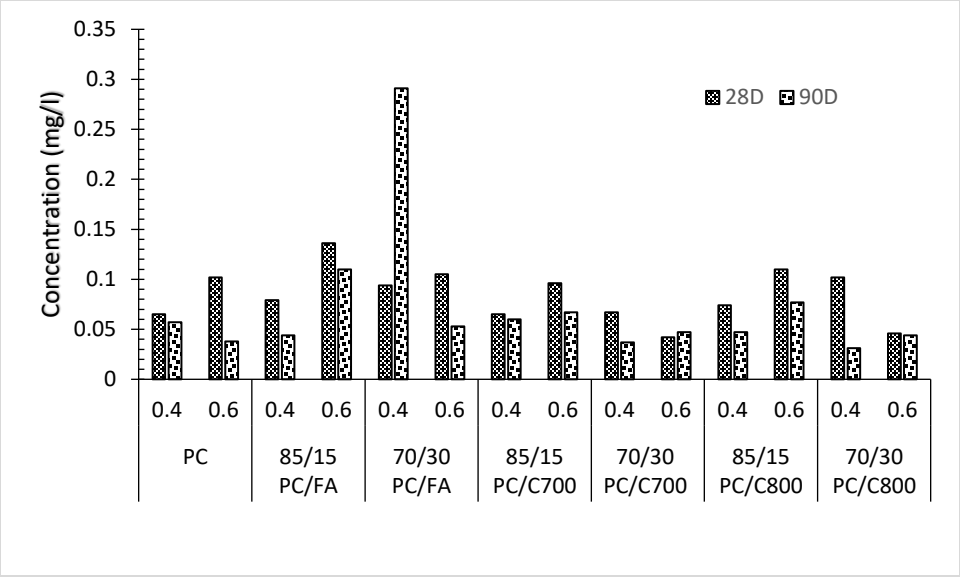

Figure 4.24: Variation of aluminium ion concentration with age and w/b ratio

4.9 Drying shrinkage results

The drying shrinkage strain with time is presented in Figure 4.25 to Figure 4.29. The results show that the rate of drying of the specimens vary with the binder type, water to binder ratio, duration of initial curing prior to testing and PC replacement level. The shrinkage strain for all the mixes increases with time. The shrinkage strain increases at an increasing rate for the first two weeks (this is subsequently refer to as the early period of drying) irrespective of whether initial water curing process was done or not. This rapid development of strain is followed by a decreasing rate of increase in strain. This is evident in the steep slope of the curve at the early drying period followed by a gradual flattening of the curve showing that the rate of drying at the early period was rapid before slowing down beyond the first two weeks. This implies that the rate of drying at early period of drying differs to the rate at later period of drying and this is largely impacted by the differences in the relative humidity influenced by the moisture gradient between the sample and the environment at these stages of drying.

At the early period of drying (the first two weeks), the internal relative humidity of the samples is high compared to the relative humidity of the exposure environment, there is a net loss of moisture to the environment, which is largely controlled by capillary forces. The loss of moisture through the capillary pores is induced by the surface tension formed in the capillary pores as a result of water-vapour meniscus formed in partially filled pores (Di Bella et al., 2017). The surface tension

induces capillary stress on the wall of the pores leading to a compressive stress on the surrounding solid phase thereby resulting in deformation (Bentz, 2005). Similarly, as hydration is in progress during the early drying period, part of the internal water is consumed with a preference for adsorbed water at interparticle pores, which are smaller in comparison to the capillary pores. Water is drawn from these pores to the surface of the developing C-S-H, the loss of moisture leads to a reduction in the interparticle pore size which tend to compress the particles as well as the C-S-H layers leading to shrinkage.

The average strain of the early period (first two weeks) of drying for PC-FA at all w/b ratio and replacement levels is lower compared to plain PC (p-value range from 0.0013 to 0.0124) except at 15% and w/b ratio of 0.6 which is similar (p-value of 0.499). The average strain for PC-CCA is significantly higher compared to plain PC (p-value range from 8.001E-07 to 8.69E-05). This shows that the inclusion of CCA increases drying shrinkage, an effect attributed to the unburnt carbon content. The unburnt carbon due to its surface area is a potential site for adsorption of water, as drying proceeds, the disjoining pressure between the surfaces decreases as the adsorbed water is lost to the environment. The interparticle distances reduces as water is lost to the environment leading to macroscopic deformation. This is in addition to the deformation induced by capillary tension hence the higher shrinkage in CCA system.

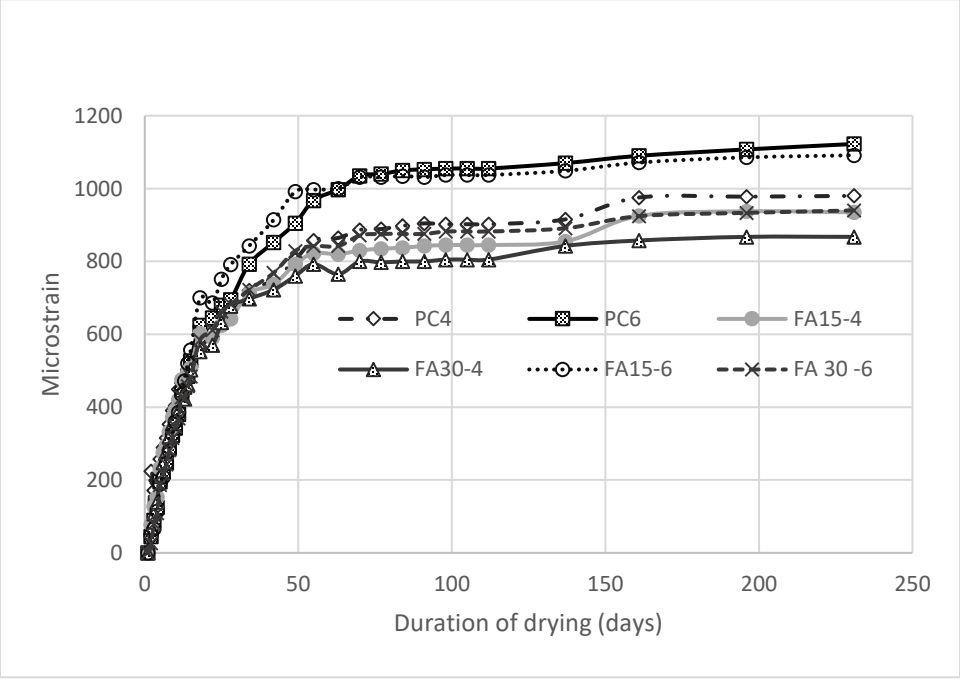

Figure 4.25: Shrinkage strain of FA compared to plain PC for air-cured samples

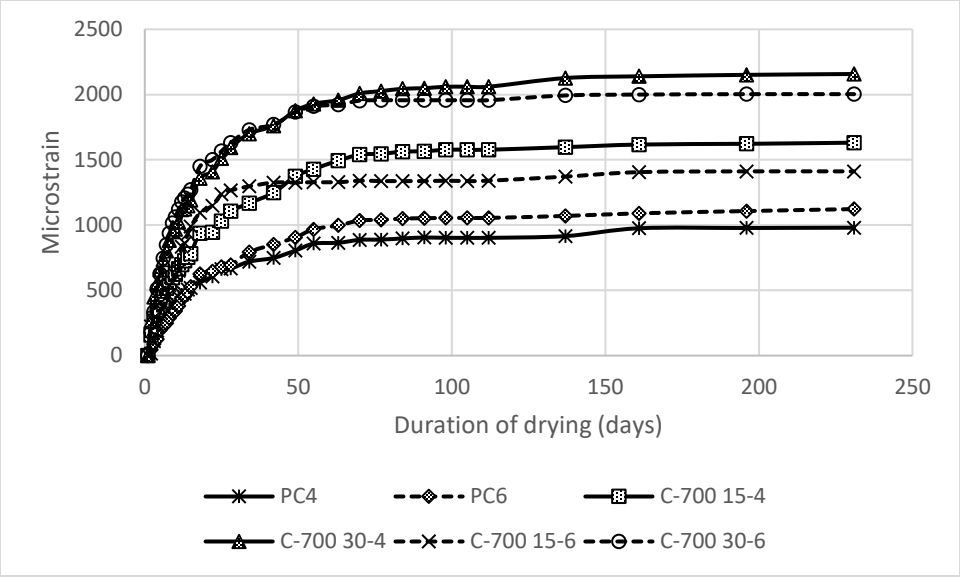

Figure 4.26: Shrinkage strain of C700 compared to plain PC for air-cured samples

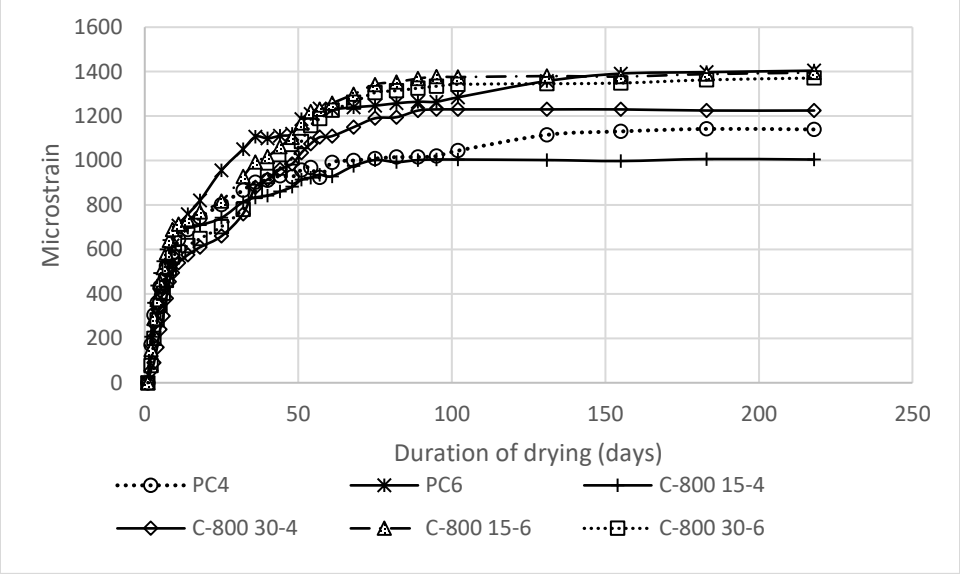

Figure 4.27: Shrinkage strain of C800 compared to plain PC for water-cured samples

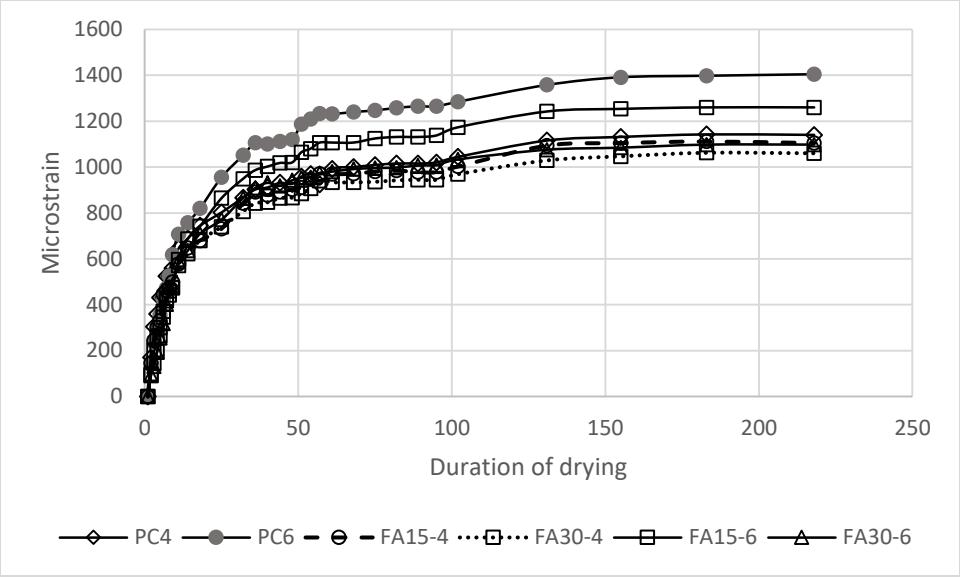

Figure 4.28: Shrinkage strain of FA compared to plain PC for water-cured samples

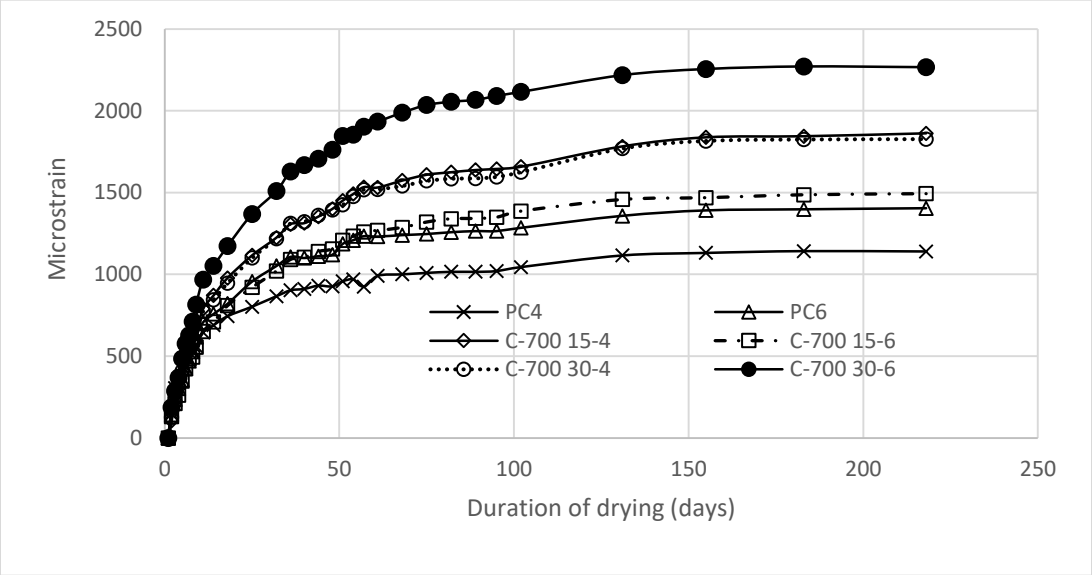

Figure 4.29: Shrinkage strain of C700 compared to plain PC for water-cured samples

4.9.1 Effect of binder type and w/b ratio on drying shrinkage development

For PC/C-700, shrinkage strain increases with increasing replacement level and reduces with increase in w/b ratio. The increase in strain with increasing replacement level is associated with the reducing PC content and increasing unburnt carbon content. As PC content reduces in the system, the dominant mechanism of shrinkage is attributed to capillary pressure. As the internal

relative humidity reduces as drying proceeds, moisture loss to the environment is induced by the capillary tension acting in the pore water in the partially filled pores with a resulting compressive stress developed to counteract the tensile stress set-up in the pores (Bentz, 2005). The tensile capillary pressure induces a compressive stress on the solid skeleton leading to a macroscopic deformation. The unburnt carbon particles adsorbs part of the mix water, which is not utilised in the hydration reaction but lost to the environment with time as previously explained. Also, with reducing PC content, the amount of C-S-H formed due to plain PC hydration is reduced and given the largely crystalline nature of C-700, contribution to C-S-H formation is limited hence the degree of stability due to hydration product formation and growth is reduced leading to a higher shrinkage. The correlation presented in Figure 4.31 between the shrinkage strain of plain PC and C-700 shows this clearly, with shrinkage strain increasing with increasing replacement level. The shrinkage strain at early period of drying is similar for each of the replacement level irrespective of w/b ratio implying that shrinkage for the sample is more sensitive to changes in PC replacement level than w/b ratio at early stage of drying.

In addition, the effect of paste content can be noticed on the shrinkage strain for C-700 at 15% and 30% replacement levels for air-cured samples with a higher strain observed at lower w/b ratio. The influence of paste content on shrinkage is due to the decreasing disjoining pressure between C-S-H layers separated by structurally held water in the interlayers. As hydration progresses, internal relative humidity reduces and part of the internal pore water is adsorbed between the C-S-H layers and as such is constrained between the C-S-H layers. As relative humidity decreases, the disjoining pressure reduces thereby reducing the interlayer distance between the C-S-H layers, with the compression of the C-S-H layers resulting in shrinkage (Tran et al., 2021). This effect is envisaged to dominate over the effect of capillary pressure at later age of drying beyond the first two weeks of drying.

For C-800, shrinkage strain increases with increasing w/b ratio and increasing replacement level similar to plain PC and FA. This is attributed to the increase in w/b ratio, which makes free water available in the system at higher w/b ratio. Beyond w/c ratio of about 0.4, it is often believed that water is in excess of that required for complete hydration of PC. The excess water is held in capillary pores and is lost through the action of capillary pressure inducing a compressive stress on the solid phase as previously explained. The increase in strain with increasing replacement level is contrary to the effect noted with FA samples and this shows the effect of reducing PC content

as previously discussed for C-700. The shrinkage strain of C-800 is lower compared to that of C-700 and this is linked to the differences in their unburnt carbon content. The unburnt carbon being higher in C-700 contributes to the higher shrinkage strain. As previously explained, the unburnt carbon absorbs water during mixing which is lost to the environment during drying resulting in the compression of the solid phase.

Figure 4.32 shows the correlation of the shrinkage strain of PC-FA and PC-CCA. The shrinkage strain of PC-CCA is higher than that of PC-FA. This is linked to the higher K_2O content in the CCAs in addition to the unburnt carbon and largely crystalline structure. Being largely crystalline, contribution to hydration product formation through pozzolanic reaction is limited and as such could not stabilise volume change in the paste compared to FA. Also, the effect of the unburnt carbon relates to the affinity of its microstructure to absorb water in addition to the water in the capillary pores. The absorbed water do not participate in the hydration reaction and as such is readily lost to the environment. A previous study by Chatveera & Lertwattanaruk (2011) reported a higher shrinkage in black rice husk ash compared to plain PC concrete alluding it to the effect of unburnt carbon on shrinkage. The mechanism of alkali effect on shrinkage is not clear but previous studies (Beltzung & Wittmann, 2005; Rezvani & Proske, 2017) have reported higher shrinkage, especially with cements containing higher alkali. Alkali content was noted by Blaine et al. (Smaoui, Bérubé, Fournier, Bissonnette, & Durand, 2005) to contribute significantly to higher drying shrinkage of pastes and mortars containing high alkali cement. The high alkali content of the ash as determined by XRF, can also be linked to the higher shrinkage strain. A likely mechanism by which alkali content influence drying shrinkage is probably connected to the effect on hydration of the system. As K_2O is highly soluble it goes into solution with the cation adsorbed by the negatively charged surface of C-S-H (Beltzung & Wittmann, 2005). As internal relative humidity reduces, the distance between adjoining C-S-H layers reduces and so is the repulsive forces of the adsorbed water within the interlayer, which results in shrinkage.

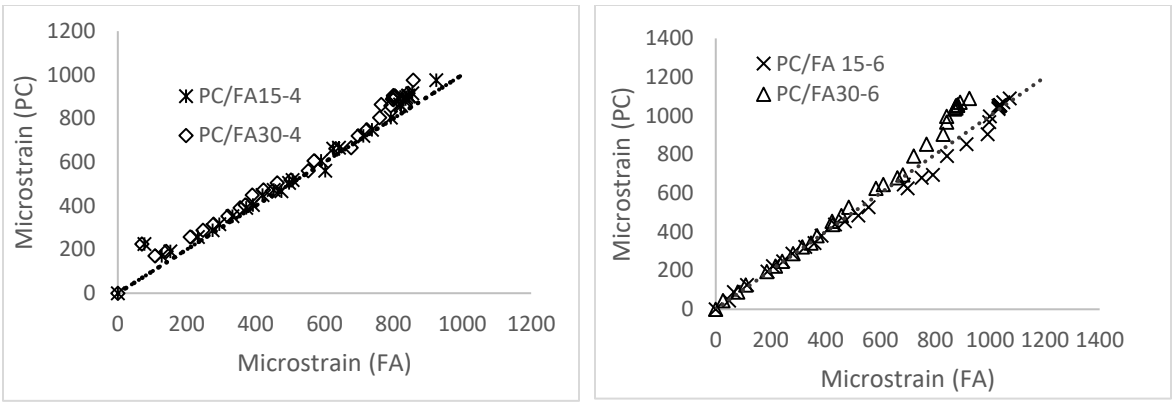

Figure 4.30: Comparison of microstrain of PC and FA at (a) w/b ratio of 0.4 (b) w/b ratio of 0.6

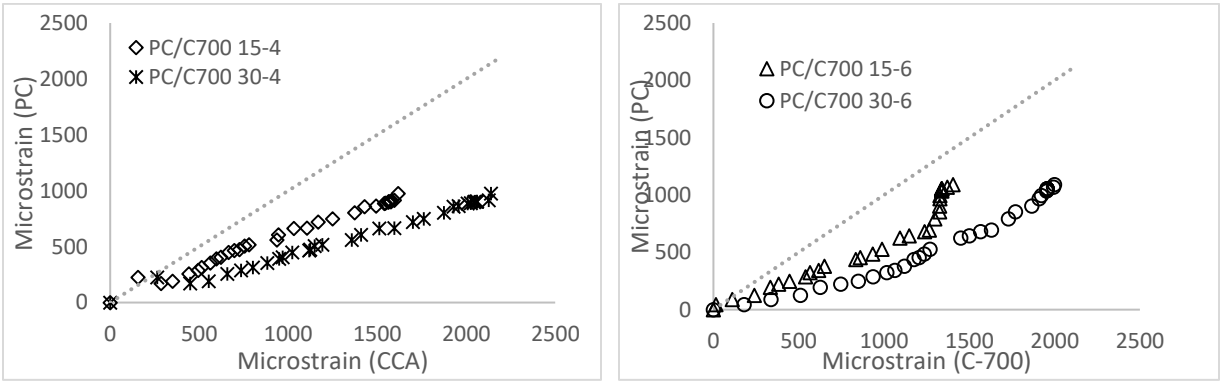

Figure 4.31: Comparison of microstrain of PC and C700 at (a) w/b ratio of 0.4 (b) w/b ratio of 0.6

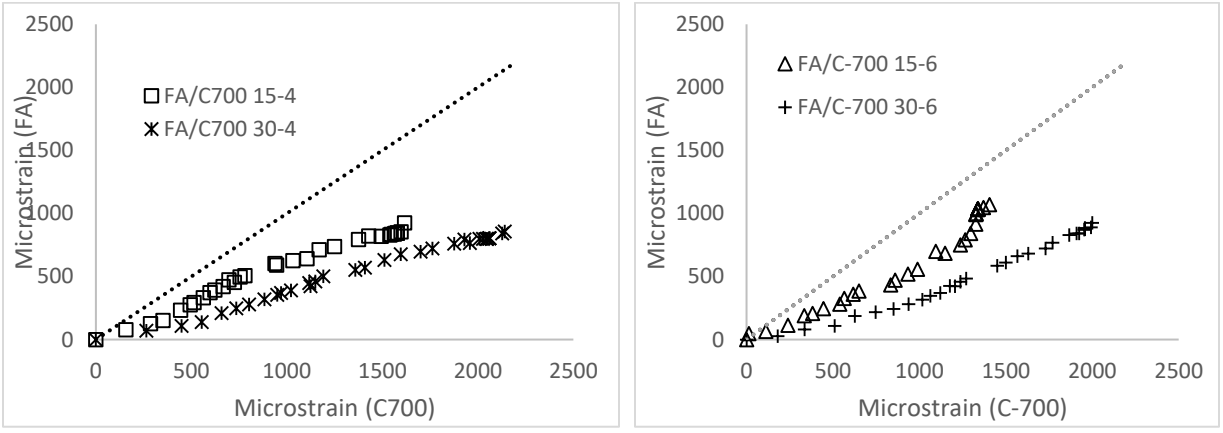

Figure 4.32: Comparison of microstrain of FA and C700 at (a) w/b ratio of 0.4 (b) w/b ratio of 0.6

4.9.2 Effect of initial curing on shrinkage strain development

A correlation of the shrinkage strain of PC-FA between air-cured and water cured samples showed that the shrinkage strain of air-cured samples were generally lower than the strain of the water-cured samples (Figure 4.33). The rate of drying evident in the slope of the shrinkage curve at early

drying times is higher in the water-cured samples than in the air-cured samples. This is attributed to the changing internal relative humidity of the samples due to continued hydration and capillary pressure. As the internal relative humidity reduces, capillary tension increases and moisture is lost to the environment. More moisture is lost from the water-cured samples to reach equilibrium with the exposure environment thereby leading to higher shrinkage strain. This coupled with the continued hydration of PC which is further enhanced by the excess cure water in the capillary pores of the water-cured samples contributes to the high shrinkage strain for the samples. This implies that the initial moisture content in the samples has an effect on the drying shrinkage strain and rate of drying at the early and later drying stage with a subsequent effect on the magnitude of strain measured. It is also worth noting that the slope of the curve flattens earlier in air-cured samples than in the water-cured samples showing that air-cured samples were able to overcome the effect of capillary pressure on shrinkage earlier than the water-cured samples.

A comparison of the mean of the strain measurement for the air-cured samples showed the following trend from the highest to the lowest strain measured; C-700 30-4 > C-700 30-6 > C-700 15-4 > C-700 15-6 > FA15-4 = PC6 > PC4 > FA30-6 > FA30-4 > FA15-6.

Figure 4.33 shows the correlation of the shrinkage strain of PC-C-700 between water-cured and air-cured samples. The shrinkage strain of air-cured samples is higher or similar to that of water-cured samples at 30% replacement level. This shows that there is some degree of stability against shrinkage in the water-cured samples, which could possibly be due to continuous hydration of PC. The initial water curing of the samples enhances the progress of hydration of PC resulting in the formation of more C-S-H and refinement of some of the capillary pores than in the air-cured samples (Tran et al., 2021). The formed C-S-H creates some form of internal restraint to deformation hence the lower shrinkage strain compared to air-cured samples. On the other hand, the shrinkage strain of the air-cured samples is lower or similar to that of the water-cured samples at 15% replacement level. This is influenced by the change of surface tension of an adsorbing particle at relative humidity below 50% inducing macroscopic strain. As the relative humidity of the environment of hydration product reduces, water molecules are gradually lost to the surrounding, inducing increase in surface tension and particle shrinkage (Beltzung & Wittmann, 2005).

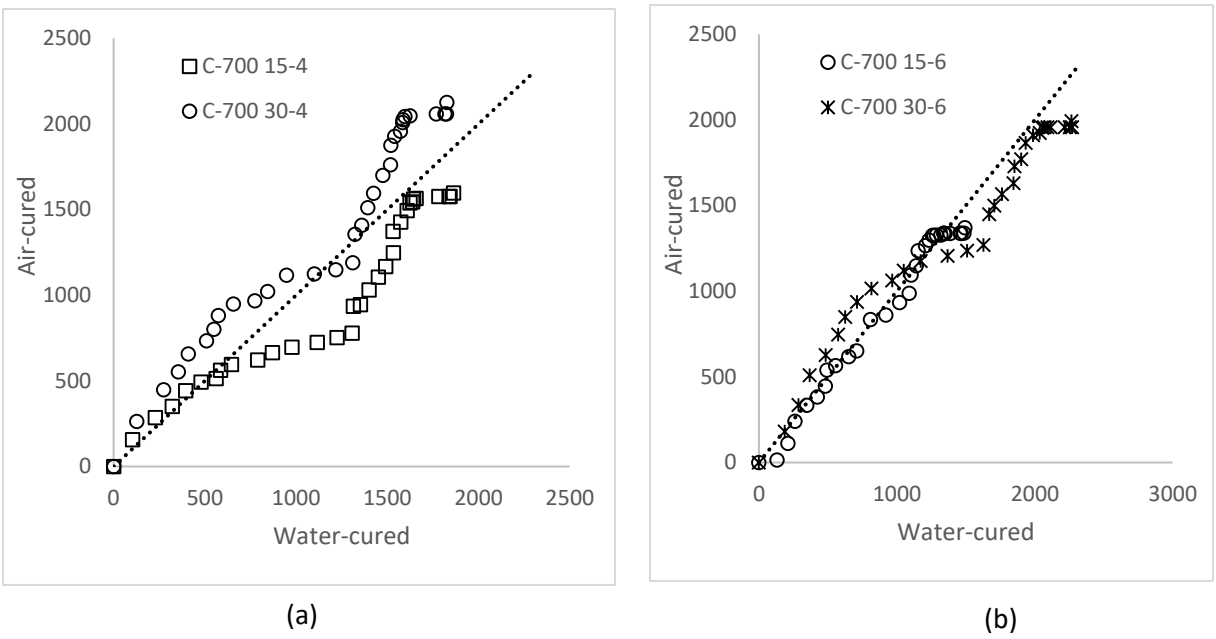

(a) (b)

Figure 4.33: Comparison of the effect of initial curing on the shrinkage of PC/CCA

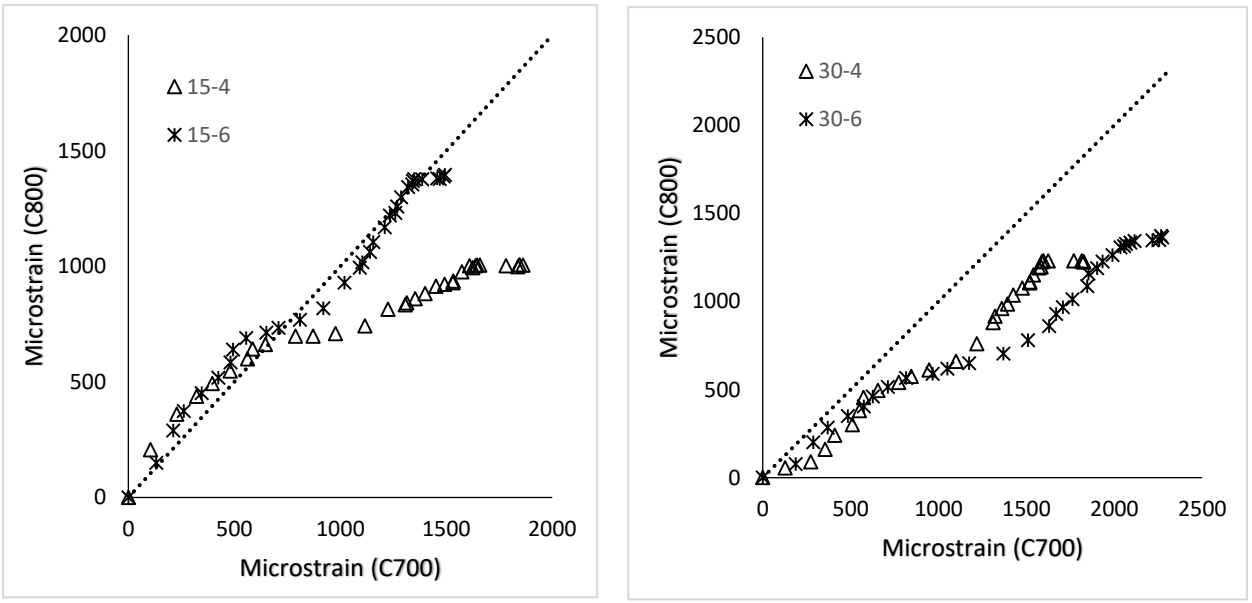

(a) (b)

Figure 4.34: Comparison of the effect of calcination temperature on the shrinkage of PC/CCA

4.9.3 Effect of calcination temperature on drying shrinkage development

Figure 4.34 shows the correlation between the PC-C800 and PC-C700 for the two replacement levels. At 15% replacement level, the shrinkage strain for C700 is higher than that of C800 at later age (beyond the first two weeks) of drying at w/b ratio of 0.4 while the shrinkage strain is similar

at w/b ratio of 0.6 for both ashes. The difference in strain at both w/b ratio may imply the dilution effect of increased water content at w/b ratio of 0.6 coupled with the lower content of ash compared to w/b ratio of 0.4 has compensated to certain extent the effect of K_2O concentration on shrinkage. However, at 30% replacement level, the shrinkage strain of C700 is higher than C800 at both w/b ratio. This is attributed to the differences in their chemical composition with respect to the K_2O content and the unburnt carbon content (as previously explained) which becomes significant with decreasing plain PC content. The higher K_2O and unburnt carbon content of C700 contributes to its higher shrinkage strain compared to C800. Also, the differences in the particle size and effect on the hydration product growth and nucleation may contribute to the differences in strain of the two ashes. C800 has finer particles which contributes to the stability of the paste against shrinkage with respect to pore refinement and interparticle distance within the paste better than C700.

4.10 Durability index tests results

The results of the three durability index tests; oxygen permeability, water sorptivity and chloride conductivity are discussed in this section. The variation of the indices with binder type, replacement level and age is examined. Each of the index examined a different transport mechanism of fluid or ionic transport through the cover concrete. Oxygen permeability relates to the concrete penetrability by oxygen, which can increase the risk of carbonation and lead to deterioration over the service life of the structure. Water sorptivity relates to penetrability by moisture through capillary action and chloride conductivity relates to diffusion of chloride ions through ionic concentration. Subsequently concrete quality was evaluated using each of the indices as an indication of the performance of the cementitious materials.

4.10.1 Oxygen permeability index

The oxygen permeability index (OPI) for each of the mixes studied is presented in Figure 4.35. For plain PC mix, the index increases with increase in w/b ratio and increase in curing age such that the OPI value at w/b of 0.6 is higher than at w/b ratio of 0.4 for the curing ages investigated. For PC/FA mix, at both replacement levels, OPI increases with increase in w/b ratio at 28 days and decreases at 90 days with increase in w/b ratio. OPI also decreases with increasing fly ash content at 28 days but increases with increasing ash content at 90 days. Similarly, for the two CCAs, OPI increases with increasing w/b ratio at 28 days for all replacement levels, while for C-

700 it reduces with increasing w/b ratio at 90 days but for C-800 at 15%, OPI is similar for both w/b ratios while at 30%, it increases with increasing w/b ratio.

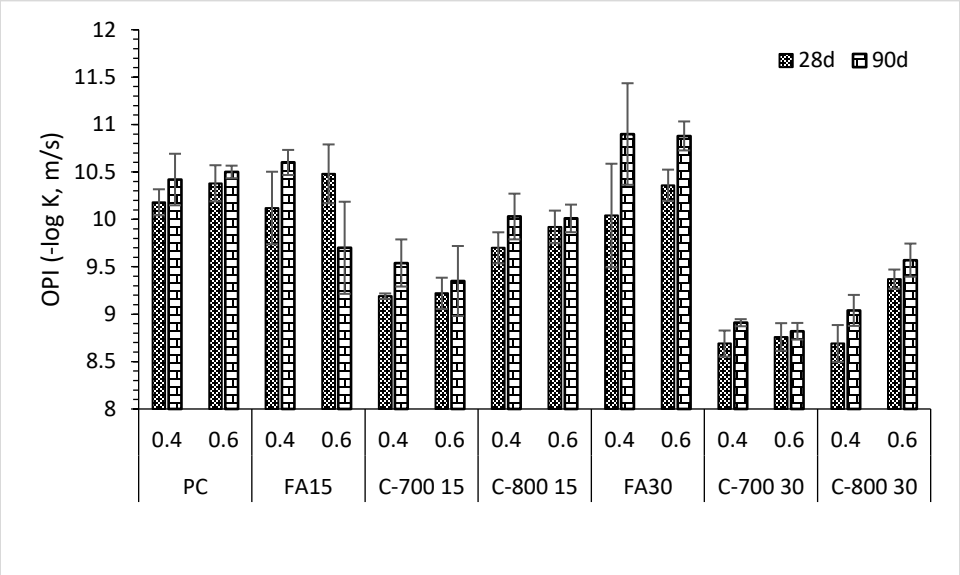

Figure 4.35: variation of oxygen permeability indices with curing age and w/b ratio

This trend of results is contrary to what has been reported in literature (Githachuri, Alexander, & Moyo, 2012). The increase in OPI with increasing w/b ratio is unexpected but can be linked to differences in the workability of the concrete mix for the two w/b ratios as admixture was not used in the preparation of the concrete samples for the test. This is evident in the slump value recorded, which ranged between 10 and 25 mm at w/b ratio of 0.4 and between 60 and 115 mm at w/b ratio of 0.6.

At the same water content, the mix at w/b ratio of 0.6 was more workable than at w/b ratio of 0.4 and it is believed this affected the interfacial bonding between the aggregates and the cement paste and have contributed to the higher permeability at w/b ratio of 0.4 which is more permeable to gas ingress than that at w/b ratio of 0.6. To enhance the performance of the concrete in terms of permeability to gas, there may be need to use admixture to enhance workability at w/b ratio of 0.4 without unnecessarily increasing water content. Even though, it is believed that hydration reaction and pozzolanic reaction (in case of fly ash) will not be affected but that the macro and microstructure as well as the interfacial transition zone may have been impacted resulting in a more permeable concrete at 0.4 w/b ratio. The result also showed that there is a limit to which adequate compaction can compensate for low workability without affecting the permeability of

concrete. This has to do with the flow of cement paste around the aggregates within the concrete to achieve a dense macrostructure and microstructure, hence, to achieve the benefit of using a low w/b ratio, it may be necessary to adjust the water content otherwise the use of workability aid is recommended.

Another factor that may have contributed to the trend of result is the higher binder content for w/b ratio of 0.4 compared to w/b ratio of 0.6 giving rise to a higher paste content at the same water content. Cement paste has been identified as a porous phase in concrete with a subsequent effect on the permeability, diffusion and absorption characteristics of concrete (Angelucci, Beushausen, Alexander, & Mackechnie, 2017). However, the mechanism by which high paste content affect permeability in this context is not clearly understood given the higher compressive strength at w/b ratio of 0.4. The result further confirmed that higher strength do not always correspond to higher durability as there are factors which affect durability more than they affect strength development.

Also, for most of the mixes, OPI increases with increasing curing age showing that there is a change in the microstructural properties with age, which can be linked to the reaction of the binder phase and there is also the modification of the pore structure of the system. For plain PC, hydration reaction of PC is solely the binder phase reaction contributing to the microstructural changes, while for PC/FA both hydration and pozzolanic reaction is contributing to the changes but for PC/CCA system, hydration reaction contributes more significantly than pozzolanic reaction (given the largely crystalline nature of the ashes), which could be a reason for lower OPI values in the system compared to both plain PC and PC/FA systems. The modification of the pore structure also comes from the hydration/pozzolanic reaction and microfiller effect of the SCM. Hydration is a continuous process with age with an increase in the precipitation of products, as hydration products fills the pores between the particles in the paste and between the paste and the aggregates. This leads to the densification of the microstructure and limits the tortuosity and interconnectivity of the pores with the obstruction of some of the pores by hydration products. Also similar to this is the pozzolanic reaction, which contributes to the formation of products and densification of the microstructure. The microfiller effect is associated with the SCM as their inclusion in the system leads to refinement of pores reducing the interparticle pores between plain PC particles. As fly ash particles is finer than those of the CCA, its microfiller effect contributes more to the reduction in the sizes and distribution of the pores than CCA resulting in a less permeable concrete than CCA.

For the CCAs, the lower OPI values recorded compared to plain PC and PC/FA system can be linked to the limited pozzolanic reaction in the system due to their largely crystalline nature. Pore refinement and microstructural densification is significantly influenced by the microfiller effect than pozzolanic reaction. This further impacts on the tortuosity and interconnectivity of the pores with the pressure decay being more than that recorded for plain PC and PC/FA systems. Both pore refinement and microstructural densification in PC/CCA system is further limited by the larger particle size of the CCAs compared to FA particles. The finer particles of FA makes the PC/FA system denser than PC/CCA system. Further, the OPI values of C-800 is higher than that for C-700 and this can be linked to the difference in the processing method of the ashes. C-700 has a higher LOI, which means a higher unburnt carbon than C-800. The unburnt carbon coupled with the high potassium oxide content interferes with plain PC hydration. In addition, the difference in particle size between the two CCAs also had some effect, as C-800 is finer than C-700 its OPI values are higher showing its fineness to be of advantage in achieving a less permeable concrete.

4.10.2 Water sorptivity index (WSI)

The result of WSI performed on concrete disc is presented in Figure 4.36. WSI for plain PC decreases with increasing w/b ratio but increases with increasing curing age. For PC/FA, WSI increases with increasing curing age for 15% replacement level and decreases with increasing curing age at 30% replacement level. No definite pattern can be observed for the effect of w/b ratio. For C-700, WSI reduces with increasing curing age and w/b ratio at both replacement levels. For C-800, WSI reduces with increasing curing age and increases with increasing w/b ratio at both replacement levels. Generally, the mixes can be grouped into two classes; those in which sorptivity increases with increasing curing ages (PC and FA15) and those in which sorptivity decreases with increasing curing age.

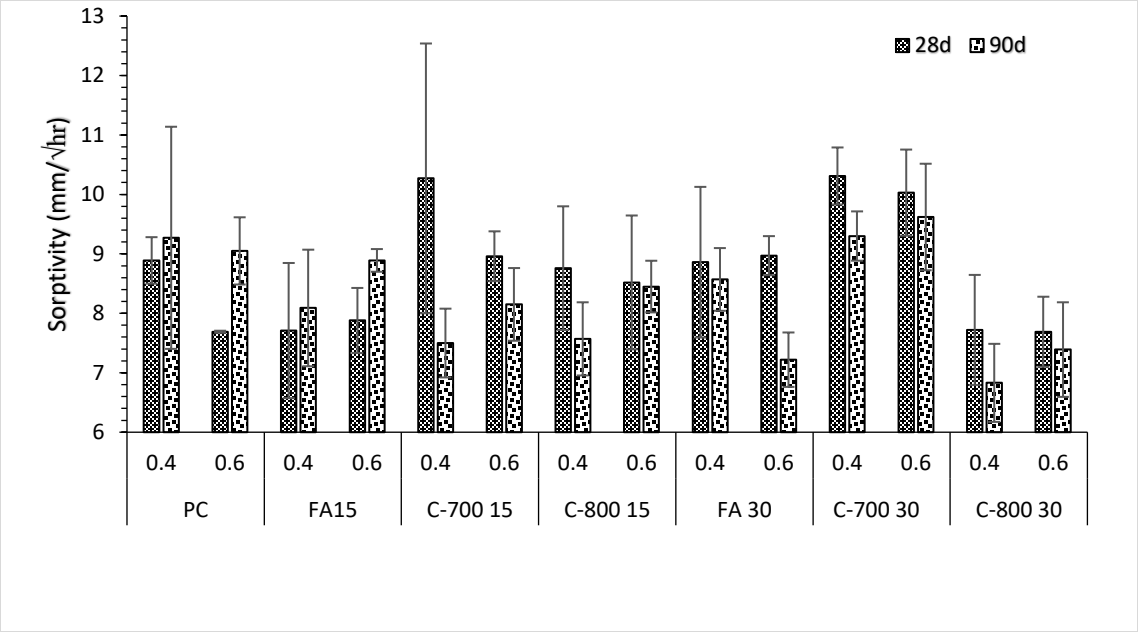

Figure 4.36: variation of water sorptivity index with curing age and w/b ratio

The increase in WSI with increasing curing age for plain PC contradicts the result obtained for OPI showing that the mechanism of transport of fluids through the cover concrete is different for the two tests. OPI is carried out under pressure and is more sensitive to the tortuosity and interconnectivity of the pores, while WSI is largely due to absorption of moisture under the influence of capillary action with the wetting of the paste along the passage of the pores taking place. The wetting of the hydrated paste being influenced by the size and distribution of the capillary pores.

The decrease in WSI with increasing w/b ratio can be linked to the differences in workability as explained for OPI and likewise it could be linked to the increase in hydration product due to the higher cement content at w/b ratio of 0.4. The movement of the wetting front into the concrete cover through the capillary pores at the surface implies that part of the moisture is absorbed into the unsaturated hydrated paste, which is wetted as suction takes place. As the paste content at w/b ratio of 0.4 is more than at w/b of 0.6, there is a reduction in the size of the capillary pores and an increase in the fine capillary pores and hence sorptivity increases at lower w/b ratio. Also, as the hydration product increases with increasing curing age, the absorption of water into the hydrated paste and hence wetting becomes significant.

For PC/FA mix, the trend at 15% differs to that at 30%, at 15%, there is an increase in sorptivity with increasing curing age, which is linked to the absorption of moisture and wetting of the hydrated paste. The increase in sorptivity with increasing w/b ratio showed that mix at 0.6 w/b ratio is more permeable than 0.4 w/b ratio and this implies that there are more capillary pores influenced by the increase in w/b ratio and hence a higher rate of suction. Here, suction through capillary pores plays more significant role than wetting of the hydrated paste. This may have been further influenced by the additional pozzolanic reaction of FA, which may have reduced the interconnectivity of the pores at w/b ratio of 0.4 compared to at w/b ratio of 0.6 thereby reducing the rate of absorption of moisture and wetting of the hydrated paste. Although, there is an increase in sorptivity with increasing curing age, the absorption of moisture and wetting becomes significant with age. At 30% FA content, sorptivity reduces with increasing curing age showing that the higher replacement level has an advantage in reducing moisture absorption by capillary suction. This is likely due to the refinement of pores occasioned by the fine particles of FA as well as the additional pozzolanic reaction.

For C-700 and C-800, the reduction in sorptivity with increasing w/b ratio is influenced by workability and paste content as paste content increases with increasing cement content. The effect of workability and paste content can be said to be the controlling factor on sorptivity at the age of 28 days while the 90 days sorptivity can be said to be controlled by the effect of w/b ratio and hydration. At higher w/b ratio, more capillary pores are formed which are passage for the moving wetting front in concrete while with increase in the degree of hydration, some of the pores are filled with the growing hydration product. However, the effect of hydration product reducing the sizes and interconnectivity of pores becomes significant at higher cement content, hence the reduction in the sorptivity at w/b ratio of 0.4 at 90 days.

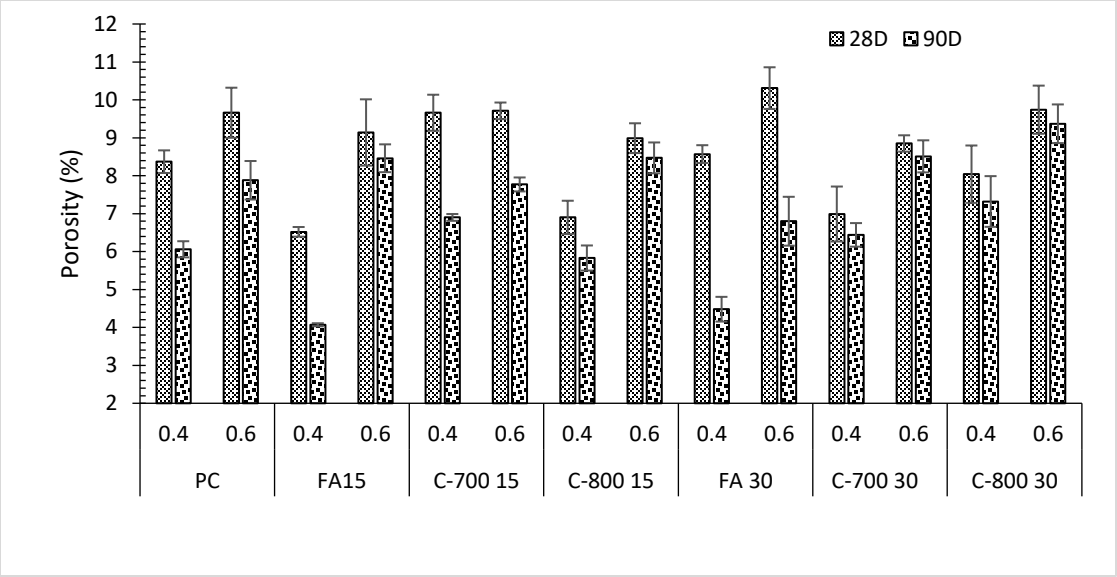

Figure 4.37: variation of porosity with curing age and w/b ratio

4.10.3 Porosity versus sorptivity

A consideration of the porosity (Figure 4.37) of the different mixes showed a clear cut trend with respect to the variation with curing age and w/b ratio. For all the mixes, porosity decreases with increasing curing age and increases with increasing w/b ratio. The trend of results obtained suggest that the porosity is more sensitive to variation in material properties and age influenced by the pozzolanic and/or hydration reaction occurring in the samples. The decrease in porosity with increasing curing age indicates growth of hydration products, which reduces the permeability of the capillary pores to moisture movement and hence a decrease in the degree of interconnectivity and tortuosity of the pores. Likewise, the increase in porosity with increasing w/b ratio showed that water penetrable pores increases with increase in w/b ratio to which the cement content contributes.

For PC/FA mix, both sorptivity and porosity increases with increasing ash content at 28 days whereas at 90 days, both porosity and sorptivity increases slightly with increasing ash content at w/b ratio of 0.4 and reduces with increasing ash content at w/b ratio of 0.6. The increase in sorptivity implies an increase in the rate of moisture absorption in the capillary pores which can be an indication of the tortuosity of the pores while an increase in porosity points to an increase in water-penetrable depth (Moore et al., 2021) and an increase in the volume of fine capillary pores with increasing ash content. At 28 days, the dilution effect of partially replacing PC with FA is yet

to be fully compensated for by the additional pozzolanic reaction of FA hence the increase in both parameters but at 90 days, there is a synergistic effect of the hydration reaction, pozzolanic reaction and pore refinement all influencing the property of the system. This was further substantiated by the lower values of porosity recorded at 90 days compared to the values at 28 days. For PC/C-800, porosity increases with increasing ash content at both curing ages, while sorptivity reduces with increasing ash content at both curing ages. The increase in porosity indicates that there is an increase in the water penetrable pores and therefore the dilution effect of partially replacing PC with CCA was not adequately compensated for by additional pozzolanic reaction. As the values of porosity at 90 days were lower than at 28 days coupled with reducing sorptivity with increasing ash content, the system properties could be said to be influenced by hydration reaction and pore refinement to certain extent.

For PC/C-700, sorptivity increases with increasing ash content for both curing ages, while at 28 days, porosity reduces with increasing ash content but at 90 days variation in porosity with increasing ash content is dependent on w/b ratio. The increase in sorptivity indicates an increase in tortuosity and interconnectivity of the capillary pores acting as conduits for the absorbed moisture. The reduction in porosity is an indication of the obstruction of some of the pores and path of moisture movement in the microstructure. At w/b ratio of 0.4, porosity reduces slightly with increasing ash content showing that there is likely improvement in microstructure with respect to capillary pores distribution and interconnectivity. At w/b ratio of 0.6, porosity increases with increasing ash content which shows the effect of w/b ratio on capillary pores formation, distribution and interconnectivity.

4.10.4 Chloride conductivity index (CCI)

The CCI values for the concrete mixes is presented in Figure 4.38. The CCI for plain PC increases with increasing w/b ratio and decreases with increasing curing age. This is similar to the trend of result for porosity and an indication that the diffusion of chloride ions increases with increasing w/b ratio. This points to increase in capillary pore volume with increasing w/b ratio. The lower CCI values at w/b ratio of 0.4 showed a reduced porosity of the microstructure with a better resistance to the flow of ions under concentration gradient than at w/b ratio of 0.6. The decrease in CCI with increasing curing age showed the effect of hydration progress contributing to the

densification of the microstructure as some of the pores that exist at day 28 have been filled by hydration product by day 90.

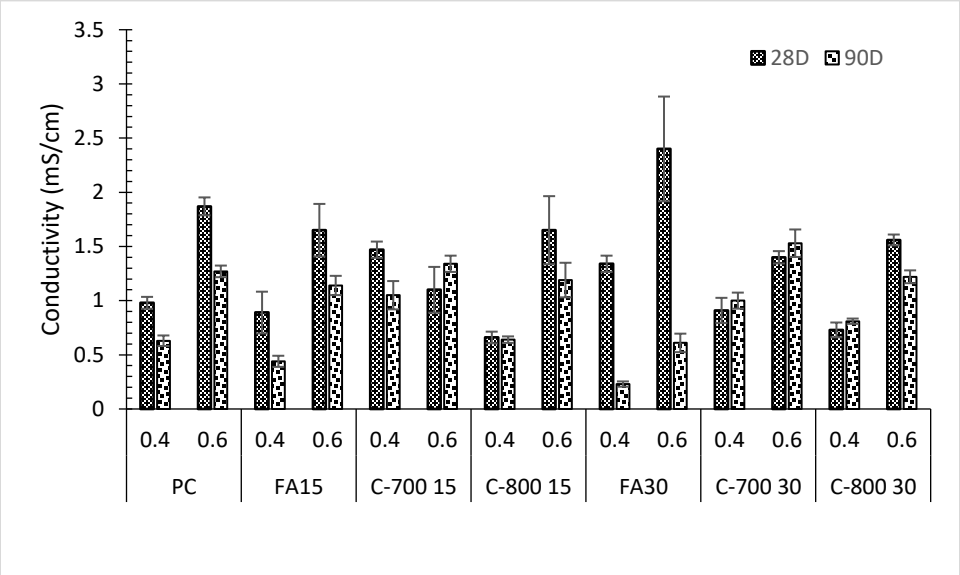

Figure 4.38: Variation of chloride conductivity index with curing age and w/b ratio

For PC/FA, CCI values increases with increasing w/b ratio and decreases with increasing curing age. The trend is similar to that observed for plain PC but the difference lies in the mechanism responsible for the trend of result. The decrease in CCI values with increasing curing age is influenced by the combined effect of hydration reaction of plain PC and pozzolanic reaction of FA both affecting the microstructure of concrete. FA relies on the hydration of PC for its pozzolanic reaction and this could be said to be effectively in place by age 90 days and generally at this age the CCI values for PC/FA is lower than plain PC. Whereas at 28 days, the pore structure could be said to be influenced by the increasing number of fine pores due to the quantity and fineness of FA particles in the system. Also, as the degree of pozzolanic reaction increases, the pores are filled by the growing pozzolanic reaction product alongside hydration product from plain PC. This trend of result is in line with literature, that chloride conductivity reduces with extended moist curing (Beushausen et al., 2021). Porosity is expected to increase with increasing w/b ratio and this is responsible for the higher values of CCI at w/b ratio of 0.6 when compared to that of w/b ratio of 0.4. At the same water content, the ratio of water to the binder particles is more at w/b ratio of 0.6 as there are more water molecules to binder particle than at 0.4 w/b ratio which has less water to binder particle.

For PC/CCA, CCI values for C-700 has different trend for each of the mixes, as CCI values reduces with increasing curing age at w/b ratio of 0.4, it increases with age at w/b ratio of 0.6 for 15% replacement level. However, at 30% replacement level, CCI values increases with increasing curing age but it generally increases with increasing w/b ratio at both replacement levels. For C-800, at 15% replacement level, CCI values reduces with increasing curing age and increases with increasing w/b ratio. The increase in CCI values with increasing w/b ratio showed the effect of porosity, which increases with increasing w/b ratio as expected. The trend of result recorded for PC/CCA showed that a large quantity of the particles are not reactive unlike FA where additional pozzolanic reaction influenced the microstructural property. For CCA, their influence on the microstructure of concrete is more physical than chemical effect due to their presence in the concrete. The only active chemical effect influencing microstructure is the hydration reaction of plain PC the extent of which is limited by the quantity of PC in the system. Also, there is a limit to which the physical effect can enhance the microstructure without an additional reaction from the blended material. Generally, the CCI values obtained for C-800 are lower than that obtained for C-700 except at w/b ratio of 0.6 and curing age of 28 days. The differences can be attributed to the differences in the processing method of the ashes, which impacted on the carbon content of the ashes. It is however not certain whether the differences in the unburnt carbon content (obtained from the loss on ignition) or differences in other chemical constituents (for example the potassium oxide) contributes and to what extent to the trend of the result. It is reported in literature that CCI is sensitive to binder chemistry (Beushausen et al., 2021), hence, this might have played some role though it could not be ascertained.

4.11 Microstructural characterisation results

The result of microstructural characterisation using back scattered electron mode in scanning electron microscopy (SEM) is here presented. One advantage of the back scattered mode is the presentation of features in different shades of grey level scale, which enables distinction of features. However, high-resolution images could not be taken as the microscope is a Tungsten SEM, focusing of image becomes difficult with increase in magnification. As such, images showing the interface between aggregate and hydrated cement paste were obtained at magnification of x1000, while images of the hydrated cement paste was taken at magnification of x3000. The features of interest are the interfacial zone between the hydrated paste and the

aggregate and the hydrated cement paste as both features have significant influence on the strength and durability performance of concrete. It should be noted that most of the microcracks are envisaged to be as a result of the sample preparation.

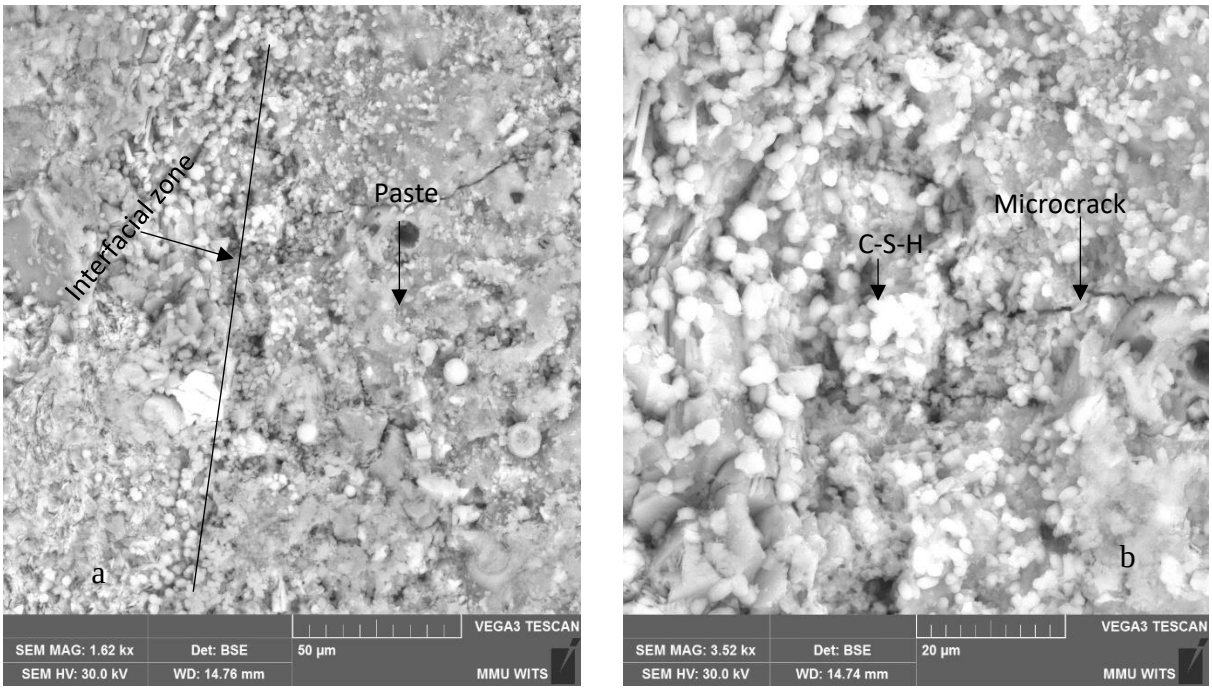

Figure 4.39: Micrograph of (a) Interface and (b) hardened cement paste of concrete containing 15% FA at w/b ratio of 0.4 and 90 days of curing

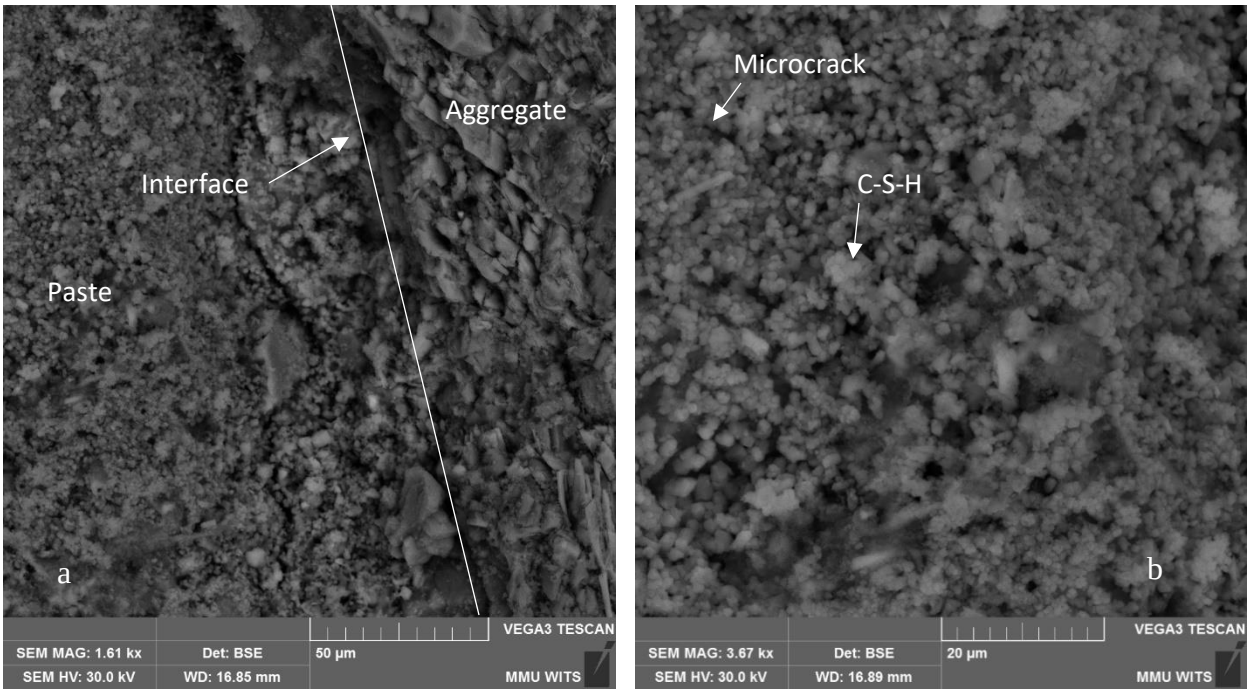

Figure 4.40: Micrograph of (a) Interface and (b) hydrated paste containing 15% C-700 at w/b ratio of 0.4 and curing age of 90 days

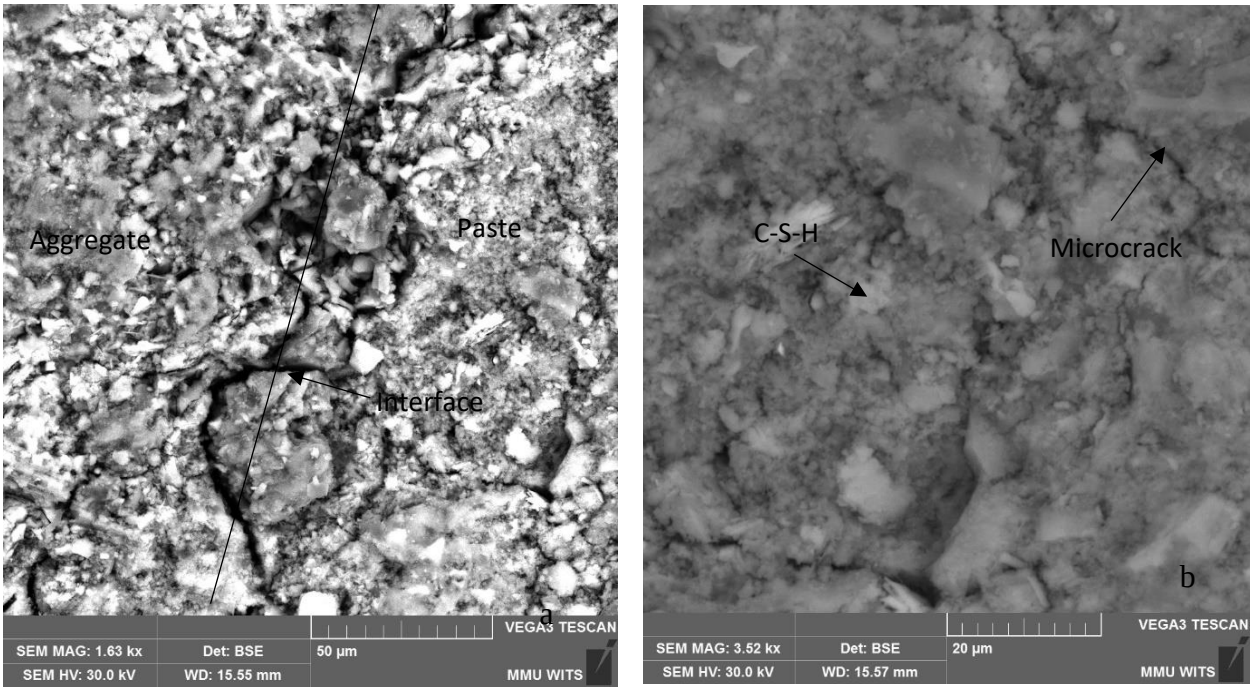

Figure 4.41: Micrograph of (a) Interface and (b) hydrated paste containing 15% C-800 at w/b ratio of 0.4 and curing age of 90 days

The microstructure of the interface between an aggregate and the hardened cement paste is shown in Figures 4.39(a), 4.40(a) and 4.41(a) for FA, C-700 and C-800 respectively for 15% cement replacement level and w/b ratio of 0.4. The interfacial zone for FA is not clearly distinguishable and it is better packed than that observed for C-700 and C-800. The interface of C-700 is better packed compared to C-800 as the later tends to be more porous with a more pronounced wall effect of aggregate. The better packing of the interface enhances the bonding at the interface between aggregate and the hardened cement paste and this significantly contributes to the higher strength measured for FA compared to the CCAs. For C-700, the bonding between the aggregate and the paste can be said to be good given the crack, which occurred within the paste close to the interface compared to the same crack occurring at the interface for C-800. The crack is envisaged to occur during sample preparation, and that it occurred at the interface in C-800 showed that its interface may be weaker than the paste. This further showed that the enhanced strength in C-800 compared to C-700 is influenced by the paste characteristics than the interfacial bonding and this could be as a result of its lower unburnt carbon content. Also, the porous interface zone in C-800 further showed its weakness compared to the hardened paste and this could explain the lower strength compared to FA besides the influence of reactivity. The porosity of the interface and its influence on strength can be linked to less cement grains at the interface in the fresh state and higher water to cement ratio compared to the bulk paste (K. L. Scrivener, Crumbie, & Laugesen, 2004).

The microstructure of the hardened cement paste is shown in Figures 4.39(b), 4.40(b) and 4.41(b) for FA, C-700 and C-800 respectively. For C-700, the formation and growth of C-S-H within the hydrated paste is uniform and evenly distributed with a higher degree of nucleation within the microstructure compared to FA and C-800. The surfaces of the FA and CCA particles are expected to form nucleation points for the growth of C-S-H due to the filler effect. There is a fusion of the growing C-S-H nuclei with the underlying C-S-H structure bridging the interlayer pores with a higher degree of densification of the microstructure in FA. The additional pozzolanic reaction of FA also contributes to the reduction of the interlayer and gel pores accounting for the higher OPI values in FA. However, for CCA (see Fig. 4.39(b)), there is a higher degree of fusion between the individual growing nucleus of C-S-H than with the underlying C-S-H structure resulting in a porous interlayer while the gel pores are not adequately bridged due to the largely crystalline nature of the CCAs. It is also envisaged that there is a higher degree of interconnectivity of the pores in system containing CCA, which can explain the lower OPI values compared to FA. This can also

explain the lower strength of the C-700 in spite of the higher density and distribution of the C-S-H compared to FA, which points to a weaker form of hydration product. This weaker form of C-S-H is due to the binding of the silicates to either K^+ or Na^+ rather than to Ca^{2+}. The growth and distribution of C-S-H within the paste is expected to result in a dense microstructure but the porous and weaker nature of the hydration product reduces its effective packing and dense microstructure.

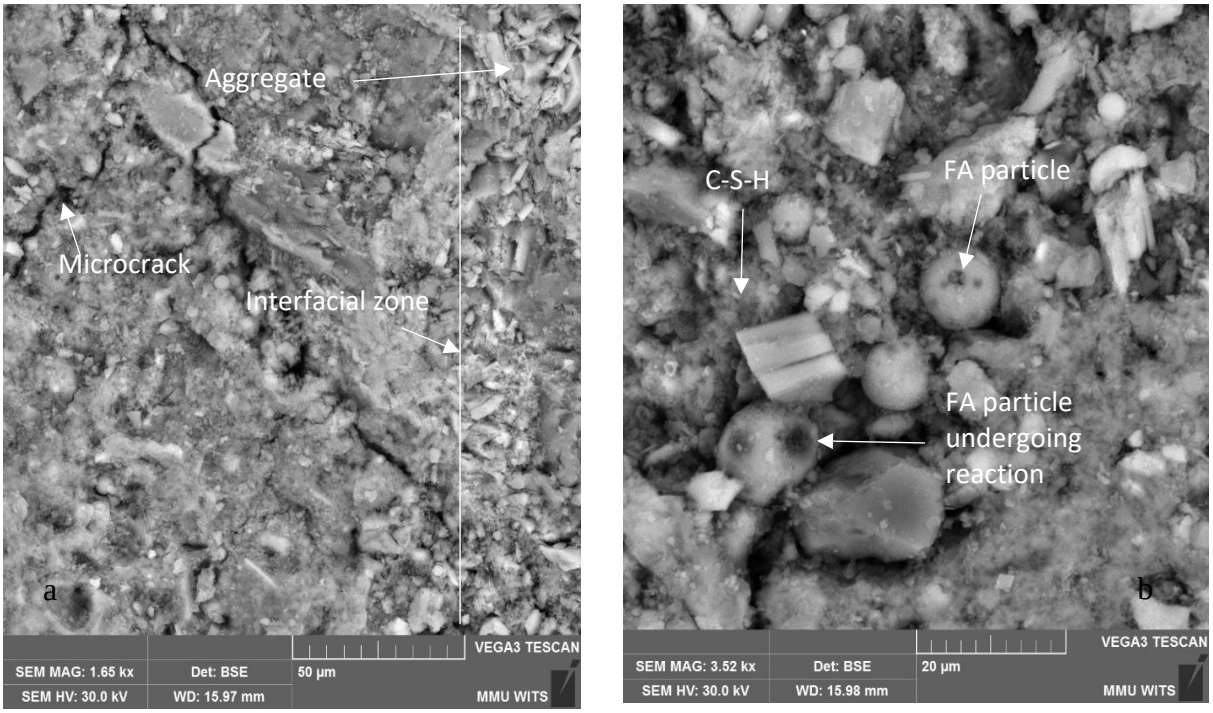

Figure 4.42: Micrograph of (a) Interface and (b) hardened cement paste of concrete containing 15% of FA at w/b ratio of 0.6 and curing age of 90 days

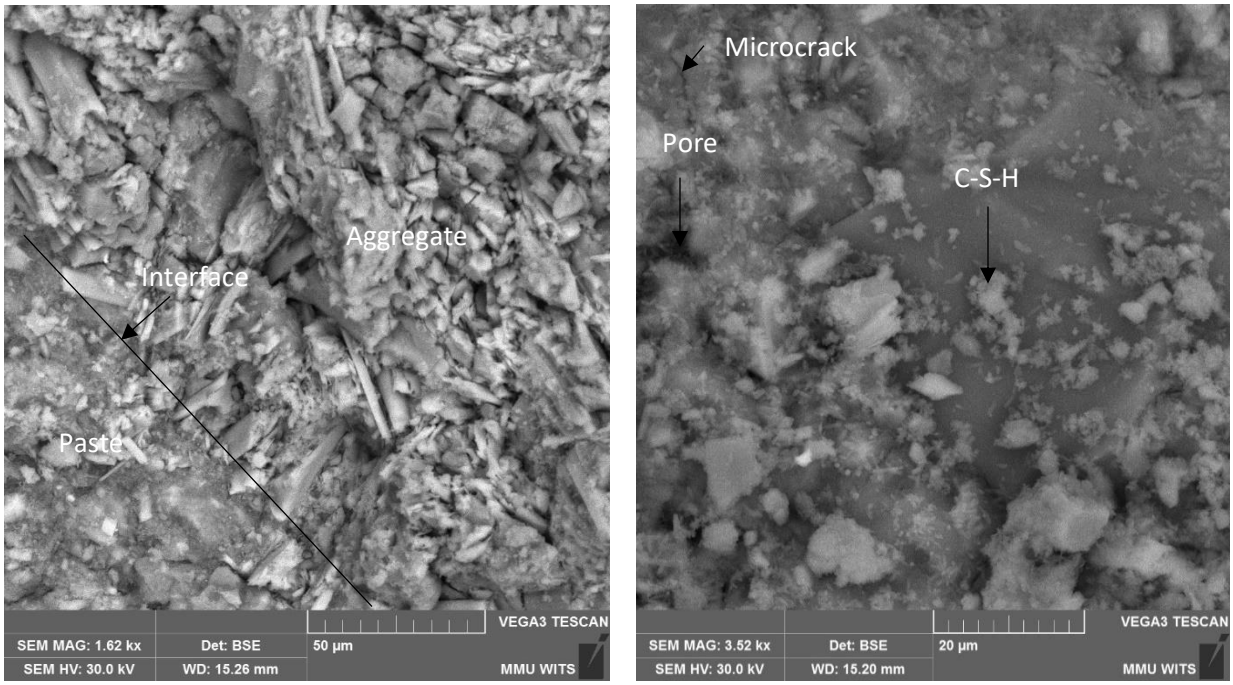

Figure 4.43: Micrograph of (a) Interface and (b) hydrated paste containing 15% C-700 at w/b ratio of 0.6 and curing age of 90 days

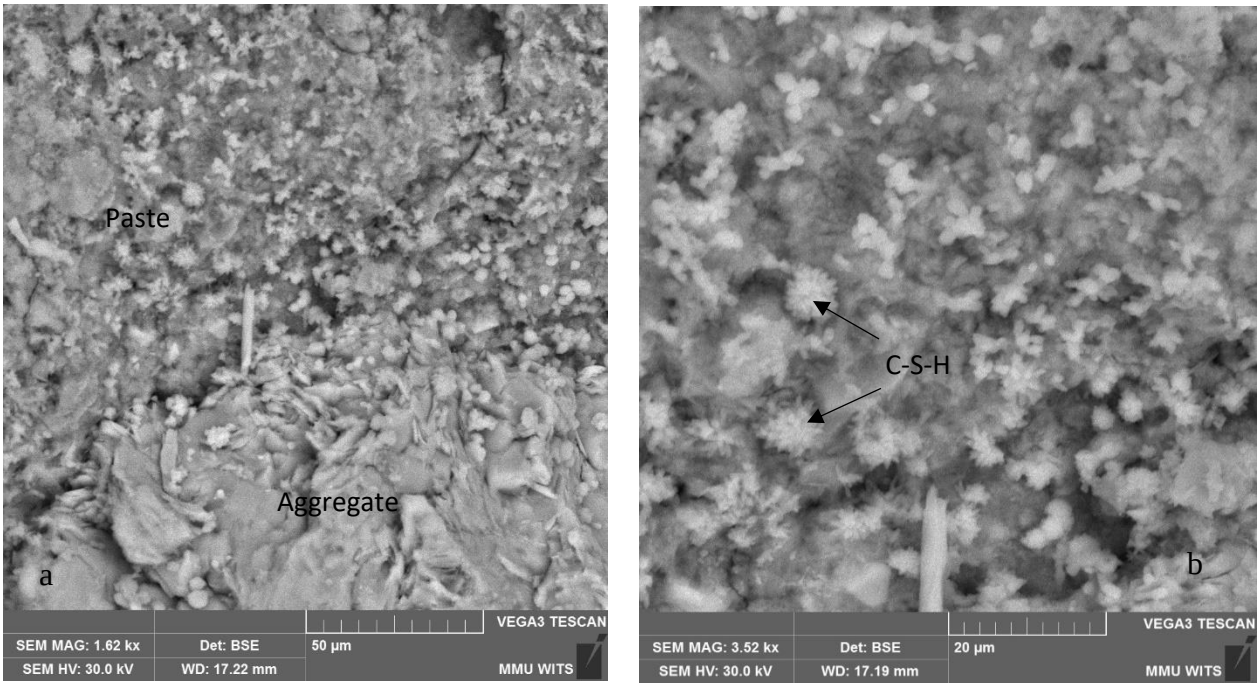

Figure 4.44: Micrograph of (a) Interface and (b) hydrated paste containing 15% C-800 at w/b ratio of 0.6 and curing age of 90 days

The micrographs of the interface are presented in Figures 4.42(a), 4.43(a) and 4.44(a) for FA, C-700 and C-800 respectively for 15% PC replacement level and w/b ratio of 0.6. The interface for C-700 is comparable to FA and is not clearly distinguishable when compared to that of C-800. This shows a relatively good bonding, which could be a result of good compaction and good workability. The interface of C-800 presents a porous microstructure, which as discussed before can be linked to lesser cement grains and increased w/c ratio compared to the adjoining bulk of hardened cement paste. The porosity of the interface is a factor that can influence the permeability of concrete to aggressive fluids, this may have contributed to the lower OPI values of CCA compared to FA.

The micrographs of the hardened cement paste for FA, C-700 and C-800 at w/b ratio of 0.6 and 15% PC replacement level are presented in Figures 4.42(b), 4.43(b) and 4.44(b) respectively. The C-S-H is sparsely distributed within the microstructure compared to w/b ratio of 0.4 showing the dilution effect of increased w/b ratio. With increasing w/b ratio, there is a reduction in the PC content for the same water content, this coupled with the further reduction due to partial replacement of PC by either FA or the CCAs. The sparse distribution of hydration product showed little interconnectivity between the hydrates, which is reflective of the increased interparticle spacing within the microstructure and this to an extent accounts for the low strength recorded at w/b ratio of 0.6 compared to w/b ratio of 0.4 in addition to the reduced PC content. The dilution effect in C-700 and C-800 was not adequately compensated compared to FA where the particles are undergoing reaction due to pozzolanic nature. The density of distributed C-S-H within the microstructure is higher for C-800 than for C-700 showing some extent of increased PC hydration and this could have been responsible for the higher OPI values of C-800 compared to C-700.

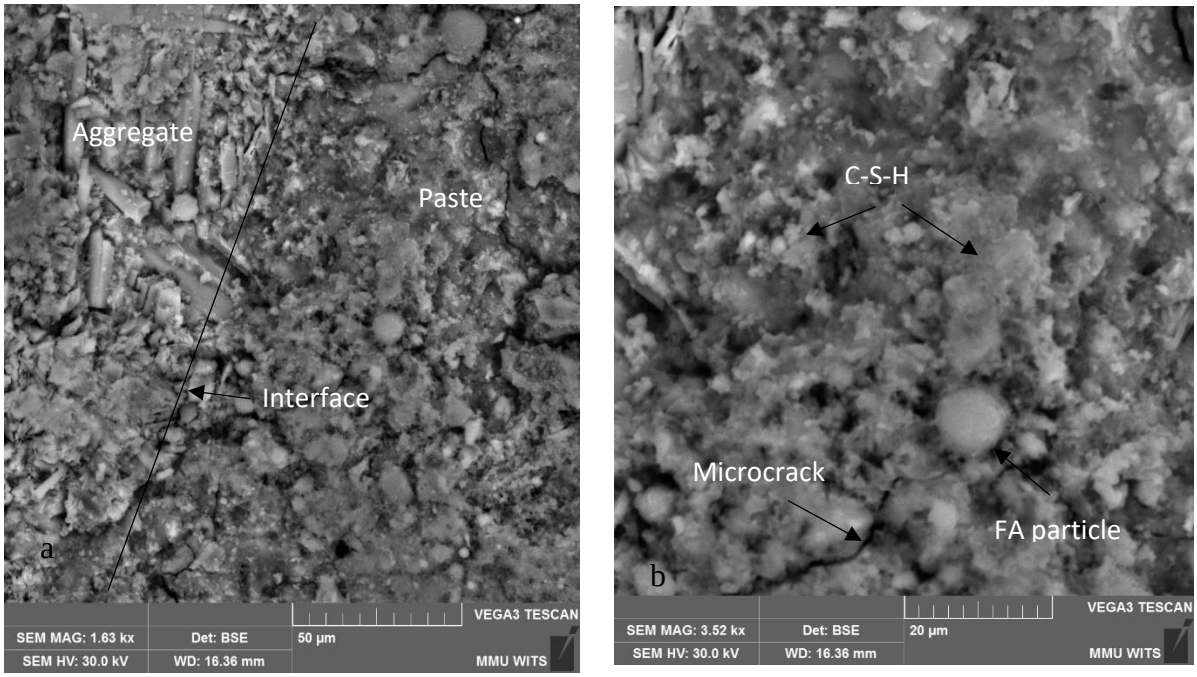

Figure 4.45: Micrograph of (a) Interface and (b) hydrated paste containing 30% FA at w/b ratio of 0.4 and curing age of 90 days

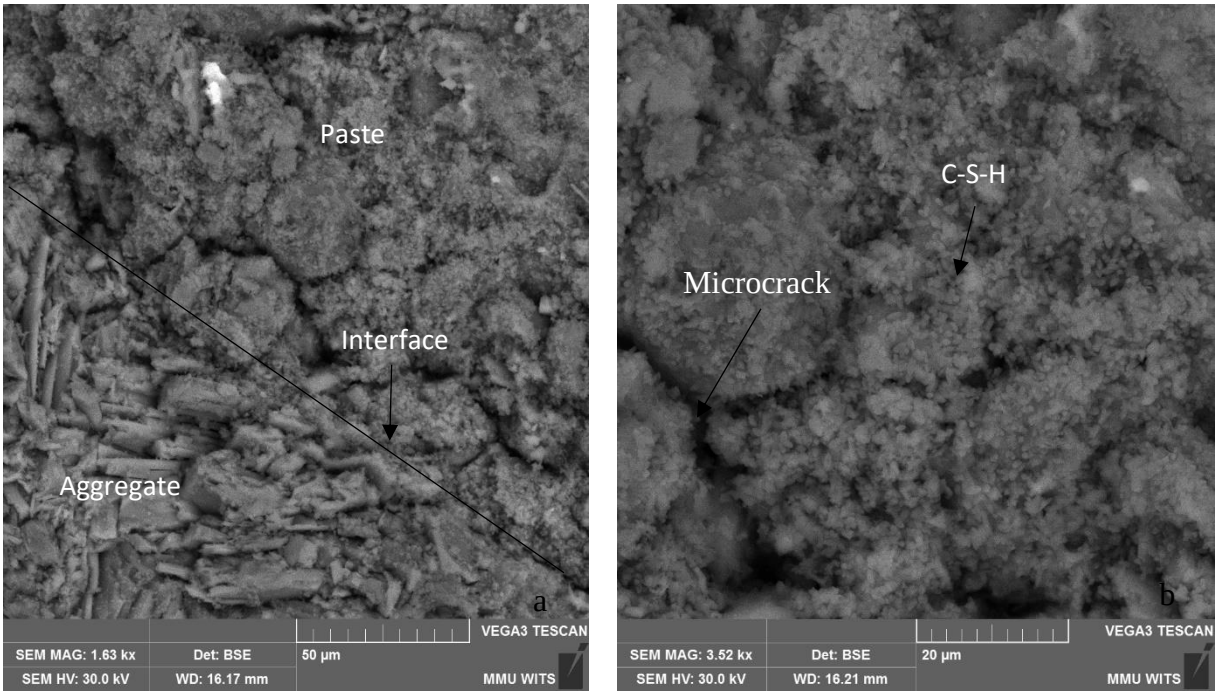

Figure 4.46: Micrograph of (a) Interface and (b) hydrated paste containing 30% C-700 at w/b ratio of 0.4 and curing age of 90 days

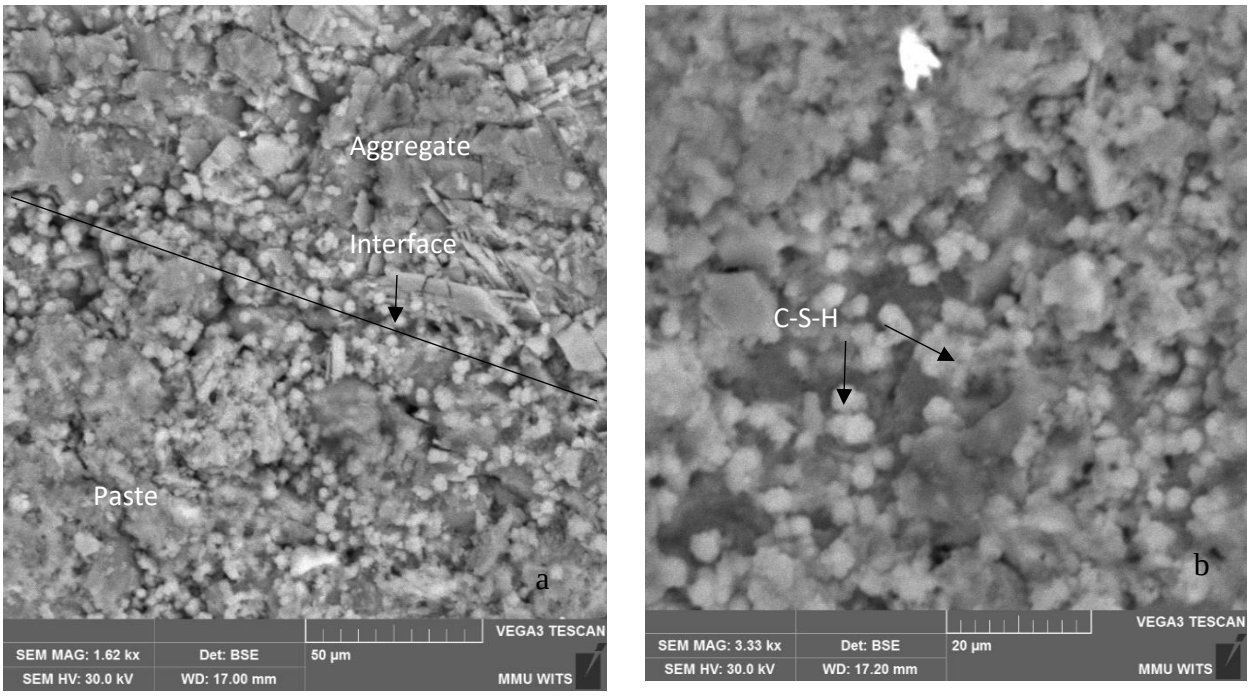

Figure 4.47: Micrograph of (a) Interface and (b) hydrated paste containing 30% C-800 at w/b ratio of 0.4 and curing age of 90 days

The micrographs of an interface is presented in Figures 4.45(a), 4.46(a) and 4.47(a) for FA, C-700 and C-800 respectively for 30% PC replacement level at w/b ratio of 0.4. The interface is not clearly distinguishable for each of the materials indicative of a good bonding. Compared to FA the interfaces for C-700 and C-800 are porous reflective of the wall effect of the aggregate. The wall effect of the aggregate results from heterogeneous bonding between the aggregate and paste characterised by high w/c ratio and fewer cement grain. These effects are induced at fresh state and may have been also influenced by the low workability of the concrete due to high water demand of C-700 and C-800 compared to fly ash. Porosity of interface influences its strength resulting in a weaker interface thereby contributing to the lower compressive strength recorded for the CCAs.

The micrographs of the hardened cement paste are presented in Figures 4.45(b), 4.46(b) and 4.47(b) for FA, C-700 and C-800 respectively. The formation and growth of C-S-H is uniformly distributed within the microstructure for each material which reflects the progress of hydration. The nuclei of C-S-H formed with C-700 is small compared to C-800 while for both C-700 and C-800 the nuclei of C-S-H are less connected when compared to FA and 15% replacement level. The lesser connectivity of the growing C-S-H network for the CCAs can be seen as an effect on PC

hydration affecting the extent of growth and connectivity of the C-S-H nuclei. This further results in continuous pores that are highly connected thereby contributing to their penetrability and strength development resulting in a higher permeability (lower OPI values) and lower strength compared to FA. This further reflect the largely crystalline nature of the CCAs with little if any contribution to the hydration product formation compared to the reactive FA, which contributes to the formation of product through pozzolanic reaction. The uniformly distributed C-S-H nuclei within the microstructure showed that the surfaces of CCA particles contributes to the nucleation and growth of C-S-H but this do not result in significant densification of the microstructure compared to additional product formation.

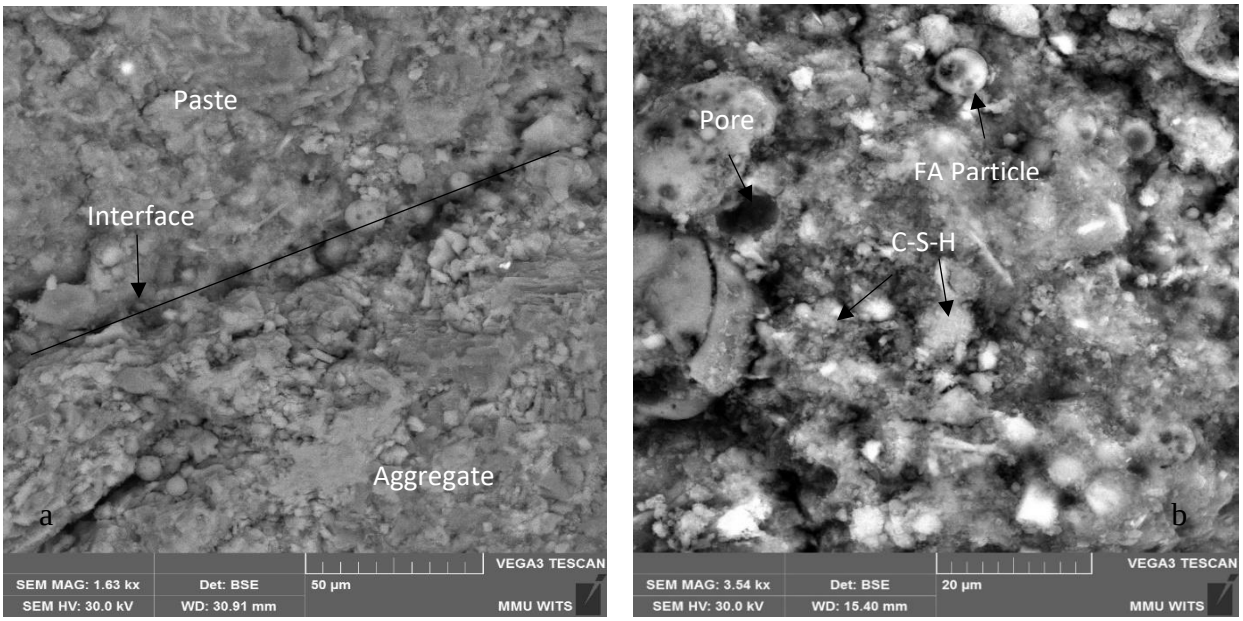

Figure 4.48: Micrograph of (a) Interface and (b) hydrated paste containing 30% FA at w/b ratio of 0.6 and curing age of 90 days

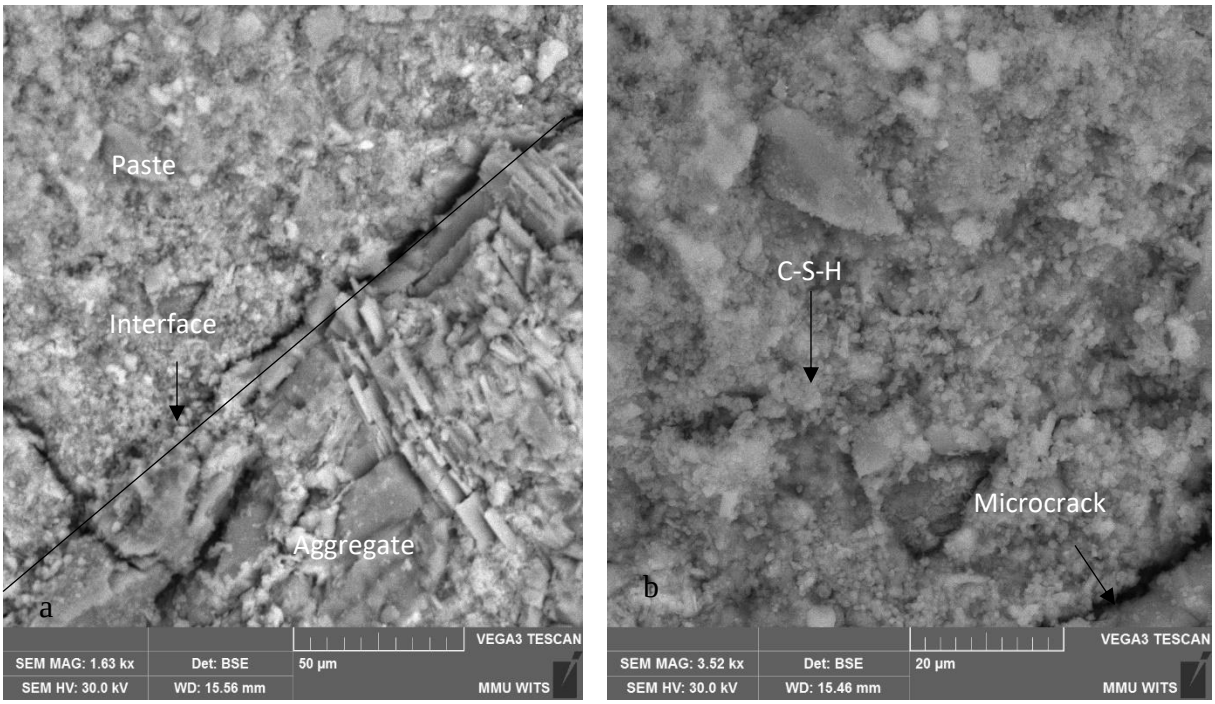

Figure 4.49: Micrograph of (a) Interface and (b) hydrated paste containing 30% C-700 at w/b ratio of 0.6 and curing age of 90 days

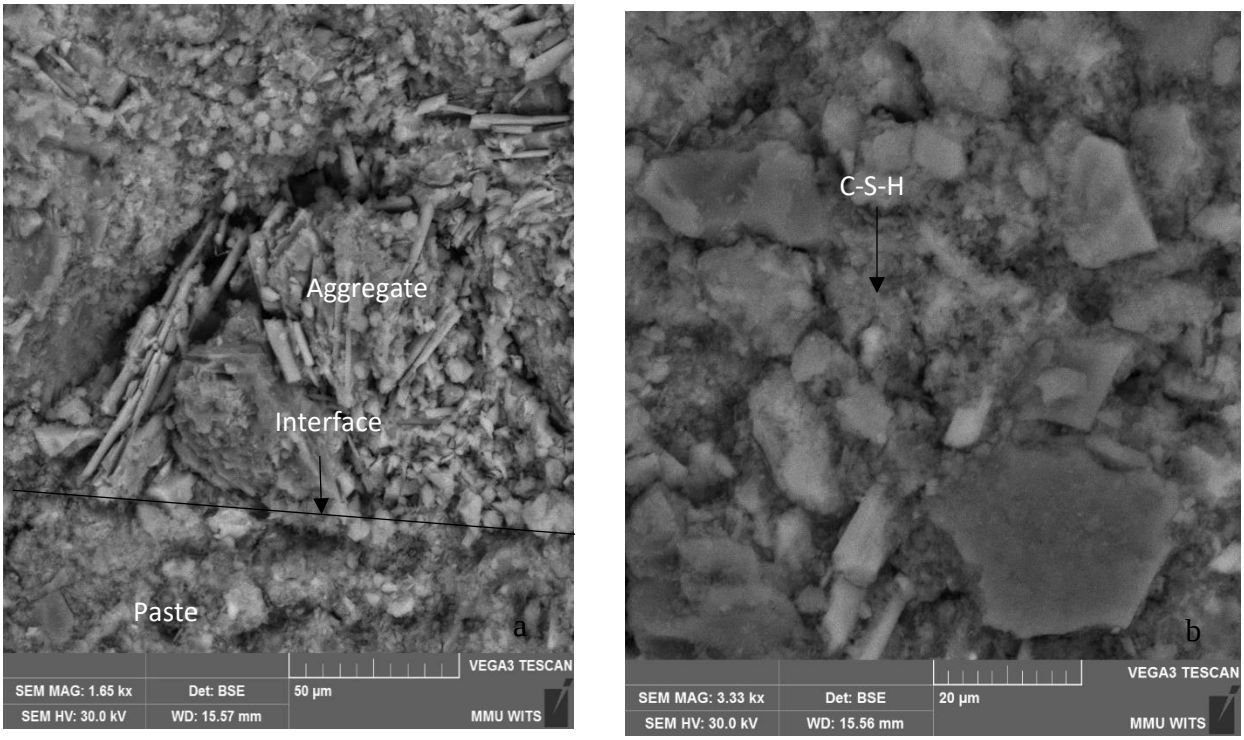

Figure 4.50: Micrograph of (a) Interface and (b) hydrated paste containing 30% C-800 at w/b ratio of 0.6 and curing age of 90 days

The micrographs of the interface are presented in Figures 4.48(a), 4.49(a) and 4.50(a) for FA, C-700 and C-800 respectively. Generally for the three materials, the interfaces can be distinguished and is porous, which shows the effect of increased w/b ratio particularly resulting in a local increase in w/c ratio at the interface. The porosity is influenced by wall effect of the aggregate characterised by low amount of cement particles compared to the bulk paste (K. L. Scrivener et al., 2004).

The micrographs of the hardened cement paste are presented in Figures 4.48(b), 4.49(b) and 4.50(b) for FA, C-700 and C-800 respectively. Generally, there is a reduction in the density and distribution of C-S-H within the microstructure and this could be attributed to the dilution effect of increased w/b ratio and reduced cement content compared to the same system at w/b ratio of 0.4. The reduced density and distribution of C-S-H is linked to the lower strength at w/b ratio of 0.6 when compared to w/b ratio of 0.4.

4.11.1 Effect of microstructure on drying shrinkage

Generally, for both C-700 and C-800, the uniform distribution of C-S-H in the microstructure depicts an increase in fine capillary pores, and this fine pores have an influence drying shrinkage. Drying shrinkage in concrete or mortar is significantly influenced by capillary pressure building up in partially filled pores (Bentz, 2005). These fine pores are emptied as drying time increases leading to a decrease in the internal relative humidity and inducing capillary tension in the pore fluid thereby causing deformation. As this pores are very small the induced capillary tension is high leading to a higher shrinkage and this explains the higher shrinkage strain in the CCAs compared to FA.

5.1 Introduction

This chapter presents the empirical model developed based on the relationship between compressive strength and porosity of concrete based on the results obtained from the experimental work. It is known that the porosity of a material has an influence on its strength (Chen, Wu, & Zhou, 2013) and this is further explored to understand the behaviour of CCA compared to FA. Strength-porosity relationship was explored to know the extent at which porosity influence strength development in concrete containing CCA compared to fly ash. Porosity here depicts the total porosity, inclusive of the porosity of the cement paste and the interfacial transition zone determined on vacuum saturated concrete disc samples. The porosity was estimated from the mass of water through unidirectional absorption of water through exposed surface of concrete disc cored from concrete cubes as explained in section 3.9. Time-dependent evolution of porosity was considered using the strength and porosity values at 28 and 90 days as input parameters in the model. Relationships established in literature were used to know the agreement with the experimental data.

5.2 Relationship between strength and porosity of concrete

Quite a number of relationship have been used in literature to define the dependence of strength on porosity for engineering materials, the most common expression of the relationship between strength and porosity followed power law (Balshin model), linear relation (Hasselman), exponential relation (Ryshkevitch) and logarithmic relation (Schiller) (Chen et al., 2013; Matusinović, Šipušić, & Vrbos, 2003). These models are based on empirical framework to relate the strength and porosity of porous materials and have been used by extension for cement mortar (Chen et al., 2013) and calcium aluminate cement paste (Matusinović et al., 2003). The Balshin equation was developed to relate the tensile strength of ceramic metal to its porosity and the relation is given by the equation below

$$\sigma = \sigma_o (1 - p)^c \quad \text{.....5.1}$$

Where σ is the strength, p is the porosity, σ_o is the strength at zero porosity and c is an empirical constant.

The Hasselman equation describes a linear relationship between strength and porosity and the relation is given as follows

$\sigma = \sigma_o - cP$ ……..5.2

The parameters are as previously defined

The Ryshkevitch equation defines the relation between strength and porosity as being exponential given by

$\sigma = \sigma_o e^{-cp}$ …….5.3

The Schiller equation describes the relationship between strength and porosity of gypsum plaster as a logarithmic function given by

$\sigma = c \ln\left(\frac{p_o}{p}\right)$ ……..5.4

Where p_o is the porosity at zero strength and other parameters are as previously defined.

5.3 Development of the model

The relationship defined by previous authors between strength and porosity shows the interdependence of strength and microstructural evolution, which is significantly influenced by the binder type among other factors. Even though these relationships were developed for other porous materials, their application to concrete is being explored. Concrete is a porous material and its porosity varies with w/b ratio, curing age and SCM type as discussed in section ….. The models were developed for each SCM type and showed sensitivity to the influence of w/b ratio, hence, model has to be developed per w/b. At 28 days, most of the samples had gained more than 70% of the 270 days strength except fly ash at both 15% and 30% replacement level and w/b ratio of 0.6 while at 90 days, all the samples have gained more than 80% of the 270 days strength. The strength at 270 days of curing can be referred as the ultimate strength measured in this study. The percentages shows that significant strength have been attained at both 28 and 90 days and is an indication of significant microstructural development.

The fit of the experimental data using each of the models discussed in section 5.2 is presented in Appendix A7. The linear fit of the experimental data obtained in this study similar to the Hasselman model indicated that the strength and porosity are related by the equation 5.5.

$\sigma = \sigma_o - cP$ ---------- 5.5

Where σ_o and c are empirical constants and vary with SCM type and w/b ratio. The values of the empirical constants are presented in Table 5.1. The fit showed a strong to moderate correlation between the variables except for C-700 at 30% content and w/b ratio of 0.4 which showed a scatter around the line of fit. A good correlation exist between the variables and the empirical constant σ_o can be taken to be the mean strength when the porosity is zero, the value of which varies with mix and w/b ratio. The constant is a mathematical figure to keep the model unbiased since concrete is known to be a porous material, the value is however outside of the data range obtained in this study. The model further showed that strength is inversely proportional to porosity which is consistent with literature, as the strength of a porous material decreases with increase in its porosity (Li & Aubertin, 2003). The strong correlation between the strength and porosity of C-700 at 15% replacement level indicates that the strength-porosity relationship is similar to that obtained for plain PC concrete and concrete containing fly ash.

Table 5.1: Values of the empirical constants for linear fitting

Mix type	**w/b ratio**	**C**	σ_o	$\mathbf{R^2}$
PC	0.4	-6.1111	120.69	0.72
	0.6	-4.1159	87.206	0.86
FA 15	0.4	-4.4839	100.17	0.74
	0.6	-8.0912	118.7	0.68
C-700 15	0.4	-3.454	81.664	0.95
	0.6	-2.1406	49.718	0.87
FA 30	0.4	-3.2422	91.68	0.99
	0.6	-4.13	74.684	0.98
C-700 30	0.4	-6.2627	82.269	0.48
	0.6	-2.0475	44.075	0.77

The empirical relation between strength and porosity similar to Ryshkevitch's model is given in equation 5.6, while the relation similar to Balshin's model and Schiller;' model are given in equations 5.7 and 5.8 respectively.

$\sigma = \sigma_o e^{-cP}$ ……..5.6

$\sigma = \sigma_o (P^{-C})$……..5.7

$\sigma = \sigma_o - c \ln P$……5.8

The empirical constants in equations 5.6, 5.7 and 5.8 are presented in Tables 5.2, 5.3 and 5.4 respectively. The constants are as defined for equation 5.5. Generally, it can be seen for all the mixes and especially for C-700 that the strength-porosity relation can be described by power law, exponential law and logarithm law with a good correlation between the variables. The only exception is C-700 at 30% replacement level and w/b ratio of 0.4. For each of the relation, strength decreases as porosity increases, which is in agreement with the behaviour of porous materials. The pores, which are formed in concrete creates point of discontinuity of paste and thus serves as weak points within the microstructure, hence have an effect on the strength. Concrete being a heterogeneous material is affected by the arrangement of the particles making up its internal structure. The porosity in concrete result from the interparticle space, voids initially occupied by mix water and the interfacial transition zone. Both strength and porosity development in concrete are age dependent and using the age effect as an input parameter in the model resulted in a good correlation as depicted by the models. The continuous hydration of plain Portland cement alongside pozzolanic reaction of pozzolanic SCMs contribute to the variations in the internal structure from one mix to the other. It is postulated that it is the internal structure influenced by the prevailing strength-affecting mechanism have a significant effect on the strength-porosity relation of concrete. Also, the strength-porosity relation holds true for the mixes studied irrespective of the material used as a partial replacement for plain Portland cement.

The models depict the strength of concrete as a function of its porosity, however, porosity of concrete

The effectiveness of using fly ash as an SCM increases with increasing content with the coefficient of correlation tending towards unity at 30% compared to C-700 whose effectiveness reduces with increasing content. For C-700 at 30% content and w/b ratio of 0.4, the predicted strength at 28 days is slightly higher than the actual for strength values lower than the mean, while for 90 days, the predicted strength is lower than the actual strength. For plain PC at w/b ratio of 0.6 and fly ash at 15% content and w/b ratio of 0.6, there is no clear trend in the predicted strength with reference to the mean, as both higher and lower predicted strength was noted for strength values higher or lower than the mean. For 15% C-700 at w/b ratio of 0.6, predicted strength were lower than the actual at 28 days, while for 90 days, strength lower than the mean have higher predicted values than the actual. For 30% fly ash at w/b ratio of 0.6, for actual strength higher than the mean, predicted strength is higher than the actual and vice versa but for actual strength close to the mean,

Table 5.2: Values of the empirical constants for exponential fitting

Mix type	w/b ratio	C	σ_o	R^2
PC	0.4	-0.084	139.35	0.68
	0.6	-0.079	102.06	0.86
FA 15	0.4	-0.058	103.69	0.76
	0.6	-0.177	224.34	0.68
C-700 15	0.4	-0.065	90.696	0.96
	0.6	-0.069	56.298	0.89
FA 30	0.4	-0.046	94.823	0.99
	0.6	-0.108	96.874	0.98
C-700 30	0.4	-0.16	116.82	0.49
	0.6	-0.077	51.398	0.77

Table 5.3: Values of the empirical constants for power law fitting

Mix type	w/b ratio	A	C	R^2
PC	0.4	-0.595	244.86	0.66
	0.6	-0.7	231.87	0.88
FA 15	0.4	-0.303	125.25	0.76
	0.6	-1.623	1598.3	0.69
C-700 15	0.4	-0.54	163.98	0.96
	0.6	-0.601	113.35	0.9
FA 30	0.4	-0.287	118.3	0.99
	0.6	-0.912	267.87	0.97
C-700 30	0.4	-1.103	324.71	0.49
	0.6	-0.666	110.86	0.77

Table 5.4: Values of the empirical constants for logarithm fitting

Mix type	w/b ratio	A	C	R^2
PC	0.4	-43.45	161.88	0.7
	0.6	-36.39	129.89	0.88
FA 15	0.4	-23.36	114.72	0.76
	0.6	-74	208.28	0.69
C-700 15	0.4	-28.57	113.03	0.95
	0.6	-18.78	71.598	0.86
FA 30	0.4	-20.19	107.25	0.99
	0.6	-35.09	113.89	0.98
C-700 30	0.4	-43.23	122.4	0.48
	0.6	-17.66	64.462	0.77

variation between the actual and predicted strength varies with dispersion of data points from the mean. For C-700 at 30% content and w/b ratio of 0.6, for actual strength lower than the mean strength for the group, the predicted strength is higher than the actual and vice-versa for all the models.

5.4 Considering the effect of material property on strength development

From the model obtained above, strength is predicted from solely porosity but it is known that there are materials factors that can significantly influence the strength development of concrete which have not been considered in the model. Compressive strength development of concrete as discussed in chapter four is affected by material factors such as the w/b ratio, binder type and PC replacement level. The model developed in section 5.3 is based on using a hardened state property of concrete to predict performance which in this case is compressive strength. However, it is opined that compressive strength development of concrete can better be described by incorporating both the influence of material properties and hardened state property. A general linear model is proposed to obtain a more general model that can be used to predict strength of concrete giving consideration to the influence of material parameters such as binder type, w/b ratio, PC replacement level and curing age.

The model incorporates both numerical variables and categorical variables. The numerical variables are curing age, w/b ratio and replacement level while the categorical variable is binder type. For curing age, the age of the concrete in days can be substituted directly into the equation while for replacement level, the percentage PC replacement level is substituted directly into the equation to obtain the predicted value of strength. Also, for w/b ratio, the w/b ratio is substituted directly into the equation to obtain the predicted value of strength. For binder type, use of dummy variables was employed to represent the effect of the variable on the model. To each of the binder type, a dummy code was assigned thus, 1 for PC, 2 for FA and 3 for CCA.

The general linear model for such a relationship is given below:

$$\sigma = 148.38 - 11.99(B) - 18.12\left(\frac{w}{b}\right) - 0.16(R) + 0.04(A) - 3.24(p) \quad \ldots\ldots\ldots 5.9$$

Where σ represent the strength, B the binder type (which in this case is plain PC, FA and CCA), w/b the water to binder ratio, R the replacement level, A the curing age and p the porosity.

Equation 5.9 above describes compressive strength of concrete as a function of the material properties (i.e. binder type, w/b ratio, PC replacement level), age effect and porosity. The incorporation of these five predictors into the model describe about 88% of the variation in strength which is as good as the individual models presented in section 5.3 but more comprehensive. Binder type, w/b ratio, PC replacement level and porosity has a similar effect on strength as an increase in the values of these variables result in a reduction in strength, while compressive strength increases as curing age increases.

Table 5.5: Summary of regression analysis

	Coefficients	*Standard Error*	*t Stat*	*P-value*	*Lower 95%*	*Upper 95%*
Intercept	148.3804	6.389801	23.22143	8.94E-30	135.5696	161.1911
Binder type	-11.9885	1.457708	-8.22421	4.3E-11	-14.911	-9.06597
w/b	-90.6004	11.80046	-7.6777	3.27E-10	-114.259	-66.9419
RPL Level	-0.16599	0.098041	-1.69309	0.0962	-0.36255	0.030568
Age	0.044344	0.039626	1.119049	0.268073	-0.0351	0.12379
Porosity	-3.23823	0.877475	-3.6904	0.000522	-4.99747	-1.479

The summary of the regression indicates that both PC replacement level and age do not have a significant effect on the prediction of strength (as the coefficients of both is closer to zero while the p-value is greater than 0.05) when compared to the other variables (binder type, w/b ratio and porosity). This shows that inasmuch as both curing age and replacement level are known to influence strength development, the significance of such effect is dependent on other factors. It is also likely that this may have been due to the different behaviour exhibited by each of the binders notably the increase in strength of PC/FA with increasing PC replacement level while for PC/C700 strength decreases with increasing PC replacement level. One limitation of the model is that the interaction between predictors was not explored as it is possible to see combination of factors that can significantly influence the response variable. However, this can also reduce the strength of the model.

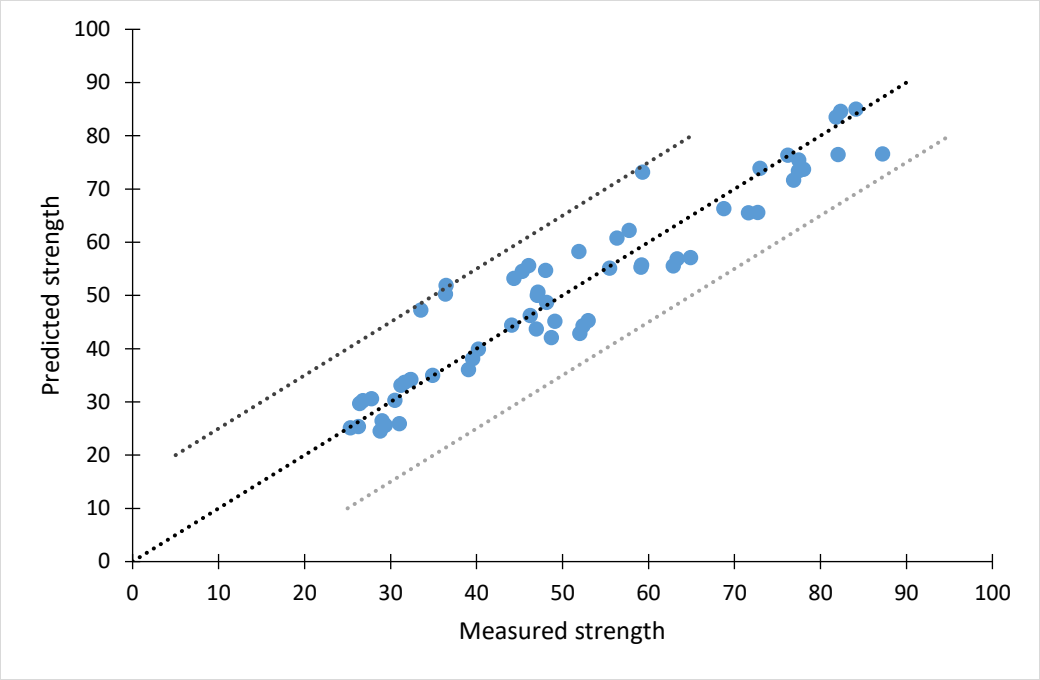

Figure 5.1: Scatterplot of the predicted strength versus the measured strength values

The scatterplot shown in Figure 5.1 indicates that the model predicts strength values that are higher, lower and similar to the measured strength values. For plain PC, the model predicted higher strength than the measured strength while for PC/FA and PC/CCA, the model predicted higher, lower strength than the measured as well as strength similar to the measured values. The underestimation and overestimation of strength by the model shows that the accuracy of prediction is influenced by the predictors when there is a change in binder type. The data points are fairly distributed around the equality line with more than 95% of the standard residuals within the -2 and +2 interval recommended by Montgomery et al. (2011). A major limitation of the model is that it requires material related inputs such as replacement level, binder type and w/b ratio as well as age and porosity to be known for strength to be predicted. This however has an advantage in that it allows the simultaneous consideration of several factors known to influence strength to be put into consideration as predictors of strength.

5.5 Consideration of the effect of w/b ratio on strength-porosity model

The w/b ratio considered as a parameter in the model in section 5.4 has a strong effect on the prediction of strength as presented when compared to the other parameters. The effectiveness of

w/b ratio as a sole predictor is being considered given that it also influences the porosity of cementitious materials significantly. Going by Abram's law, strength is inversely related to w/b ratio, and from properties of conventional concrete, porosity increases as w/b ratio increases. This two relationships are further explored as follows; from the plot of strength and w/b ratio, an equation for strength in terms w/b ratio was obtained as given in Equation 5.10 below for concrete containing fly ash:

$\sigma = 20.171 w/b^{-1.419}$ ($R^2 = 0.78$)……..5.10

Also, a similar relation was obtained for concrete containing CCA and is given in Equation 5.11 below:

$\sigma = 15.666 w/b^{-1.176}$ ($R^2 = 0.74$) ……..5.11

Similarly by considering the relation between porosity and w/b ratio the following Equations were obtained for concrete containing fly ash and CCA respectively:

$P = 15.226 w/b^{1.0853}$ ($R^2 = 0.46$) …….5.12

$P = 10.615 w/b^{0.3961}$ ($R^2 = 0.29$) ……..5.13

The terms in the equations are as previously defined.

The empirical relations expressed in Equations 5.10 to 5.13 are based on average compressive strength and porosity. To further account for the effect of w/b ratio on strength prediction from porosity, Equations 5.12 and 5.13 were substituted into Equations 5.10 and 5.11 respectively. The obtained relations is presented in Equations 5.14 and 5.15 respectively for concrete containing fly ash and CCA.

$$\sigma = 20.171 \left[\frac{1}{\left(P/_{15.226}\right)^{1.307}}\right] \quad \text{…….5.14}$$

$$\sigma = 15.666 \left[\frac{1}{\left(P/_{10.615}\right)^{2.969}}\right] \text{……5.15}$$

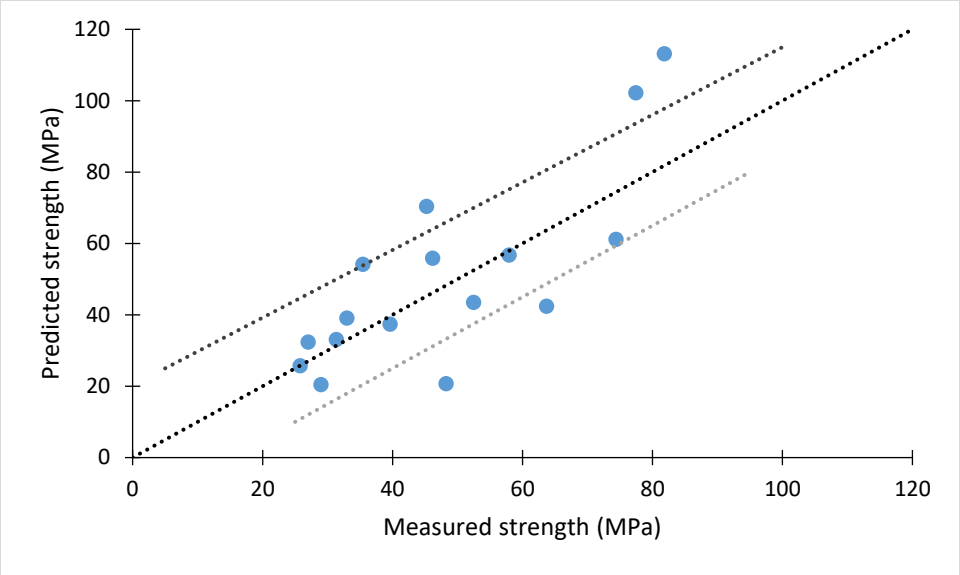

Figure 5.2: Scatter plot of predicted strength versus measured strength

The new model predicted strength fairly well as shown in Figure 5.2, with the predicted strength being higher, lower and similar to the measured strength. The model predicted well strength up to 60 MPa as shown in Figure 5.2 with strength values clustering around the line of equality. A major limitation of the models is that it may not be generalised to other binder types than fly ash and CCA used in its development. This may be as a result of limited data used in development of the model. The model can be improved upon in the future using a wider scope of parameters most especially the w/b ratio.

6.1 Introduction

The performance of CCA as a partial replacement for plain PC has been studied combining both reactivity test approach and performance test approach to determine its suitability as a partial replacement for Portland cement as well as to understand its reaction mechanism with Portland cement. This study has been able to combine two different methods of obtaining CCA from raw corn cobs. Calcination in a drum furnace typifies a simple and easy to adopt method but with the calcination temperature difficult to control but can be measured. On the other hand, calcination of previously pyrolysed corn cob powder in an electric furnace seeks an improvement in the method of calcination whereby the calcination temperature could be controlled. Combining both methods affords the opportunity to investigate the influence of calcination method on the characteristics of the ash.

Investigation on the reactivity and performance of CCA is essential to its adoption and use or otherwise as a partial replacement for cement. Reactivity tests were carried out to assess the likely reaction mechanism by which the material influences the performance (strength and durability) of cementitious systems following tests protocol of R3 test using the bound water approach and strength activity index estimated from compressive strength of 50mm mortar cubes. Performance testing on the other hand assesses the effect of the material on specific properties of cementitious systems which is essential to understanding the behaviour and scope of practical application of the material. Performance tests that were done are compressive strength of concrete, drying shrinkage test, durability index tests and microstructural characterisation. The details of the test procedure and findings were presented in chapters 3 and 4 respectively. Furthermore, a generalised linear relationship between the strength and durability indicator (namely porosity) was sought for the prediction of performance of the material in concrete considering the effect of material parameters (PC replacement level, w/b ratio) and age effect (curing age).

6.2 General conclusion

The calcination methods of obtaining the ashes contribute significantly to the characteristics of the ashes and their performance in cementitious systems. The process of calcining in a drum furnace results in ash that is largely crystalline with a loss on ignition greater than the 10% and 6%

recommended for class N pozzolans and fly ashes respectively by ASTM C618. The crystallinity of the ash obtained can be linked to the long duration involved in the reduction of the raw cobs to ashes which is necessary to obtain the ash required for investigation. This is a limitation of the method as the unburnt carbon remaining in the ash affects the workability of the ash. The second method adopted by calcining previously pyrolysed corn cob powder in a furnace also yields a largely crystalline ash but with a lower loss on ignition which is within limits specified by ASTM C618. A major challenge that remains is obtaining a reactive material from calcination of corn cob with the only promising alternative being envisaged to be industrial calcination in a controlled environment or combustion in thermal power plant (typical of fly ash) which this study was not able to achieve. The significant difference between the loss on ignition of the CCA and fly ash is evidence of the better quality control associated with industrial processing of fly ash.

In terms of particle size distribution, the CCAs used in this study are coarser than the fly ash used as a reference material. The D_{10}, D_{50} and D_{90} particle parameter was significantly higher in the CCAs compared to fly ash. This is indicative of a lesser space filling and filler effect and hence a less dense microstructure with CCA compared to fly ash in cementitious systems.

In terms of the chemical composition, the CCAs used in this study are largely siliceous with a high potassium oxide content. The high potassium oxide is considered a major limitation to their use in concrete as this increases the risk of alkali-silica reaction where favourable conditions exist. It also influences the structure and nature of hydration product formed by binding to the C-S-H thereby weakening the calcium-to-silica bonding with a consequential effect on compressive strength development. The ashes were largely crystalline with the amorphous content being less than 3% and this has a limitation on the use of CCA as a pozzolanic material in cementitious system.

From the reactivity test results, limited level of pozzolanic activity can be attributed to the CCAs given a higher bound water value than andesite sand (an inert material) but a lower bound water value than FA (a known pozzolanic material). The limited pozzolanic reactivity in the CCAs can be associated to the limited amorphous content of the ashes as depicted by the XRD results and this was insufficient to enhance the performance of the system as it is with fly ash.

The inclusion of CCA has an effect on the hydration reaction of plain PC as measured by isothermal calorimetry, with a prolonged induction phase and delay in the evolution of the main heat peak compared to fly ash, andesite sand and plain PC pastes. This effect is attributed to the

dissociation of the k+ ions in solution and subsequent effect on the dissolution of C_3S and the nucleation and growth of C-S-H. The effect on both the induction phase and main heat peak has a significant effect on the magnitude of strength gained in concrete.

The pore solution analysis using cold water extraction method showed that the potassium oxide and sodium oxide present in the CCAs are highly soluble and go readily into solution in the presence of moisture. This is evident in the high concentrations measured at both 28 days and 90 days compared to the concentration in PC/FA and plain PC. This has an implication for the use of CCA with reactive aggregates as this can increase the risk of alkali-aggregate (and alkali-silica) reaction which is a known deterioration mechanism in concrete. This will necessitate the need for pre-treatment of the cobs in order to reduce to certain extent the alkalis present in the raw cobs prior to calcination otherwise the high alkali content in the raw cobs is a limitation to its use in cementitious system where alkali-aggregates reaction is envisaged.

The use of CCA in concrete resulted in low strength development compared to plain PC concrete and fly ash containing concrete, although there is increase in strength gain of the concrete with age. The increase in strength with age can be associated to the hydration reaction of plain PC being the main chemical process resulting in strength gain while the low strength can be attributed to dilution effect which predominates over the filler effect. The dilution effect of using CCA as a partial replacement of PC was not adequately compensated due to its' largely crystalline nature. The filler effect of CCA in concrete was also affected by its coarser particle size compared to that of fly ash resulting in a lower strength than that of andesite crusher sand (an inert material) used for its comparison. The low strength is also attributed to the interference of the high alkali content of the CCAs with hydration product formation envisaged to alter the structure of the C-S-H formed by a likely binding of the alkalis to the C-S-H thereby resulting in low strength.

On the influence of CCA on durability, the inclusion of the material in concrete affects the permeability to oxygen gas, absorption of water through the capillary pores and chloride ion diffusion with a behaviour inferior to plain PC and fly ash. This effect is due to the interconnectivity and tortuosity of pores, increase in pore size with increasing w/b ratio and increase in pore volume. The durability indices improved with age depicting the influence of continued plain PC hydration in modification of the microstructure.

On the influence of CCA on the drying shrinkage of mortar, the inclusion of CCA in mortar resulted in high drying shrinkage strain compared to plain PC and fly ash. This is associated with the largely crystalline nature of the ashes and the carbon content adsorbing water. The mechanism of influence on drying shrinkage is linked to capillary tension and disjoining pressure. As drying proceeds, the adsorbed water is lost through capillary action inducing tensile stresses in the capillary pores and subsequently compressive stresses on the solid phase leading to shrinkage strain. Also, as hydration proceeds simultaneously with drying, C-S-H layers are formed with water adsorbed in the interlayer. As drying proceeds, the internal relative humidity reduces and the forces of repulsion within the interlayer tends to reduce leading to greater attraction between the C-S-H layers which results in macroscopic deformation.

The use of CCA also influence the microstructure of concrete with CCA surface acting as points for nucleation and growth of C-S-H while the C-S-H formed is uniformly distributed but with lesser degree of connectivity between the nuclei compared to fly ash and plain PC concrete.

A generalised linear relationship can be obtained between the strength and porosity of concrete which considers the influence of material parameters like binder type, w/b ratio and PC replacement level, and the age effect.

The following conclusions have been drawn from the study

1. The two methods of calcining corn cob have an influence on the chemical and mineralogical composition as well as the reactivity of the ashes with the ash produced being largely crystalline and the mechanism of reaction in cementitious with respect to compressive strength development mainly influenced by the filler effect rather than by amorphous content. This brings to the fore the limiting effect of calcination method on the quality of ash.
2. The high potassium oxide content of the ashes influences the mechanisms of hydration reaction of plain PC at dissolution and induction phases with a subsequent effect on compressive strength, drying shrinkage and microstructure of concrete and mortar.
3. The low strength development in concrete containing CCA compared to plain Portland cement concrete is due to the low reactivity of the ash and the influence of the high potassium oxide of the ash on the structure of the C-S-H formed with plain PC.

4. The partial replacement of PC with CCA has an influence on volume change resulting in an increase in drying shrinkage of mortar, an effect associated to the largely crystalline nature of the ash, the carbon content of the ash as well as the high potassium oxide content of the ash. Similarly, it is expected that the use of CCA will influence the drying shrinkage of concrete but to a lower degree due to the restraining effects of coarse aggregates in concrete.
5. The use of CCA in concrete resulted in increase in permeability of concrete to gas ingress through the pores and interface between the hydrated paste and aggregates as well as water absorption through the capillary pores. This has an implication on the durability of concrete implying that the use of the ash may increases the risk of deterioration of concrete in service.
6. Partial replacement of PC with CCA up to 15% showed some potential in terms of strength development but the increased risk of deterioration compared to fly ash and plain PC indicate a need for the use of a more reactive ash which could contribute to the microstructural development of the system through a beneficial pozzolanic reaction. This could not be achieved in this study, this may help increase the potential use of CCA and its adoption for use in construction.

6.3 Recommendations

1. The two methods of calcination employed in this study resulted in crystalline ash which impacted the reactivity in cementitious systems, hence there is a need for improvement of method especially exploring calcination in a controlled environment based on industrial application. This may help overcome the challenges associated with calcination and quality of the ash as it is envisaged that the unburnt carbon content may be significantly reduced.
2. As the calcination of previously pyrolysed carbon black CCA powder showed some potential compared to calcination in a drum furnace, this can further be scaled for further laboratory investigation to see any improvement in the quality of the ash with respect to amorphous content of the ash.

3. As corn cob similar to other agro-based wastes is bulky with low ash content, the cost-benefit assessment needs to be done to ascertain the sustainability vis-à-vis waste cobs collection, calcination process, ash yield and ash quality.
4. Given the high alkali content of CCA, the influence on alkali-silica reaction needs to be investigated to quantify the likely contribution to concrete deterioration.
5. The calcination of large quantities of cobs to obtain the ash remains a challenge coupled with the availability of suitable facility to calcine the material and this has been noted to be a major contributory factor to the properties, quality and performance of the ash in concrete. To overcome this challenge will necessitates industrial engagement and collaboration towards the utilisation of the raw cobs as fuel. This will help in quality control and assurance as well as the availability of the ash.

Adesanya, D. A., & Raheem, A. A. (2009a). A study of the workability and compressive strength characteristics of corn cob ash blended cement concrete. *Construction and Building Materials*, *23*(1), 311–317. https://doi.org/10.1016/j.conbuildmat.2007.12.004

Adesanya, D. A., & Raheem, A. A. (2009b). Development of corn cob ash blended cement. *Construction and Building Materials*, *23*(1), 347–352.

Adesanya, D. A., & Raheem, A. A. (2010). A study of the permeability and acid attack of corn cob ash blended cements. *Construction and Building Materials*, *24*(3), 403–409.

Al-Shmaisani, S., Kalina, R. D., Ferron, R. D., & Juenger, M. C. G. (2022). Critical assessment of rapid methods to qualify supplementary cementitious materials for use in concrete. *Cement and Concrete Research*, *153*(January), 106709. https://doi.org/10.1016/j.cemconres.2021.106709

Alexander, M. G. (1994). Deformation properties of blended cement concretes containing blastfurnace slag and condensed silica fume. *Advances in Cement Research*, *6*(22), 73–81. https://doi.org/10.1680/adcr.1994.6.22.73

Alexander, M. G., & Griesel, E. J. (2004). Effect of Controlled Environment Conditions on Durability Index Parameters of Portland Cement Concretes. *Concrete Beton*, *107*(September), 7–13.

Angelucci, M., Beushausen, H., Alexander, M. ., & Mackechnie, J. . (2017). Specifying cement content for concrete durability : why less is more Specifying cement content for concrete durability : why less is more. *Concrete Beton*, *150*(September), 12–17.

Antiohos, S. K., Papadakis, V. G., & Tsimas, S. (2014). Rice husk ash (RHA) effectiveness in cement and concrete as a function of reactive silica and fineness. *Cement and Concrete Research*, *61–62*, 20–27.

Arif, E. (2016). *Development of value added products from sugarcane boiler ashes : utilisation in cements , mortars and concretes*. Southern Cross University.

Asonja, A., Desnica, E., & Radovanović, L. Z. (2017). Energy efficiency analysis of corn cob used as a fuel. *Energy Sources, Part B: Economics, Planning and Policy*, *12*(1), 1–7.

ASTM C1897. (2020). Standard Test Methods for Measuring the Reactivity of Supplementary Cementitious Materials by Isothermal Calorimetry and Bound Water Measurements. *ASTM International, West Conshohocken, PA*, *04*(August), 7–11. https://doi.org/10.1520/C1897-20.2

Augustine, A., & Michael, T. (2016). Partial replacement of cement with corn cob ash. *International Journal of Innovative Research in Multidisciplinary Field*, *2*(7), 159–169.

Avet, F., Snellings, R., Alujas, A., Ben, M., & Scrivener, K. (2016). Development of a new rapid , relevant and reliable (R 3) test method to evaluate the pozzolanic reactivity of calcined kaolinitic clays. *Cement and Concrete Research*, *85*, 1–11. https://doi.org/10.1016/j.cemconres.2016.02.015

Bahurudeen, A., & Santhanam, M. (2015). Influence of different processing methods on the pozzolanic performance of sugarcane bagasse ash. *Cement and Concrete Composites*, *56*, 32–45.

Barahira, D. S., Okudoh, V. I., & Eloka-Eboka, A. C. (2021). Suitability of crop residues as feedstock for biofuel production in south africa: A sustainable win-win scenario. *Journal of Oleo Science*, *70*(2), 213–226. https://doi.org/10.5650/jos.ess20288

Batidzirai, B., Valk, M., Wicke, B., Junginger, M., Daioglou, V., Euler, W., & Faaij, A. P. C. (2016). Current and future technical, economic and environmental feasibility of maize and wheat residues supply for biomass energy application: Illustrated for South Africa. *Biomass and Bioenergy*, *92*, 106–129.

Bellmann, F, Sowoidnich, T., Ludwig, H.-M., & Damidot, D. (2012). Analysis of the surface of tricalcium silicate during the induction period by X-ray photoelectron spectroscopy. *Cement & Concrete Research*, *42*, 1189–1198.

Bellmann, Frank, Damidot, D., Möser, B., & Skibsted, J. (2010). Improved evidence for the existence of an intermediate phase during hydration of tricalcium silicate. *Cement and Concrete Research*, *40*(6), 875–884.

Bellmann, Frank, Sowoidnich, T., Ludwig, H. M., & Damidot, D. (2015). Dissolution rates during the early hydration of tricalcium silicate. *Cement and Concrete Research*, *72*, 108–116.

Beltzung, F., & Wittmann, F. H. (2005). Role of disjoining pressure in cement based materials.

Cement and Concrete Research, *35*(12), 2364–2370. https://doi.org/10.1016/j.cemconres.2005.04.004

Bentz, D. P. (2005). Curing with Shrinkage-Reducing Admixtures. *Concrete International*, Vol. 27, pp. 55–60. Retrieved from http://search.proquest.com/docview/198707241?accountid=27917%5Cnhttp://linksource.ebsco.com/linking.aspx?sid=ProQ%3Asciencejournals&fmt=journal&genre=article&issn=01624075&volume=&issue=&date=2005-10-01&spage=55&title=Concrete+International&atitle=Curing+

Berodier, E., & Scrivener, K. (2014). Understanding the filler effect on the nucleation and growth of C-S-H. *Journal of the American Ceramic Society*, *97*(12), 3764–3773.

Bhatty, J. I., & Reid, K. J. (1985). Use of thermal analysis in the hydration studies of a type 1 portland cement produced from mineral tailings. *Thermochimica Acta*, *91*(C), 95–105.

Boström, D., Skoglund, N., Grimm, A., Boman, C., Öhman, M., Broström, M., & Backman, R. (2012). Ash transformation chemistry during combustion of biomass. *Energy and Fuels*, *26*(1), 85–93.

Brouwers, H. J. H. (2011). *A hydration model of Portland Cement using the work of Powers and Brownyard*. Eindhoven University of Technology, Portland Cement Association.

Bullard, J. W., & Flatt, R. J. (2010). New insights into the effect of calcium hydroxide precipitation on the kinetics of tricalcium silicate hydration. *Journal of the American Ceramic Society*, *93*(7), 1894–1903.

Bullard, J. W., Jennings, H. M., Livingston, R. A., Nonat, A., Scherer, G. W., Schweitzer, J. S., … H, T. (2015). Mechanisms of cement hydration. *Science and Technology of Concrete Admixtures*, *41*(12), 129–145.

Bullard, J. W., Jennings, H. M., Livingston, R. A., Nonat, A., Scherer, G. W., Schweitzer, J. S., … Thomas, J. J. (2011). Mechanisms of cement hydration. *Cement and Concrete Research*, *41*(12), 1208–1223. https://doi.org/10.1016/j.cemconres.2010.09.011

Chao-Lung, H., Anh-Tuan, B. Le, & Chun-Tsun, C. (2011). Effect of rice husk ash on the strength and durability characteristics of concrete. *Construction and Building Materials*, *25*(9), 3768–3772.

Chatveera, B., & Lertwattanaruk, P. (2011). Durability of conventional concretes containing black rice husk ash. *Journal of Environmental Management*, *92*(1), 59–66.

Chen, X., Wu, S., & Zhou, J. (2013). Influence of porosity on compressive and tensile strength of cement mortar. *Construction and Building Materials*, *40*, 869–874. https://doi.org/10.1016/j.conbuildmat.2012.11.072

Choate, W. T. (2003). Energy and Emission Reduction Opportunities for the Cement Industry. In *U.S. Department of Energy, Energy Efficiency and Renewable Energy*.

Cogut, A. (2016). Open burning of waste: a global health disaster. In *R20 Regions of climate action*. Retrieved from https://regions20.org/wp-content/uploads/2016/08/OPEN-BURNING-OF-WASTE-A-GLOBAL-HEALTH-DISASTER_R20-Research-Paper_Final_29.05.2017.pdf?fbclid=IwAR0NDYVAdq66rdJpT1gO0R3qyeYJs8dJ6-8Vs1wNTF0yriaV8bsSnr4JLLM

Cordeiro, G. C., Toledo Filho, R. D., & Fairbairn, E. M. R. (2009). Effect of calcination temperature on the pozzolanic activity of sugar cane bagasse ash. *Construction and Building Materials*, *23*(10), 3301–3303.

Cordeiro, G. C., Toledo Filho, R. D., Tavares, L. M., & Fairbairn, E. M. R. (2008). Pozzolanic activity and filler effect of sugar cane bagasse ash in Portland cement and lime mortars. *Cement and Concrete Composites*, *30*(5), 410–418.

Cyr, M., Lawrence, P., & Ringot, E. (2005). Mineral admixtures in mortars: Quantification of the physical effects of inert materials on short-term hydration. *Cement and Concrete Research*, *35*(4), 719–730. https://doi.org/10.1016/j.cemconres.2004.05.030

Cyr, M., Lawrence, P., & Ringot, E. (2006). Efficiency of mineral admixtures in mortars: Quantification of the physical and chemical effects of fine admixtures in relation with compressive strength. *Cement and Concrete Research*, *36*(2), 264–277.

Damidot, D., & Nonat, A. (1994). C 3 S hydration in diluted and stirred suspension: (II) properties of C—S—H precipitated during the two kinetic steps. *Advances in Cement Research*, *6*(22), 83–91. https://doi.org/10.1680/adcr.1994.6.22.83

Damidot, D., & Nonat, A. (1994). C 3 S hydration in diluted and stirred suspensions: (I) study of the two kinetic steps. *Advances in Cement Research*, *6*(21), 27–35. Retrieved from

https://www.icevirtuallibrary.com/doi/pdf/10.1680/adcr.1994.6.21.27

Damidot, D., Nonat, A., Barret, P., Bertrandie, D., Zanni, H., & Rassem, R. (1995). C3S hydration in diluted and stirred suspensions: (III) NMR study of C-S-H precipitated during the two kinetic steps. *Advances in Cement Research*, *7*(25), 1–8. https://doi.org/10.1680/adcr.1995.7.25.1

Danje, S. (2011). *Fast pyrolysis of corn residues for energy production*. (December), 1–222.

De la Varga, I., Castro, J., Bentz, D. P., Zunino, F., & Weiss, J. (2018). Evaluating the hydration of high volume fly ash mixtures using chemically inert fillers. *Construction and Building Materials*, *161*, 221–228.

De Weerdt, K., Kjellsen, K. O., Sellevold, E., & Justnes, H. (2011). Synergy between fly ash and limestone powder in ternary cements. *Cement and Concrete Composites*, *33*(1), 30–38.

Deboucha, W., Leklou, N., Khelidj, A., & Oudjit, M. N. (2017). Hydration development of mineral additives blended cement using thermogravimetric analysis (TGA): Methodology of calculating the degree of hydration. *Construction and Building Materials*, *146*, 687–701. https://doi.org/10.1016/j.conbuildmat.2017.04.132

department of agriculture and fisheries, Q. government. (2018). Varieties and planting of maize. Retrieved July 12, 2018, from https://www.daf.qld.gov.au/business-priorities/plants/field-crops-and-pastures/broadacre-field-crops/maize/varieties-planting

Deschner, F., Münch, B., Winnefeld, F., & Lothenbach, B. (2013). Quantification of fly ash in hydrated, blended Portland cement pastes by backscattered electron imaging. *Journal of Microscopy*, *251*(2), 188–204.

Deschner, Florian, Winnefeld, F., Lothenbach, B., Seufert, S., Schwesig, P., Dittrich, S., … Neubauer, J. (2012). Hydration of Portland cement with high replacement by siliceous fly ash. *Cement and Concrete Research*, *42*(10), 1389–1400. https://doi.org/10.1016/j.cemconres.2012.06.009

Detwiler, R. J., & Mehta, P. K. (1989). Chemical and physical effects of silica fume on the mechanical behaviour of concrete. *ACI Materials Journal*, *86*(6), 609–614.

Di Bella, C., Wyrzykowski, M., & Lura, P. (2017). Evaluation of the ultimate drying shrinkage of

cement-based mortars with poroelastic models. *Materials and Structures/Materiaux et Constructions*, *50*(1). https://doi.org/10.1617/s11527-016-0870-0

Dittrich, S., Neubauer, J., & Goetz-Neunhoeffer, F. (2014). The influence of fly ash on the hydration of OPC within the first 44 h - A quantitative in situ XRD and heat flow calorimetry study. *Cement and Concrete Research*, *56*, 129–138.

Donatello, S., Tyrer, M., & Cheeseman, C. R. (2010). Comparison of test methods to assess pozzolanic activity. *Cement and Concrete Composites*, *32*, 121–127. https://doi.org/10.1016/j.cemconcomp.2009.10.008

Duchesne, J., & Berube, M. A. (1995). Effect of supplementary cementing materials on the composition of Cement Hydration Products. *Advanced Cement Based Materials*, *2*, 43–52. Retrieved from https://ac.els-cdn.com/1065735595900241/1-s2.0-1065735595900241-main.pdf?_tid=48634d04-376f-4f27-b283-b9205314def1&acdnat=1534422134_a44baa6b273c948016700caea796c10e

Escalante, J. I., Gómez, L. Y., Johal, K. K., Mendoza, G., Mancha, H., & Méndez, J. (2001). Reactivity of blast-furnace slag in Portland cement blends hydrated under different conditions. *Cement and Concrete Research*, *31*(10), 1403–1409.

food and agriculture organisation. (2016). FAOSTAT. Retrieved July 12, 2018, from http://www.fao.org/faostat/en/#rankings/countries_by_commodity

Fulton. (2021). Concrete technology. In G. Owens (Ed.), *Fulton's Concrete Technology* (9th ed.). Midrand: Cement & Concrete Institute.

Garci Juenger, M. C., & Jennings, H. M. (2002). Examining the relationship between the microstructure of calcium silicate hydrate and drying shrinkage of cement pastes. *Cement and Concrete Research*, *32*(2), 289–296. https://doi.org/10.1016/S0008-8846(01)00673-1

Gardner, N. ., & Lockman, M. . (2001). Design Provisions for Drying Shrinkage and Creep of Normal-Strength Concrete. *ACI Materials Journal*, *98*(2), 159–167.

Gardner, N. ., & Zhao, J. . (1993). Creep and Shrinkage Revisited. *ACI Materials Journal*, *90*(3), 236–246.

Gardner, N. J. (2004). Comparison of prediction provisions for drying shrinkage and creep of

normal-strength concretes. *Canadian Journal of Civil Engineering*, *31*(5), 767–775. https://doi.org/10.1139/L04-046

Garrault, S., Finot, E., Lesniewska, E., & and Nonat, A. (2005). Study of C-S-H growth on C 3 S surface during its early hydration. *Materials and Structures*, *38*, 435–442. Retrieved from http://demo.webdefy.com/rilem-new/wp-content/uploads/2016/09/1843.pdf

Gartner, E. (2011). Discussion of the paper "dissolution theory applied to the induction period in alite hydration" by P. Juilland et al., Cem. Concr. Res. 40 (2010) 831-844. *Cement and Concrete Research*, *41*(5), 565–567. Retrieved from http://dx.doi.org/10.1016/j.cemconres.2011.01.019

Gartner, E.M., Young, J. F., Damidot, D. . ., & Jawed, I. (2002). Hydration of Portland cement. In B. J. Barnes P (Ed.), *Structure and Performance of Cements* (second, pp. 57–111). Retrieved from https://books.google.co.za/books?id=6wPpkyrWE5oC&printsec=frontcover&source=gbs_atb#v=onepage&q&f=false

Gartner, Ellis M., & Jennings, H. M. (1987). Thermodynamics of Calcium Silicate Hydrates and Their Solutions. *Journal of the American Ceramic Society*, *70*(10), 743–749.

Gatner, E. M., Young, J. F., Damidot, D. a., & Jawed, I. (2002). Hydration of portland cement. In B. J & B. P (Eds.), *The structure and performance of cements* (2nd ed., pp. 1–19). London: Spon Press.

Gaylard, P. C., Ballim, Y., & Fatti, L. P. (2013). A model for the drying shrinkage of South African concretes. *Journal of the South African Institution of Civil Engineering*, *55*(1), 45–59.

Gilbe, C., Öhman, M., Lindström, E., Boström, D., Backman, R., Samuelsson, R., & Burvall, J. (2008). Slagging characteristics during residential combustion of biomass pellets. *Energy and Fuels*, *22*(5), 3536–3543.

Githachuri, K., Alexander, M., & Moyo, P. (2012). Durability performance of a range of marine concretes and the applicability of the South African Service Life Prediction Model. *Materials and Structures/Materiaux et Constructions*, *45*(1–2), 185–198. https://doi.org/10.1617/s11527-011-9759-0

Givi, A. N., Rashid, S. A., Aziz, F. N. A., & Salleh, M. A. M. (2010). Assessment of the effects

of rice husk ash particle size on strength, water permeability and workability of binary blended concrete. *Construction and Building Materials*, *24*(11), 2145–2150.

Goldman, A., & Bentur, A. (1989). "Bond effects in high-strength silica-fume concretes". *ACI Materials Journal*, *86*(5), 440–447.

Goldman, A., & Bentur, A. (1993). The influence of microfillers on enhancement of concrete strength. *Cement and Concrete Research*, *23*(4), 962–972.

Gouws, S. M., Alexander, M. G., & Maritz, G. (2001). Use of Durability Index Tests for the Assessment and Control of Concrete Quality on Site. *Concrete Beton*, *98*(April), 5–16. Retrieved from www.concretesociety.co.za

Grimm, A., Skoglund, N., Boström, D., & Öhman, M. (2011). Bed agglomeration characteristics in fluidized quartz bed combustion of phosphorus-rich biomass fuels. *Energy and Fuels*, *25*(3), 937–947.

Gutteridge, W. A., & Dalziel, J. . (1990a). Filler cement: the effect of the secondary component on the hydration of portland cement: Part 2: fine hydraulic binders. *Cement & Concrete Research*, *20*(6), 853–861.

Gutteridge, W. A., & Dalziel, J. . (1990b). Filler cement: The effect of the secondary component on the hydration of Portland cement. Part 1: Fine Non-hydraulic fillers. *Cement and Concrete Research*, *20*, 778–782.

Haha, M. Ben, De Weerdt, K., & Lothenbach, B. (2010). Quantification of the degree of reaction of fly ash. *Cement and Concrete Research*, *40*(11), 1620–1629.

Hall, C. (1989). Water sorptivity of mortars and concretes: A review. *Magazine of Concrete Research*, *41*(147), 51–61. https://doi.org/10.1680/macr.1989.41.147.51

Han, F., He, X., Zhang, Z., & Liu, J. (2017). Hydration heat of slag or fly ash in the composite binder at different temperatures. *Thermochimica Acta*, *655*(July), 202–210.

Hill, R. L., Sarkar, S. L., Rathbone, R. F., & Hower, J. C. (1997). An examination of fly ash carbon and its interactions with air entraining agent. *Cement and Concrete Research*, *27*(2), 193–204. https://doi.org/10.1016/S0008-8846(97)00008-2

Huang, L., & Yan, P. (2019). Effect of alkali content in cement on its hydration kinetics and

mechanical properties. *Construction and Building Materials*, *228*, 116833. https://doi.org/10.1016/j.conbuildmat.2019.116833

Idiart, A. E. (2009). *Chapter 3 DRYING SHRINKAGE AND CREEP IN CONCRETE : A SUMMARY*. Retrieved from http://www.ncbi.nlm.nih.gov/pubmed/20826935

Ikponmwosa, E. E., Salau, M. A., & Kaigama, W. B. (2015). Evaluation of strength characteristics of laterized concrete with corn cob ash (CCA) blended cement. *IOP Conference Series: Materials Science and Engineering*, *96*(1). https://doi.org/10.1088/1757-899X/96/1/012009

Isaia, G. C., Gastaldini, A. L. G., & Moraes, R. (2003). Physical and pozzolanic action of mineral additions on the mechanical strength of high-performance concrete. *Cement and Concrete Composites*, *25*(1), 69–76.

Jansen, D., Neubauer, J., Goetz-Neunhoeffer, F., Haerzschel, R., & Hergeth, W. D. (2012). Change in reaction kinetics of a Portland cement caused by a superplasticizer - Calculation of heat flow curves from XRD data. *Cement and Concrete Research*, *42*(2), 327–332. Retrieved from http://dx.doi.org/10.1016/j.cemconres.2011.10.005

Jaturapitakkul, C., Tangpagasit, J., Songmue, S., & Kiattikomol, K. (2011). Filler effect and pozzolanic reaction of ground palm oil fuel ash. *Construction and Building Materials*, *25*, 4287–4293.

Jenkins, B. M., Bakker, R. R., & Wei, J. B. (1996). On the properties of washed straw. *Biomass and Bioenergy*, *10*(4), 177–200. https://doi.org/10.1016/0961-9534(95)00058-5

Jenkins, B. M., Baxter, L. L., & Miles, T. R. (1998). Combustion properties of biomass. *Fuel Processing Technology*, *54*, 17–46. Retrieved from http://citeseerx.ist.psu.edu/viewdoc/download;jsessionid=60A12928A6A01166C64D29AB3F71E3F9?doi=10.1.1.473.6136&rep=rep1&type=pdf

Jennings, H. M., & Pratt, P. L. (1979). An experimental argument for the existence of a protective membrane surrounding portland cement during the induction period. *Cement and Concrete Research*, *9*(4), 501–506. https://doi.org/10.1016/0008-8846(79)90048-6

Jennings, H. M., Thomas, J. J., Chen, J. J., & Rothstein, D. (2002). Cement Paste as a Porous Material. In F. Schuth, K. . Sing, & J. Weitkamp (Eds.), *Handbook of Porous Solids* (pp. 2971–3028). https://doi.org/10.1002/9783527618286

Juenger, M. C. G., & Siddique, R. (2015). Recent advances in understanding the role of supplementary cementitious materials in concrete. *Cement and Concrete Research*, *78*, 71–80.

Juenger, M. C. G., Snellings, R., & Bernal, S. A. (2019). Supplementary cementitious materials: New sources, characterization, and performance insights. *Cement and Concrete Research*, *122*(February), 257–273. https://doi.org/10.1016/j.cemconres.2019.05.008

Juilland, P., Gallucci, E., Flatt, R. J., & Scrivener, K. L. (2011). Reply to the discussion by E . Gartner of the paper " Dissolution theory applied to the induction period in alite hydration ." *Cement and Concrete Research*, *41*(5), 563–564. Retrieved from http://dx.doi.org/10.1016/j.cemconres.2011.01.018

Juilland, P., Gallucci, E., Flatt, R., & Scrivener, K. (2010). Dissolution theory applied to the induction period in alite hydration. *Cement and Concrete Research*, *40*(6), 831–844.

Juilland P, G. E. (2015). Morpho-topological investigation of the mechanisms and kinetic regimes of alite dissolution. *Cement and Concrete Research*, *76*, 180–191. Retrieved from https://ac.els-cdn.com/S0008884615001702/1-s2.0-S0008884615001702-main.pdf?_tid=575b975a-d611-4ecd-a707-145653a4fe8a&acdnat=1523540572_076c49987d266b6bd6012db21ee92893

Kakali, G., Tsivilis, S., Aggeli, E., & Bati, M. (2000). Hydration products of C3A, C3S and Portland cement in the presence of CaCO3. *Cement & Concrete Research*, *30*(1073–1077), 1–14.

Kalina, R. D., Al-shmaisani, S., Ferron, R. D., & Juenger, M. C. G. (2019). False Positives in ASTM C618 Specifications for Natural Pozzolans. *ACI Materials Journal*, *116*(1), 165–172. https://doi.org/10.14359/51712243

Kianirad, M., Muazardalan, M., Savaghebi, G., Farahbakhsh, M., & Mirdamadi, S. (2010). Effects of temperature treatment on corn cob composting and reducing of composting time: A comparative study. *Waste Management and Research*, *28*(10), 882–887. https://doi.org/10.1177/0734242X09342359

Kroehong, W., Sinsiri, T., Jaturapitakkul, C., & Chindaprasirt, P. (2011). Effect of palm oil fuel ash fineness on the microstructure of blended cement paste. *Construction and Building*

Materials, *25*, 4095–4104.

Kumar, A., Oey, T., Falzone, G., Huang, J., Bauchy, M., Balonis, M., … Neithalath, N. (2017). The filler effect: The influence of filler content and type on the hydration rate of tricalcium silicate. *Journal of the American Ceramic Society*, *100*(7), 3316–3328.

L'Hôpital, E., Lothenbach, B., Scrivener, K., & Kulik, D. A. (2016). Alkali uptake in calcium alumina silicate hydrate (C-A-S-H). *Cement and Concrete Research*, *85*, 122–136.

Lam, L., Wong, Y. ., & Poon, C. . (2000). Degree of hydration and gel/space ratio of high-volume fly ash/cement systems. *Cement & Concrete Research*, *30*, 747–756.

Lasaga, A. C., & Luttge, A. (2001). Variation of crystal dissolution rate based on a dissolution stepwave model. *Science*, *291*(5512), 2400–2404.

Lawrence, P., Cyr, M., & Ringot, E. (2003). Mineral admixtures in mortars. *Cement and Concrete Research*, *33*(12), 1939–1947.

Ley-hernandez, A. M., Lapeyre, J., Cook, R., Kumar, A., & Feys, D. (2018). Elucidating the Effect of Water-To-Cement Ratio on the Hydration Mechanisms of Cement [Research-article]. *ACS Omega*, *3*, 5092–5105. https://doi.org/10.1021/acsomega.8b00097

Li, L., & Aubertin, M. (2003). A general relationship between porosity and uniaxial strength of engineering materials. *Canadian Journal of Civil Engineering*, *30*(4), 644–658. https://doi.org/10.1139/l03-012

Li, Zhengqi, Afshinnia, K., & Rangaraju, P. R. (2016). *Effect of alkali content of cement on properties of high performance cementitious mortar*. *102*, 631–639. https://doi.org/10.1016/j.conbuildmat.2015.10.110

Li, Zongjin. (2011). *Advance Concrete Technology*. New Jersey: John Wiley & Sons.

Lothenbach, B., & Nonat, A. (2015). Calcium silicate hydrates: Solid and liquid phase composition. *Cement and Concrete Research*, *78*, 57–70.

Lothenbach, B., Scrivener, K., & Hooton, R. D. (2011). Supplementary cementitious materials. *Cement and Concrete Research*, *41*, 1244–1256.

Lumley, J. S., Gollop, R. S., Moir, G. K., & Taylor, H. F. W. (1996). Degrees of reaction of the slag in some blends with Portland cements. *Cement and Concrete Research*, *26*(1), 139–151.

Luxán, M. P., Madruga, F., Saavedra, J., Lux??n, M. P., Madruga, F., & Saavedra, J. (1989). Rapid evaluation of pozzolanic activity of natural products by conductivity measurement. *Cement and Concrete Research*, *19*(1), 63–68.

Makar, J. M., Chan, G. W., & Esseghaier, K. Y. (2007). A peak in the hydration reaction at the end of the cement induction period. *Journal of Materials Science*, *42*(4), 1388–1392.

Makar, J M, Beaudoin, J. J., Sato, T., Alizadeh, R., & Raki, L. (2011). Discussion of " Dissolution theory applied to the induction period in alite hydration ." *Cement and Concrete Research*, *41*(5), 565–567. https://doi.org/10.1016/j.cemconres.2011.01.020

Makar, Jon M., & Chan, G. W. (2008). End of the induction period in ordinary portland cement as examined by high-resolution scanning electron microscopy. *Journal of the American Ceramic Society*, *91*(4), 1292–1299.

Matusinović, T., Šipušić, J., & Vrbos, N. (2003). Porosity-strength relation in calcium aluminate cement pastes. *Cement and Concrete Research*, *33*(11), 1801–1806. https://doi.org/10.1016/S0008-8846(03)00201-1

Megat Johari, M. A., Zeyad, A. M., Muhamad Bunnori, N., & Ariffin, K. S. (2012). Engineering and transport properties of high-strength green concrete containing high volume of ultrafine palm oil fuel ash. *Construction and Building Materials*, *30*, 281–288.

Mehdipour, I., & Khayat, K. H. (2017). Effect of particle-size distribution and specific surface area of different binder systems on packing density and flow characteristics of cement paste. *Cement and Concrete Composites*, *78*, 120–131.

Memon, S. A., & Khan, M. K. (2018). Ash blended cement composites : Eco-friendly and sustainable option for utilization of corncob ash. *Journal of Cleaner Production*, *175*, 442–455.

Miller, S. A., Roijen, E. Van, Cunningham, P. R., & Kim, A. (2021). *Opportunities and challenges for engineering construction materials as carbon sinks*. 105–118.

Mohlala, L. M., Bodunrin, M. O., Awosusi, A. A., Daramola, M. O., Cele, N. P., & Olubambi, P. A. (2016). Beneficiation of corncob and sugarcane bagasse for energy generation and materials development in Nigeria and South Africa: A short overview. *Alexandria Engineering Journal*, *55*(3), 3025–3036.

Mokarem, D. W., Weyers, R. E., & Lane, D. S. (2005). Development of a shrinkage performance specifications and prediction model analysis for supplemental cementitious material concrete mixtures. *Cement & Concrete Research*, *35*, 918–925. https://doi.org/10.1016/j.cemconres.2004.09.013

Monteagudo, S. M., Moragues, A., Gálvez, J. C., Casati, M. J., & Reyes, E. (2014). The degree of hydration assessment of blended cement pastes by differential thermal and thermogravimetric analysis. Morphological evolution of the solid phases. *Thermochimica Acta*, *592*, 37–51.

Montgomery, D. ., Runger, G. ., Hubele, N., & F. (2011). *Engineering Statistics* (Vol. 5).

Moore, A. J., Bakera, A. T., & Alexander, M. G. (2021). A critical review of the Water Sorptivity Index (WSI) parameter for potential durability assessment: Can WSI be considered in isolation of porosity? *Journal of the South African Institution of Civil Engineering*, *63*(2), 27–34. https://doi.org/10.17159/2309-8775/2021/v63n2a4

Mujedu, K., Adebara, S., & Lamidi, I. (2014). The use of corn cob ash and saw dust ash as cement replacement in concrete works. *The International Journal Of Engineer Ing And Science*, *3*(4), 22–28. Retrieved from http://theijes.com/papers/v3-i4/Version-1/D03401022028.pdf

Mushtaq, S. M., Siddique, R., Goyal, S., & Kaur, K. (2021). Experimental studies and drying shrinkage prediction model for concrete containing waste foundry sand. *Cleaner Engineering and Technology*, *2*(February), 100071. https://doi.org/10.1016/j.clet.2021.100071

Muthadhi, A., & Kothandaraman, S. (2010). Optimum production conditions for reactive rice husk ash. *Materials and Structures/Materiaux et Constructions*, *43*(9), 1303–1315.

Nehdi, M., Duquette, J., & El Damatty, A. (2003). Performance of rice husk ash produced using a new technology as a mineral admixture in concrete. *Cement and Concrete Research*, *33*(8), 1203–1210.

Nimityongskul, P., & Daladar, T. U. (1995). Use of coconut husk ash, corn cob ash and peanut shell ash as cement replacement. *Journal of Ferrocement*, *25*(1), 35–44.

Odler, I., & Abdul-Maula. (1984). POSSIBILITIES OF QUANTITATIVE DETERMINATION OF THE AFt-(ETTRINGITE) AND AFm-(MONOSULPHATE) PHASES IN HYDRATED CEMENT PASTES. *Cement and Concrete Research* , *14*, 133–141. Retrieved from https://ac.els-cdn.com/0008884684900899/1-s2.0-0008884684900899-

main.pdf?_tid=e709dcea-63c8-4a5d-b5d2-b09d8072d0cf&acdnat=1531403641_2eda36212dbc92826b11194cf245ce9b

Olafusi, O., & Olutoge, F. (2012). Strength Properties of Corn Cob Ash Concrete. *Journal of Emerging Trends in Engineering and Applied Sciences (JETEAS)*, *3*(2), 297–301.

Otieno, M. B. (2014). *The development of empirical chloride-induced corrosion rate prediction models for cracked and uncracked steel reinforced concrete structures in the marine tidal zone*. Retrieved from http://library.wur.nl/WebQuery/wurpubs/fulltext/353506

Otieno, M. B., Alexander, M. G., & Beushausen, H.-D. (2010). Corrosion in cracked and uncracked concrete – influence of crack width, concrete quality and crack reopening. *Magazine of Concrete Research*, *62*(6), 393–404.

Otieno, M, & Alexander, M. G. (2015). Chloride conductivity testing of concrete – past and recent developments. *Journal of the South African Institution of Civil Engineering*, *57*(4), 55–64.

Otieno, Mike. (2018). Sensitivity of the rapid chloride conductivity index test to concrete quality and changes in various test parameters. *Cement and Concrete Composites*, *86*, 110–116. https://doi.org/10.1016/j.cemconcomp.2017.11.011

Pane, I., & Hansen, W. (2005). Investigation of blended cement hydration by isothermal calorimetry and thermal analysis. *Cement and Concrete Research*, *35*(6), 1155–1164. https://doi.org/10.1016/j.cemconres.2004.10.027

Park, D. C. (2008). *Carbonation of concrete in relation to CO 2 permeability and degradation of coatings*. *22*, 2260–2268. https://doi.org/10.1016/j.conbuildmat.2007.07.032

Park, K. B., Kwon, S. J., & Wang, X. Y. (2016). Analysis of the effects of rice husk ash on the hydration of cementitious materials. *Construction and Building Materials*, *105*, 196–205.

Perraki, T., Kakali, G., & Kontori, E. (2005). Characterization and pozzolanic activity of thermally treated zeolite. *Journal of Thermal Analysis and Calorimetry*, *82*(1), 109–113. https://doi.org/10.1007/s10973-005-0849-5

Plusquellec, G., & Weerdt, K. De. (2017). Cold water extraction (CWE) - Procedure for the determination of the alkali content and pore solution composition. *Norwegian University of Science and Technology*.

Poole, J. L., Riding, K. A., Folliard, K. J., Juenger, M. C. G., & Schindler, A. K. (2007). Hydration Study of Cementitious Materials using Semi-Adiabatic Calorimetry. *Aci, SP 241*, 59–76.

Pratt, P. L., & Jennings, H. M. (1981). The Microchemistry and Microstructure of Portland-Cement. *Ann. Rev. Mater. Sci.*, *11*, 123–149.

Quarcioni, V. A., F. F. Chotoli, A. C. V. Coelho, & M. A. Cincotto. (2015). Indirect and direct Chapelle's methods for the determination of lime consumption in pozzolanic materials. *IBRACON Structures and Materials Journal*, *8*(1), 1–7.

Rahhal, V., & Talero, R. (2004). Influence of two different fly ashes on the hydration of portland cements. *Journal of Thermal Analysis and Calorimetry*, *78*(1), 191–205.

Rahhal, V., & Talero, R. (2005). Early hydration of portland cement with crystalline mineral additions. *Cement and Concrete Research*, *35*(7), 1285–1291.

Rêgo, J. H. S., Nepomuceno, A. A., Figueiredo, E. P., & Hasparyk, N. P. (2015). Microstructure of cement pastes with residual rice husk ash of low amorphous silica content. *Construction and Building Materials*, *80*, 56–68.

Rezvani, M., & Proske, T. (2017). Influence of chemical-mineralogical properties of limestone on the shrinkage behaviour of cement paste and concrete made of limestone-rich cements. *Construction and Building Materials*, *157*, 818–828. https://doi.org/10.1016/j.conbuildmat.2017.09.101

Rodger, S. A., Groves, G. W., Clayden, N. J., & Dobson, C. M. (1988). Hydration of Tricalcium Silicate Followed by29Si NMR with Cross-Polarization. *Journal of the American Ceramic Society*, *71*(2), 91–96. https://doi.org/10.1111/j.1151-2916.1988.tb05823.x

Schindler, A. K., & Folliard, K. J. (2005). Heat of hydration models for cementitious materials. *ACI Materials Journal*, *102*(1), 24–33.

Schlorholtz, S. (2006). Chapter 43-Supplementary Cementitious Materials. In *Significance of Tests and Properties of Concrete and Concrete-Making Materials, ASTM STP 169D* (pp. 495–511).

Scrivener, K. L., Crumbie, A. K., & Laugesen, P. (2004). The interfacial transition zone (ITZ) between cement paste and aggregate in concrete. *Interface Science*, *12*(4), 411–421.

Scrivener, K. L., John, V. M., & Gartner, E. M. (2018). Eco-efficient cements: Potential

economically viable solutions for a low-CO2 cement-based materials industry. *Cement and Concrete Research*, *114*, 2–26. https://doi.org/10.1016/j.cemconres.2018.03.015

Scrivener, K. L., Juilland, P., & Monteiro, P. J. M. (2015). Advances in understanding hydration of Portland cement. *Cement and Concrete Research*, *78*, 38–56.

Scrivener, K., Martirena, F., Bishnoi, S., & Maity, S. (2018). Calcined clay limestone cements (LC3). *Cement and Concrete Research*, Vol. 114, pp. 49–56. https://doi.org/10.1016/j.cemconres.2017.08.017

Scrivener, K., Snellings, R., & Lothenbach, B. (2016). A Practical Guide to Microstructural Analysis of Cementitious Materials Edited. In K. L. Scrivener, R. Snellings, & B. Lothenbach (Eds.), *A Practical Guide to Microstructural Analysis of Cementitious Materials* (First). https://doi.org/10.7693/wl20150205

Serbanoiu, A. A., Gradinaru, C. M., Muntean, R., Cimpoesu, N., & Serbanoiu, B. V. (2022). Corn Cob Ash versus Sunflower Stalk Ash , Two Sustainable. *Materials*.

Shakouri, M., Exstrom, C. L., Ramanathan, S., & Suraneni, P. (2020). Hydration , strength , and durability of cementitious materials incorporating untreated corn cob ash. *Construction and Building Materials*, *243*, 118171. https://doi.org/10.1016/j.conbuildmat.2020.118171

Simnani, S. I. (2017). *Effect of Water-Cement Ratio on Compressive Strength of Concrete*. *4*(10), 486–488. Retrieved from www.jetir.org

Singh, N. B., Singh, V. D., & Rai, S. (2000). Hydration of bagasse ash-blended portland cement. *Cement and Concrete Research*, *30*, 1485–1488.

Singh, S. B., Munjal, P., & Thammishetti, N. (2015). Role of water/cement ratio on strength development of cement mortar. *Journal of Building Engineering*, *4*, 94–100. https://doi.org/10.1016/j.jobe.2015.09.003

Smaoui, N., Bérubé, M. A., Fournier, B., Bissonnette, B., & Durand, B. (2005). Effects of alkali addition on the mechanical properties and durability of concrete. *Cement and Concrete Research*, *35*(2), 203–212. https://doi.org/10.1016/j.cemconres.2004.05.007

Snellings, R., Chwast, J., Cizer, Ö., De Belie, N., Dhandapani, Y., Durdzinski, P., … Lothenbach, B. (2018). Report of TC 238-SCM: hydration stoppage methods for phase assemblage studies

of blended cements—results of a round robin test. *Materials and Structures/Materiaux et Constructions*, *51*(4).

Snellings, R., & Scrivener, K. L. (2016). Rapid screening tests for supplementary cementitious materials: past and future. *Materials and Structures*, *49*(8), 3265–3279.

Snellings Ruben. (2016). Assessing, Understanding and Unlocking Supplementary Cementitious Materials. *RILEM Technical Letters*, *1*, 50–55. https://doi.org/10.21809/rilemtechlett.2016.12

Stanish, K., Alexander, M. G., & Balim, Y. (2006). Assessing the repeatability and reproducibility values of South African durability index tests. *Journal of the South African Institution of Civil Engineering*, *48*(2), 10–17.

Suberu, M. Y., Mokhtar, A. S., & Bashir, N. (2012). *POTENTIAL CAPABILITY OF CORN COB RESIDUE FOR SMALL POWER GENERATION IN RURAL NIGERIA*. *7*(8).

Suprenant, B. B. A., & Papadopoulos, G. (1991). Selective dissolution of portland-fly-ash cements. *Journal of Materials in Civil Engineering*, *3*(1), 48–59.

Suwanmaneechot, P., Nochaiya, T., & Julphunthong, P. (2015). Improvement, characterization and use of waste corn cob ash in cement-based materials. *IOP Conference Series: Materials Science and Engineering*, *103*(1). https://doi.org/10.1088/1757-899X/103/1/012023

Taylor, H. F. W. (1986). Proposed structure for calcium silicate hydrate gel. *Journal of the American Ceramic Society*, *69*, 464–467. https://doi.org/10.1111/j.1151-2916.1986.tb07446.x

Tran, N. P., Gunasekara, C., Law, D. W., Houshyar, S., Setunge, S., & Cwirzen, A. (2021). A critical review on drying shrinkage mitigation strategies in cement-based materials. *Journal of Building Engineering*, *38*(September 2020), 102210. https://doi.org/10.1016/j.jobe.2021.102210

UCT-WITS DI Manual. (2018). Durability Index Testing Procedure Manual. *University of Cape Town, CoMSIRU., Ver. 4.5*(July, 2017), 42.

Vassilev, S. V., Vassileva, C. G., Song, Y. C., Li, W. Y., & Feng, J. (2017). Ash contents and ash-forming elements of biomass and their significance for solid biofuel combustion. *Fuel*.

Vollpracht, A., Lothenbach, B., Snellings, R., & Haufe, J. (2016). The pore solution of blended cements: a review. *Materials and Structures*, *49*, 3341–3367.

Walker, R., & Pavía, S. (2011). Physical properties and reactivity of pozzolans, and their influence on the properties of lime-pozzolan pastes. *Materials and Structures/Materiaux et Constructions*, *44*(6), 1139–1150.

Wang, D., Shi, C., Farzadnia, N., Shi, Z., Jia, H., & Ou, Z. (2018). A review on use of limestone powder in cement-based materials: Mechanism, hydration and microstructures. *Construction and Building Materials*, *181*, 659–672.

Wang, L., Hustad, J. E., & Grønli, M. (2012). Sintering characteristics and mineral transformation behaviors of corn cob ashes. *Energy and Fuels*, *26*(9), 5905–5916.

World bank group. (2015). *Stocktaking of the Housing Sector in Sub-Saharan Africa*.

Zeng, Q., Li, K., Fen-Chong, T., & Dangla, P. (2012). Determination of cement hydration and pozzolanic reaction extents for fly-ash cement pastes. *Construction and Building Materials*, *27*(1), 560–569.

Zhang, M.-H., & Islam, J. (2012). Use of nano-silica to increase early strength and reduce setting time of concretes with high volumes of slag. *Construction and Building Materials*, *29*, 573–580. https://doi.org/10.1016/j.cemconcomp.2012.02.005

Appendix A1: Compressive strength

Tables A1 and A2 present the summary of data used to compute the compressive strength of concrete at different w/b ratios while Table A3 presents the summary of data used for the computation of the strength activity index based on compressive strength of mortar

Table A 1: Compressive strength data for concrete at w/b ratio of 0.4

Mix type	w/b ratio	Age (days)	Strength (MPa)	Std dev
PC	0.4	3	55.89	1.71
		7	61.21	0.89
		28	75.22	9.45
		90	82.77	1.22
		180	83.46	6.62
		270	84.13	2.60
85/15 PC/FA	0.4	3	48.36	1.34
		7	57.95	0.50
		28	71.04	2.03
		90	81.83	5.52
		180	85.91	10.60
		270	81.28	3.39
85/15 PC/C700	0.4	3	39.86	1.83
		7	47.05	1.45
		28	48.25	1.16
		90	57.93	1.71
		180	63.6	1.67
		270	62.48	0.86
70/30 PC/FA	0.4	3	38.87	1.29
		7	48.07	1.09
		28	63.7	1.06
		90	77.45	0.58
		180	83.08	9.18
		270	85.91	0.93
70/30 PC/C700	0.4	3	29.22	1.11
		7	33.39	0.41
		28	35.45	1.69
		90	45.23	0.86
		180	47.71	5.17
		270	46.17	2.67

Table A 2: Compressive strength data for concrete at w/b ratio of 0.6

Mix type	w/b ratio	Age (days)	Strength (MPa)	Std dev
PC	0.6	3	31.1	0.73
		7	38.99	0.74
		28	47.41	0.53
		90	55.32	3.06
		180	55.52	1.01
		270	57.58	1.36
85/15 PC/FA	0.6	3	23.17	1.22
		7	28.78	0.96
		28	39.61	0.58
		90	52.47	0.48
		180	55.75	0.38
		270	57.43	1.80
85/15 PC/C700	0.6	3	22.89	1.39
		7	25.37	1.45
		28	29.73	1.16
		90	32.96	1.71
		180	36.81	1.67
		270	36.01	0.86
70/30 PC/FA	0.6	3	18.39	0.60
		7	22.21	0.78
		28	31.33	0.89
		90	46.17	2.03
		180	53.57	1.62
		270	54.45	2.18
70/30 PC/C700	0.6	3	19.11	2.18
		7	21.09	0.34
		28	26.87	1.90
		90	27	0.72
		180	28.75	0.78
		270	29.99	0.54

Table A 3: Compressive strength data of mortar

Mix type	Age (days)	Strength (MPa)	Std dev
PC	28	48.35	0.88
	56	54.35	3.87
	90	54.99	0.79
PC/FA	28	40.37	0.85
	56	46.91	0.29
	90	49.89	0.73
PC/C700	28	33.12	0.99
	56	34.67	1.50
	90	36.32	1.53
PC/C800	28	39.95	0.88
	56	41.20	1.09
	90	43.52	0.62

Appendix A2: Drying shrinkage

The data presented in Tables A4 to A6 are the microstrain on mortar bars for air-cured and water-cured regimes.

Table A 4: Drying shrinkage data for air-cured samples

Day	PC4	FA15-4	C700 15-4	FA30-4	C700 30-4	PC6	FA15-6	C700 15-6	FA30 -6	C700 30-6
0	0.00	0.00	0.00	0.00	0.00	0.00	0.00	0.00	0.00	0.00
1	224.44	77.50	157.14	70.00	264.44	45.00	48.57	14.29	26.67	180.00
2	171.11	127.50	285.71	107.50	448.89	90.00	65.71	111.43	80.00	336.67
3	191.11	152.50	351.43	140.00	553.33	125.00	114.29	240.00	108.89	510.00
4	257.78	232.50	442.86	210.00	657.78	195.00	188.57	334.29	186.67	626.67
5	288.89	275.00	494.29	247.50	735.56	222.50	208.57	382.86	217.78	746.67
6	315.56	295.00	514.29	277.50	802.22	247.50	245.71	445.71	242.22	850.00
7	353.33	332.50	562.86	320.00	882.22	287.50	280.00	540.00	282.22	936.67
8	391.11	372.50	597.14	355.00	948.89	322.50	325.71	565.71	315.56	1016.67
9	404.44	392.50	622.86	370.00	968.89	342.50	360.00	617.14	346.67	1063.33
10	448.89	420.00	665.71	390.00	1022.22	380.00	385.71	651.43	368.89	1120.00
11	466.67	475.00	697.14	447.50	1117.78	437.50	434.29	834.29	426.67	1176.67
12	473.33	452.50	725.71	422.50	1124.44	455.00	471.43	860.00	424.44	1206.67
13	504.44	497.50	754.29	462.50	1148.89	485.00	520.00	934.29	457.78	1236.67
14	517.78	507.50	780.00	502.50	1191.11	527.50	557.14	988.57	484.44	1270.00
17	560.00	602.50	937.14	552.50	1357.78	625.00	700.00	1094.29	584.44	1450.00
21	606.67	590.00	945.71	570.00	1408.89	645.00	685.71	1148.57	611.11	1500.00
24	662.22	625.00	1031.43	632.50	1511.11	680.00	751.43	1237.14	662.22	1566.67
27	666.67	642.50	1105.71	677.50	1595.56	695.00	791.43	1265.71	682.22	1630.00
33	720.00	712.50	1168.57	697.50	1700.00	792.50	842.86	1297.14	722.22	1730.00
41	748.89	737.50	1248.57	722.50	1762.22	852.50	914.29	1325.71	768.89	1770.00
48	804.44	792.50	1374.29	760.00	1875.56	905.00	991.43	1325.71	828.89	1866.67
54	857.78	822.50	1428.57	792.50	1928.89	967.50	997.14	1328.57	842.22	1910.00
62	864.44	820.00	1494.29	765.00	1957.78	997.50	1000.00	1328.57	842.22	1923.33
69	886.67	830.00	1540.00	800.00	2008.89	1035.00	1031.43	1340.00	871.11	1953.33
76	888.89	835.00	1545.71	797.50	2026.67	1040.00	1031.43	1337.14	875.56	1956.67
83	897.78	837.50	1562.86	800.00	2044.44	1050.00	1034.29	1337.14	875.56	1956.67
90	904.44	842.50	1565.71	800.00	2048.89	1052.50	1031.43	1337.14	875.56	1956.67
97	902.22	845.00	1577.14	805.00	2060.00	1055.00	1037.14	1340.00	882.22	1956.67
104	902.22	845.00	1577.14	805.00	2060.00	1055.00	1037.14	1337.14	882.22	1956.67
111	902.22	845.00	1577.14	805.00	2060.00	1055.00	1037.14	1340.00	882.22	1956.67
136	915.56	855.00	1597.14	842.50	2126.67	1070.00	1048.57	1371.43	891.11	1993.33
160	975.56	925.00	1617.14	857.50	2140.00	1090.00	1071.43	1405.71	924.44	2000.00
195	977.78	937.50	1622.86	867.50	2151.11	1107.50	1085.71	1411.43	933.33	2003.33
230	980.00	935.00	1631.43	867.50	2157.78	1122.50	1091.43	1411.43	940.00	2003.33

Table A 5: drying shrinkage strain data for water-cured samples at w/b ratio of 0.4

DAYS	PC4	FA15-4	C700 15-4	FA30-4	C700 30-4	C800 15-4	C800 30-4
1	0.00	0.00	0.00	0.00	0.00	0.00	0.00
2	171.11	146.67	104.44	100.00	126.67	206.67	55.00
3	304.44	244.44	228.89	202.22	273.33	360.00	90.00
4	360.00	302.22	322.22	264.44	355.56	437.78	160.00
5	431.11	331.11	395.56	300.00	408.89	493.33	240.00
6	431.11	446.67	480.00	371.11	508.89	546.67	300.00
7	524.44	462.22	562.22	428.89	548.89	600.00	380.00
8	524.44	471.11	586.67	460.00	573.33	642.22	455.00
9	560.00	500.00	646.67	473.33	655.56	662.22	495.00
11	644.44	577.78	788.89	571.11	773.33	697.78	540.00
14	688.89	646.67	871.11	622.22	844.44	697.78	575.00
18	744.44	680.00	977.78	680.00	946.67	708.89	610.00
25	802.22	731.11	1115.56	740.00	1100.00	742.22	660.00
32	866.67	842.22	1224.44	806.67	1217.78	813.33	760.00
36	902.22	891.11	1306.67	842.22	1311.11	833.33	880.00
40	911.11	877.78	1313.33	846.67	1322.22	842.22	915.00
44	931.11	891.11	1353.33	864.44	1360.00	860.00	960.00
48	926.67	902.22	1400.00	866.67	1393.33	882.22	985.00
51	957.78	911.11	1451.11	884.44	1424.44	913.33	1035.00
54	968.89	946.67	1491.11	906.67	1475.56	922.22	1075.00
57	924.44	971.11	1533.33	940.00	1517.78	935.56	1105.00
61	991.11	968.89	1531.11	933.33	1520.00	928.89	1110.00
68	1000.00	971.11	1573.33	933.33	1540.00	975.56	1150.00
75	1008.89	980.00	1608.89	935.56	1571.11	1002.22	1190.00
82	1015.56	984.44	1624.44	942.22	1584.44	993.33	1195.00
89	1015.56	977.78	1637.78	944.44	1586.67	1002.22	1225.00
95	1020.00	977.78	1644.44	944.44	1595.56	1004.44	1230.00
102	1044.44	1002.22	1657.78	968.89	1624.44	1004.44	1230.00
131	1115.56	1093.33	1782.22	1028.89	1768.89	1002.22	1230.00
155	1131.11	1104.44	1837.78	1046.67	1815.56	997.78	1230.00
183	1142.22	1111.11	1844.44	1062.22	1824.44	1006.67	1225.00
218	1140.00	1104.44	1862.22	1060.00	1826.67	1004.44	1225.00

Table A 6: Drying shrinkage strain data for water-cured samples at w/b ratio of 0.6

DAYS	PC6	FA15-6	C700 15-6	FA30-6	C700 30-6	C800 15-6	C800 30-6
1	0.00	0.00	0.00	0.00	0.00	0.00	0.00
2	142.22	91.11	131.11	93.33	186.67	148.89	77.14
3	235.56	144.44	211.11	131.11	286.67	288.89	200.00
4	302.22	195.56	262.22	193.33	368.89	373.33	282.86
5	355.56	264.44	346.67	255.56	484.44	451.11	348.57
6	424.44	346.67	424.44	317.78	575.56	517.78	402.86
7	471.11	417.78	482.22	402.22	626.67	584.44	460.00
8	526.67	442.22	493.33	477.78	711.11	640.00	514.29
9	617.78	475.56	555.56	484.44	815.56	688.89	565.71
11	706.67	597.78	651.11	588.89	966.67	713.33	588.57
14	757.78	686.67	708.89	635.56	1051.11	733.33	617.14
18	820.00	742.22	808.89	708.89	1173.33	768.89	648.57
25	955.56	864.44	920.00	771.11	1368.89	817.78	702.86
32	1051.11	948.89	1020.00	864.44	1508.89	928.89	780.00
36	1106.67	986.67	1091.11	908.89	1628.89	993.33	860.00
40	1100.00	1002.22	1104.44	931.11	1668.89	1017.78	928.57
44	1111.11	1017.78	1140.00	917.78	1706.67	1062.22	965.71
48	1120.00	1020.00	1155.56	942.22	1762.22	1104.44	1011.43
51	1186.67	1064.44	1208.89	953.33	1846.67	1168.89	1085.71
54	1208.89	1080.00	1233.33	955.56	1853.33	1220.00	1157.14
57	1233.33	1106.67	1260.00	973.33	1902.22	1231.11	1188.57
61	1231.11	1106.67	1268.89	980.00	1933.33	1257.78	1225.71
68	1240.00	1106.67	1286.67	991.11	1988.89	1297.78	1262.86
75	1246.67	1124.44	1320.00	995.56	2035.56	1342.22	1305.71
82	1257.78	1131.11	1340.00	997.78	2055.56	1353.33	1314.29
89	1264.44	1131.11	1342.22	1006.67	2066.67	1368.89	1325.71
95	1264.44	1137.78	1348.89	1008.89	2091.11	1377.78	1334.29
102	1284.44	1173.33	1386.67	1033.33	2115.56	1375.56	1342.86
131	1357.78	1242.22	1457.78	1075.56	2217.78	1380.00	1345.71
155	1391.11	1253.33	1468.89	1084.44	2255.56	1377.78	1348.57
183	1397.78	1260.00	1486.67	1097.78	2271.11	1388.89	1362.86
218	1404.44	1260.00	1493.33	1097.78	2266.67	1395.56	1371.43

Appendix A3: Durability index

Table A 7: Oxygen permeability test results

Mix type	w/b ratio	Age (days)	OPI	Std dev
PC	0.4	28	10.18	0.14
		90	10.42	0.27
	0.6	28	10.38	0.19
		90	10.50	0.07
85/15 PC/FA	0.4	28	10.12	0.38
		90	10.60	0.13
	0.6	28	10.48	0.31
		90	9.70	0.49
85/15 PC/C700	0.4	28	9.19	0.03
		90	9.54	0.25
	0.6	28	9.22	0.16
		90	9.35	0.37
85/15 PC/C800	0.4	28	9.70	0.16
		90	10.03	0.24
	0.6	28	9.92	0.17
		90	10.01	0.15
70/30 PC/FA	0.4	28	10.04	0.55
		90	10.90	0.54
	0.6	28	10.36	0.16
		90	10.88	0.15
70/30 PC/C700	0.4	28	8.59	0.14
		90	8.91	0.04
	0.6	28	8.74	0.15
		90	8.82	0.09
70/30 PC/C800	0.4	28	8.69	0.20
		90	9.04	0.16
	0.6	28	9.37	0.10
		90	9.57	0.17

Table A 8: Water sorptivity index test results

Mix type	w/b ratio	Age (days)	WSI	Std dev
PC	0.4	28	8.89	0.39
		90	9.26	1.87
	0.6	28	7.69	0.02
		90	9.05	0.57
85/15 PC/FA	0.4	28	7.71	1.14
		90	8.09	0.98
	0.6	28	7.88	0.55
		90	8.89	0.19
85/15 PC/C700	0.4	28	10.27	2.27
		90	7.50	0.58
	0.6	28	8.96	0.42
		90	8.15	0.61
85/15 PC/C800	0.4	28	8.76	1.04
		90	7.57	0.62
	0.6	28	8.52	1.13
		90	8.45	0.43
70/30 PC/FA	0.4	28	8.86	1.27
		90	8.57	0.53
	0.6	28	8.97	0.33
		90	7.22	0.46
70/30 PC/C700	0.4	28	10.30	0.48
		90	9.30	0.41
	0.6	28	10.03	0.72
		90	9.62	0.90
70/30 PC/C800	0.4	28	7.72	0.93
		90	6.83	0.66
	0.6	28	7.69	0.59
		90	7.39	0.80

Table A 9: Average porosity values in percentage

Mix type	w/b ratio	Age (days)	Porosity	Std dev
PC	0.4	28	8.37	0.30
		90	6.06	0.21
	0.6	28	9.66	0.66
		90	7.88	0.51
85/15 PC/FA	0.4	28	6.52	0.13
		90	4.07	0.04
	0.6	28	9.14	0.87
		90	8.46	0.37
85/15 PC/C700	0.4	28	9.66	0.48
		90	6.90	0.09
	0.6	28	9.71	0.22
		90	7.77	0.18
85/15 PC/C800	0.4	28	6.90	0.44
		90	5.83	0.33
	0.6	28	8.99	0.39
		90	8.47	0.41
70/30 PC/FA	0.4	28	8.57	0.23
		90	4.48	0.33
	0.6	28	10.31	0.55
		90	6.80	0.64
70/30 PC/C700	0.4	28	6.99	0.72
		90	6.44	0.31
	0.6	28	8.85	0.21
		90	8.51	0.42
70/30 PC/C800	0.4	28	8.04	0.76
		90	7.32	0.67
	0.6	28	9.74	0.63
		90	9.37	0.51

Table A 10: Chloride conductivity index test results

Mix type	w/b ratio	Age (days)	CCI (mS/cm)	Std dev
PC	0.4	28	0.98	0.06
		90	0.63	0.05
	0.6	28	1.87	0.08
		90	1.27	0.06
85/15 PC/FA	0.4	28	0.89	0.19
		90	0.44	0.05
	0.6	28	1.65	0.24
		90	1.14	0.09
85/15 PC/C700	0.4	28	1.10	0.08
		90	1.05	0.13
	0.6	28	1.47	0.21
		90	1.34	0.07
85/15 PC/C800	0.4	28	0.66	0.05
		90	0.64	0.03
	0.6	28	1.65	0.31
		90	1.19	0.16
70/30 PC/FA	0.4	28	1.34	0.08
		90	0.23	0.02
	0.6	28	2.40	0.48
		90	0.61	0.09
70/30 PC/C700	0.4	28	0.91	0.12
		90	1.00	0.07
	0.6	28	1.40	0.06
		90	1.53	0.13
70/30 PC/C800	0.4	28	0.73	0.07
		90	0.81	0.02
	0.6	28	1.56	0.05
		90	1.22	0.06

Appendix A4: Pore solution analysis

Table A 11: Concentration of ionic species in pore solution

		Concentration (mg/l)					
		OH^-		k^+		Ca^{2+}	
Muix type	w/b ratio	**28d**	**90d**	**28 d**	**90d**	**28d**	**90d**
PC	0.4	28.52	7.13	40.3	26.9	61.96	65.69
	0.6	10.12	7.3	30.5	22.3	52.76	61.23
FA 15	0.4	27.92	7.51	34.7	21.1	53.97	47.38
	0.6	11.36	6.85	37.7	27	19.94	39.72
FA 30	0.4	23.72	8.01	32.9	23.7	41.46	39.54
	0.6	8.8	6.28	41.2	23.8	11.62	23.4
C700 15	0.4	23.2	7.62	46.4	274	51.47	30.37
	0.6	10.2	8.13	38.6	31	24.11	45.1
C700 30	0.4	17	7.67	144	222	31.09	32.64
	0.6	8.8	7.43	84.2	190	12	46.12
C800 15	0.4	29.28	6.98	47.1	39.4	53.61	29.67
	0.6	15.4	9.41	38	161	26.1	5.86
C800 30	0.4	15.64	7.34	144	253	27.52	15.67
	0.6	8.56	7.19	33.6	46.1	16.42	8.91

Table A 12: Concentration of ionic species in pore solution

		Concentration (mg/l)					
		Na^+		Si^{4+}		Al^{3+}	
Mix type	w/b ratio	**28d**	**90d**	**28d**	**90d**	**28d**	**90d**
PC	0.4	34	54	0.408	0.144	0.065	0.057
	0.6	36	37	0.415	0.408	0.102	0.038
FA 15	0.4	93	55	1.251	0.558	0.079	0.044
	0.6	177	66	1.15	0.367	0.136	0.11
FA 30	0.4	39	31	0.503	0.807	0.094	0.291
	0.6	126	40	0.437	0.157	0.105	0.053
C700 15	0.4	104	193	0.487	0.135	0.065	0.06
	0.6	114	174	0.478	0.227	0.096	0.067
C700 30	0.4	161	260	0.57	0.29	0.067	0.037
	0.6	117	188	0.18	0.649	0.042	0.047
C800 15	0.4	51	85	0.785	0.449	0.074	0.047
	0.6	65	102	0.472	0.747	0.11	0.077
C800 30	0.4	54	225	0.276	0.173	0.102	0.031
	0.6	90	143	0.253	0.552	0.046	0.044

Appendix A5: Filler effect comparison

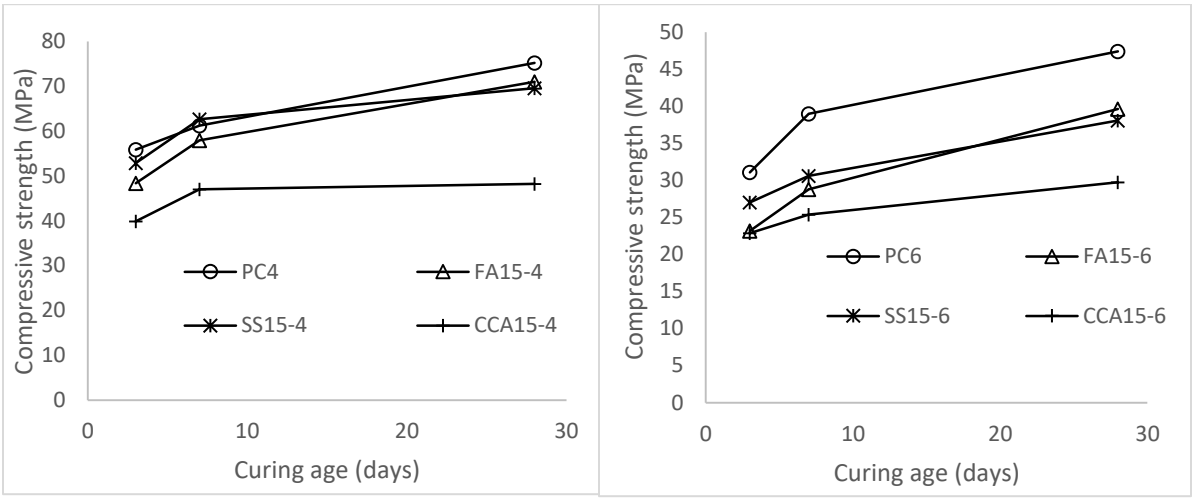

Figure A 1: Comparison of filler effect of FA and CCA at 15% replacement level

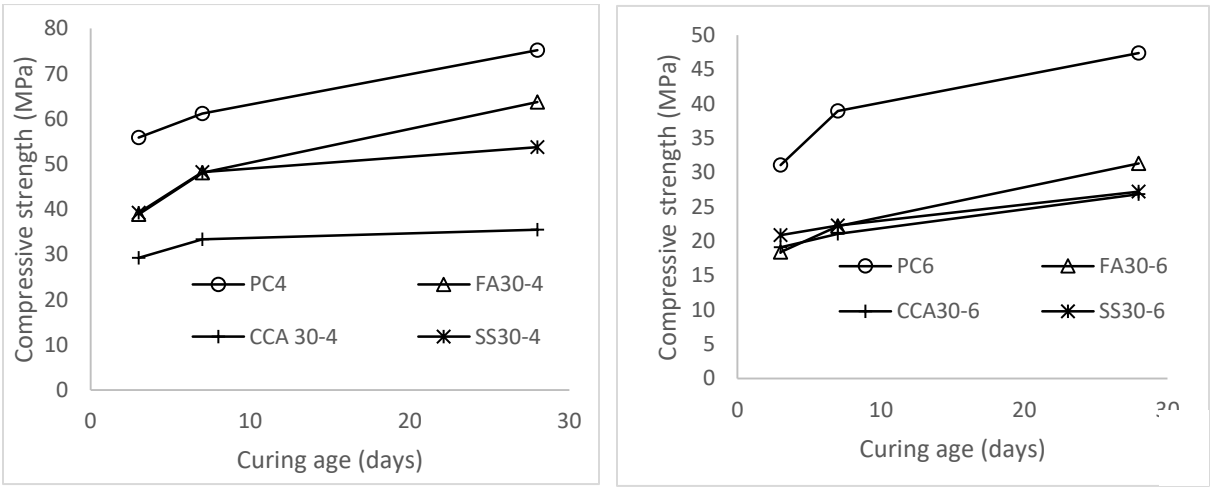

Figure A 2: Comparison of filler effect of FA and CCA at 30% replacement level

Appendix A6: Drying shrinkage strain

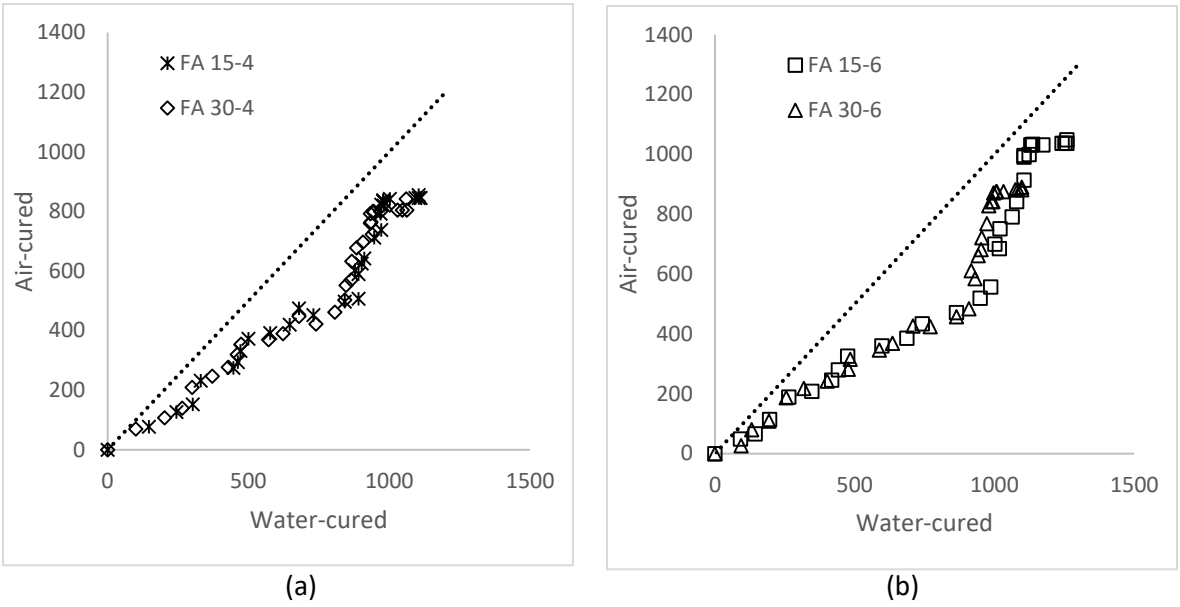

Figure A 3: Comparison of the effect of initial curing on drying shrinkage of PC-FA

Appendix A7: Strength-porosity regression curve

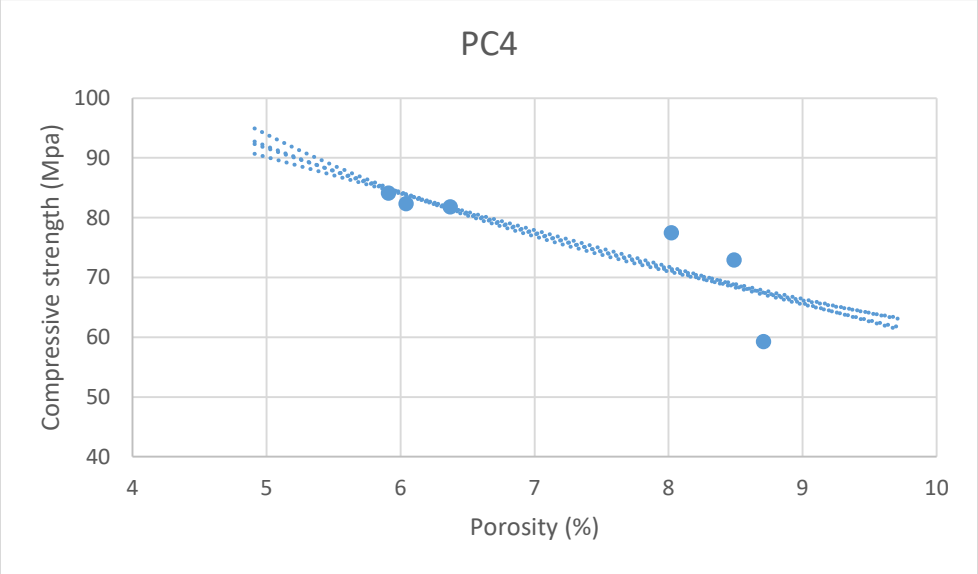

Figure A 4: Strength-porosity relation for PC at w/b of 0.4

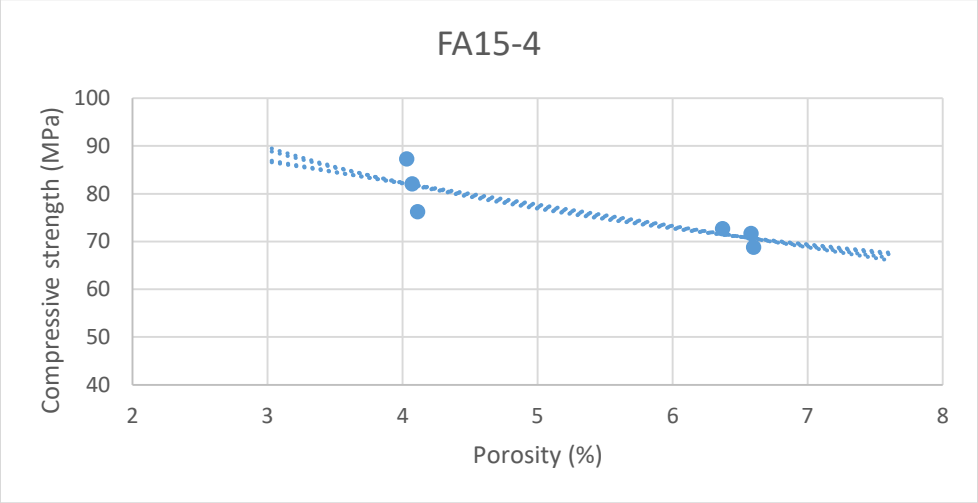

Figure A 5: Strength-porosity relation for FA at 15% replacement level and w/b of 0.4

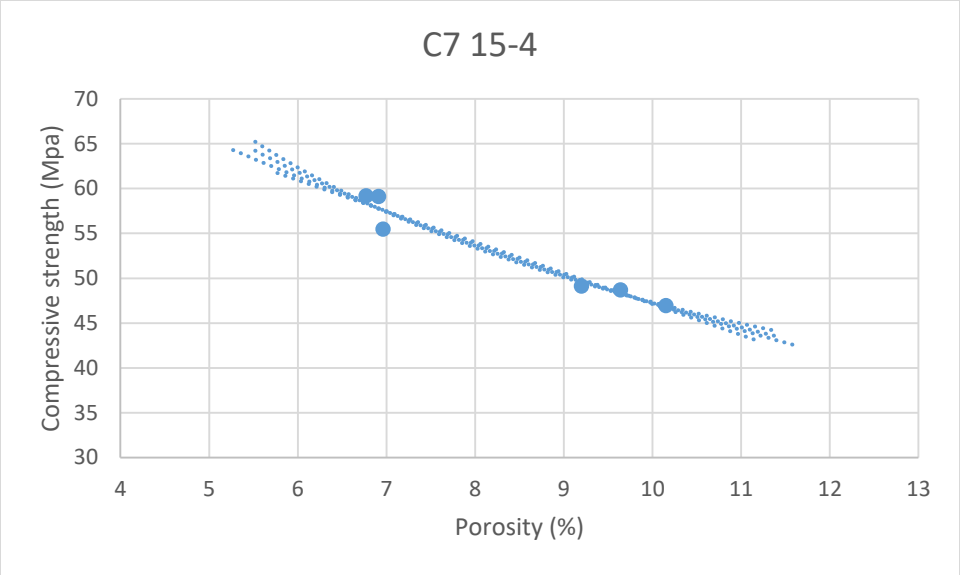

Figure A 6: Strength-porosity relation for C700 at 15% replacement level and w/b of 0.4

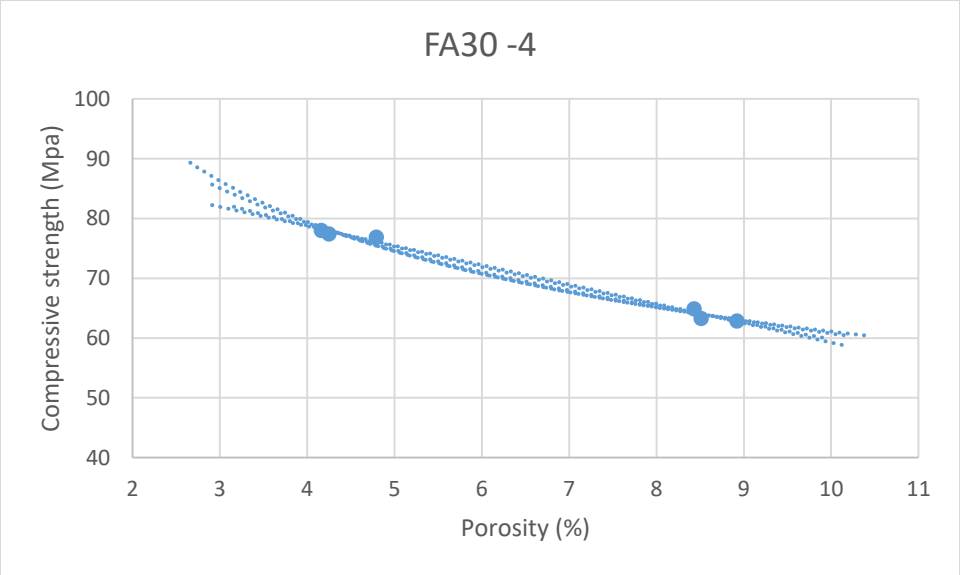

Figure A 7: Strength-porosity relation for FA at 30% replacement level and w/b of 0.4

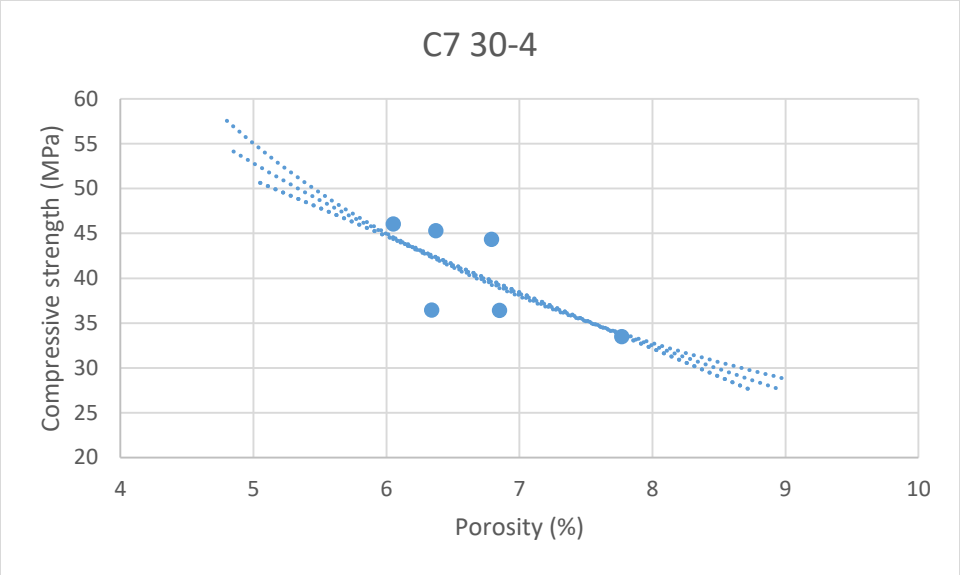

Figure A 8: Strength-porosity relation for C700 at 30% replacement level and w/b of 0.4

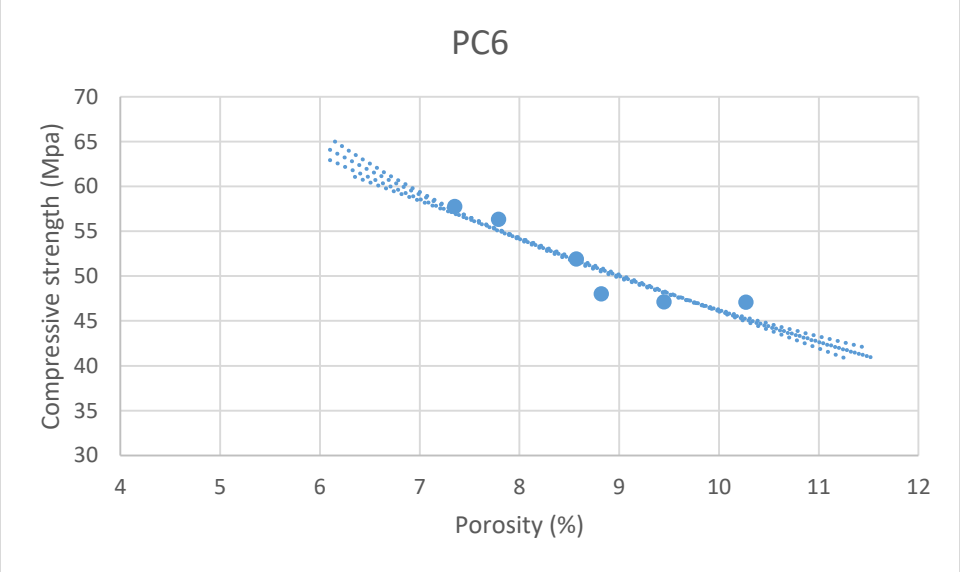

Figure A 9: Strength-porosity relation for PC at w/b of 0.6

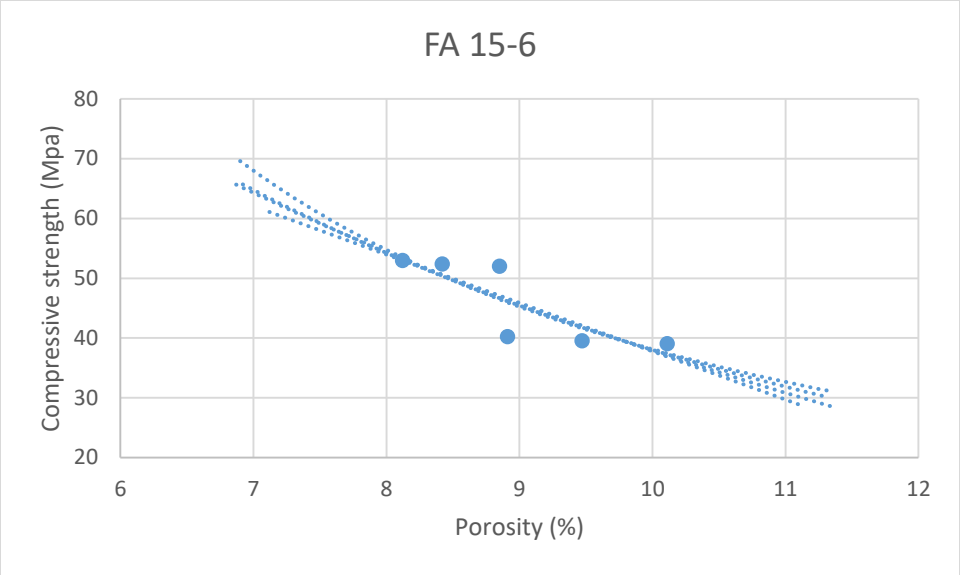

Figure A 10: Strength-porosity relation for FA at 15% replacement level and w/b of 0.6

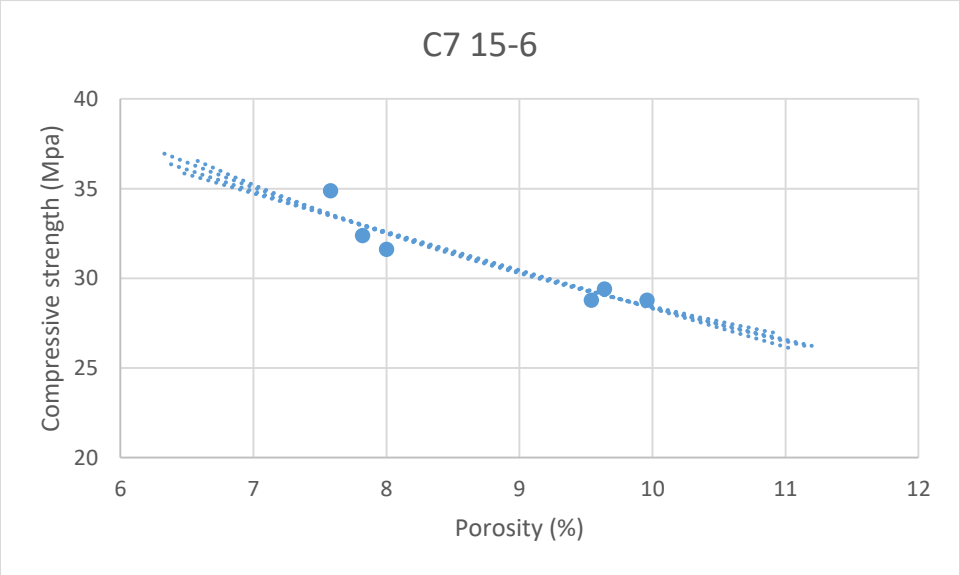

Figure A 11: Strength-porosity relation for C700 at 15% replacement level and w/b of 0.6

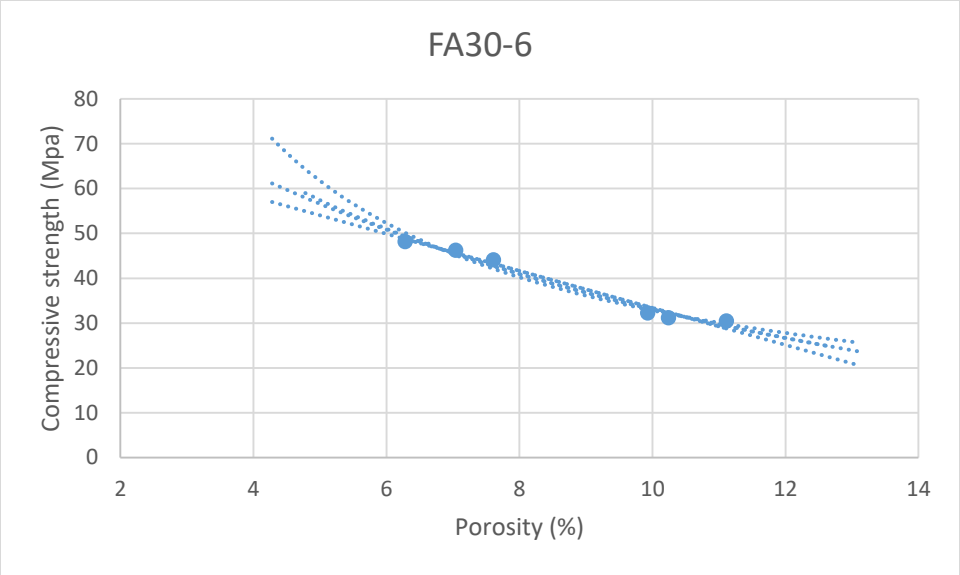

Figure A 12: Strength-porosity relation for FA at 30% replacement level and w/b of 0.6

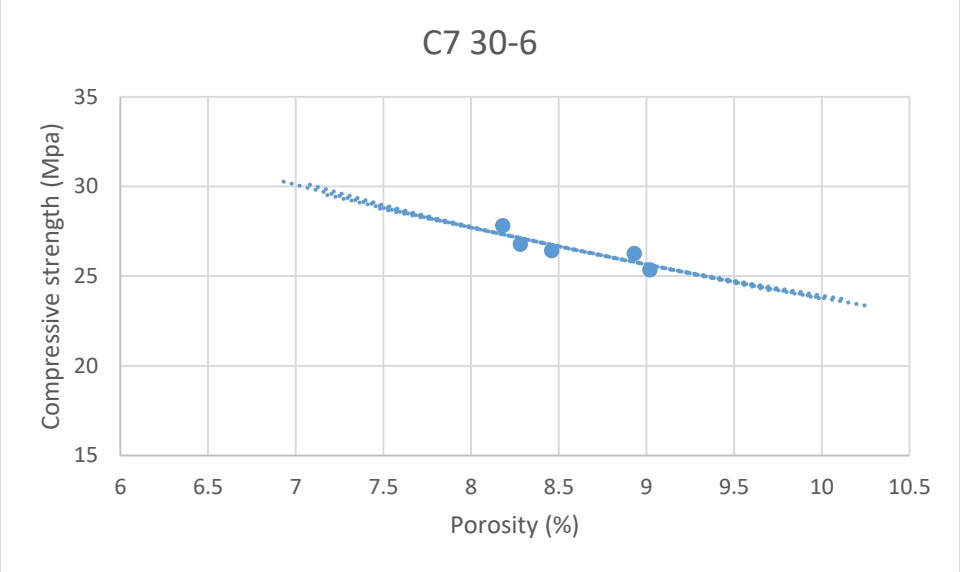

Figure A 13: Strength-porosity relation for A at 30% replacement level and w/b of 0.6

Appendix A8: Note on statistical analysis

The models reported in the study were based on regression analysis. Regression analysis involves the combination of statistical tools for determining the estimates of the parameters in a regression model which can be used in the prediction of future observation of the dependent variable. Regression analysis uses least squares estimates to calculate the parameters of the regression model. The parameters of the regression model are estimated from the following equations

$$S_{xx} = \sum_{i=1}^{n} x_i{}^2 - \frac{\left(\sum_{i=1}^{n} x_i\right)^2}{n} \quad \text{..... A1}$$

$$S_{xy} = \sum_{i=1}^{n} x_i y_i - \frac{\left(\sum_{i=1}^{n} x_i\right)\left(\sum_{i=1}^{n} y_i\right)}{n} \quad \text{.....A2}$$

The least square estimate of the slope and intercept is given by

$$\beta_{.1} = \frac{S_{xy}}{S_{xx}} \text{.....A3}$$

$$\beta_{.0} = y_m - \beta_{.1} x_m \text{.....A4}$$

The equation of the regression line is given as

$$y_E = \beta_{.0} + \beta_{.1} x \text{.....A5}$$

Where n represents the number of observations, y_m is the mean of the dependent variable, x_m is the mean of the independent variable, y_E is the estimated value of the dependent variable, $\beta_{.0}$ is the intercept of the regression equation and $\beta_{.1}$ is the slope of the regression equation.

The residuals from the fitted model are estimated from the difference between the measured dependent variable and the predicted values from the model and are used to estimate the variance of the errors of the model. The model errors are assumed to be normally distributed with mean zero and constant variance. For normally distributed errors, it is expected that about 95% of the standardized residuals will fall within the interval ±2 while values outside this range indicates the likely presence of outliers. An outlier is an observation which differs from the population. One method of identifying an outlier is the Grubb's test which is based on the following relations

$$T_u = \frac{X_u - x_m}{\sigma} \text{.....A6}$$

$$T_l = \frac{x_m - X_l}{\sigma} \text{.....A7}$$

Equation A6 is used when the potential outlier is greater than the mean of the sample population while Equation A7 is used when the outlier is lower than the mean of the sample. The value obtained from either equations is compared to a critical value based on the confidence level and number of replicates. The data point in question maybe rejected if it is greater than the critical value. The treatment of a data point as an outlier can be subject to engineering judgement as this can help in the decision of whether the data point can be rejected or retained.

Note: The information presented above is obtained from Montgomery et al. (2011) and Otieno, (2014).

Appendix A9: Particle size distribution charts

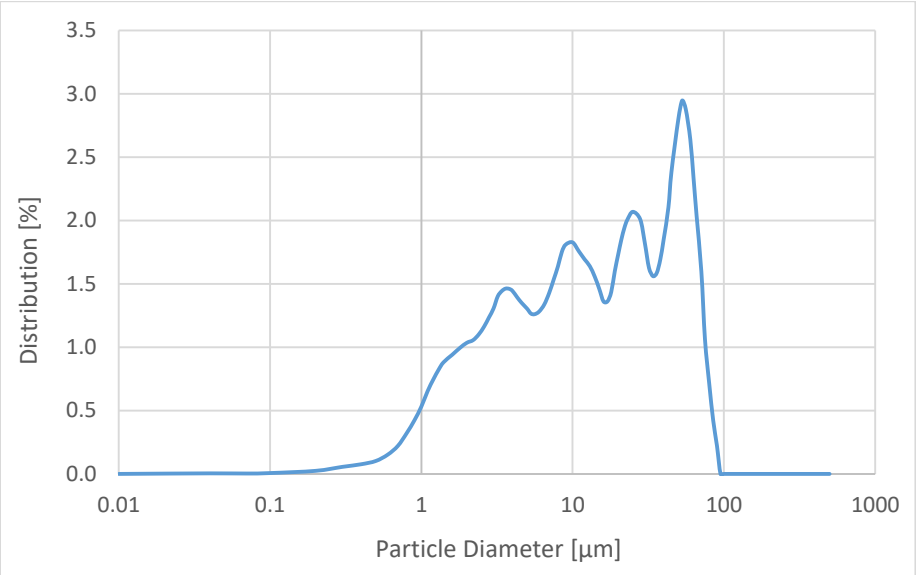

Figure A14: Particle size distribution for C700

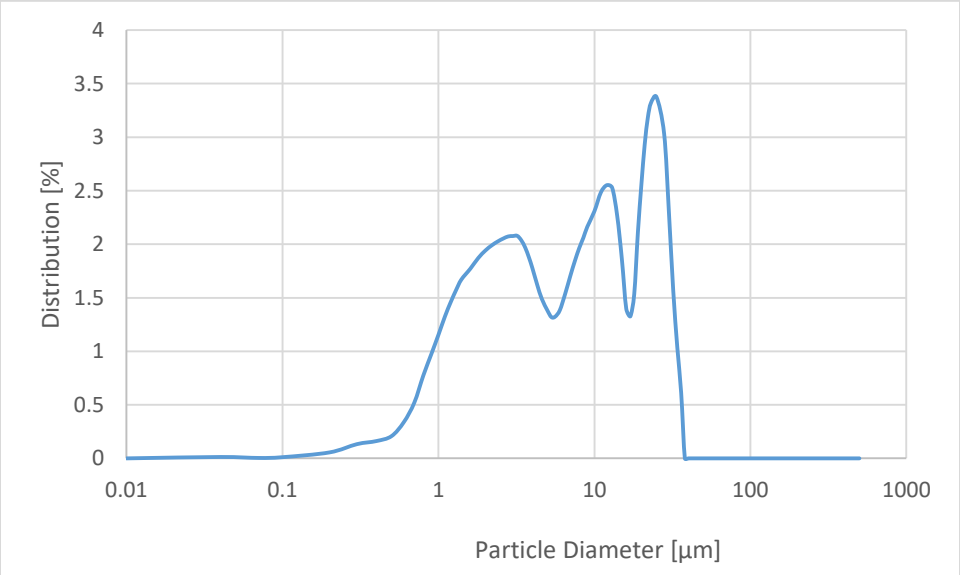

Figure A15: Particle size distribution for C800

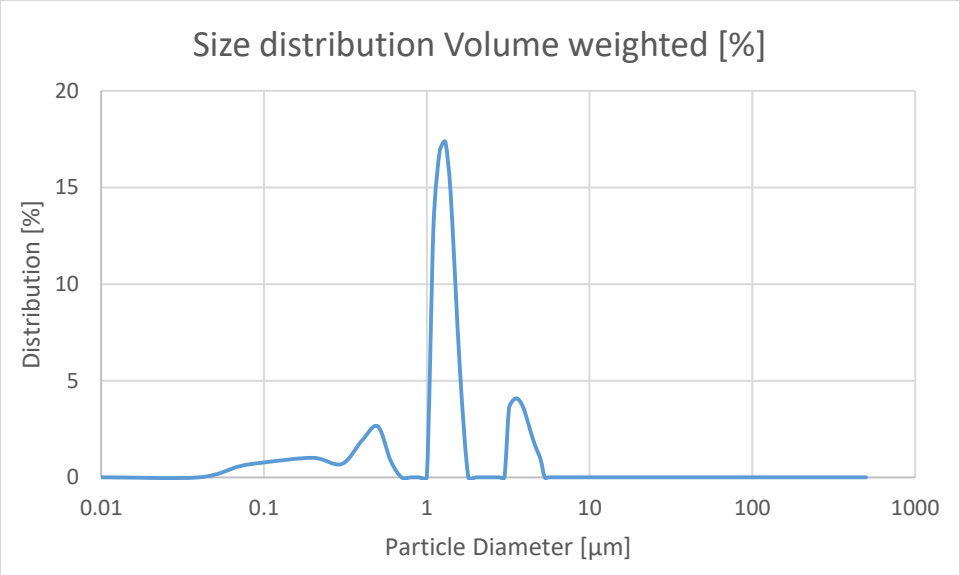

Figure A16: Particle size distribution for fly ash

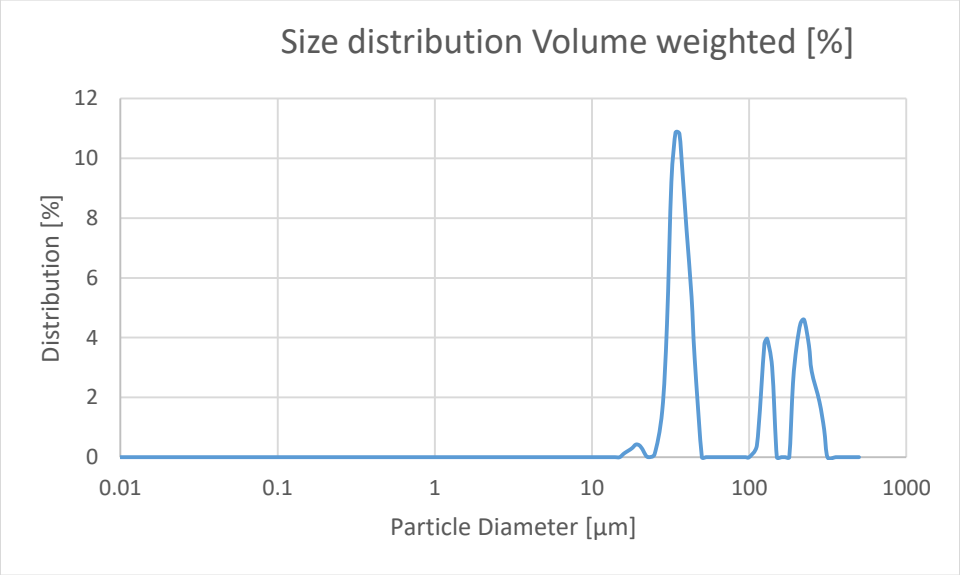

Figure A17: Particle size distribution for PC

Appendix A10: XRD diffractogram for phase quantification

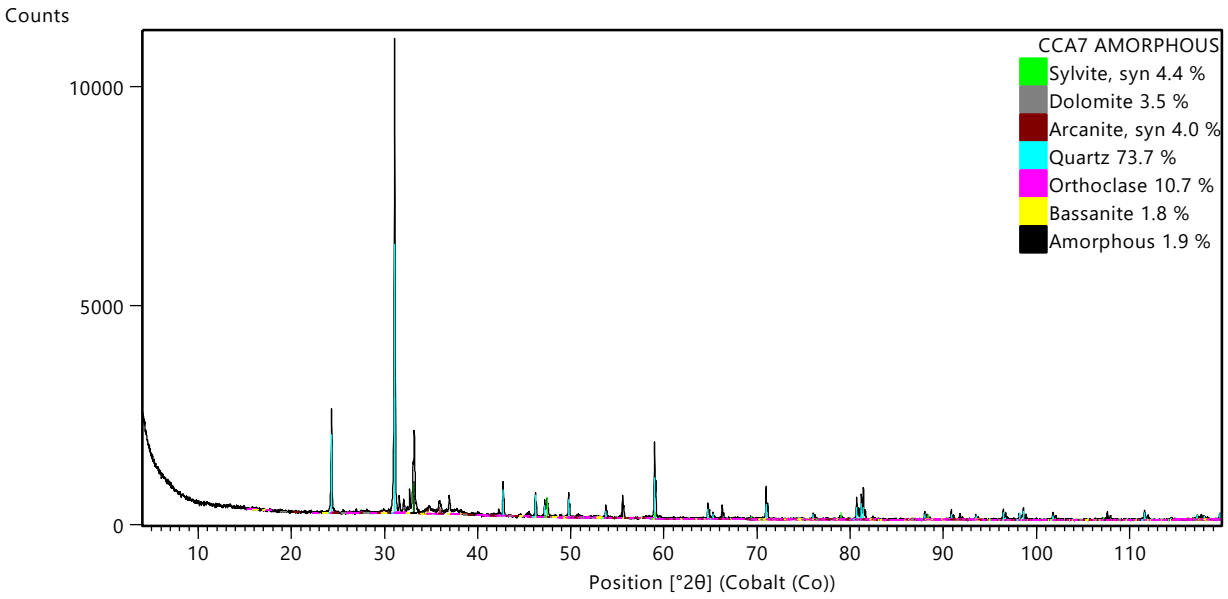

Figure A18: XRD diffractogram for corn cob ash calcined at 700°C

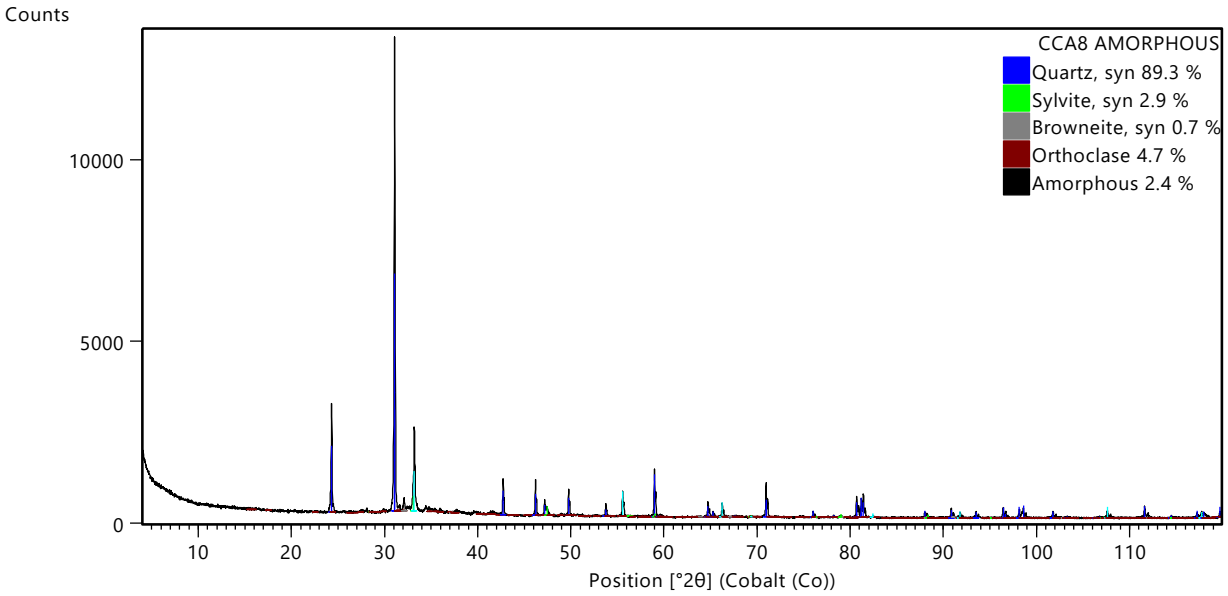

Figure A19: XRD diffractogram for corn cob ash calcined at 800°C

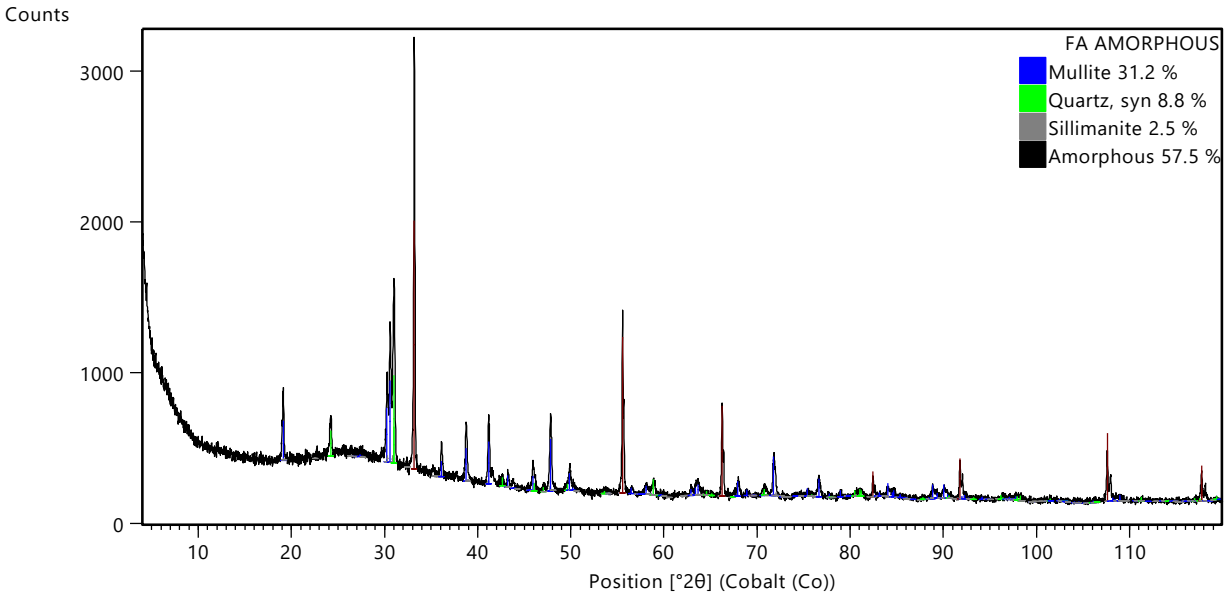

Figure A20: XRD diffractogram for fly ash

Appendix A11: Picture of materials used in the investigation

Figure A21: Raw corn cobs

Figure A22: Portland cement

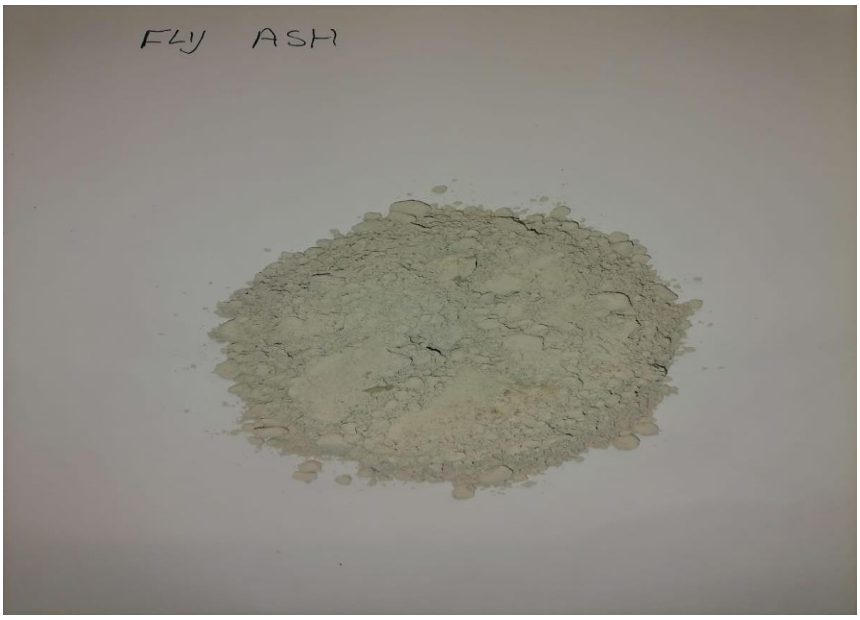

Figure A23: Fly ash

Appendix A12: Setting times result

Table A13: Setting times

Mix	**Initial setting time (mins)**	**Final setting time (mins)**
100PC	160	320
85/15/PC/FA	230	370
70/30/PC/FA	240	440
85/15/PC/C700	20	190
70/30PC/C700	30	160
85/15/PC/C800	126	510
70/30/PC/C800	20	462